UNIVERSITÄT DUISBURG ESSEN

Open-Minded

Zwitterion-Perylene diimide-Modules for switchable supramolecular systems

Dissertation

zur Erlangung des akademischen Grades eines Doktors der Naturwissenschaft

- Dr. rer. nat. -

vorgelegt von Diplom Chemikerin

Ina Krebs

geboren in Mainz

Institut für Organische Chemie der Universität Duisburg-Essen

Essen 2015

Zwitterion-Perylene diimide-Modules for switchable supramolecular systems

Gutachter:	Prof. Dr. Carsten Schmuck
	Prof. Dr. Georg Jansen
Prüfungsvorsitzender:	Prof. Dr. B. Siebers
Tag der mündl. Prüfung:	30.11.0215

Erklärung

Die vorliegende Arbeit wurde von Januar 2010 bis August 2015 im Institut für Organische Chemie der Universität Duisburg–Essen unter der Anleitung von Herrn Prof. Dr. Carsten Schmuck angefertigt.

Ich erkläre hiermit des Eides statt, dass ich die vorliegende Arbeit selbst verfasst und mich dabei keiner anderen als der von mir bezeichneten Quellen und Hilfen bedient habe.

Ich erkläre hiermit, dass ich an keiner anderen Stelle ein Prüfungsverfahren beantragt beziehungsweise die Dissertation in dieser oder anderer Form bereits anderweitig als Prüfungsarbeit verwendet oder einer anderen Fakultät als Dissertation vorgelegt habe.

Essen, im August 2015

.....

Ina Krebs

Curriculum Vitae

Aus Datenschutzgründen in der elektronischen Version nicht enthalten.

Danksagung

Als erstes möchte ich mich bei Prof Dr. Carsten Schmuck dafür bedanken, dass ich dieses spannende und abwechslungsreiche Thema bearbeiten durfte. Ich danke dir für deine Geduld und für den kreativen Spielraum den du mir in den Jahren gegeben hast. Bei Prof. Dr. Jansen bedanke ich mich für die Übernahme des zweiten Gutachtens.

Mein Dank gilt außerdem der Studienstiftung des deutschen Volkes sowie der Universität Duisburg-Essen, die mit ihrer finanziellen Förderung diese Arbeit überhaupt erst ermöglicht haben.

Ich möchte mich besonders bei Wilhelm Sicking für den immensen Beitrag zur erfolgreichen Fertigstellung meiner Arbeit bedanken. Ohne deine Rechnungen wären meine Ergebnisse immer noch völlig verwirrend für mich. Des Weiteren möchte ich mich für die Hilfe bei allen analytischen Methoden bedanken: für die Messung der NMR-Spektren insbesondere am 500er und 600er bei Heinz Bandmann und Dr. Torsten Schaller; bei Werner Karow für die enge Zusammenarbeit und das Austoben am MALDI sowie bei Ulla Nüchter für die Hilfe bei allen UV/vis Messungen sowie den damit zusammenhängenden Fragen. Ein großer Dank auch an Elisabeth Verheggen vor allem dafür, dass du mir gelegentlich mit der dritten Stufe ausgeholfen hast und für die lustige Zeit im Labor. Weiterhin danke ich Dr. Hans-Gert Korth sowie Christine Cangemi für die Unterstützung im Umgang mit den alltäglichen Fragestellungen.

Meinen Kooperationspartnern danke ich für die tollen Messungen sowie die interessanten Diskussionen über supramolekulare Chemie. Dabei danke ich besonders Henning Vieker für die HIM Messungen, sowie Boris Rybtchinski für die generelle Kooperation und Haim Waisman für die cryo-TEM Bilder.

Meinen jetzigen wie auch ehemaligen Arbeitskollegen möchte ich für ihre Unterstützung und die schönen Jahre im Arbeitskreis danken. Ich danke dabei vor allem Lina, Jule, Ute und Sandra für die schöne Zeit und die lustigen Gespräche im Kaffeeraum. Ich muss heute noch vor mich hin Grinsen, wenn jemand vom Laichen spricht und dabei an unseren Kühlschrank denken. Es war eine wirklich wunderschöne Zeit mit euch! Ganz besonders bedanke ich mich bei meiner Labornachbarin Kerstin, mit der die Laborarbeit jeden Tag ein tolles Erlebnis war. Ich danke dir für die vielen durchlachten Stunden und lustigen wie auch spannenden Momente. 👀 Außerdem vielen Dank, dass du mein Chaos so stoisch ertragen hast. Ebenso danke ich allen Auszubildenden, Studenten sowie Christian Schlütting für die tolle Arbeit, die er im Vertiefungspraktikum geleistet hat.

Für die Durchsicht des schriftlichen Teils meiner Doktorarbeit möchte ich mich bei Kerstin Grossert sowie Dr. René Nagelsdiek bedanken.

Außerdem möchte ich meiner Familie und meinen Freunden danken, die mich auf meinem Lebensweg begleitet und unterstützt haben. Ich danke meiner Schwester Maren, dass sie mich immer aufmuntert und an meiner Seite steht. Du hast mir gezeigt, wie wichtig es ist für sich selbst einzustehen. Des Weiteren danke ich Anja dafür, dass sie immer für mich da ist und mir geholfen hat viele schwierige Momente in der Vergangenheit zu meistern. Ebense danke euch beiden, dass ihr euch durch das fachfremde chemische Manuskript gearbeitet habt.

Abschließend möchte ich mich bei meinem Partner und zukünftigen Mann Jan bedanken. Du gibst mir die Kraft und die Motivation nochmal ein Stückchen mehr über mich hinaus zu wachsen. Vielen Dank für deine unendliche Geduld und Unterstützung während der Doktorarbeit, vor allem während der letzten Schreibphase. Du bereicherst mein Leben und ich bin froh, dass es dich gibt.

There is nothing like looking, if you want to find something.
You certainly usually find something, if you look,
but it is not always quite the something you were after.

J.R.R. Tolkien

Content

1. Introduction 1

2. State of Art 4

2.1 Supramolecular Chemistry 4

2.2 Zwitterionic GCP binding motif 13

2.2.1 Basic research 13

2.2.2 Supramolecular Assemblies 17

2.2.3 Smart Materials 21

2.3 Perylene diimides 24

2.3.1 Introduction 24

2.3.2 Synthesis 24

2.3.3 Optical properties 26

2.3.4 Supramolecular PDI assemblies 27

2.3.4.1 Assemblies without additional binding motif 30

2.3.4.2 Assemblies with additional binding motif 34

2.3.4.3 Aggregates in water 37

3. Concept 47

3.1 Ditopic Modules 49

3.2 Monotopic Modules 51

4. Ditopic Modules 54

4.1 Concept 54

4.2 Retrosynthesis 56

4.2.1 Imide linked Module 56

4.2.2 Core linked Module 61

4.3 Aggregation behavior 65

4.3.1 Spectroscopy 65
4.3.2 Microscopy 68
4.3.3 Assembly mode 72
4.3.4 Aging of the core linked Module 79
4.4 Switching ability 85
4.4.1 Acid and Base 85
4.4.2 Reduction 92
4.5 Summary 96
5. Monotopic Modules 97
5.1 Concept 97
5.2 Retrosynthesis 100
5.2.1 3-Pentyl Module 100
5.2.2 Cyclohexyl Module 104
5.3 Aggregation behavior 107
5.3.1 Spectroscopy 107
5.3.2 Microscopy 110
5.3.3 Assembly mode 114
5.4 Switching ability 119
5.4.1 Acid and base 119
5.4.2 Sodium Dithionite 124
5.5 Assembly in water 125
5.5.1 3-Pentyl Module 125
5.5.2 Cyclohexyl Module 128
5.6 Gel formation 131
5.7 Summary 132
6. Summary 133
6.1 Ditopic Modules 134
6.2 Monotopic Modules 139

6. Zusammenfassung 144

6.1 Ditopische Module 145

6.2 Monotopische Module 151

7. Experimental Part 156

7.1 GCP and other precursor molecules 159

7.2 Ditopic Modules 167

7.3 Monotopic Modules 182

8. Abbreviations 198

9. Bibliography 200

1. Introduction

The noblest pleasure is the joy of understanding.

These are the words of Leonardo da Vinci (1452-1519), one of the most outstanding minds of modern history. His life was driven by the search of a better understanding of both natural and technical things. He was known for his exceptional observation of nature, the human body and his detailed studies of all natural forces. He was especially fascinated by the most essential element of life, water.[1] Da Vinci investigated the properties of water in one of his notebooks known as Codex Leicester or also Hammer Codex.[2] He was intrigued by the way it moved und curious about the unusual behavior of the liquid. During his life he looked for an understanding of the principles behind this behavior and worked on the development of technical constructions to make use of water.

Figure 1: Sketch of flowing water drawn by Leonardo da Vinci.[1]

This ubiquitous foundation of life shows indeed many unusual features compared to other liquids. One of these features is for example the surface tension whereby Da Vinci was the first to describe this property. More than 400 years passed until the mystery of these properties could be unraveled.[3] The exceptional behavior of water can be explained by the existence of weak forces which enable interactions between the molecules. The formation of hydrogen bonds between H_2O molecules leads to a three dimensional network of the tilted molecules.[4] Based on these structural features which are founded by these weak interactions, one can understand the unusual behavior of water.

Hydrogen bonds are not the only weak interactions known in nature though, there are also various other interactions. Interactions between molecules based on weak forces were summarized under the term supramolecular chemistry by Jean Marie Lehn.[5] The concept is described as "chemistry beyond the molecule" and regarded as link between the simplicity of basic motifs and complexity in structure. All non-covalent interactions except the ionic bonds in salts are regarded as such weak forces summarized under the term supramolecular chemistry.

These weak interactions are the basis for the formation of reversible bonds needed for various processes in nature, whereby they can to be divided into intra- and intermolecular interactions. Protein folding for example is based on weak intramolecular interactions. Specific parts of the side chains of the amino acids interact with adjacent side chains which leads to a coiling or folding to form the secondary, tertiary and quaternary structure of the protein.[6] Another example is the formation of the DNA double strand through an intermolecular interaction of two single DNA strands. Thereby the DNA base pairs interact with another to form hydrogen bonds between the two strands.[7]

Supramolecular interactions lay the foundation for a better understanding of assembled systems and processes in nature. In a certain sense, nature gives the blueprint for the assembly of structures and provides a supramolecular toolbox for the creation of new systems. Like da Vinci did with his flight machines, it is possible to employ concepts known from nature and utilize them to develop new materials. This can be done in two ways: imitating nature to artificially form similar systems or employing certain concepts to create completely new systems. The development of smart materials thereby has been a research focus in the last decade. This research field focuses on the intelligent combination of supramolecular interactions and functional units to create systems with special characteristics. In recent years, the focus especially lay on functional and adaptive systems. Nature has various examples where a reversible formation of architectures takes place or where a system reversibly reacts to different stimuli. Several research groups therefore tried to develop smart materials that exhibit a reversible switching ability. Emphasis is being placed especially on the creation of supramolecular gels that show a responsive change in viscosity.[8]

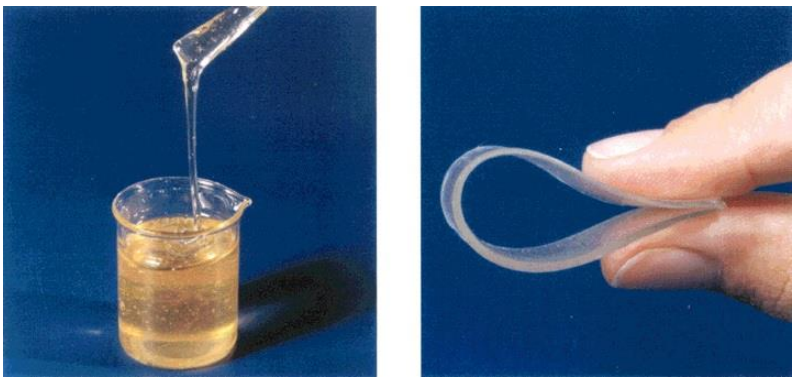

Figure 2: Left: Pure polymer without supramolecular binding sites. Right: Assembled supramolecular gel formed by the polymer with supramolecular binding sites. Reprinted with permission.[8]

Moreover, optical properties are often in focus for the development of smart materials. One functional unit that has been investigated intensively is the perylene diimide which shows outstanding photoelectronic properties.[9] This dye was used to form artificial light harvesting systems having the

light harvesting system in plants as model.[10] Due to the exceptional photoelectronic properties it is also an excellent candidate for the creation of new materials e. g. for organic light emitting diodes or solar cells.[11] What is still challenging though is the creation of functional supramolecular systems in water. Due to the significant hydrophobic effect there is often either a problem with the solubility or the stability of the formed system. Assembled systems based on hydrogen bonds for example are stable in unpolar solvents, but usually disaggregate upon addition of water. To obtain supramolecular systems in water, a unit is needed that forms stable assemblies in polar media. Our working group reported the zwitterionic guanidiniocarbonyl-pyrrole-carboxylate (GCP), a binding motif which is stable in polar solvents and shows an extraordinary pH switching ability. Like the perylene diimide, this unit is suitable for the formation of smart materials.[12]

This thesis will therefore explore the combination of these two particular supramolecular units to provide a basis for the creation of responsive smart materials that are stable in polar environment. The aim is to design small bi-functional Modules that self-assemble into complex systems in polar media and to explore the switching possibilities of these systems with various stimuli.

2. State of Art

2.1 Supramolecular Chemistry

As mentioned in the introduction, this thesis will be based on the concepts of supramolecular chemistry since the goal is the creation of complex assemblies by a combination of several weak forces. Therefore the theory of supramolecular chemistry as well as the involved forces which lead to non-covalent interactions will be outlined in this chapter.

Jean Marie Lehn coined the term supramolecular chemistry when he described the topic as "chemistry beyond the molecule", targeting the interplay between two moieties, while the interactions can both be intermolecular between two separate molecules as well as intramolecular within one molecule. Nature has numerous examples for supramolecular chemistry e.g. in molecular recognition or the assembly of the DNA double helix.

The interactions responsible for supramolecular chemistry are often called weak interactions, even though the term is not completely sufficient. Per definition all non-covalent interactions are regarded as supramolecular forces and therefore defined as being weak at least compared to covalent bonds between two atoms. The following part of the chapter will outline the involved forces in detail.

In principle all interactions between atoms and/or molecules can be divided in three principle classes:[13]

1) purely electrostatic, which arise from Coulomb interactions and include charges, ions, permanent and induced dipoles
2) entropic, which are present in osmotic forces
3) quantum mechanical, whereby chemical bonds as well as van der Waals, charge-transfer or steric forces fall under this class

These interactions form the basis of all matter, whereby some can be regarded as weak or as strong force depending on the moieties involved in the interaction as well as the conditions present. Electrostatic interactions for example can be both. When being involved in a salt formation, the interaction is regarded as strong interaction leading to a tight binding of the naked ions. In supramolecular interactions, the charges are incorporated in molecules and therefore not as localized and isolated as in a salt, leading to a weaker interaction. Since covalent &strong interactions are not

the focus of supramolecular chemistry, this thesis will concentrate on weak non-covalent interactions employed to build up complex structures. The most relevant supramolecular interactions for this thesis shall be outlined in the following based on the book *Intermolecular and Surface Forces* written by J. N. Israelachvili.[13]

One of the often quoted interactions is the van der Waals force, which is always present in the interplay between atoms and molecules. Van der Waals forces are divided in three main parts which contribute to the overall interaction. Dispersion forces are one part of the van der Waals forces and probably the most important contribution since they are always present. Features like surface tension, properties of physical states or structures of condensed macromolecules are determined by these forces. They are basically quantum mechanical since they are based on the current position of the electron shell of a molecule or atom. The electrons of an atom are not always equally distributed around the positively charged core. A spontaneous uneven distribution of the electrons can cause a dipole moment for the atom. This dipole can itself induce a second dipole in a nearby entity which can be regarded as a polarization force. The dispersion forces can either be attractive or repulsive, depending also on the electronic situation in the nearby atom. They bring molecules together, but can also align and orient them. In sum, van der Waals forces are always attractive since also constant dipol interactions contribute to the overall strength.

As already mentioned all electrostatic interactions are based on coulomb interactions between at least two charges. They have to be divided in two classes; the isolated charges like in salts and the incorporated charges which can be regarded as part of a dipolar molecule, whereby the latter will be in focus in this thesis. Thereby a negatively charged atom interacts with a positively charged atom to form an intermolecular weak bond between two involved molecules.

The formation of hydrogen-bonds is one of the best known interactions, as mentioned in the introduction of this thesis. Water owes its properties to the existence of such interactions between the molecules. In principle H-bonds are a dipole-dipole interaction between a partially negatively charged atom and the positively polarized hydrogen atom of a neighbored group. Thereby the hydrogen has to be bound to an electronegative heteroatom. Because the bond moment of such groups like N-H, O-H or F-H is unusually large, other electronegative atoms can get close to the hydrogen. This results in an interaction, whereby the hydrogen atom is located between the two electronegative atoms building a bridge between these molecules, which is called H-bond.

One of the most feasible interactions for supramolecular chemistry is the aromatic π-π-stacking.[14] It describes the stacking of two or more molecules with large π-electron systems, e.g. porphyrins with a

parallel orientation of the aromatic systems. The term is somehow misleading though, since the interaction between two aromatic systems is not caused by an attraction of the π-systems, but the σ-π-attraction. The interacting molecules are arranged in an offset to reduce the coulomb repulsion between delocalized π-electron clouds to enable the stabilizing σ-π-interaction.

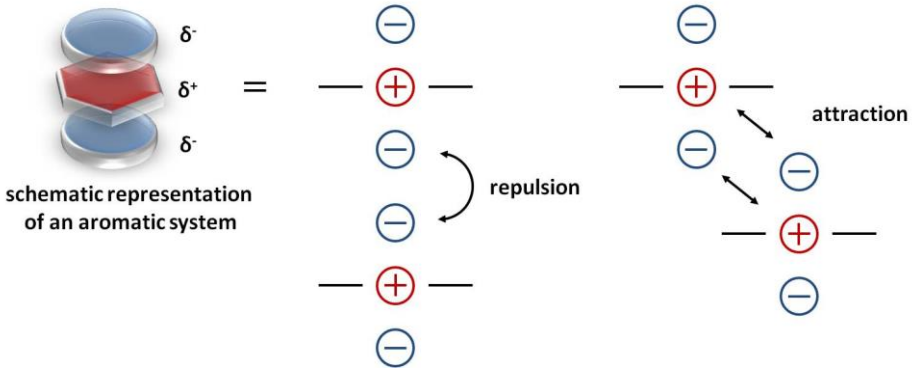

Figure 3: Schematic presentation of the interactions leading to a π-π-stacking.[14]

The major contributions to this stacking come from electrostatic and van der Waals interactions. Since the van der Waals forces are proportional to the π-overlap, they cannot be the whole driving force, otherwise this would result in a complete overlap without offset. Additionally an interaction of the π-electron systems would not lead to a charge transfer and therefore no change in the UV/vis spectrum which is normally observed with π-stacked systems. For that reason the key is the electrostatic part of the π-π-interaction. When a contour plot for the charge distribution is calculated based on the electrostatic interactions, it reflects the overlapping regions of the molecules when being stacked. The inclusion of van der Waals forces in the calculation leads to no alteration of the contour plot but highly influence the net interaction energy. Therefore it can be stated that the electrostatic part of the interaction influences the geometry while the van der Waals interactions affects the magnitude.

The hydrophobic effect occurs, when an unpolar substance is introduced in a polar environment of water. When this molecule has no possibility to form H-bonds, one part of the water molecule has to face towards the molecule and is lost for the internal H_2O H-bond. When unpolar molecules are not too large, all water molecules can pack around without losing H-bonds. Bringing water and unpolar molecules together therefore means a reorientation of the water molecules to maintain all H-bonds. However some H-bonds have to bend which is entropically highly disfavored. The term hydrophobic solvation means the minimization of the area that has to be restructured and the unpolar molecules are crowded together to minimize the exposed surface. If the dissolved molecule has a hydrophilic surface, this will then face outwards to maintain H-bonds with water, which is the driving force for e.g.

a membrane formation. When the molecules get larger, greater cavities have to be created to distribute the molecule in the aqueous medium.

What also has to be mentioned are repulsive steric forces. There are several examples in which a specific aggregate could be observed after assembly due to a steric repulsion of interacting groups. This repulsion is caused by the van der Waals packing radius of a molecule.

An interaction which is also widely used in supramolecular chemistry is the metal ligand coordination. Some examples will be shown in this chapter, but since the following part of this thesis will not focus on these kind of interactions the principle will not be outlined any further.

All these above mentioned weak interactions are utilized in supramolecular chemistry to build up artificial systems. Through an intelligent combination of the interactions, tailor made systems can be created that exhibit special properties. Besides these weak interactions there are some concepts used to build up complex systems in supramolecular chemistry. These concepts form the basis of this thesis and will be outlined in the next part of this chapter based on the book of Jean Marie Lehn.[5]

- The commonly used term self-assembly describes the spontaneous association of components to form assemblies. By the interplay of supramolecular interactions small units rearrange into complex architectures. Depending on the geometry and the involved interactions, different types of one, two or three dimensional aggregates are formed.
- The term self-organization describes a dynamic process with a spontaneous change in structural and/or temporal order. These changes are caused by supramolecular forces, whereby the information for the process is encoded in the profile of the supramolecular interactions within the molecule.

Since the coining of the term supramolecular chemistry, numerous research groups concentrated on this topic and utilized interactions to build up more complex structures. Thereby the concept of the supramolecular binding motif evolved. A binding motif is a structural unit responsible for the supramolecular assembly with a specific interaction pattern. It incorporates one or more units which enable weak interactions and is utilized for the build-up of larger structures. Nature is the model for this concept and the most prominent example is the interaction between nucleic acids to form the DNA double helix. Based on hydrogen bonds, the DNA base pairs form dimers to link the two separate strands together. Thereby thymine-adenine form the first base pair and guanine-cytosine form the ssecond base pair.[7]

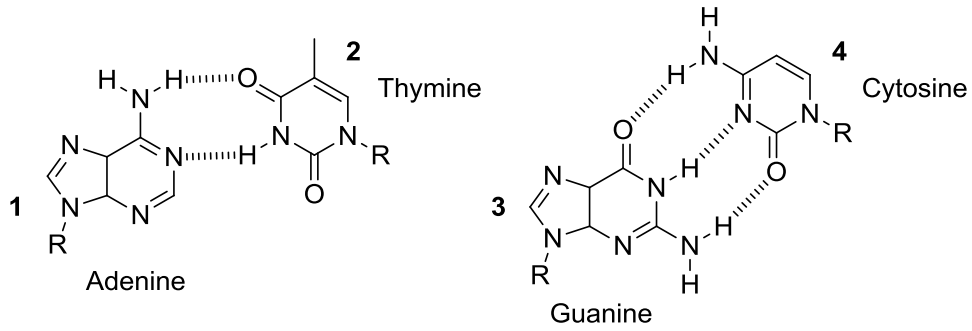

Figure 4: DNA base pairs: adenine **1** and thymine **2** are complementary binding motifs as well as guanine **3** and cytosine **4**.[7]

On that basis several groups worked on designing motifs with a similar function. Thereby it can be distinguished between a complementary and a self-complementary binding motif. The expression self-complementary describes a molecule that aggregates with a second molecule of its own kind with the same chemical build-up (e.g. molecule **7**). Here the term homo-assembly is used to describe the aggregation pattern. A complementary binding needs two different motifs which have a complementary interaction pattern like the DNA base pairs. The chemical build up is different in this case since two different molecules are needed for the interaction (e.g. molecule **5** and **6**) and therefore named hetero-assembly. Two examples for supramolecular binding motifs based on hydrogen bonds are given below in Figure 5.

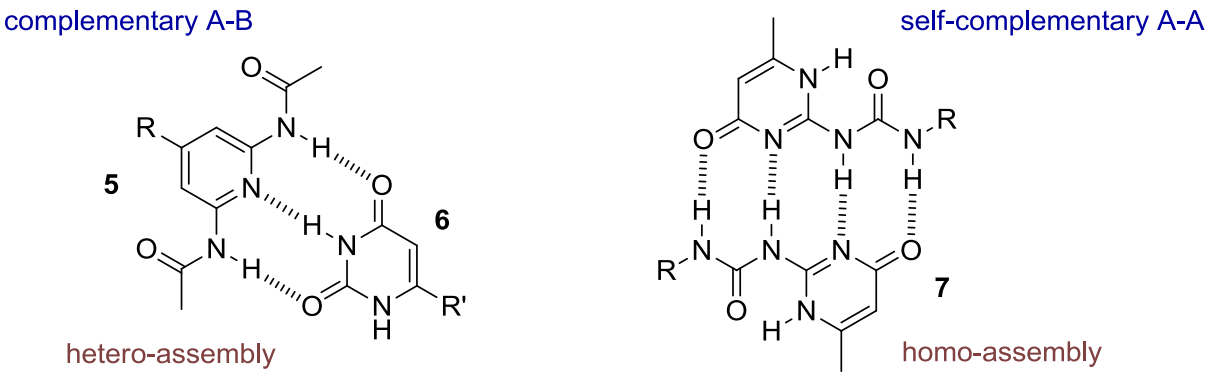

Figure 5: Left: Example for a complementary binding motif introduced by Fouquey and coworkers;[15] Right: Example for a self-complementary binding motif introduced by Folmer and coworkers.[8]

When speaking of binding motifs one can further distinguish between a monotopic and a ditopic attachment of a binding unit to another molecule. While the term "monotopic" describes a molecule where only one binding motif is attached to the parent molecule, "ditopic" illustrates a molecule where two units are attached. Often the binding motifs are attached at opposite sides of the parent molecule to obtain linear or polymeric aggregates after assembly.

The first example to be mentioned here was presented by Fouquey and coworkers. [15] They designed two subunits in a complementary fashion which form an assembly through three donor acceptor interactions. Subsequently these two binding motifs were attached to a linker based on tartaric acid in a ditopic fashion (A-A and B-B). The researchers showed that alternating supramolecular polymers (A-AB-BA-AB-B) can be formed, when these two ditopic molecules are mixed in a 1:1 ratio.

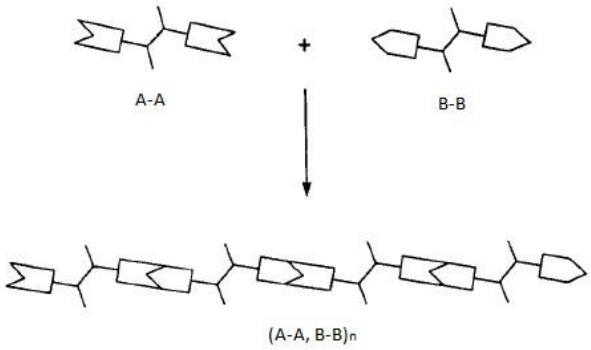

Figure 6: Schematic representation of the formation of a polymeric supramolecular species (A-A, B-B)$_n$ by association of two complementary ditopic components A-A and B-B. C. Fouquey, J.-M. Lehn, A.-M. Levelut, *Adv. Mater.* **1990**, *2*, 254-257. Copyright (c) 2014 WILEY-VCH Verlag GmbH.[15]

The second example is a motif (**7**) presented by Folmer et al. and shows a self-complementary binding through four H-bonds.[8] They supplied a flexible polymer with this motif at both sides to get a ditopic molecule. Through the supramolecular assembly of the binding motifs even larger polymers were formed which altered the physical state. While the initial polymer showed a honey like state, the assembled polymers formed a rubber like material.

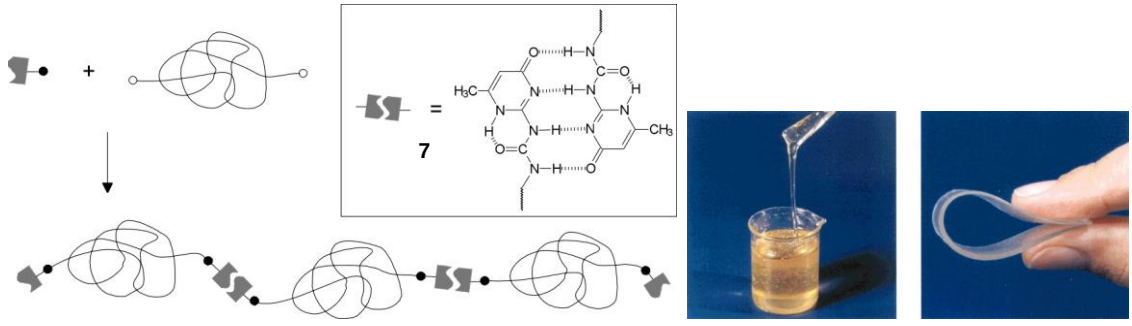

Figure 7: Schematic drawing of functionalization of telechelic polymers with quadruple hydrogen-bonded ureidopyrimidinone units. : Poly(ethylene/butylene) with OH end groups (left), poly(ethylene/butylene) functionalized with hydrogen-bonded units (right). B. J. B. Folmer, R. P. Sijbesma, R. M. Versteegen, J. A. J. van der Rijt, E. W. Meijer, *Adv. Mater.* **2000**, *12*, 874-878. Copyright (c) 2014 WILEY-VCH Verlag GmbH.[8]

The two given examples show that indeed complex materials can evolve from an intelligent combination of weak interactions.

Depending on the system and the environment, the mechanism of the build-up of the assembly is different. The last part of this chapter will therefore focus on different mechanistic concepts of aggregation for supramolecular polymers. There are three reversible pathways known to form supramolecular polymers which are outlined in the following part and were described in the review paper of de Greef and coworkers:[16]

- isodesmic
- cooperative
- ring-chain

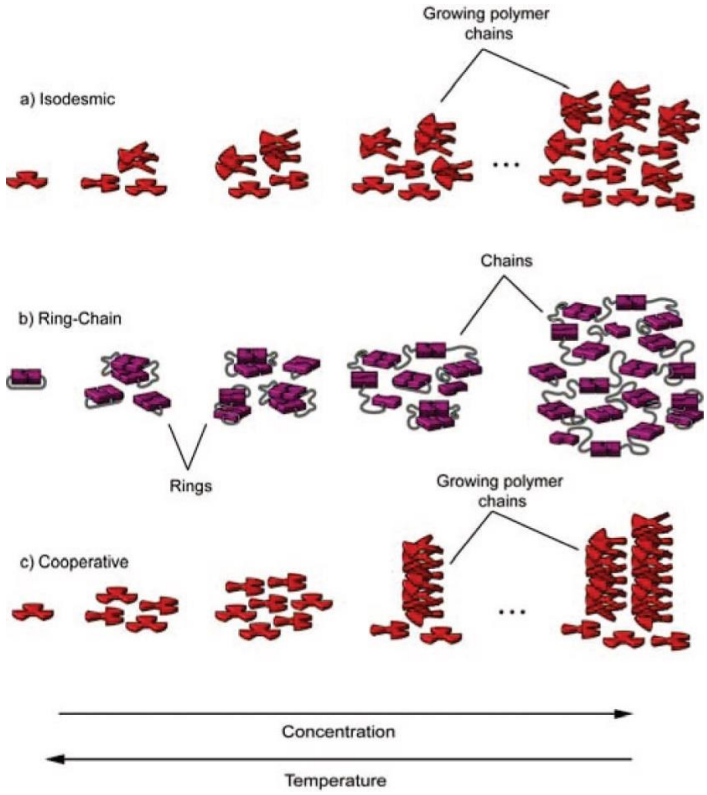

Figure 8: Different aggregation models. Reprinted with permission from T. F. A. De Greef, M. M. J. Smulders, M. Wolffs, A. P. H. J. Schenning, R. P. Sijbesma, E. W. Meijer, *Chem. Rev.* **2009**, *109*, 5687-5754. Copyright 2015 American Chemical Society.[16]

For an **isodesmic** aggregation mechanism each polymerization step is thermodynamically identical which means that also the binding constant for all polymerization steps is identical. In a chemical sense this leads to the conclusion that all end groups of the polymer are equally reactive. This furthermore leads to a constant decrease in free energy. Since all polymerization steps are identical, the mechanism is characterized by a broad distribution of polymer lengths that lead to high polydispersity. Also no critical temperature or concentration can be observed for an isodesmic polymerization mechanism. This kind of aggregation is typically reported for the group of perylene diimide dyes. The isodesmic aggregation process can be described by equation (1):

$$\alpha(c) = \frac{2Kc + 1 - \sqrt{4Kc + 1}}{2K^2c^2} \quad (1)$$

whereby α(c) is the degree of aggregation, K is the binding constant and c is the total concentration in the sample.

The **ring-chain** aggregation is a two step process. In the first step of assembly rings are formed which in a second step convert into linear aggregates. This means that both states exist in solution whereby the linear polymers are in equilibrium with their cyclic counterpart whereby two different binding constants can be distinguished: K_{intra} for the ring formation and K_{inter} for the chain formation. The mechanism is characterized by a critical concentration after which the polymerization occurs.

For a **cooperative** aggregation a polymerization nucleus is needed and the growth of the polymer occurs in two stages. Up to the formation of the nucleus the binding constant is smaller than afterwards which means that the binding constants of these two steps are different. In principle two versions of cooperative polymerization exist. For the cooperative nucleated supramolecular polymerization the nucleus is the energetically least favored species and therefore the bottleneck for a polymer formation. To form a polymer, an energetical barrier has to be overcome after nucleation. For the cooperative downhill supramolecular polymerization the nucleus is not energetically disfavored and less stable than the monomer. This simply means that the formation of the nucleus is slower than the actual polymer formation. Both versions are characterized by a critical concentration though. The cooperative aggregation can be described by equation (2)

$$\alpha(c) = \frac{2Kc + \sigma - \sqrt{4Kc + \sigma}}{2K^2c^2} \quad (2)$$

whereby σ is the degree of cooperativity, the proportion between the different binding constants. For the isodesmic aggregation, σ = 1 since all binding constants are equal.

While the ring-chain aggregation is unique due to the formation of a separate aggregate species, isodesmic and cooperative aggregation only differ in the binding constants of the system. To distinguish between isodesmic and cooperative aggregation, temperature dependent or concentration dependent UV/vis measurements can be utilized for analysis.[17] The aggregation of monomers leads to changes in UV/vis due to the interaction of these units. The decrease or increase of the extinction coefficient correlates with aggregation and allows conclusions concerning the aggregation mechanism.

Taking the definition of α(c) into account:

$$\alpha(c) = \frac{\varepsilon(c) - \varepsilon_a}{\varepsilon_m - \varepsilon_a} \tag{3}$$

whereby ε(c) denotes the extinction coefficient obtained from the spectra; ε_m and ε_a are the extinction coefficients for the monomeric and the aggregated species, a connection to the absorption spectra can be drawn from equation (4):

$$\varepsilon(c) = \frac{2Kc + \sigma - \sqrt{4Kc + \sigma}}{2K^2c^2}(\varepsilon_m - \varepsilon_a) + \varepsilon_a \tag{4}$$

Data point for the analysis of the aggregation mode is the extinction coefficient for the wavelength of themaximum absorption band. A concentration variation leads to a decrease or increase and therefore other values for the extinction coefficient. The extinction coefficient is then plotted as a function of the dimensionless concentration and then fitted by a nonlinear regression analysis according to equation (4).

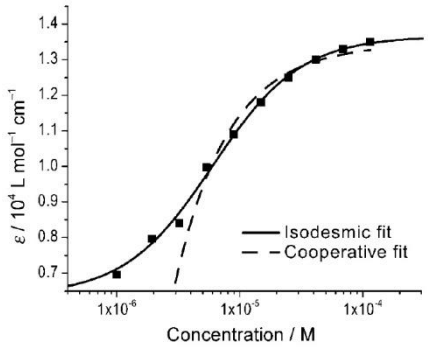

Figure 9: Example for an isodesmic and cooperative fit. M. M. J. Smulders, M. M. L. Nieuwenhuizen, T. F. A. de Greef, P. van der Schoot, A. P. H. J. Schenning, E. W. Meijer, *Chem. Eur. J.* **2010**, *16*, 362-367. Copyright (c) 2015 WILEY-VCH Verlag GmbH.[17]

In Figure 9, the isodesmic fit is represented by the black curve and the cooperative fit by the dashed curve. The data points in the example can be best fitted with the isodesmic fit which means that the supramolecular polymer formation also follows the isodesmic path. With this easy method it can be distinguished between both aggregation models.

This part of the chapter introduced the main concepts of supramolecular chemistry and outlined the main principles of the research field. The next part of this chapter will provide an insight into the important chemical units for this thesis.

2.2 Zwitterionic GCP binding motif

2.2.1 Basic research

As mentioned in the previous chapter, supramolecular chemistry is all about weak forces. The term describes the build-up of complex structures from small units by intermolecular interactions. It has been shown that tremendous changes in e.g. structure or physical state can occur upon assembly of supramolecular systems, nevertheless these weak interactions have some limitations in stability of the assembled systems. When looking at systems held together only by H-bonds as introduced previously, their stability is usually limited to unpolar solvents like chloroform.[8] In more polar protic solvents like methanol or water, the binding sites for the H-bonds are occupied by solvent molecules and the supramolecular assembly is weakened. There are several approaches to enable supramolecular assemblies even in polar protic solvents like water. Whereby other groups created completely new supramolecular binding motif, without using H-bonds as interaction in the final binding motif, Schmuck approached the topic by combining H-bonds with ionic interactions. [18]

The starting point for the development of this new binding motif was the interaction between guanidinium cations and carboxylates (**8**). Originally this interaction is found in the amino acid arginine, whereby the guanidinium part is known to bind anionic substrates and stabilize the tertiary structure of proteins through an interaction with carboxylate units.[19] Normally this interaction is relatively weak in polar protic solvents. If the guanidinium is isolated, no binding can be observed in water. Schmuck developed a possibility to improve the binding ability of guanidinium cations with additional interaction sites. [20] The acidic character of the of the guaninidinium is enhanced through an acylation which leads to a better binding of the carboxylate (e.g. **10**). For this purpose he chose to attach a pyrrole unit as well as another amide function to enhance the binding of the carboxylate with additional H-bonds even further.

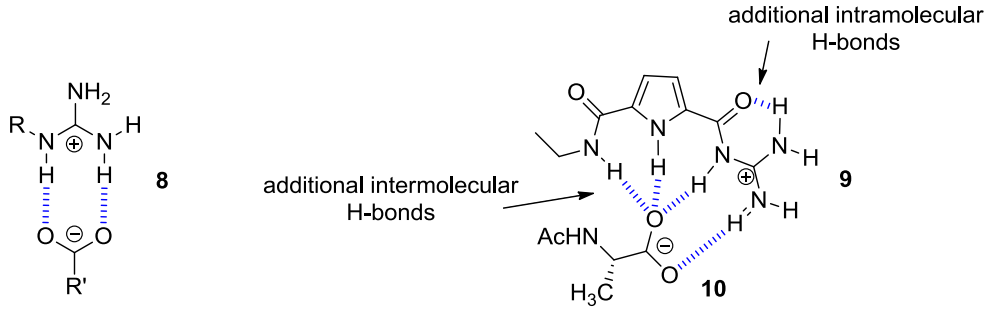

Figure 10: A general guanidinium cation - carboxylate interaction (**8**) is shown on the left, whereby the altered pyrrole guanidinium cation **9** is depicted on the right side.

The devised [5-(N-ethylcarbamoyl)-1Hpyrrol-2-ylcarbonyl]guanidinium cation **9** enables two additional intermolecular H-bonds which face towards the carboxylate and one intramolecular H-bond that forms between the carboxylic group and one guanidinium hydrogen at the back side of the molecule. NMR binding studies in 40% water in DMSO revealed a binding constant of K ≈ 2800 mol^{-1} for the pyrrole-guanidinium cation, whereby the parent N-actetyl guanidinium cation shows a binding constant of K ≈ 50 mol^{-1}. This states a significantly higher binding strength of the derivatized guanidinium for carboxylates in polar solvents.

On this basis the two interacting subunits - guanidinium cation and carboxylate - were combined in one molecule, to yield in a 5-(Guanidiniocarbonyl)-1*H*-pyrrole-2-carboxylate (GCP) zwitterion **11**. Thereby a zwitterionic binding unit was created which perfectly assembles into dimers in a self-complementary way. The synthesized molecule as well as a schematic representation of the proposed self-assembly are shown below.

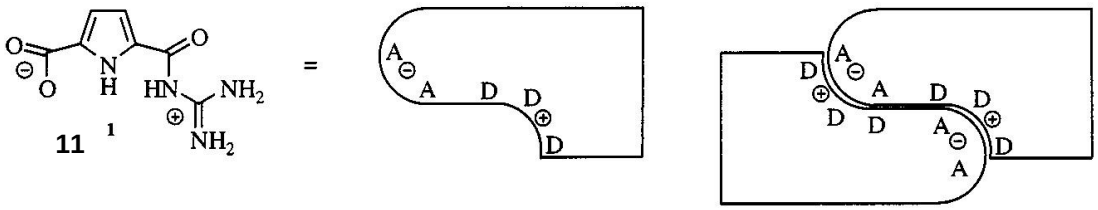

Figure 11: 5-(Guanidiniocarbonyl)-1*H*-pyrrole-2-carboxylate (**11**) as a rigid molecule with complementary hydrogen-bond donor (D) and acceptor (A) sites capable of dimer formation. C. Schmuck, *Eur. J. Org. Chem.* **1999**, 2397-2403. Copyright (c) 2014 European Journal of Organic Chemistry. [18]

The rigidity which is obtained by the pyrrole core hinders the carboxylic and guanidinium subunits from interacting intramolecularly. These GCP dimers are held together by eight H-bonds and two ionic interactions (see Figure 13), whereby six of the hydrogen bonds are build-up intermolecularly between the separate molecules and two H-bonds form intramolecularly in the same fashion as described above for the receptor molecule. MM studies reveal indeed the formation of discrete dimes for the zwitterionic GCP unit whereby the x-ray structure of the cationic GCP unit shows a planar dimer depicted in Figure 12.

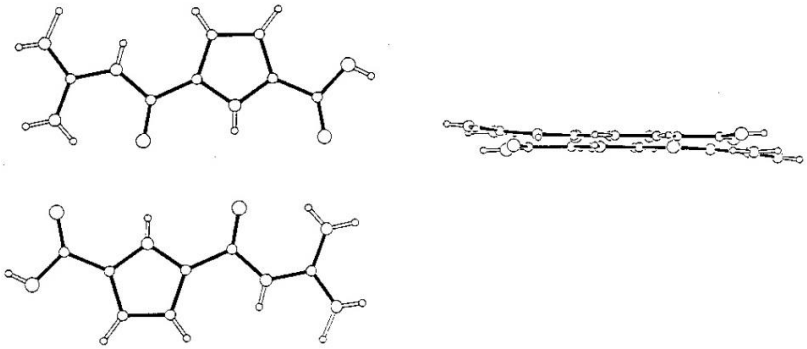

Figure 12: X-ray crystal structure of **molecule 11+** (chloride salt); top view (left), and side view (right) (chloride anions and water molecules have been omitted for the sake of clarity). The structure shows the formation of discrete dimers. C. Schmuck, *Eur. J. Org. Chem.* **1999**, 2397-2403. Copyright (c) 2014 European Journal of Organic Chemistry. [18]

The binding unit exhibits an extremely stable binding even in polar solutions. Because of the limited solubility in other solvents besides DMSO, the binding strength of the aggregate could only be estimated. Therefore several parts had to be taken into account and the sum of these assumptions lead to a binding strength of approx. 10^{12} M^{-1} in DMSO. Additional to the extremely high binding strength, the binding motif exhibits another unusual feature. Because of the ionic interactions, the dimeric aggregates can be reversibly switched on and off with acid and base. Upon addition of base, the guanidinium unit is deprotonated which switches off the ionic interaction. In the acidic case, the carboxylate is being protonated which also leads to a loss of the ionic interactions and therefore a deaggregation.

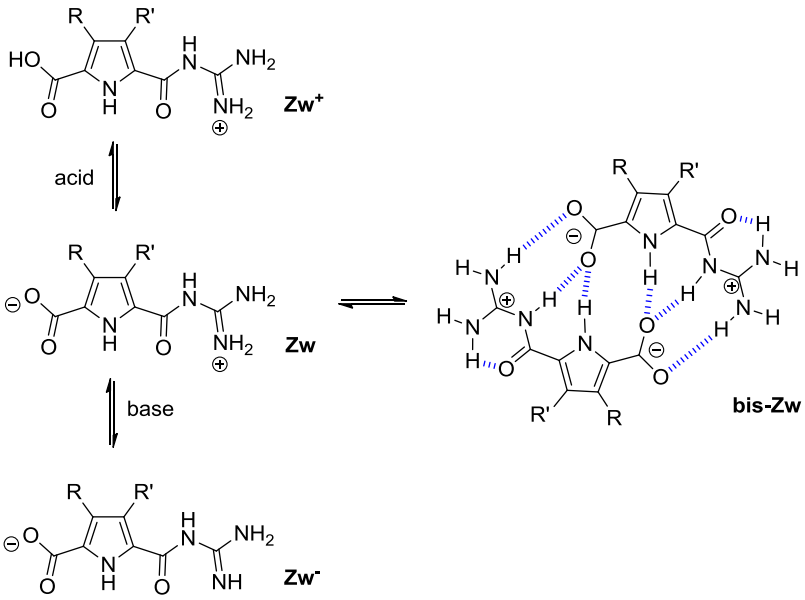

Figure 13: Molecule **11** = **Zw** with R = R' = H forms a stable dimer **bis-Zw** based on multiple hydrogen bonds as well as ionic interaction, whereby the protonated **Zw**$^{+}$ and the deprotonated **Zw**$^{-}$ version do not show this tendency to dimerize.

A few years later, Schmuck et al. reported a derivative (molecule **12**) of the zwitterionic binding motif which overcomes the limited solubility of the initial dimer.[21] They attached two triethylene glycole (TEG) chains at the pyrrole backbone to enhance the solubility in water.

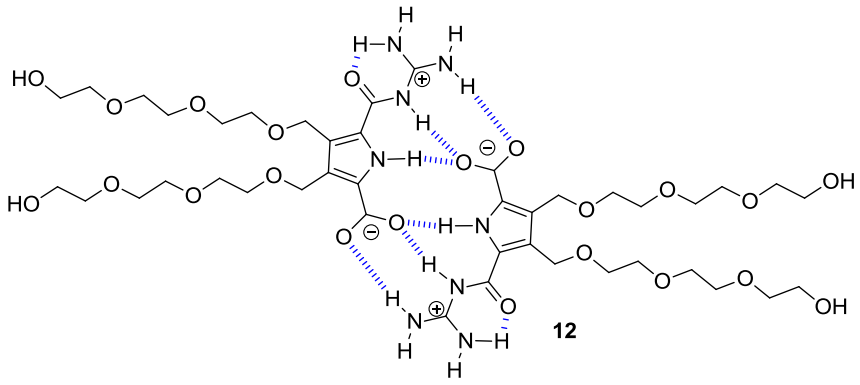

Figure 14: Ditriethylene glycol derivative of GCP **12** that forms disscrete dimers in aqueous medium.

With this functionalization of the GPC zwitterion, they could obtain water soluble assemblies. An ESI measurement revealed the existence of the dimeric form of the zwitterion at least in methanol. This was underlined by the NMR-spectrum, in which a set of 4 sharp signals as well as a significant downfield shift was observed.

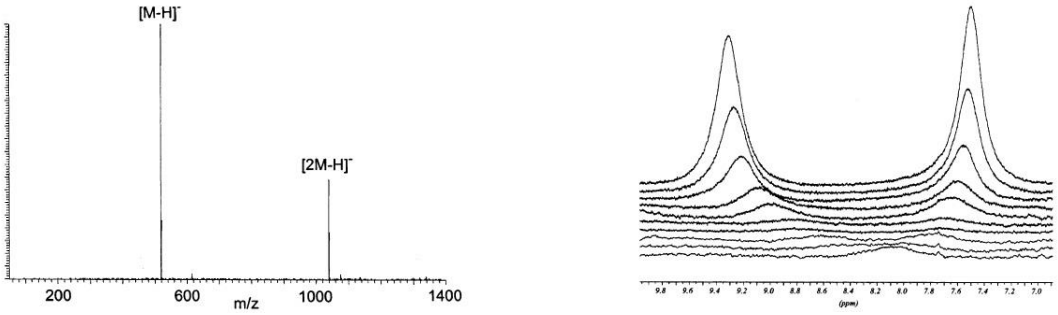

Figure 15: Left: ESI mass spectrum of compound **2** (*m*/*z* = 519 au) from a solution in methanol showing the formation of a discrete 1:1 dimer at *m*/*z* = 1039 au. Right: Part of the ^{1}H NMR spectrum of in 2.5% DMSO-d_6 in water showing the complexation-induced shift changes of the guanidinium NHs (concentrations from bottom to top: 1, 2, 3, 4, 5, 7, 12, 17, and 22 mM). Reprinted with permission from C. Schmuck, W. Wienand, *J. Am. Chem. Soc.* **2003**, *125*, 452-459. Copyright 2014 American Chemical Society.

The binding constant of the dimer was determined with concentration dependent NMR studies. Since an initial NMR measurement in pure water did not show any signals for the -NH protons, mixtures of water and DMSO were chosen to obtain the binding constant. When the binding constants of the measurements in 2.5%, 5% and 10% DMSO content are compared, all give the same binding constant. Therefore it is safe to assume, that the binding constant in pure water is the same. These

measurements revealed a dimerization constant of K = 170 M^{-1}, which is surprisingly high for an assembly which is solely based on weak interactions.

These two examples underline the principle features of the introduced binding motif. The motif is stable in polar solutions and upon addition of acid or base a loss in aggregation was observed. To follow the path that Jean Marie Lehn outlined in his book, the creation of complex assemblies is the logical next step for a binding motif.

2.2.2 Supramolecular Assemblies

In the last 10 years, the development of the GCP unit toward complex systems has taken place. To investigate what kind of larger aggregates could be formed based on the GCP binding motif different approaches were reported:

- Attachment of additional functionalities at the side chain of the GCP
- Connecting two GCP units with a linker

Fenske et al. reported a set of GCP derivatives which form assemblies through an additional π-π-stacking of the GPC dimers. [22] This was accomplished by attaching an alkyl amine to the residual carboxylic acid of the GCP backbone to give an amide functionality which can form intermolecular H-bonds.

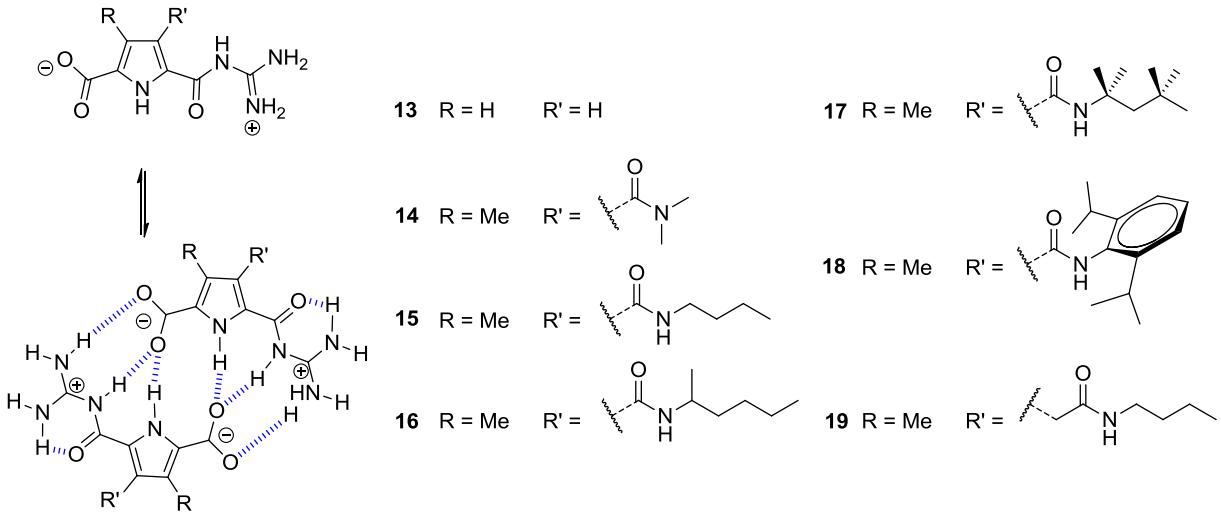

Figure 16: Molecular structures of the reported molecules. [22]

AFM, SEM and TEM measurements show the formation of one dimensional aggregates. Where the AFM and SEM images do not provide any more detail, TEM pictures of the molecules with the amide

functionality (**15** and **16**) show bigger bundles which are comprised of several smaller fibers whereby the minimum width of one fiber is about 1.7 nm. The analogue without the amide functionality did not show any microscopically observable assembly. This comparison shows that the amide is indeed essential for the assembly into larger aggregates. The structure found to be the energetically favorable one in molecular mechanic calculations has the same linear conformation as the ones in the microscopic images. A deeper look into the calculated assembly reveals a slightly bended structure of the zwitterionic dimers and the ability of the presented molecules to stack onto each other.

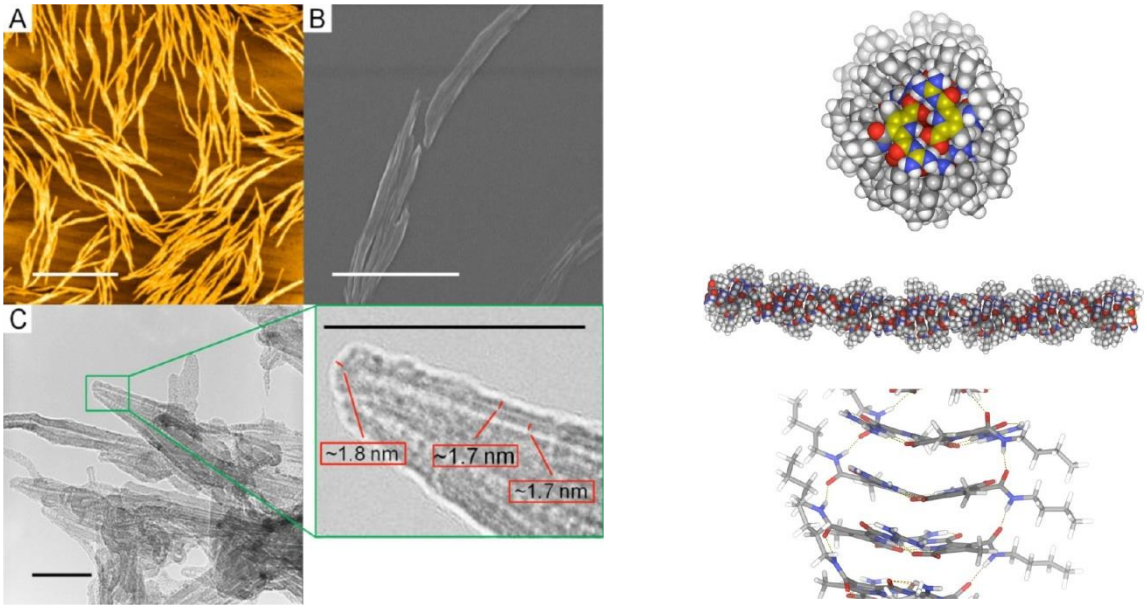

Figure 17: Left: AFM- (A), SEM- (B), and TEM-images (C) of 1.0 mM solutions (DMSO) of zwitterions **15** (A, B) and **16** (C) Right: Calculated structure of a one-dimensional rod obtained from the stacking of discoid dimers. Reprinted with permission from M. T. Fenske, W. Meyer-Zaika, H.-G. Korth, H. Vieker, A. Turchanin, C. Schmuck, *J. Am. Chem. Soc.* **2013**, *135*, 8342-8349. Copyright 2014 American Chemical Society. [22]

Since concentration dependent UV/vis measurements can give detailed insight into the aggregation mechanism, a concentration dependent measurement of **15** from 0.11 mM to 18 nM was made. With decreasing concentration, a bathochromic shift of about 20 nm is observed. A bathochromic shift occurred due to electronic changes during the deaggregation of the larger assembly. When plotting the degree of the aggregation against the dimensionless concentration, a cooperative aggregation mechanism was found.

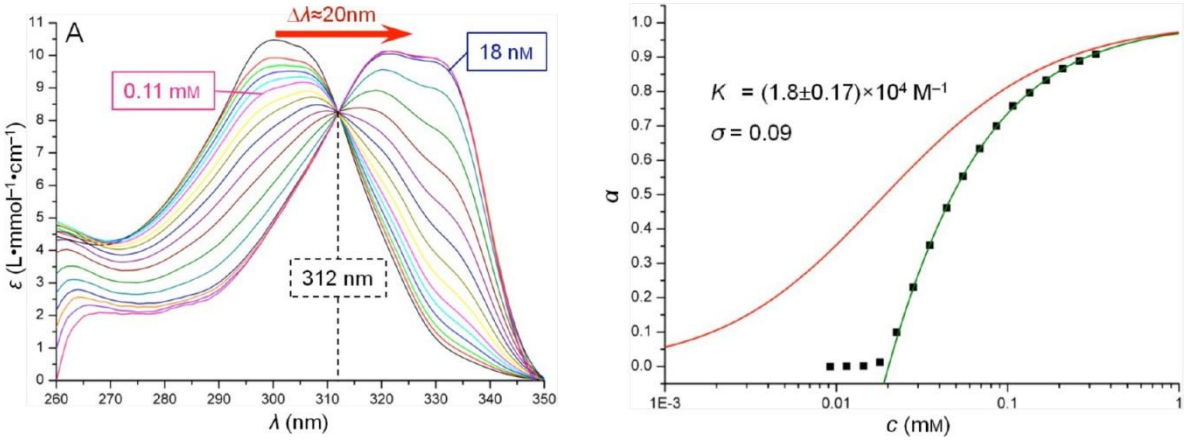

Figure 18: Left: Concentration dependent UV/vis absorption spectra of **15** (0.33 mM to 9 nM in DMSO). Arrow indicates the direction of change with decreasing concentration. Right: Plotting the degree of aggregation α of **15** against the concentration (black squares). Cooperative aggregation mode (green), isodesmic growth model (red). Reprinted with permission from M. T. Fenske, W. Meyer-Zaika, H.-G. Korth, H. Vieker, A. Turchanin, C. Schmuck, *J. Am. Chem. Soc.* **2013**, *135*, 8342-8349. Copyright 2014 American Chemical Society. [22]

As reported earlier, the zwitterionic dimer is prone to protonation and therefore the switching ability of the assembly was investigated. While the addition of base only resulted in precipitation, the assembly could successfully be altered by the addition of acid. In the case of **15** , a change of rod like structures into vesicles occurred. The initial assembly could be obtained again by the addition of base, which represents a reversible switching of the supramolecular aggregate. This example shows, that one dimensional aggregates can be formed based on the zwitterionic binding motif.

That it is also possible to form aggregates which elongate in more than one dimension with the GCP binding motif was shown by Schmuck et al. in 2006. They reported the investigation of a GCP derivative, in which two pyrrole subunits were connected by a flexible linker (**20**).[23] The GCP precursor was functionalized with an unpolar alkyl chain at the guanidinium side. Subsequently two of these derivatized GCP precursor units were linked by coupling of the acid ester with a short diamine linker. This resulted in an amphiphilic molecule with an unpolar core, two amide functionalities in the middle and the ditopic attacgment of two zwitterionic GCP units at the sides.

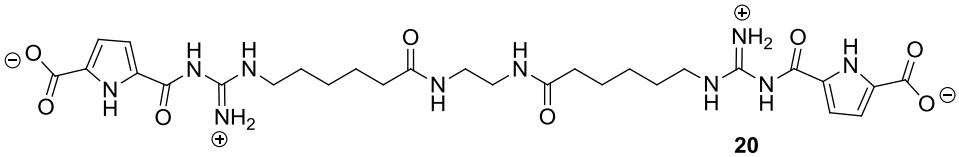

20

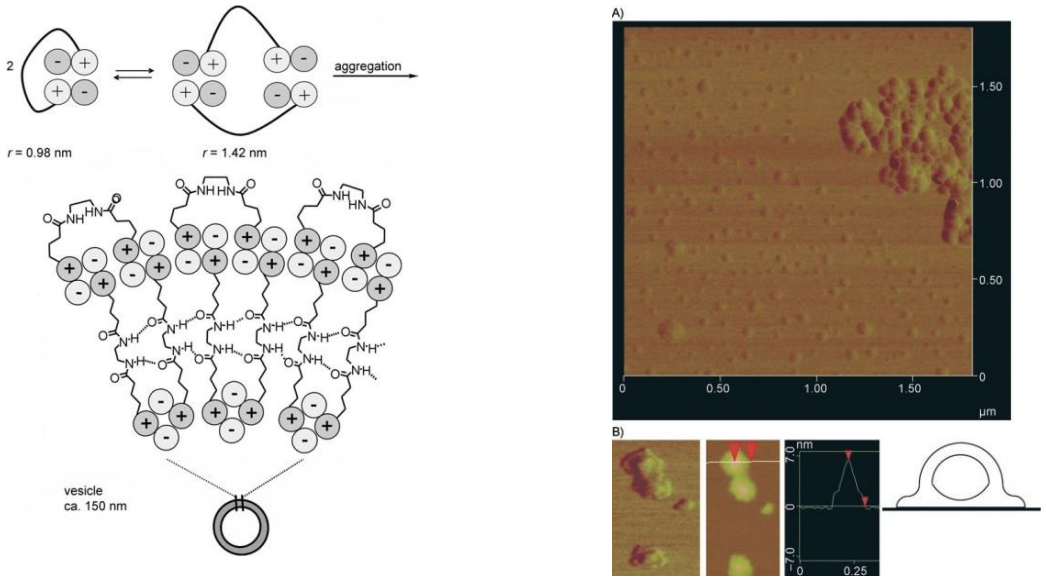

Figure 19: Previous page: Molecular structure of the amphiphilic zwitterion dimer **20**. This page left: Schematic drawing of the assembly of the molecule. Right: AFM pictures. A) Overview picture with vesicles and larger particles. B) Detailed images of the vesicles, from left to right: Phase image, height image, contour plot, schematic drawing of the vesicle on the surface. C. Schmuck, T. Rehm, K. Klein, F. Gröhn, *Angew. Chem. Int. Ed.* **2007**, *46*, 1693-1697. Copyright (c) 2014 Angewandte Chemie International Edition [24]

In a more detailed investigation in 2007, AFM studies of the bis-zwitterionic molecule **20** showed that the supramolecular aggregation lead to spherical assemblies.[24] While the AFM height image only reveals the formation of spherical particles, the contour plot confirms the formation of a vesicular assembly. Thereby the existence of two shoulders beneath the main curve depicts the presence of a vesicle, which is attributed to a flattening of the vesicle on the surface. To get additional insight in the dimension of the aggregate, dynamic light scattering (DLS) measurements were performed. While AFM measurements only provide information of the assembly that forms on the surface, these measurements give account about the assembly in solution.

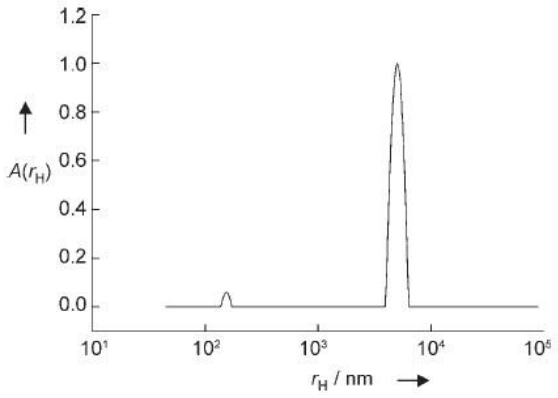

Figure 20: DLS measurement of of the amphiphilic zwitterion dimer **20**. C. Schmuck, T. Rehm, K. Klein, F. Gröhn, *Angew. Chem. Int. Ed.* **2007**, *46*, 1693-1697. Copyright (c) 2014 Angewandte Chemie International Edition [24]

The number weighted distribution shows an overall size of approximately 150 nm for the aggregates which is in good accordance with the AFM height curves which showed a width of 140 nm. Based on Small angle neutron scattering (SANS) measurements which give insight into the vesicle wall thickness, Schmuck et al. explained the vesicle structure by the formation of a monolayer of the amphiphilic molecule. Thereby two molecules create a dimer through the interactions of the zwitterions which folds through intermolecular H-bonds of the amides of the two molecules and therefore build up the vesicle layer. Additional monomers interact with this monolayer inducing the curvature in the particle which then leads to vesicle formation.

These examples demonstrate that the binding motif can be utilized to form complex self-assembled systems. The assemblies themselves are not limited to one dimension, but also form aggregates which are more dimensional. Additionally these assemblies can be reversibly switched on and off by addition of acid and/or base.

2.2.3 Smart Materials

With the successful formation of complex aggregates which are based upon the dimer formation of the GPC zwitterion, the question arises if also functional materials can be created with this binding motif. Hisamatsu et al. recently reported a quadruple zwitterion which forms a reversibly switchable supramolecular gel.[12] Therefore they took the next step of complexity and crossed the threshold between basic research and the development of smart materials. The described molecule **21** is comprised of four GCP subunits which were connected to a tetrahedral pentaerythriol core by click chemistry.

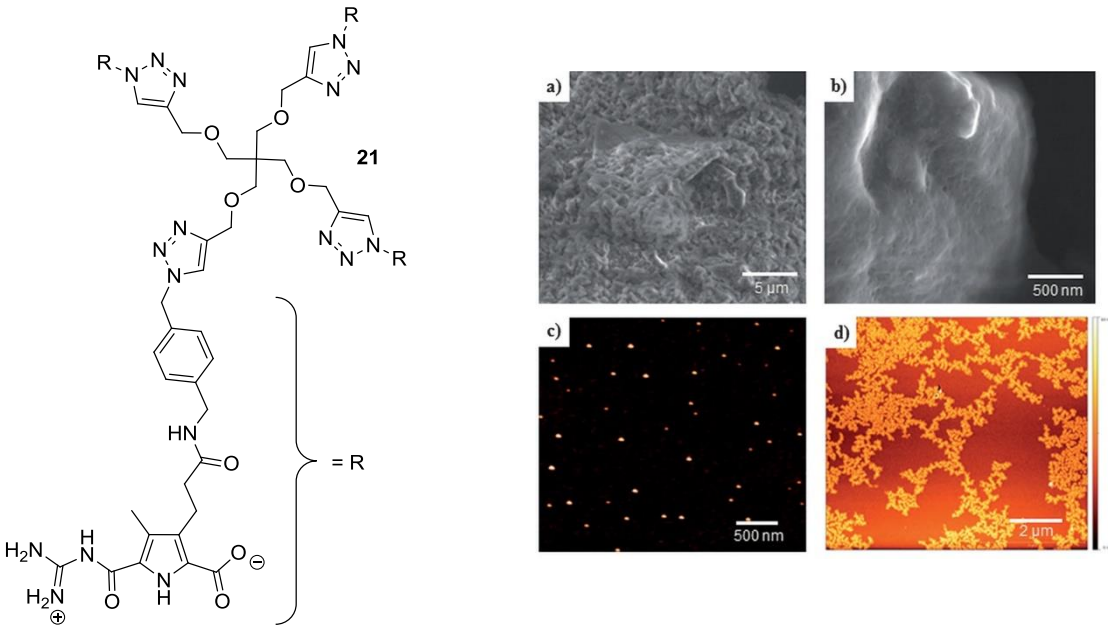

Figure 21: Left: Molecular structure of the quadruple zwitterion **21**. Right: Microscopic examination of different states of the molecule. a)+b) FESEM images of the gel at 50 mM. c) AFM height image at 0.1 mM. d) AFM height image at 5 mM. Y. Hisamatsu, S. Banerjee, M. B. Avinash, T. Govindaraju, C. Schmuck, *Angew. Chem. Int. Ed.* **2013**, *52*, 12550-12554. Copyright (c) 2014 Angewandte Chemie International Edition.[12]

The reported gel could be obtained at a concentration 50 mM in DMSO. To take a closer look into the morphology, the gel was examined by FESEM. The images show densely entangled polymeric strands. AFM measurements reveal polymeric structures even at lower concentrations of 5 mM. If the concentration is lowered even further to 0.1 mM, vesicular particles can be observed.

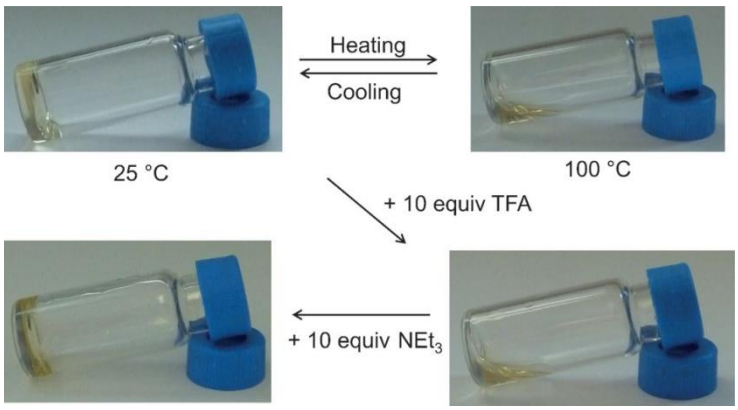

Figure 22: Reversible gel-sol transitions upon heating/cooling and by the addition of acid and base at 50mM. Y. Hisamatsu, S. Banerjee, M. B. Avinash, T. Govindaraju, C. Schmuck, *Angew. Chem. Int. Ed.* **2013**, *52*, 12550-12554. Copyright (c) 2014 Angewandte Chemie International Edition. [12]

Not only the formation of the gel is quite spectacular, but also the reversible switching ability with acid, base or temperature. The switching causes a change in the physical state from gel to sol which can be monitored with AFM as well as DLS measurements. The addition of acid results in the formation of

vesicular assemblies, which can be observed in the AFM images. After the addition of the respective amount of base, the polymeric assembly is restored. The same behavior can be seen in DLS measurements when the initial 16 nm sized particles are converted into aggregates which are only 3 nm in size after the addition of acid. Upon addition of the respective amount of base the initially present larger aggregates of 15 nm size are re-assembled again.

This poses an outstanding example of straightforward research and intelligent combination of supramolecular interactions. Here the question arises, if there might be an additional step in complexity which can be taken. By combining the zwitterionic GPC with a functional unit that brings special features itself, interesting complex systems could be created. This might be a functional unit that for example shows fluorescence, is prone to reduction or oxidation or can be switched in other ways than the zwitterionic GCP.

Fenske presented an example of such combination between GCP zwitterion and functional unit in his dissertation.[25] He created a ditopic GCP molecule with an azobenzene core motif whereby the zwitterions were attached symmetrically at both sides of the azobenzene. This unit was chosen because of its aromaticity and its specific size to check if also other units can stack onto a zwitterionic dimer and not mainly due to its functionality. The azobenzene molecule has two isomeric states - cis and trans - which can be reversibly interconverted by light of a specific wavelength. The aggregation behavior of the two states was investigated in detail with AFM. The trans-version of the molecule assembles into bimolecular layers while the cis-version which was created by irradiation with a wavelength of 366 nm shows vesicles in the microscopical measurements. He thereby showed that the type of assembly can be altered due to external stimuli other than the manipulation of the zwitterion with acid or base. Depending on the functional unit, very interesting systems could evolve through an intelligent combination with the zwitterionic GCP unit. The next chapter will highlight a functional dye which is one of the most feasible functional units and forms the other pillar of this thesis.

2.3 Perylene diimides

2.3.1 Introduction

This chapter introduces the functional dye used in this thesis. The following examples do not claim to be a comprehensive overview of the diverse field of perylene diimides, but will give a selection of significant and important insights into the potential of this chromophore. The general overview given in this thesis is based on two review papers which give an extremely eclectic insight into the versatility of perylene diimides. [26, 27]

Originally, perylenes were used as pigments since the early ninetieth century. Their insolubility and stability made them a perfect fit for high grade industrial applications as fiber coloring or in industrial paints as in automotive coating. Their excellent performance and the wide color range thereby easily outweighed their relatively high cost compared to inorganic colorants. Whereas the insolubility of the pigments made them a high performance material, a completely new field of application opened up, when the first soluble PDI was synthesized in 1959.[28] In the following years, it was discovered that the soluble PDI dyes were not only extremely photostable but also highly fluorescent. As their insoluble relatives they are also very stable and additionally found to be electron deficient and reversibly reducible. Their favorable optical and chemical properties as well as their semiconductivity made them suitable candidates for several optical and electronic applications especially with focus on absorbing light, emitting light or transferring electrons. Although it would be quite interesting to explore the novel utilization of PDI dyes, this thesis will focus on the outstanding supramolecular properties and the versatility of this dye group.

2.3.2 Synthesis

Perylene diimides are polycyclic aromatic ring systems with imide substituent at both sides based on perylene tetracarboxylic acid bisanhydride (PTDCA). The acidic anhydride derivative of perylene is the most important precursor for the synthesis of perylene diimides. In the PDI molecule there are different positions which can be addressed for functionalization. These can be divided into the imide position and the so called bay or core position. While the imide position is only accessible for derivatization with amines, the bay position can variously be functionalized.

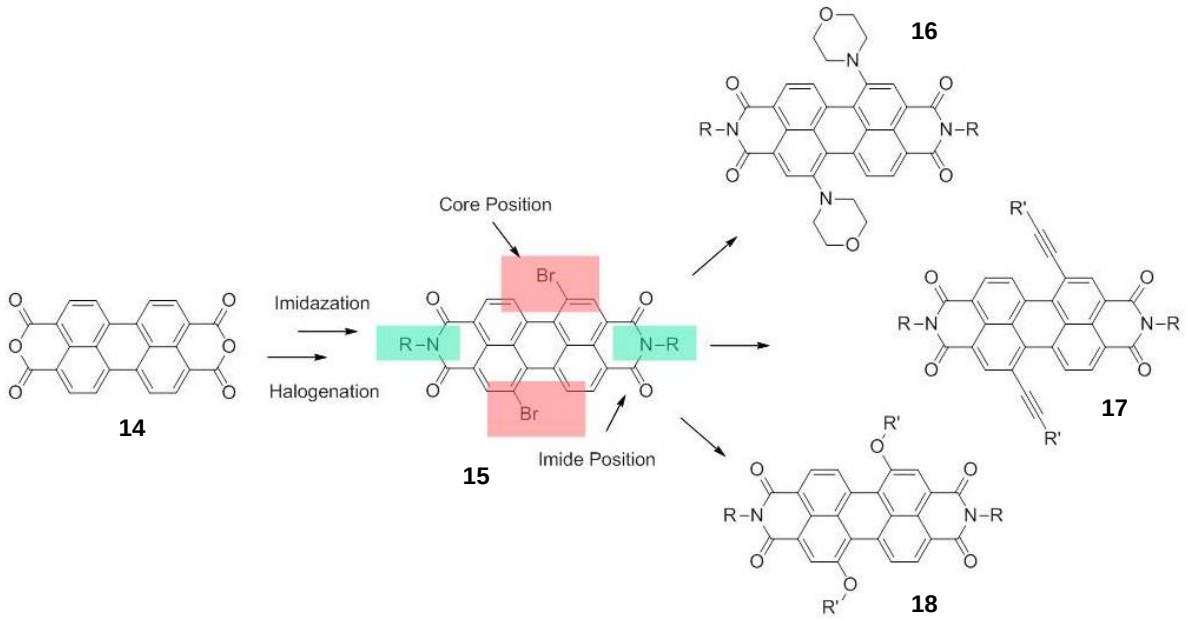

Figure 23: Possible synthetic routes to functionalize the perylene diimide at the core position. The so called core position is marked in red, while the imide position is marked in green.

In the scheme above the most frequently used synthetic routes to functionalize a perylene at the bay position are shown. While this scheme depicts the twofold derivatization of the perylene core these reactions are likewise used for a fourfold functionalization of the perylene. The main reaction types possible at the bay position are listed below:

- electrophilic substitution to introduce chlorine or bromine at the core to make this position available for other reactions (e.g. **14** → **15**)
- nucleophilic substitution whereby the halogen is substituted with an O, S or N containing moiety (e.g. **15** → **16, 15** → **18**)
- catalytic reactions are used to introduce alkines at the bay (e.g. **15** → **17**)

Based on PTCDA different approaches can be chosen to attach substituents to the perylene anhydride. Thereby it is possible to first introduce a group at the imide position followed by a further functionalization with a halogen at the core position or to do it the other way around. The halogen at the core position it is then the starting point for further reactions at this position. This vast synthetic accessibility is also a favorable feature of perylene diimides.

2.3.3 Optical properties

As mentioned in the introduction, PDIs show outstanding absorption and fluorescence properties. PDI **19** shown in Figure 24 for example has an absorption maximum at 526 nm and a fluorescence maximum at 533 nm with a quantum yield of nearly 100%.[27] The spectra themselves are strong vibronically structured, which can be attributed to the planar constitution of the aromatic core of the dye.

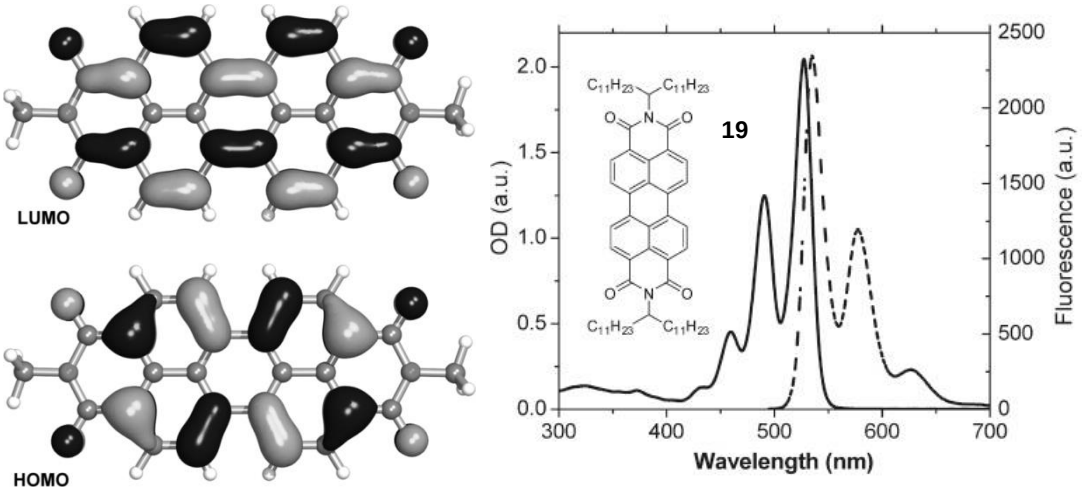

Figure 24: Left: Frontier orbitals of N,N'-dimethyl PDI, according to DFT calculations. Right: UV/vis absorption (solid line) and emission (dashed line) spectra of **19** in toluene. C. Huang, S. Barlow, S. R. Marder, *J. Org. Chem.* **2011**, *76*, 2386-2407. Copyright 2014 American Chemical Society.[26]

Looking at the HOMO and LUMO of a simple PDI obtained by DFT-calculations, the nitrogen atoms are located on the nodal planes of the molecular orbital. Therefore the HOMO-LUMO excitation can be regarded as $S_0 \rightarrow S_1$ transition where the optical transition is polarized along the molecular N-N axis (x-axis), which provokes that the imide substituent has no influence on the optical properties of the PDI dye. In contrast to the functionalization at the imide position, a substitution at the bay position has quite a large impact on the optical and constitutional properties of a PDI. When a PDI is substituted at the bay position, the aromatic system is distorted into a twisted version of the perylene core and which affects the molecular orbitals. The large influence of the substituents induces mainly a bathochromic shift of the absorption and a loss of the vibronic structure through a stabilization of the LUMO or the destabilization of the HOMO. A second absorption band evolves at lower wavelengths which is attributed to the electronic $S_0 \rightarrow S_2$ transition with a transition dipole moment perpendicular to the molecular N-N axis.

The shift of the absorption is proportional to the π-donor strength of the substituent. In the case of halogen or oxygen at the core position only a weak bathochromic shift is observed, due to the weak

respective medium donor strength of the substituent. When being substituted with a strong π-donor like nitrogen, a strong bathochromic shift is visible in the absorption spectrum, caused by a quadrupolar charge transfer from the nitrogen to the perylene. The substitution with a carbon through a catalytic coupling leads to an enlargement of the conjugated π-system and the change in absorption is depending on the nature of the substituent bound to the carbon. [26]

2.3.4 Supramolecular PDI assemblies

This chapter will now describe the supramolecular behavior of the PDI dye. As mentioned above, the PDI without any substitution at the bay position, has a large planar aromatic core. Therefore it tends to form aggregates by π-π-stacking, whereby the principle π-π-interaction has been described in detail in the previous part of this chapter. When looking at the arrangement of a simple PDI in solid, a parallel stacking is observed. The two dye units in this example have a distance of 3.34 - 3.55 Angström and are slightly offset.[27]

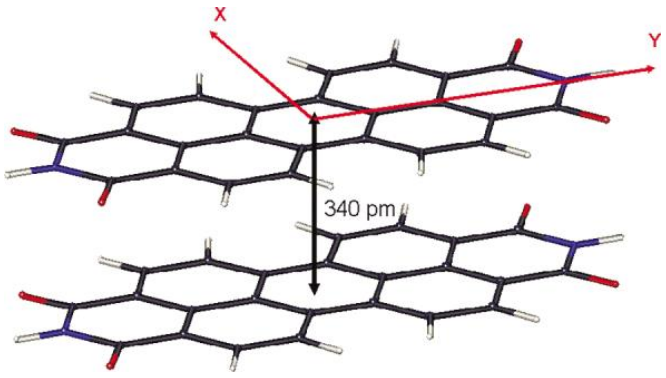

Figure 25: Exemplary π–π-stacking of a simple perylene diimide in the solid state, involving longitudinal and transverse offsets. Reproduced from F. Würthner, *Chem, Commun.* **2004** , 1564-1579 with permission of The Royal Society of Chemistry.[27]

It is possible to arrange two dyes in different positions, therefore one can differentiate between H- and J-aggregates in the description of perylene diimide π-π-assemblies. These terms describe the correlation between morphology and photophysical properties of the assembly and were first ascribed by Jelley[29] and Scheibe[30] (J) as well as West and Carroll[31] (H).

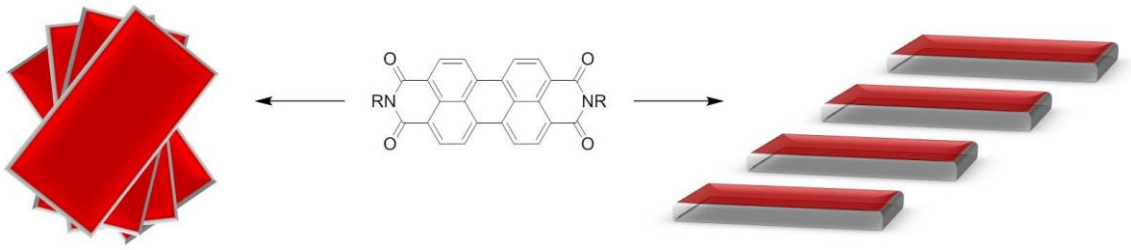

Figure 26: Schematic representation of H- (left) or J-type (right) aggregation.

J-aggregates are characterized by a head to tail arrangement of the assembled dyes with a longitudinal displacement. Due to a negative exitonic coupling between the aggregated units upon excitation compared to the excitation of a not aggregated molecule, the allowed optical transition is $S_0 \rightarrow S_1$. This leads to a red shift of the maximum absorption band with respect to the monomer which is also called bathochromic shift. The H-aggregate on the other hand describes a parallel or side by side orientation of the stacked molecules whereby the units do not exactly overlap but show a rotational displacement to minimize the π-π-repulsion. This type exhibits a blue (hypsochromic) shift in the absorption upon excitation which is caused by a positive excitonic coupling that leads to a $S_0 \rightarrow S_2$ transition. The following scheme depicts the allowed transitions upon excitation depending on the aggregation type.

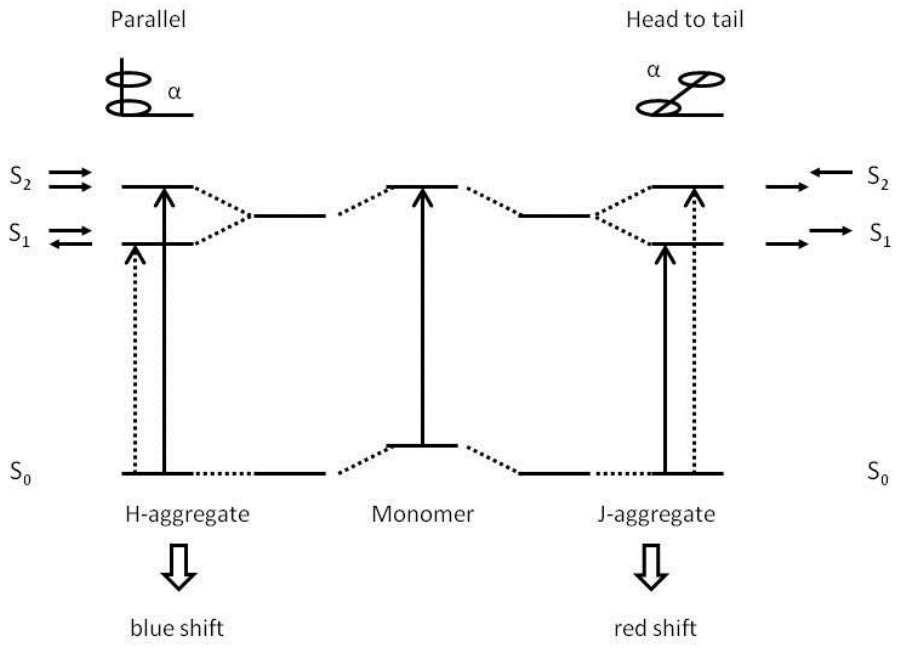

Figure 27: Schematic representation of the possible excitation pathways for J- and H-aggregates of perylene diimides. Adapted from a presentation of T. Pradeep, Professor at DST Unit of Nanoscience, Indian Institute of Technology Madras. [32]

Through this correlation between morphology and photophysical properties of the assembly, the aggregation process can be monitored with UV/vis spectroscopy. Thereby the assembly type is clearly distinguished by the shift of the spectrum.

These two aggregation types form the basis of supramolecular PDI chemistry, but the further assembly is far more complex. The supramolecular structures formed by the interaction of perylene diimides are extremely manifold and far too many to list them here. Therefore only the principle aggregation behavior shall be categorized in this thesis.

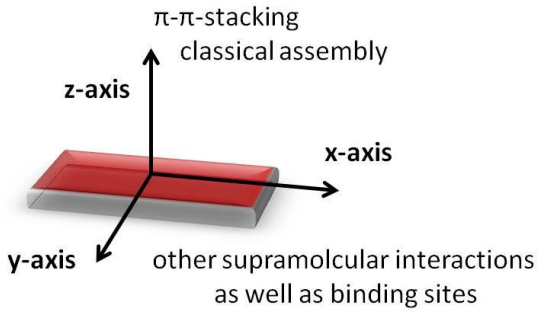

Figure 28: Supramolecular binding axes of a perylene diimide.

In principle there are three possible ways for a perylene diimide to form assemblies; along the imide position (x-axis), along the core position (y-axis) und perpendicular to the π-system (z-axis). The prevailing type of aggregation is along the z-axis through π-π-stacking, what represents the classical PDI assembly. An assembly along the x-axis is possible when a supramolecular binding site is attached at the imide position. For a binding along the y-axis also another weak interaction is needed at the core position, but these assemblies are extremely rare. Even though a main interaction is responsible for an elongation along a certain axes, no assembly form is prerequisited by the binding axis. The principle supramolecular chemistry of PDIs can therefore be divided in two main classes

- without binding motif, based on π-π-stacking, assembly perpendicular to the PDI axis which can nonetheless be accompanied also by influence of other supramolecular interactions
- with binding motif, based on other interactions with additional π-π-stacking, assembly along PDI axis as well as perpendicular

The following parts of this chapter therefore will give a few significant examples to outline the PDI aggregation behavior. This thesis will also outline the PDI assembly in water.

2.3.4.1 Assemblies without additional binding motif

As mentioned above, the PDI aggregation without binding motif is mainly driven by π-π-interaction. One of the first π-π-stacks of a PDI dye in solution was reported by Ford in 1986. [33] He synthesized a dianionic PDI which showed a bathochromic shift in the absorption upon increasing concentration. For these concentration dependent changes he stated a dimerization of the perylene diimide which nowadays would be designated as aggregation into J-type assemblies.

Since this first reported π-π-stack of PDIs in solution, a lot of detailed investigations of perylene assemblies were made. A deeper look into the aggregation behavior provides the investigation of Würthner et al. with five structurally different dyes.[34] They differ in core substitution, whereas one dye is not substituted at the bay position, one dye has phenoxy substituents at the 1 and 7 position of the PDI and the three other dyes are fourfold bay substituted with varying phenoxy side groups. Even though more dyes were presented in the publication, only two significant ones are shown below.

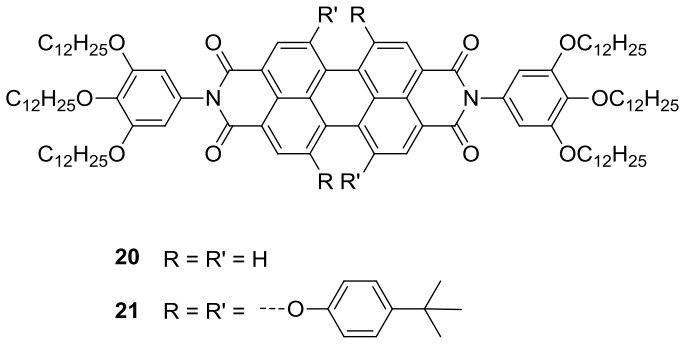

Figure 29: Two representative dyes of Würther et al. whereby molecule **20** is not substituted at the bay position and molecule **21** is fourfold bay substituted with a phenoxy side group.[34]

The UV/vis spectra of the compounds represent all characteristics of PDI dyes bearing zero, two or four substituents at the bay position as mentioned in the previous part of this chapter. The absorption maximum shows a bathochromic shift with increasing number of substituents as well as a loss in the vibronic structure accompanied by a broadening of the peaks.

To investigate the aggregation behavior, concentration dependent UV/vis measurements were presented. A remarkable change in all UV/vis spectra can be observed, which correlates well with the dye assembly. In the case of the planar PDI **20**, the vibronic fine structure is almost completely lost at higher concentrations, which can be attributed to a strong π-π-interaction of the large aromatic systems. However, in the case of the fourfold substituted perylene **21**, a less significant change in the vibronic structure can be observed at higher concentrations. The individual shift of the spectra also

differed, while the unsubstitued PDI **20** showed a hypsochromic shift, a bathochromic shift was observed for the fourfold perylene diimide **21**.

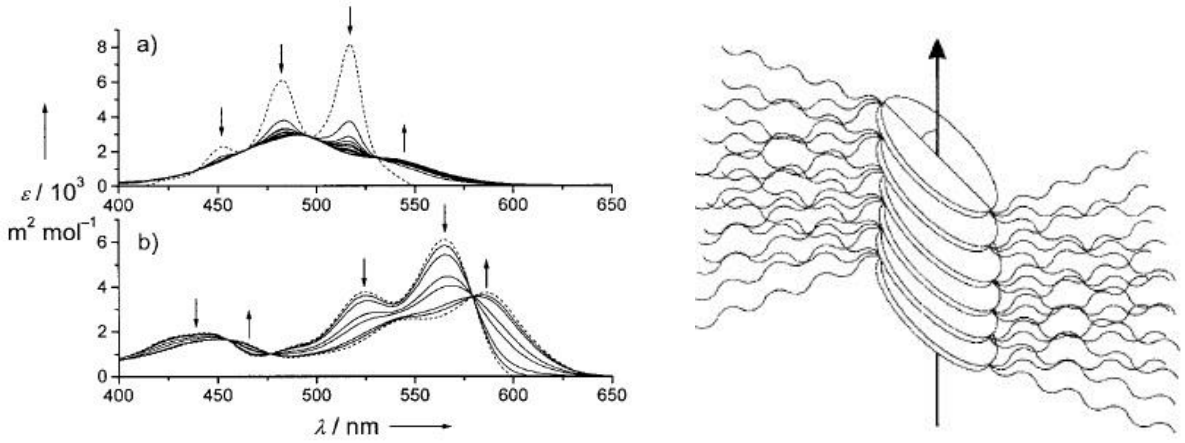

Figure 30: Left: Concentration-dependent UV/Vis absorption spectra in methylcyclohexane (MCH) for a) **20** (concentration range 10^{-7}-10^{-5} M) and b) **21** (concentration range $5x10^{-7}$-10^{-4} M). Arrows indicate the direction of change with increasing concentration. Dotted lines represent spectra for the free and the aggregated chromophore calculated from the respective data set. Roght: Model of the arrangement in the columnar mesophase, based on electrostatic interactions between the perylene diimide chromophores and steric demand of the substituents in the bay positions which lead to a longitudinal offset. F. Würthner, C. Thalacker, S. Diele, C. Tschierske, *Chem. Eur. J.* **2001**, *7*, 2245–2253. Copyright (c) 2014 WILEY-VCH Verlag GmbH.[34]

The concentration range in which the aggregation from monomer to π-π-stacked assemblies occurs, differs quite significantly for the three different kinds of substituted PDIs. The concentration at which the dimerization and the further assembly takes place correlates with the sterical hinderance at the core position. The strongest aggregation was therefore observed with the unsubstituted perylene. The aggregation is also dependent on the twisting of the PDI, which means that a twisted perylene does not stack as good as a less twisted one, whereby the twisting is logically also connected to the sterical demand of the substitutes. This also leads to a larger distance of the π-π-systems for the fourfold perylene diimide. The schematic model of the aggregation shows a longitudinal offset which corresponds with the J-type stacking for the substituted perylene diimides. For the unsubstituted perylene diimide, a rotational offset is stated, which was not termed H-type aggregate though. Around the π-π-stacks an interlacing of the surrounding alkyl chains can be observed that leads to a shielding of the PDI core.

To investigate the influence of the bulkiness of the side chain at the imide position on the aggregation behavior of the PDI dye, Würthner et al. introduced a series of perylene diimides with different alkyl chains at the imide.[35] To enhance the π-π-stacking behavior, amide functions were attached within the

substituents, so that intermolecular H-bonds could stabilize the dimeric PDI assembly compared to the monomeric dye.

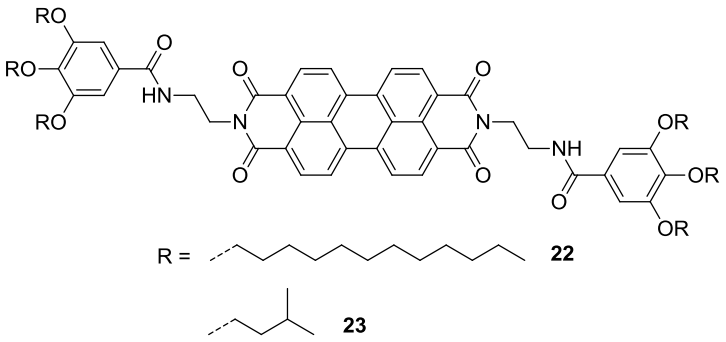

Figure 31: Two exemplary perylene diimides of Würther et al. with different alkyl chains at the imide position.[35]

To take a deeper look into the aggregation behavior, concentration and solvent dependent UV/vis studies were performed. The self assembly of **22** indeed occurred at highly diluted solutions, which indicates a significant influence of the amide function in the side chain. The solvent dependent measurements reveal a hypsochromic shift upon decrease of the solvent polarity, which is normally linked to the formation of an H-aggregate. Looking at dye **23**, a completely different shift is observed. The increase of the methylcyclohexane (MCH) content leads to a strong bathochromic shift which indicates the formation of a J-aggregate.

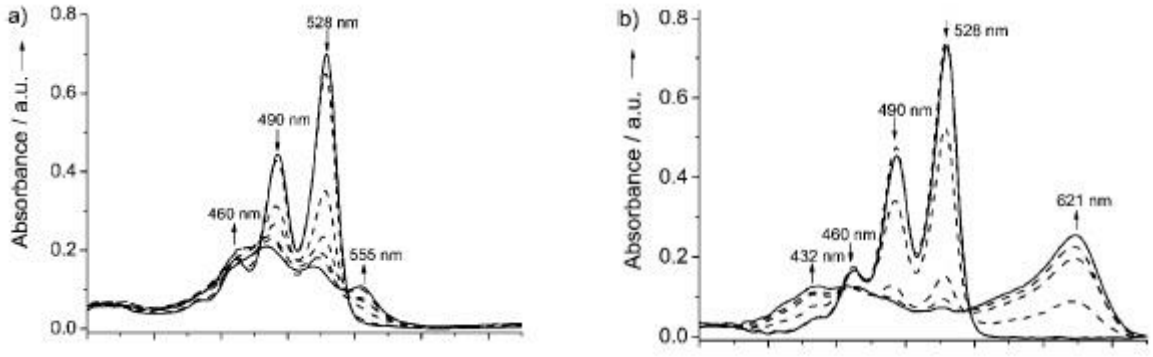

Figure 32: Solvent-dependent (in various MCH/DCM (dichloromethane) mixtures) UV-visible absorption spectra of left: **22** (50:50 to 80:20), right: **23** (40:60 to 70:30), at a concentration of $1x10^{-5}$M at 25°C. Arrows indicate the spectral changes upon increasing the amount of MCH (from 40 to 90%). S. Ghosh, X.-Q. Li, V. Stepanenko, F. Würthner, *Chem. Eur. J.* **2008**, *14*, 11343-11357. Copyright (c) 2014 WILEY-VCH Verlag GmbH.[35]

For **22** that contains linear side chains at the imide position, an H-aggregate is the most stable assembly form due to a tight stacking of the chromophores. Thereby a helical assembly is formed with a perfect shielding of the perylene core. Wüthner et al. suggest the bulkiness of the gamma-methyl

groups as explanation for the different aggregation of **23**. This leads to a significant longitudinal displacement that corresponds to a J-type stacking to minimize the sterical crowding in the aggregate.

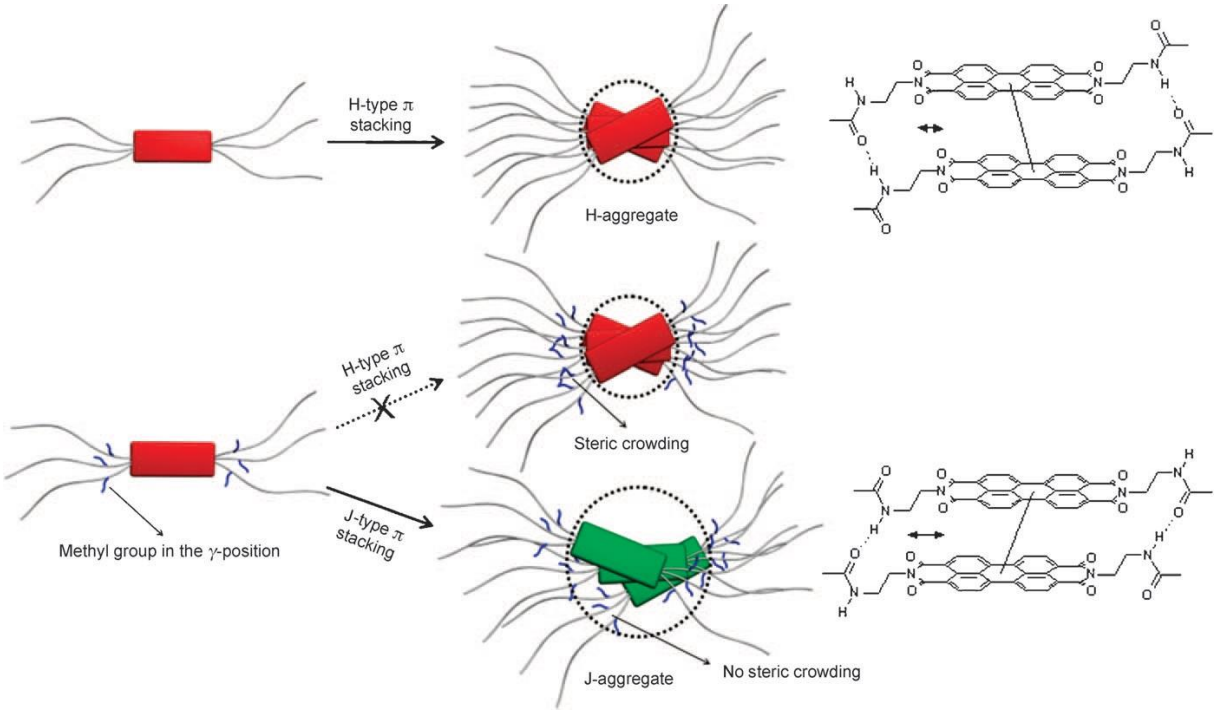

Figure 33: Left: Schematic representation of PDI chromophores with linear (top) and branched (bottom) alkyl substituents. Middle: The transition from H- (top) to J-type (bottom) π-stacking with increasing steric demand of the peripheral alkyl side chains. Right: Packing model for H- (top) and J-type (bottom) π stacking. In both cases additional rotational offsets are needed to enable both close π-π contact and hydrogen bonding. S. Ghosh, X.-Q. Li, V. Stepanenko, F. Würthner, *Chem. Eur. J.* **2008**, *14*, 11343-11357. Copyright (c) 2014 WILEY-VCH Verlag GmbH.[35]

In both cases, microscopic measurements show, that linear aggregates are formed. Since the π-π-stacking behavior is additionally stabilized through intermolecular H-bonds, a gel formation occurs upon dissolution in hot toluene for all six PDI which contain the amide function in the side chain. The aggregates without hydrogen bonds are not stable enough in toluene, so a deaggregation takes place for these cases. The amide in the side chain stabilizes the aggregates in toluene, so the alkyl chains that surround the linear aggregate can interpenetrate to form a disordered network which is then macroscopically observed as gel.

These examples underline the principles of the supramolecular behavior of perylene diimides. As mentioned earlier, an assembly along the z-axis takes place without binding motifs attached at the perylene. With additional interactions that add onto the perylene π-π-stacking, macroscopic changes like a gel formation are also possible. As described before, either an H- or a J-aggregate is formed, whereby unsubstituted perylenes tend to form H-aggregates and twisted, core substituted perylenes tend to form J-aggregates. In summary it can be stated that the lateral growth in one dimension can be

both simple regarding the macroscopic structure which was build up and complex regarding the constitution of these aggregates.

2.3.4.2 Assemblies with additional binding motif

While the assemblies of PDIs without additional binding motif are naturally limited to a lateral growth in one dimension, the following examples will introduce some ways to add complexity to supramolecular PDI chemistry. One of the most simple and intriguing examples of this, was the work of Kaiser and coworkers.[36] They introduced an additional binding axis for an aggregation through H-bonding via the imide position of the PDI dye. Therefore, the initial PTCDA was functionalized with ammonia to give the most simple diimide compound with only an NH-group at the imide position. With this functionalization they created a binding motif within the molecule to enable the possibility of H-bonding via the NH and CO groups. They attached solubilizing phenoxy groups at the bay position which results in a twisted PDI with a sterical shielding of the core (**24**).

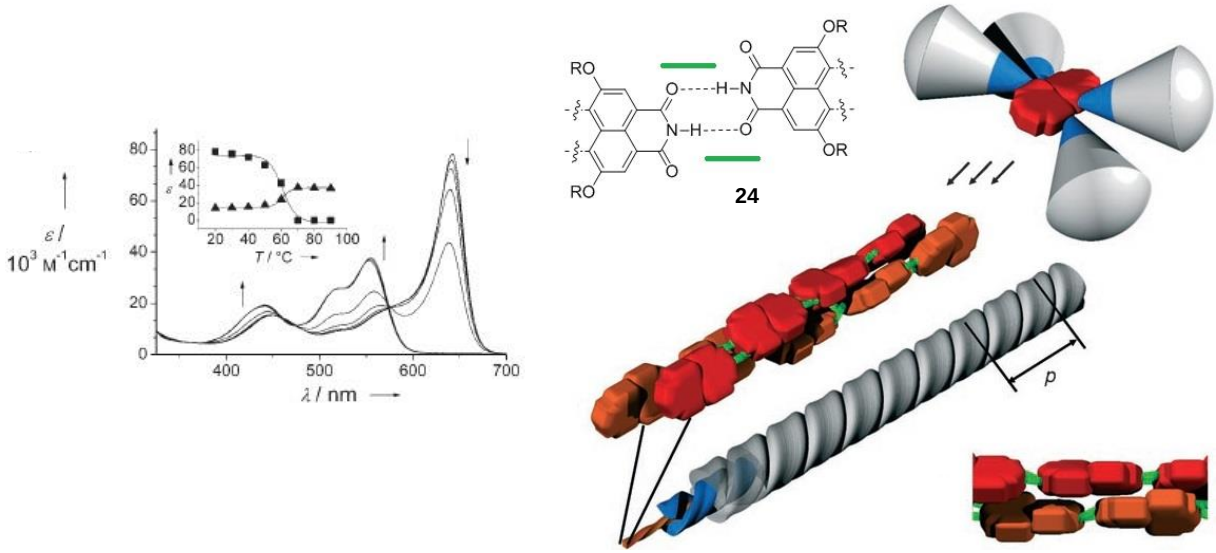

Figure 34: Left: Temperature-dependent UV/vis spectra of **24** in MCH (1.5×10^{-5} M) from 10 to 90 °C. Arrows indicate the spectral changes with increasing temperature. (Inset) Change of absorption at 633 nm (9) and 556 nm (2) upon increasing temperature and calculated lines according to sigmoidal fit. Right: Schematic illustration of self-assembly of the perylene diimide dye **24** into J-type aggregates with R = phenoxy. T. E. Kaiser, H. Wang, V. Stepanenko, F. Würthner , *Angew. Chem. Int. Ed.* **2007**, *46*, 5541-5544. Copyright (c) 2014 Angewandte Chemie International Edition.[36]

The shape of the absorption curve in the UV/vis spectrum of the monomeric dye reflects a typical curve for twisted PDIs in dichloromethane (DCM) like previously mentioned. In less polar solvents a strong bathochromic shift combined with further loss of the fine structure can be observed. The reported temperature dependent UV/vis spectrum links those two extremes because the transition

from aggregated to monomeric species can be followed upon heating of the solution. They suggested an assembly mode where strings of the PDI are formed through H-bonding along the x-axis, whereby two of these strings then stack onto each other forming J-type aggregates along the z-axis. Due to the bulky substituents at the core and the resulting sterical shielding of the core, a further π-π-stacking is prevented. They compared this behavior with a dye to which a bulky substituent was a attached at the imide position. This dye only showed a slight bathochromic shift due to the blocked imide position, which has now no ability to form hydrogen bonds and could only form dimers.

While the previous example outlined the supramolecular aggregation with a binding motif which was incorporated within the molecule, the following part describes perylene diimides in which a separate binding motif was attached to the perylene. The use of metal-ligand interactions is a common way to build up structures in supramolecular chemistry. A widely used binding motif which is based on this interaction type is the terpyridine (TP) which forms 2:1 complexes with various metals, that for example also has been connected to the GCP zwitterion to give supramolecular polymers.[37] Dobrawa et al. reported the investigation of a series of PDI dyes to which one (**25**) and two (**26**) of these TP units was attached at the imide position of the PDI to investigate the aggregation behavior of this molecule.[38]

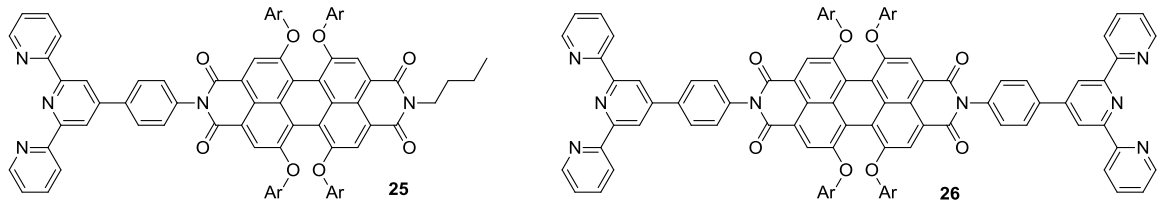

Figure 35: Molecules of Dobrawa and coworkers, Left: monotopic TP-derivative **25**; Right: ditopic TP-derivative **26**.[38]

While the monotopic TP-PDIs were not subject to a deeper aggregation study, the ditopic compound was investigated in detail. While the single ditopic PDI did not show any tendency to form aggregates, aggregation studies with the addition of Zn^{2+} ions were made. The Zn^{2+} ions form a 2:1 complex with the terpyridine which leads to a supramolecular polymer formation. This aggregation was monitored with UV/vis, whereby the complexation with Zn^{2+} does not influence the absorption properties of the PDI, but the terpyridine-related part.

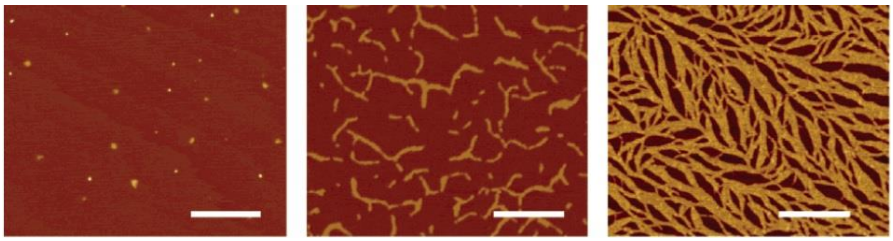

Figure 36: Left: AFM image of ligand **26** on mica and the corresponding coordination polymer prepared from dilute (middle, 0.1 mM) and concentrated (right, 1 mM) dimethylformamide (DMF) solution on mica; In all AFM images, the scale bar corresponds to 250 nm, the z data scale is 5 nm. All samples were prepared by spin-coating. Reprinted with permission from R. Dobrawa, M. Lysetska, P. Ballester, M. Grüne, F. Würthner, *Macromolecules* **2005**, *38*, 1315-1325. Copyright 2014 American Chemical Society.

A stepwise polymer formation was thus reported for the ditopic TP-PDI **26**. AFM pictures clearly show the formation of polymer strands, so it can be seen that only a one dimensional aggregation along the x-axis is observed. Even though the complexation of the terpyridine with Zn^{2+} can be reversed upon addition of a chelating ligand, the switching ability was not investigated.

In most examples of supramolecular chemistry with PDI derivatives the additional supramolecular interaction is accomplished by a binding site at the imide position.[39] As mentioned earlier in this chapter this attachment of a binding site leads to assemblies which elongate along the x-axis. One of the few examples where the binding sites are attached at the bay position, is the work of Sariola-Leikas and coworkers.[40] The goal of their work was to obtain an assembly which elongates along the y-axis. As well as in the previous example, they also synthesized a monotopic and a ditopic TP-PDI derivative.

Since the TP unit was attached at the core position without spacer in between to generate a completely conjugated system, the complexation with Zn^{2+} ions led to a significant change in the UV/vis spectrum. Unfortunately no further study of the exact assembly has been done due to the limited solubility of the ditopic derivative in chlorinated solvents like chloroform. Therefore it is not possible to compare the assembly which results of the binding via the x-axis with the one resulting of the interactions via the bay position and therefore the y-axis. As far as this thesis could evaluate, there is no example for an elongation along the y-axis known up to this point.

2.3.4.3 Aggregates in water

While in the previous part of this chapter a few significant examples were given to illustrate the principle supramolecular behavior of perylene diimides, this part will focus on assemblies in water. Normally, perylene diimides are completely insoluble in water due to the large aromatic core, but there are several possibilities to accomplish a solubility in water without changing their principle chemical structure. An easily accessible method is the attachment of side chains which are themselves highly soluble in water like polytheylene glycol (PEG) chains, sugars or dendrons.[41,42,43] One other possible method is the attachment of ionic parts to enhance the solubility in aqueous solution.[44] These methods result in a molecule that has an amphiphilic character due to the unpolar core and the polar substituents. Nevertheless it is a thin line between a gain in water solubility and a complete shielding of the perylene core with a loss of aggregation.

Even though water soluble PDIs are known for many years, a detailed investigation was not performed until recently. Structures in water are not so easily predictable because of an undirected hydrophobic effect, although the advantage of assemblies in water is the amplification of other supramolecular forces. Görl et al. gave a comprehensive overview about PDI chromophores in water in their recent review paper. [45] They reported the whole spectrum of PDI assemblies of water even though most examples are formed by planar unsubstituted PDIs. The review does not only describe supramolecular assemblies, but also biochemical topics like the intercalation of specifically designed PDIs into DNA. Some significant examples for the supramolecular behavior of PDIs in water shall be given in the following part of this chapter, which are not necessarily mentioned in the review paper of Görl et al., but being chosen to highlight different aspects like e.g. the incorporation of binding motifs.

One of the most recent examples of perylene diimide chemistry in water is the paper of Zhang et al. were the complexity of supramolecular chemistry of PDIs is shown.[46] They investigated a planar PDI **27** that has been reported previously and initially was subject to an investigation of the influence of various solvents on the π-π-stacking of perylenes. The water soluble perylene diimide was obtained through an attachment of three ethylene oxide groups on both imide positions.

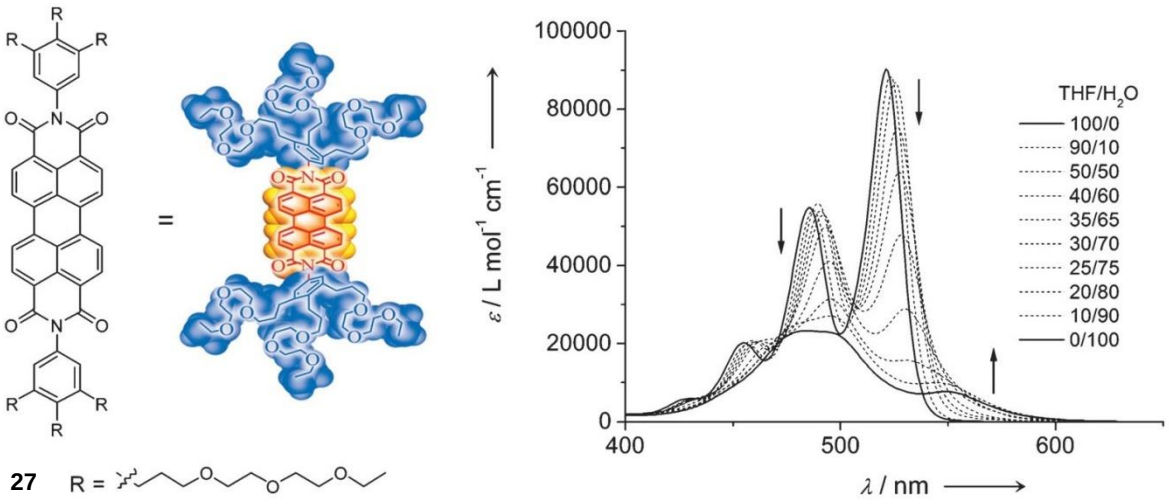

Figure 37:Left: Presented molecule **27** of Zhang et al. with three triethylene glycol chains at both imide positions and schematic coloring of the dye. Right: UV/Vis spectra of 2.0×10^{-6} M **27** in THF/water mixtures at 20°C. Arrows indicate spectral changes upon increase of water content.[46]

Whereby the spectrum in THF shows a significant vibronic structuring typical for planar PDIs, the maximum absorption band undergos a hypsochromic shift with increase of the solvent polarity. TEM measurements reveal the formation of helical rods through a π-π-stacking of the core and therefore an elongation along the z-axis. The probable explanation is an H-type stacking of the dyes whereby the hydrophobic PDI core faces inside the aggregate while the hydrophilic triethylene glycol chains face outwards to shield the inner part. The molecules additionally exhibit a further concentration dependent aggregation behavior that does not stop at single rods. The stepwise increase of the concentration leads to a fusion of single rods to ribbons. The high resolution pictures show that a continuous sticking of the rods is taking place until the ribbon forms.

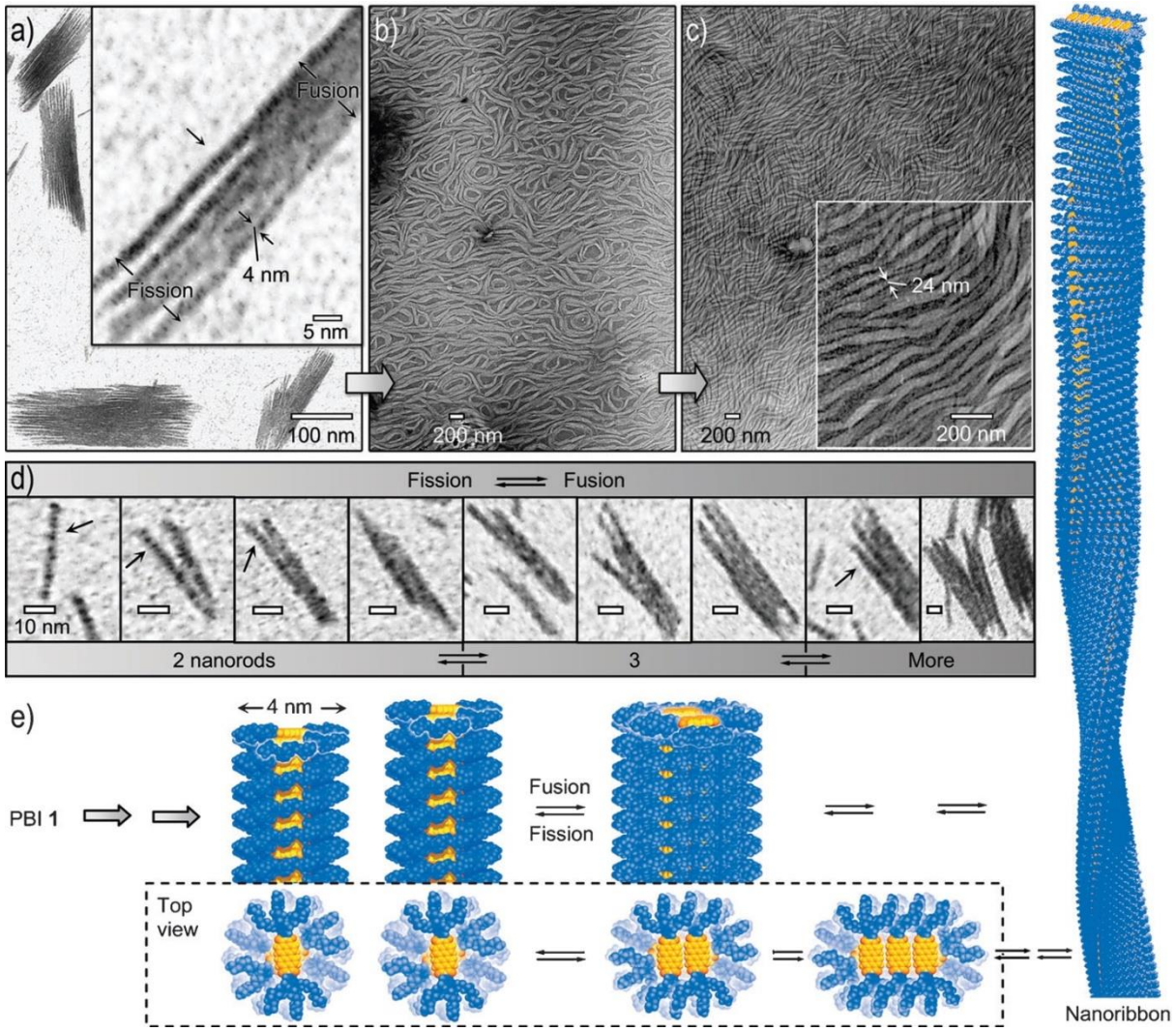

Figure 38: a–c) TEM images of **27** aggregates prepared from water, [**27**]=0.25 mg mL^{-1} (a), 0.76 mg mL^{-1} (b), and 1.0 mg mL^{-1} (c). d) TEM images of the fusion and fission of two, three, or more nanorods; arrows indicate the segmented nanostructures, [**27**]=0.25 mg mL^{-1}; scale bar: 10 nm. e) Schematic illustration based on space-filling (CPK) models for the hierarchical self-assembly from nanorods to nanoribbons by fusion and fission. X. Zhang, D. Görl, V. Stepanenko, F. Würthner, Angew. Chem. Int. Ed. 2014, 53, 1270-1274. Copyright (c) 2014 Angewandte Chemie International Edition.[46]

Zhang et al. state that these ribbons are composed of PDIs in a side by side orientation which was also reported by Percec et al. recently.[47] This arrangement is further underlined by fluorescence measurements whereby the enhanced quantum yield of the ribbons is attributed to a denser packing of the dyes. This packing leads to a disfavoring of the structural relaxation into a less fluorescent eximer species. MakroModel (MM)-calculations hint that the hydrophobic inside of a single nanorod is not completely shielded by the hydrophilic oligoethylene (OEG) chains. Conversely, the ribbon exhibits a significantly better shielding of the core which is siggested to be the driving force of this assembly.

Jouault et al. reported the assembly of a similar planar PDI derivative, which was decorated with one PEG chain at each side of the PDI at the imide position, whereby they investigated different PEG chain lengths to enhance the solubility.[48]

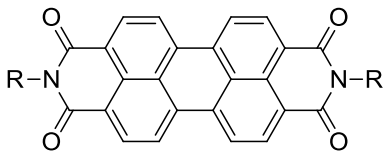

28 R = PEG_7
29 R = $OPEG_7$
30 R = PEG_{16}
31 R = $OPEG_{16}$

Figure 39: Molecules studied by Jouault et al. with varying PEG chains at the imide position.[48]

The introduced PDIs assemble through π-π-stacking along the z-axis, but are limited in the lateral growth compared to the previous system due to the sterical crowding of the PEG chains. This limitation results in short stacks which then interlink into densely packed globular aggregates through an entanglement of the PEG chains. The large structures which can be observed with AFM measurement in aqueous solution are 100-250 nm in height.

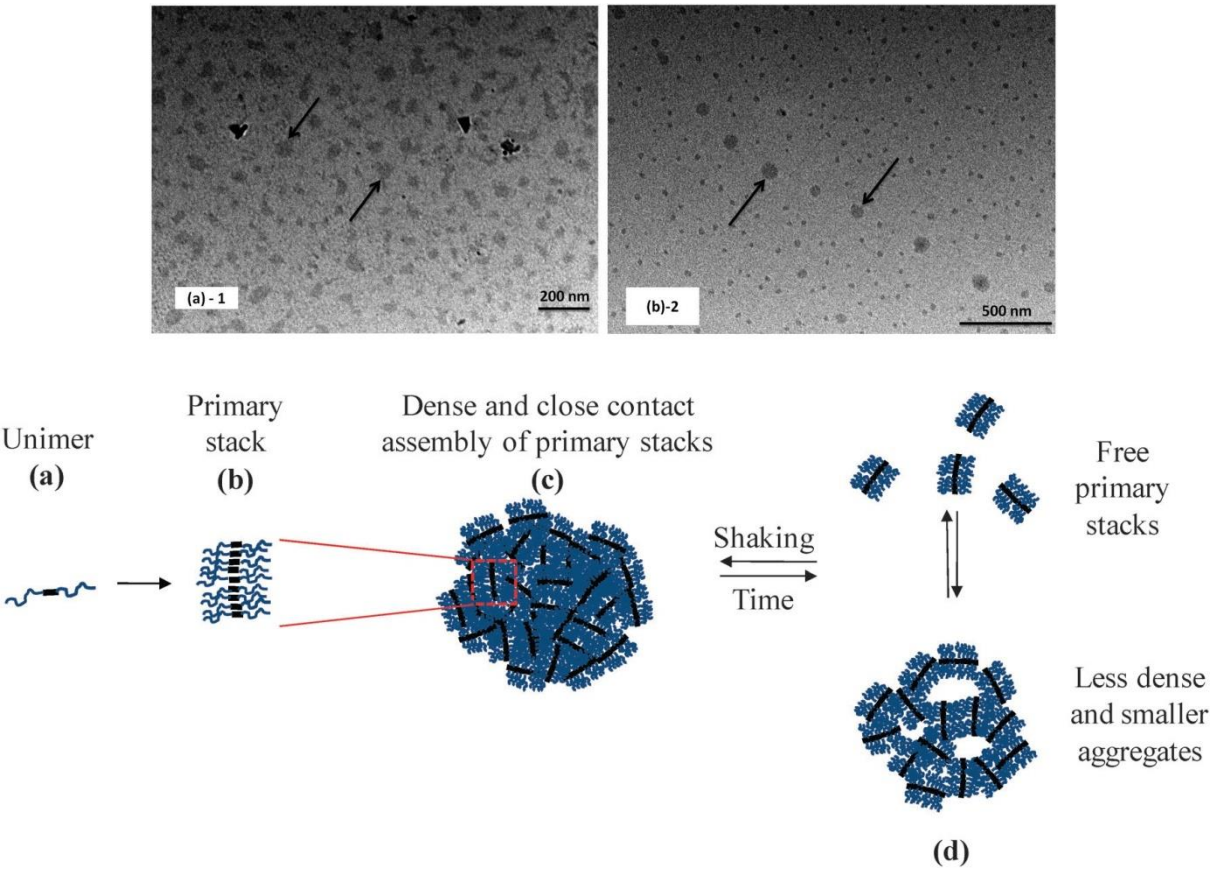

Figure 40: Above: TEM images. Left: **28** at C = $1x10^{-4}$ M. Right: **31** at C = $2.7x10^{-3}$ M. Below: Schematic diagram depicting the effect of time (or equivalently of concentration) and of shaking on the structure of the PEG–PDI system. Reproduced from N. Jouault, Y. Xiang, E. Moulin, G. Fuks, N. Giuseppone, E. Buhler, *Phys. Chem. Chem. Phys.* **2012**, *14*, 5718-5728 with permission of The Royal Society of Chemistry.[48]

SAXS measurements indeed revealed that this assembly is composed of linear stacks which further agglomerate into larger aggregates. The length of these stacks is dependent on the PEG chain length. Larger PEG chains form shorter stacks due to a sterical crowding in the aggregate. Additionally an aging behavior is observed, whereby a deaggregation into primary stacks occurs over time. This can be explained by a progressive re-solubilization of the PEG chains. When the sample is shaken, a reassembly of the stacks is taking place through an interpenetration of the PEG chains. This is related to mechanical effects which have been reported by the same working group previously.[49]

These two examples showed beautifully that, even though the aggregates are based on the same principle build-up, the systems form two completely different assemblies. Also a lot more architectures are known for planar water soluble dyes which are based on PDI π-π-stacking, but they will not be mentioned in detail in this thesis due to the manifold examples. For twisted PDIs only a few examples for an assembly in water are known which will be highlighted in the following.

The next introduced self-assembly motif was proposed by Baram and coworkers.[50] The molecule **32** consists of two PDI subunits that were connected through an alkyne linker at the core position and decorated with PEG at the other side of the core. Since this unit is equally important for the latter assembly, it shall be mentioned that a 3-pentyl chain is attached at the imide position. The synthesized amphiphilic PDI molecule is not completely soluble in water though and therefore the aggregation was investigated in water/THF (4:1) mixtures.

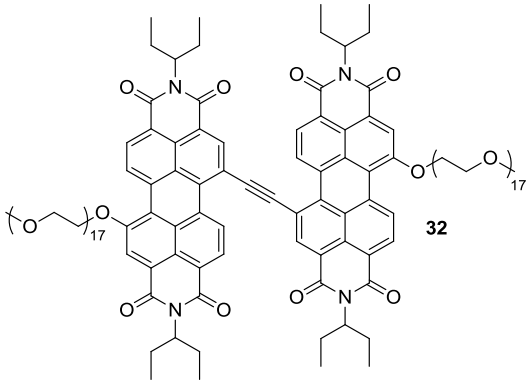

Figure 41: Presented molecule (**32**) of Baram et al. whereby two PDI subunits are connected through an alkine linker at the core position and decorated with PEG at the other sides of the core.[50]

The molecule forms long fibers which exhibit a ribbonlike structure as observed by cryo-TEM measurements. Like in the example of Jouault et al.[48] the formation of short stacks is proposed which are called segments by Baram and coworkers. But opposite to the previous example no disordered assembly of these stacks takes place, but an ordered assembly is observed. Since the PEG is attached to the core, the imide position is free for other interactions. The 3-pentyl chain at the imide

position of the perylene then enables an interaction of the segments through interlinking which leads to the creation of ordered segmented fibers.

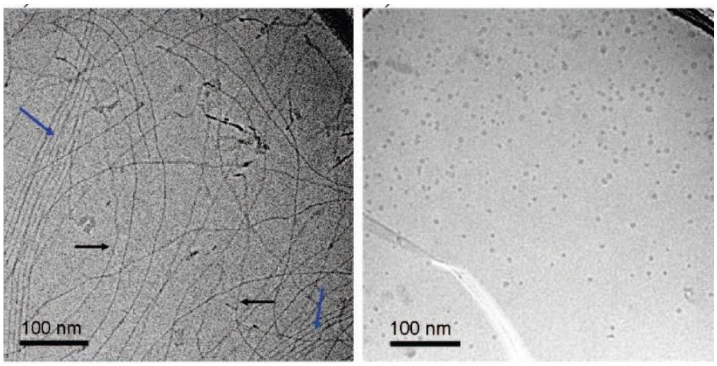

Figure 42: Cryo-TEM images of **32** in water/THF mixture (4:1, v/v), $1x10^{-3}$ M. Left: Neutral system: black arrows, fiber twists; blue arrows, ordered domains. Right: Reduced system (the feature in the lower left part is due to a crack in the vitrified solvent). Reprinted with permission from J. Baram, E. Shirman, N. Ben-Shitrit, A. Ustinov, H. Weissman, I. Pinkas, S. G. Wolf, B. Rybtchinski, *J. Am. Chem. Soc.* **2008**, *130*, 14966-14967. Copyright 2014 American Chemical Society.[50]

One extraordinary feature which was introduced by this work is a switching of the assembly with sodium dithionite. The sodium dithionite acts as a reducing agent which reduces the PDI from a neutral to an anionic state. The switching to the anionic state leads to a rearrangement of the assembly resulting in a depolymerization and therefore loss of assembly. This is accompanied by a loss of viscosity due to polymer fission. Cryo-TEM images depict circular aggregates that are being formed in the anionic state. The initial assembly is reformed upon oxidation with O_2, so a reversible switching can be stated.

A similar PDI (**33**) to the previously reported one has been published by Krieg et al. which shows some outstanding features.[51] The difference between the reported dyes is an additional bipyridyl moiety to connect the two PDIs in this example. Since the unit is a good metal ligand, it is normally used as supramolecular binding motif. In the reported paper, the unit is solely used as linker though and no further investigation of a metal addition has been published yet.

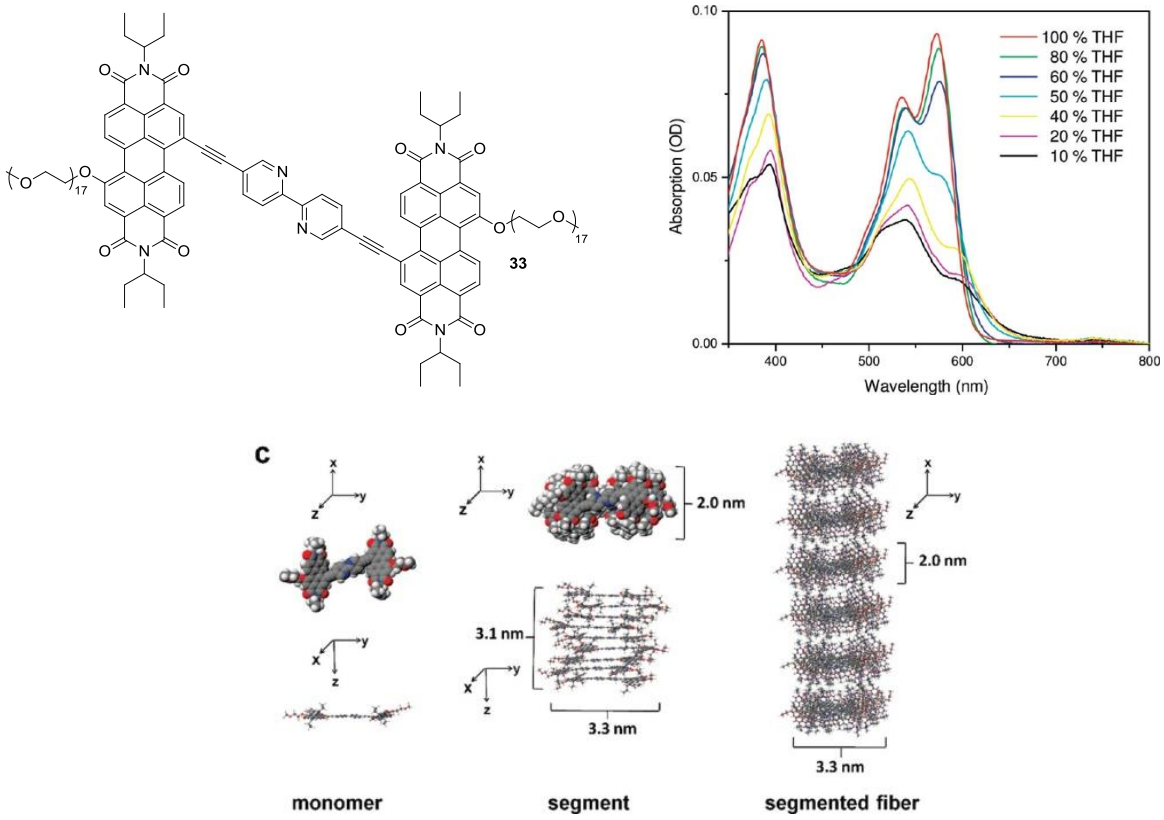

Figure 43: Above left: Presented molecule of Krieg et al. whereby two PDI subunits are connected through an additional bipyridyl moiety at the core position and decorated with PEG at the other sides of the core. Above right: UV/vis spectrum of **33** (2.4 x10^{-6} M) in THF and different water/THF mixtures. Below: Molecular modeling of **33** and its supramolecular structures. For simplification, PEG chains are modeled as the -O(CH_2-CH_2)OCH_3 group. Reprinted with permission from E. Krieg, E. Shirman, H. Weissman, E. Shimoni, S. G. Wold, I. Pinkas, B. Rybtchinski, *J. Am. Chem. Soc.* **2009**, *131*, 14365-14374. Copyright 2014 American Chemical Society.[51]

The synthesized PDI **33** is reported to be disaggregated in DCM, chloroform ($CHCl_3$) and tetrahydrofuran (THF) since a monomeric spectrum is measured by UV/vis. The solvent dependent UV/vis spectrum shows a slight hypsochromic shift upon increase of solvent polarity. An aggregation can be observed upon addition of water up to 90%, after which only a precipitation can be seen. Concurrently an increase of viscosity happens upon addition of water.

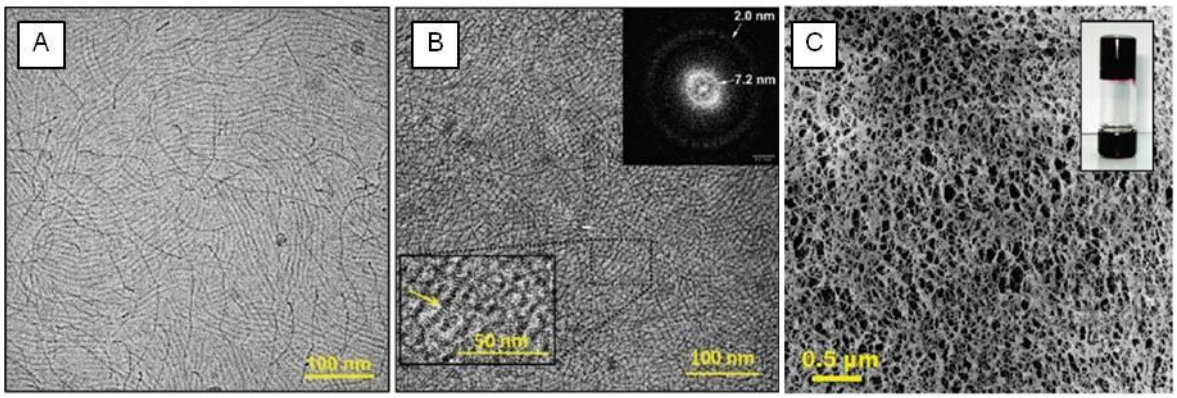

Figure 44: A: Cryo-TEM image of aggregated solution (10^{-4} M) of **33** in water/THF mixture (80:20, v/v). The image shows ordered fibers (high contrast cores: 3.3 (0.4 nm, low contrast spacings: 3.9 (0.4 nm). B: Cryo-TEM image of **33** at higher concentration ($3.3x10^{-3}$ M). Some individual fibers show distinct segments (yellow arrow). Inset: FFT calculation showing spacing of 7.2 nm (fiber-fiber distance) and 2.0 nm (segment-segment distance). C: Cryo-SEM images of the gel of **33** ($8x10^{-3}$ M, water/THF mixture (80:20)). Thereby the nanoporous structure of the three-dimensional network can be seen. Inset: vial inversion test.. Reprinted with permission from E. Krieg, E. Shirman, H. Weissman, E. Shimoni, S. G. Wold, I. Pinkas, B. Rybtchinski, *J. Am. Chem. Soc.* **2009**, *131*, 14365-14374. Copyright 2014 American Chemical Society.[51]

In the microscopic measurements, again segmented fibers can be observed. The formation of segmented fibers is according to the example of Baram and coworkers. First an aggregation along the z-axis takes place followed by the assembly along the x-axis through an interlinking of 3-pentyl chains. The interpenetration of the attached PEG chains leads then to a network formation which is visible by cryo-TEM measurements. As extraordinary feature, the reported molecule forms a supramolecular gel through an interconnected three dimensional network at higher concentration.. This robust gel shows additionally a multiple stimuli responsiveness. Similar to the above reported molecule of Baram et al. the perylene diimide is prone to a switching with sodium dithionite, whereby the transformation from gel to fluid solution occurs. The gel is being reformed upon oxidation and the switching series can be repeated several times. A temperature treatment leads to shrunken gel, which is reformed to the gel after cooling again.

One of the few papers that reported perylene based supramolecular chemistry in water with a binding motif was the publication of Golubkov and coworkers.[52] They introduced molecule **34**, which is similar to the monotopic molecule earlier reported by Sariola-Leikas and coworkers.[40] Like in this example, a terpyridine is used as metal binding unit and attached via an alkyne linker to the core. Similarly to the above examples a polyethylene glycol is bound to the core of the perylene diimide.

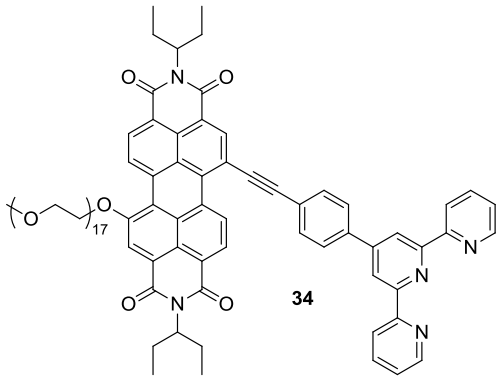

34

Figure 45: Presented molecule of Golubkov et al. with a monotopic attachment of a TP unit.

As already mentioned before, TP is used as coordination site for metal ions. To utilize the TP as binding motif to connect two units, a metal has to be used that results in a sixfold coordination and

would lead to a formation of dimers in this case. Golubkov et al. did not investigate this option though but the complexation with fourfold metals like Palladium or Platinum. The complexation here also has a huge impact on the UV/vis spectrum due to a conjugated attachment of the TP to the PDI core. With microscopic measurements, different morphologies can be observed depending on the used metal. While the molecule alone also forms segmented fibers, the metal complexes aggregate differently. In the case of Palladium addition (molecule Pd-**34**) tubular aggregates form which aggregate in a face to face fashion which is known for H-aggregates. The molecule coordinated with Platinum (Pt-**34**) shows an assembly into vesicles that are composed of bilayers of the molecule. The fourth investigated molecule with Silver (Ag-**34**) aggregates into platelets or layers.

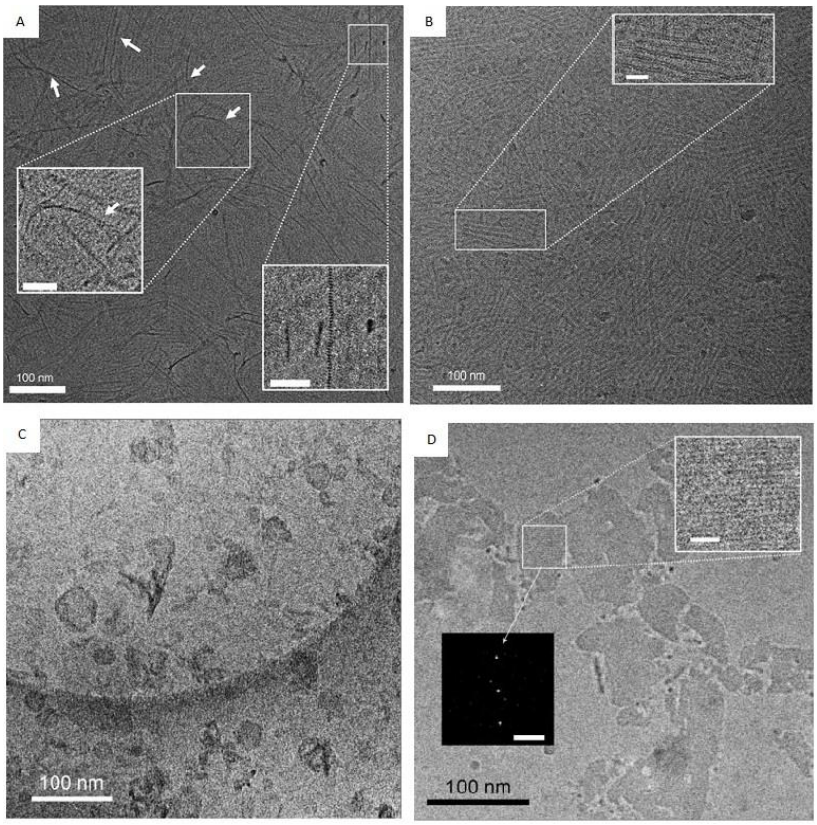

Figure 46: A) Cryo-TEM image of $2x10^{-4}$ M solution of **34** in a water/THF (9:1 v/v) mixture. The right inset shows an enlarged image of a segmented fiber (scale bar 40 nm) and the left inset shows an enlarged image of a fiber twist (scale bar 20 nm). The white arrows point at twisting regions (from the narrow edge to the wider face) of ribbonlike fibers. B) Cryo-TEM image of a solution of Pd-**34** ($2x10^{-4}$ M) in water/THF (9:1 v/v). The inset shows an enlarged image of a nanotube (scale bar 20 nm). C) Cryo-TEM image of a solution of Pt-**34** ($2x10^{-4}$ M) in water/THF (9:1 v/v). D) Cryo-TEM image of a solution of Ag-**34** ($2x10^{-4}$ M) in water/THF (9:1 v/v). The inset surrounded by a white frame shows an enlarged image of a nanoplatelet (scale bar 10 nm) and the inset in a black square (scale bar 0.5 nm) shows a fast Fourier transform image (performed on the region in the white frame), which shows high crystallinity with the pattern that corresponds to 1.85 nm spacing. G. Golubkov, H. Weissman, E. Shirman, S. G. Wolf, I. Pinkas, B. Rybtchinski, Angew. Chem. Int. Ed. 2009, 48, 926 -930. Copyright (c) 2014 Angewandte Chemie International Edition.[52]

Even though the terpyridine aggregation can be reversed with the addition of a chelating ligand as described earlier, the switching ability of these systems was not investigated. Also the TP binding motif is not used for a dimerization and therefore an elongation of the assembly along the binding axis is not achieved.

In summary perylene diimides are feasible supramolecular units that form aggregates that can elongate along various axes. Even though this thesis concentrated on the principle supramolecular behavior there are several examples where perylene diimides were used to form smart materials e.g. as semiconductor, liquid crystals or in organic solar cells.[9,11]

3. Concept

As reported previously, PDI dyes are a group of chromophores with very interesting supramolecular properties which are subject to various fields of research and application like e.g. OLEDs or solar cells and therefore are chosen to be the first building block in this thesis. It is possible to form assemblies through π-π-stacking of the aromatic dyes which can be distinguished between H- and J-aggregates depending on the respective orientation of the involved dyes. Perylene diimides exhibit a feasible switching ability, whereby the formation of the assembly is directed mostly by adjusting concentration or solvent. It is not only possible to form assemblies solely based on the π-π-stacking ability of the perylene core, but also supramolecular assemblies with additional binding motifs attached to the dye.

The typical assembly for PDIs without additional binding motifs is a linear aggregation along the z-axis through π-π-stacking. As outlined in the previous chapter, there are far more examples for a one dimensional aggregation for perylene diimides even though also spherical assemblies are frequently reported. Various architectures can be build-up with perylene diimides that incorporate an additional binding motif in the molecule whereby the assembly is predominately formed along the x- and z-axis. Examples for a directed elongation along the y-axis could not be found during the literature screening of this thesis. There are several water soluble PDIs that form assemblies in aqueous medium, whereby the driving force for the assembly is mostly a hydrophobic interaction. There are furthermore only few examples for perylene diimides with additional binding motif that form stable assemblies in water, since most of the binding motifs reported in the previous chapter form aggregates based on hydrogen bonds and are limited to unpolar solvents. Ionic interactions - as one of the more stable interactions in water - were not investigated as supramolecular binding interactions in water for perylene diimides yet.

The zwitterionic GCP mentioned in the previous part which was created by Schmuck is also an outstanding supramolecular binding motif and will therefore be the second building block in this thesis. This self-complementary unit forms extremely stable dimeric aggregates in polar solutions due to a feasible combination of ionic interactions and H-bonds. It is one of the few binding motifs known to form stable supramolecular assemblies even in water based on electrostatic interactions. Besides its versatile functionalization through various synthetic routes, it shows an outstanding reversible switching ability with acid and/or base.

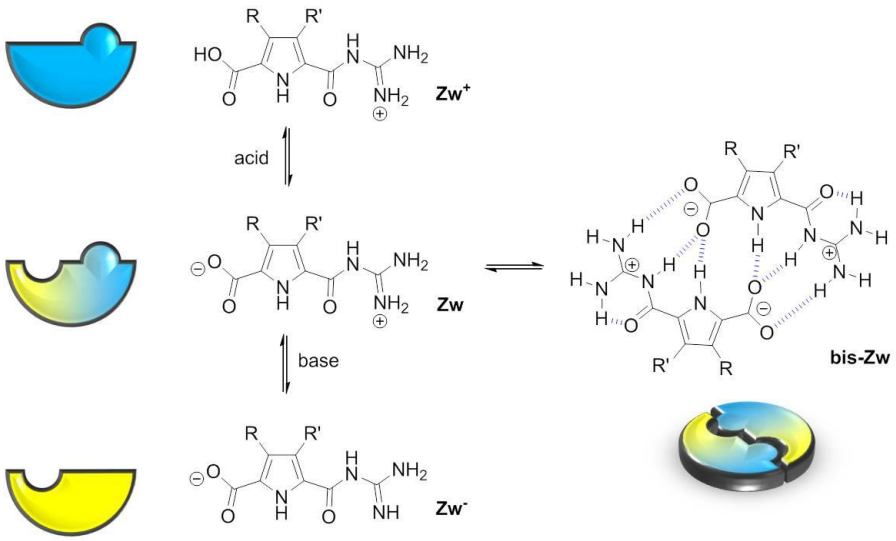

Figure 47: Molecule **11** = **Zw** with R = R' = H forms a stable dimer **bis-Zw** based on multiple hydrogen bonds as well as ionic interaction, whereby the protonated **Zw**$^{+}$ and the deprotonated **Zw**$^{-}$ version do not show this tendency to dimerize.

It is possible to form various assemblies with the zwitterionic GCP unit, whereby extensive research resulted even in the development of a reversibly switchable functional material. Additionally, the binding motif is not limited to dimeric assemblies but these dimers themselves can aggregate by orthogonal interaction through π-π-stacking.

The goal of this thesis is the creation of bi-functional supramolecular systems through the combination of perylene diimide and zwitterionic GCP binding motif. As described in the last chapter, perylene diimides are often utilized as functional core unit due to its unique photophysical as well as electronic properties and decorated with a binding motif which is used to tune or change the assembly. In the example of Dobrawa and coworkers, an assembly into linear string is accomplished by the attachment of the zinc complexed terpyridine binding motif while the single molecule does not form any observable assembly due to the bulky phenoxy groups at the core position. This work therefore wants to investigate the principal properties of perylene diimide - GCP zwitterion - Modules and possibly even lay the foundation for the develop of new functional materials. Through the combination of both functional units, a supramolecular system shall be created that exhibits a manifold switching ability based on the known stimuli for the two respective units. The goal is furthermore to form aggregates that are stable in polar media.

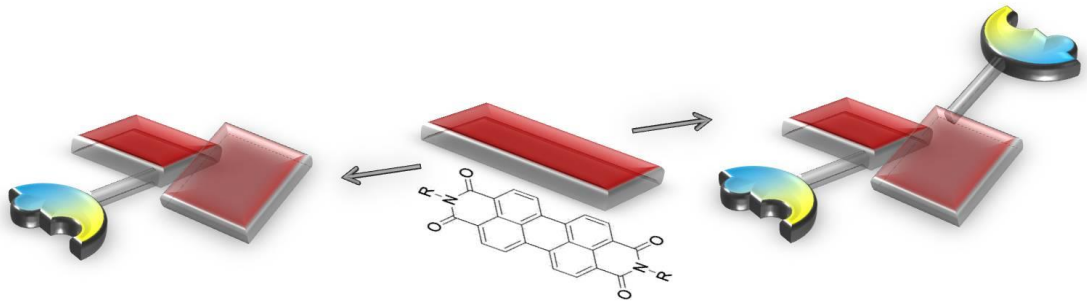

Figure 48: Schematic representation of the monotopic (right) and the ditopic (right) attachment of the GCP binding motif to the perylene core. The tilted red rectangles shall represent the twisting of the core upon substitution.

Binding motifs can in principal be attached to various positions at the perylene diimide. Most examples have the binding motifs attached on either one or two sides though. Therefore this thesis will investigate a monotopic as well as a ditopic attachment of the zwitterionic GCP unit to the perylene diimide core. The schematic representation of the monotopic and ditopic Modules is depicted in Figure 48 and the objectives for both concepts are outlined hereafter.

3.1 Ditopic Modules

Two binding motifs shall be attached to either side of the perylene diimide to enable an elongation along binding axes of the motif additional to the π-π-stacking of the perylene diimide. Within this ditopic Module, several different supramolecular interactions shall enable stable aggregates in polar media with an elongation in more than one dimension:

- π-π interactions through stacking of the perylene core or the planar zwitterion dimer
- ionic interactions through the zwitterionic binding motif
- H-bond through the zwitterionic binding motif and the linker moiety

The binding motif will additionally be attached in two ways to enable a comparison of two different binding axes, since an elongation of the binding along the core axis (y-axis) was not investigated before. The binding along the imide axis (x-axis) which has been investigated intensively is accompanied by an attachment of the binding motif to the imide position of the perylene diimide, while the elongation along the y-axis shall be enabled through an attachment of the binding motif at the core position. The influence of the binding axis on the assembly will then be investigated in this thesis. To accomplish that goal, two molecules comparable in size and solubility are designed. A flexible linker will be used to connect the perylene diimide with the GCP unit via an amide bond to ensure to

flexibility and solubility of the molecule. The binding motif as well as the solubilizing group shall only be attached at the 1,7-position to minimize the sterical hindrance of the side group so that the PDI is still prone to aggregation. Therefore the molecules shown in Figure 49 were designed.

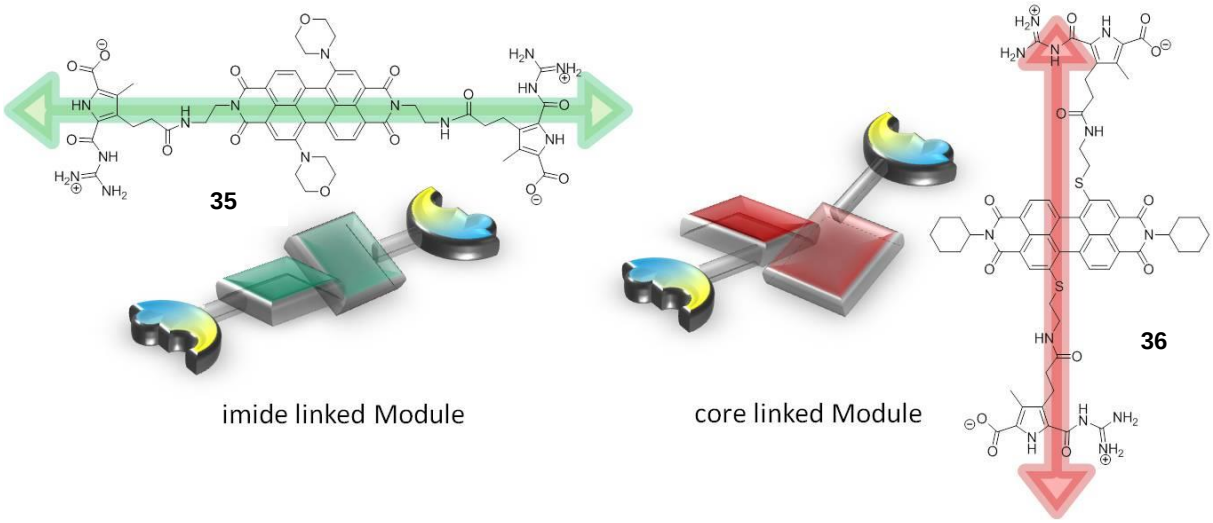

Figure 49: Imide linked Module **35** and core linked Module **36**: Structural formula and schematic representation.The arrow along the molecules shall illustrate the aspired binding axes.

Molecule **35** on the left side shows an attachment of two GCP binding motifs at both imide positions of the perylene diimide and the respective molecule will be referenced in this thesis as **imide linked Module**. As mentioned earlier, this attachment is commonly known from literature and can therefore be regarded as reference molecule to compare the new system with the conventional PDI assemblies. The second molecule (**36**) on the right side shows an attachment of two GCP binding motifs at the perylene core and will be referenced as **core linked Module** in the following chapters. This Module is designed to investigate the differences in assembly upon variation of the binding axis. The schematic representation of both ditopic Modules is also shown in Figure 49. The GCP binding motif is represented in yellow and blue while the perylene core is marked in green for the imide linked Module and in red for the core linked Module to be able to distinguish between both easily.

The ditopic Modules should be prone to a polymer formation along the zwitterionic binding axis through the self assembly of the GCP binding motif as well as the perylene binding axis through a π-π-stacking of the perylene core. It is anticipated that the introduced Modules form a two dimensional assembly, if the aggregation is not limited in one dimension. Therefore a sheet like assembly is expected for both ditopic Modules. If a limitation of some kind occurs in one dimension, the aggregation might also yield in a polymeric assembly. Additionally, a homotopic stacking is anticipated, whereby perylene stacks onto perylene and GCP dimer stacks onto GCP dimer. The schematic representation of this anticipated layered assembly is shown in Figure 50. Of special

interest is the investigation of the stacking behavior of the perylene cores, whether H- or J-type of aggregates are being formed and if both ditopic Modules form the same type of assembly.

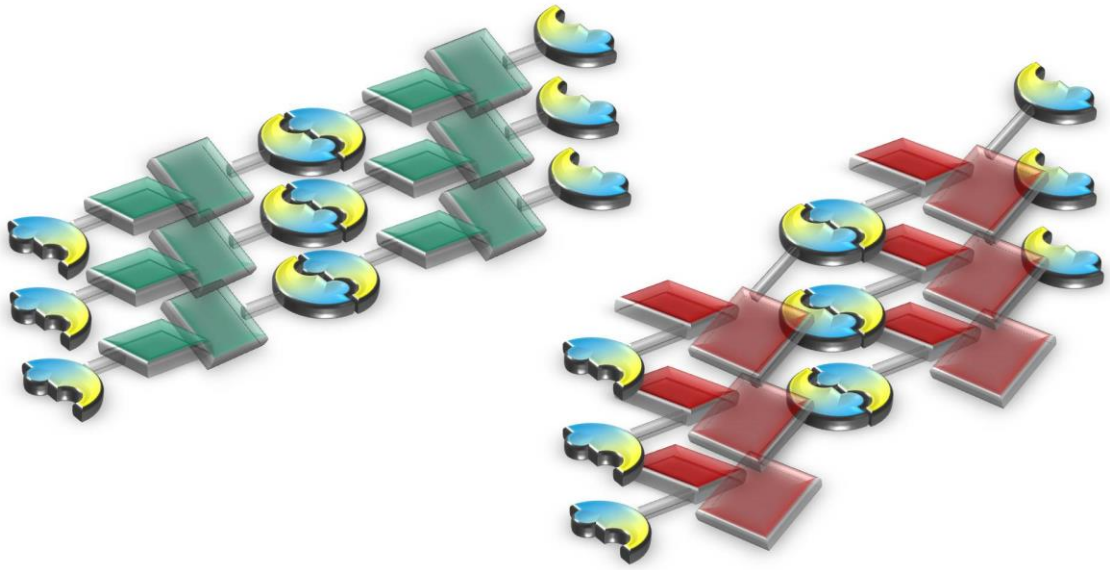

Figure 50: Schematic representation of the proposed aggregation of the imide linked Module **35** and the core linked Module **36**.

One extraordinary feature of these assemblies shall be the versatile and manifold switching ability. Up to now, the switching of perylene diimides on one hand is mostly achieved with a variation of the concentration or a change of solvent polarity. A novel switching was reported by the working group of Rybtchinski, whereby the addition of sodium dithionite leads to a formation of a radical anion species of the perylene accompanied by a loss of the initial assembly. The zwitterionic GCP binding motif on the other hand is prone to a switching with acid and base like mentioned earlier. The addition of acid protonates the carboxylic acid while the addition of base leads to a deprotonation of the guanidinium unit, both leading to a loss of the dimeric GCP assembly. Based on the switching possibilities of the incorporated functional units, this thesis wants to investigate the aggregation changes upon switching in each case.

3.2 Monotopic Modules

Opposite to the ditopic attachment that shall be accomplished, also one binding motif shall be introduced to the perylene core to have the possibility to attach other substituents at the other side of the perylene core. For a good solubility in water PEG chains shall be connected to the perylene core.

which are also expected to add an additional supramolecular interaction through an interpenetration of adjacent PEG chains. Furthermore this thesis will investigate the influence of a 3-pentyl-chain at the imide position. With these 3-pentyl groups an interlinking with of adjacent molecules that also have 3-pentyl groups at the imide position is enabled as previously reported by Krieg and coworkers.[51] Two molecules were designed to study the change in assembly with and without such interlinking possibility. Therefore one Module with 3-pentyl chains at the imide positions (molecule **38**) was designed (**3-pentyl Module**) while the comparable molecule **37** has a closed cyclohexyl chain at the imide position (**cyclohexyl Module**), inhibiting the interlinking possibility in this case. The zwitterionic binding motif itself will be again connected through a flexible linker at the perylene core.

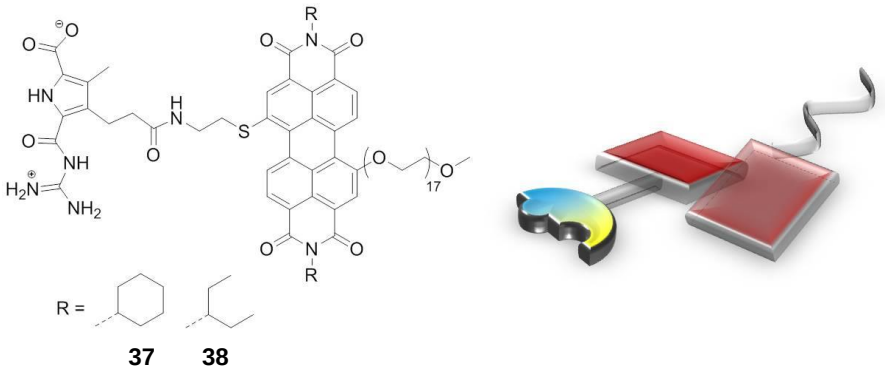

Figure 51: Monotopic Modules **37** (cyclohexylamine substituted) and **38** (3-pentylamine substituted): Structural formula and schematic representation.

The monotopic Modules shown in Figure 51 are expected to form dimers through the self-complementary assembly of the GCP binding motif. This self assembled dimer is similar to various molecules reported by the working group of Rybtchinski and is therefore anticipated to form similar assemblies. The elongation possibility in one dimension is cut short compared to the ditopic Modules due to the fact, that only a dimer can be formed by the monotopic zwitterion at the perylene core. When stacked onto each other, these dimers can assemble into rods, whereby again a homotopic stacking of perylene onto perylene and GCP dimer onto GCP dimer is anticipated. The cyclohexyl Module should be only prone to a rod formation through such homotopic π-π-stacking. For the 3-pentyl Modules, various assemblies may be formed through an additional interaction of adjecent 3-pentyl groups. If the polymer growth along the z-axis is limited, the most probable assembly is the formation of segmented fibers like suggested in Figure 52. If the growth is not limited in this dimension and a homotopic polymeric assembly forms, even the formation of layers through interlinking of the 3-pentyl chain is possible. Additionally the PEG chains may overcome the elongation limitation of the dimer through interpenetration of neighbored chains to enable a supramolecular continuation of the aggregation even in this dimension. With the interlinking possibility of the 3-pentyl

amine at the imide position, it might be possible to enable the binding even in three dimensions depending on the assembly formed. This leads to a variety of possible assemblies that might be observed.

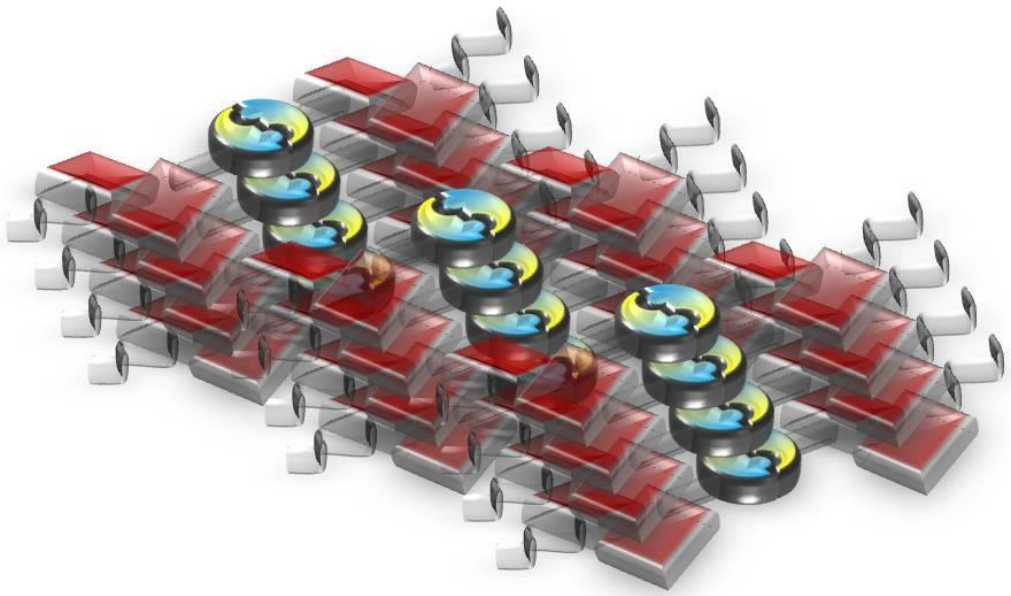

Figure 52: Suggested aggregation mode for the 3-pentyl Module based on a homotopic stacking of the Module accompanied by an interlinking of the 3-pentyl chains.

Depending on which assembly is being formed and on whether the interpenetration of the PEG chain leads to regular or irregular assemblies, it might be possible to form a supramolecular gel as reported by Krieg et al. for a similar molecule. As well as in the ditopic part of this chapter, the introduced molecules shall create assemblies, which show a versatile and manifold switching ability. The assembled systems should be prone to various stimuli like mentioned for the ditopic Modules. Again, it will be of high interest, how the aggregation mode is being changed upon switching in each case. Especially, if a supramolecular gel can be formed, which then could switched with an outstanding amount of different stimuli.

The next chapter will now describe the synthesis of the presented Modules and investigate the aggregation behavior as well as the switching ability.

4. Ditopic Modules

4.1 Concept

This chapter will describe the synthesis and the investigation of the two ditopic Modules. As mentioned in the last chapter, the goal of this work was the combination of the properties of a perylene diimide with the supramolecular ability of two zwitterionic binding sites. With the interaction of those different supramolecular forces a manifold switchable functional system shall be created. At the same time the influence of the binding axis on the supramolecular assembly shall be investigated. Therefore two molecules were developed which are comparable in size and solubility. To attach the zwitterionic binding motif to the imide and the core position of the PDI, different synthetic routes were taken.

It is possible to introduce a large variety of amines at the imide position, therefore various possibilities exist to connect pyrrole and perylene for the imide linked Module. Since the GCP precursor has a carboxylic group for functionalization at the backbone, a diamine is most suitable as linker. The first amine can form an imide with the perylene dicarboxylic acid, while the second amine is then accessible for a coupling reaction with the carboxylic acid of the GCP. To enable a good solubility and some flexibility, alkyl derivatives are more suitable as linker than aromatic compounds. Therefore an ethylene diamine linker was chosen for the attachment of the pyrrole subunit. To obtain a good solubility in polar media, morpholine was chosen for the functionalization at the core position of the imide linked Module.

For the binding of the zwitterionic binding motif to the core position of the core linked Module, different possibilities exist for the connection of both subunits. A possible way is to attach an alkyne to the GCP by coupling[53] and then perform a Suzuki coupling to connect the GCP to the perylene core. This option was not chosen due to the significant influence of the alkyne unit on the spectral properties of the perylene. Additionally a lower solubility is anticipated for this alternative. Therefore a flexible linker was preferred for the attachment of the GCP, also in regard to the comparability to the imide linked Module. For the coupling with the carboxylic acid of the GCP a free amine is needed that was attached to the perylene as just mentioned. In principal it might be also possible to use a diamine linker, but Santosh and coworkers reported the facile reaction of cysteamine with PDI with extremely good yields.[54] Since the two Modules would still be comparable in size and both be connected with the GCP through a flexible linker, the cysteamine was chosen as linker between both units. To obtain a

molecule that is comparable in size with the imide linked Module, a cyclohexylamine was attached at the imide position of the core linked Module.

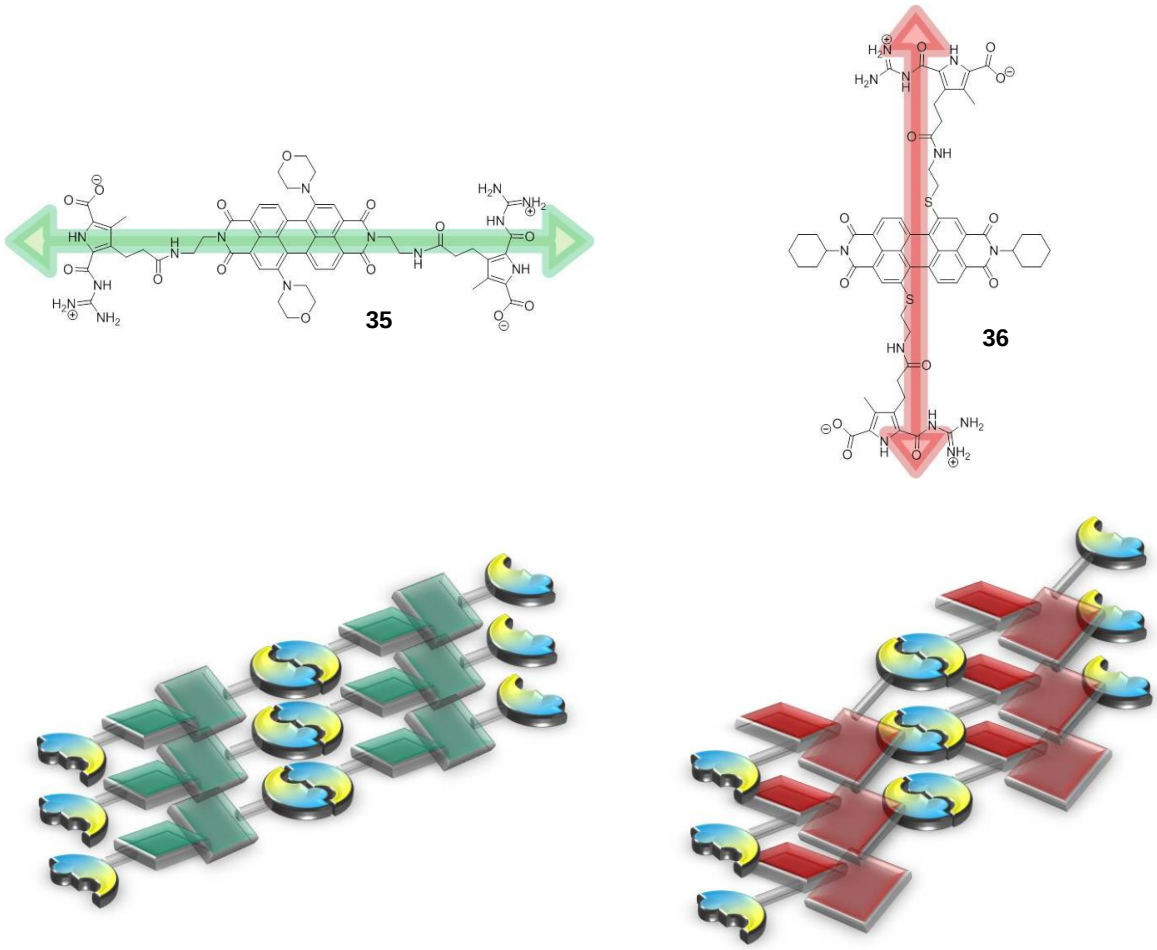

Figure 53: Imide linked Module **35** and core linked Module **36**: schematic representation and proposed aggregation.The arrow along the molecule shall illustrate the aspired binding axis.

The final molecules and the anticipated aggregation behavior are shown in Figure 53. As described in the previous chapter, a two dimensional aggregate is anticipated to form. In the following parts of this chapter, the synthesis as well as the investigation of the aggregation behavior shall be presented. Thereby particular attention will be given to the differences between the two Modules as well as the switching ability of the formed systems.

4.2 Retrosynthesis

4.2.1 Imide linked Module

For the synthesis of the ditopic Module with the binding axis along the imide position, various literature known synthesis were adjusted to fit the desired synthesic route. The principle retrosynthetic route is shown in Figure 54.

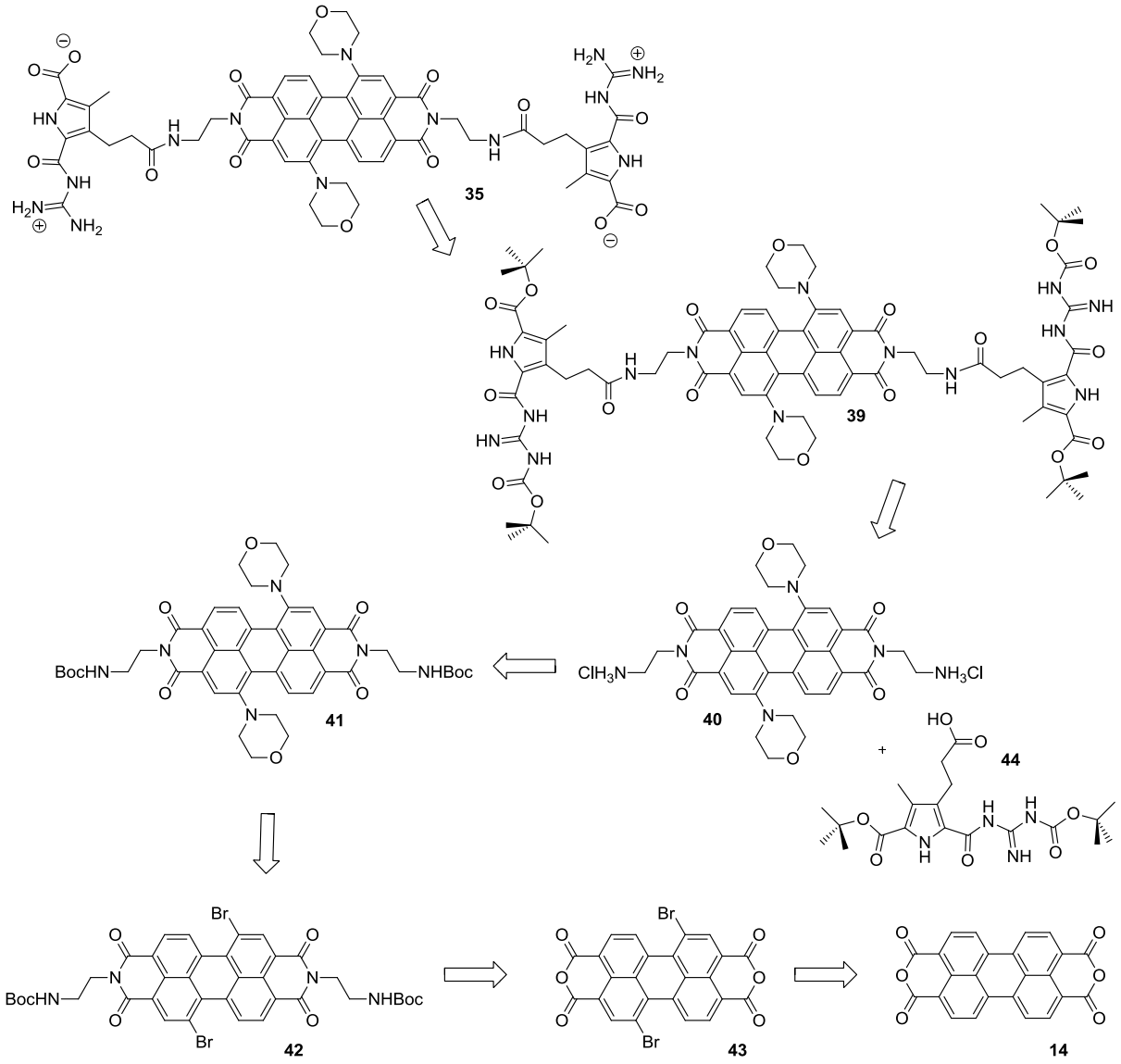

Figure 54: Retrosynthesis of the imide linked Module **35**.

To obtain a functionalized PDI dye which is still prone to aggregation, a 1,7-substitution at the core position was chosen. Therefore the synthesis was based on the literature known dibromo-perylene compound **43**.[54] To accomplish the functionalization at the imide position, the short but flexible ethylene diamine linker was introduced at the imidization step. The linker needs to be Boc-protected,

because otherwise a polymerization along the imide axis takes place. The morpholino group was inserted at the core position afterwards to ensure the solubility in polar solvents. The GCP precursor molecule **44** with the free carboxylic group at the backbone was synthesized according to literature known procedures and will not be described in detail in this thesis.[55,25] To obtain a free amine function which is required for the following coupling to the GCP precursor the Boc-protecting group needed to be removed in advance. The coupling was then followed by the deprotection of the Boc-groups of the GCP units to give the final imide linked Module **35**.

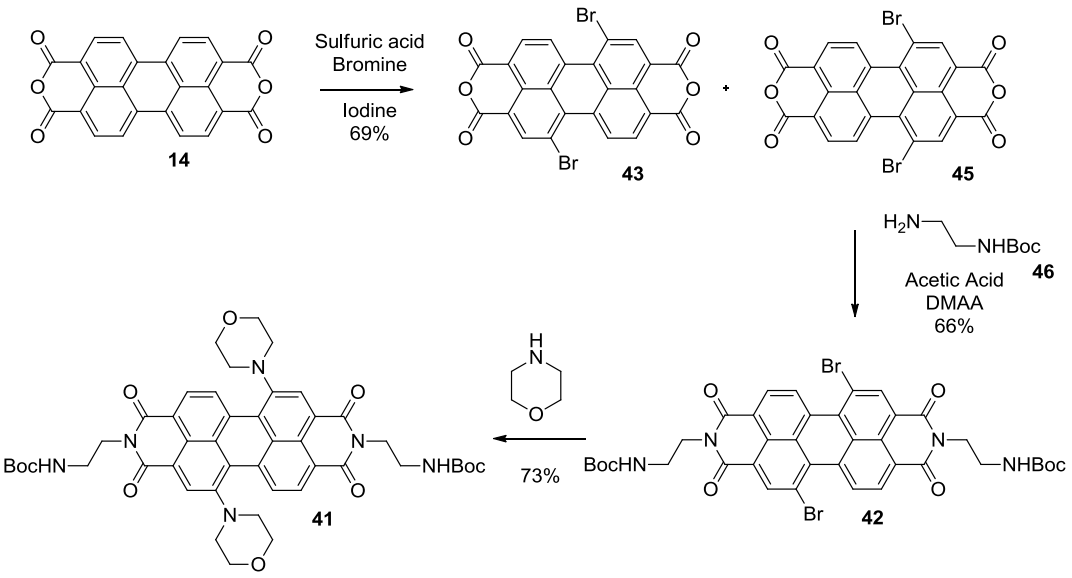

Figure 55: Synthesis of molecules boc-protected morpholine-PDI precursor **41**.

To obtain the brominated PTCDA **43**, the synthesis was performed according to literature.[54] In the first step, PCTDA **14** was dissolved in concentrated sulfuric acid and stirred at room temperature for one day to ensure the complete dissolution of the perylene dye. After 24 hours, a catalytic amount of iodine was added to the solution, the mixture was subsequently heated to 85°C and bromine added slowly. After additional 24 hours, the mixture was cooled to room temperature and the precipitate filtered off. The brick red solid was washed and lyophilized to give 73% of the mixture of the 1,6- and 1,7-regioisomers of the di-bromo-PTCDA (**43** (1,7) and **45** (1,6).

The following step was based on the synthesis of a literature known dibromo-perylene **49**, but slightly altered concerning the recrystalization step.[54] Starting material for this step was the mixture of 1,6- and 1,7-dibromo-PTCDA **43** and **45** and boc-protected ethylene diamine **46**, which was synthesized according to literature.[56] These reactants were dissolved in dimethylacetamide and acetic acid and stirred for 24 hours at 100°C. After cooling, the solution was diluted with methanol and the formed precipitate was filtered off. A chromatographic purification using dichloromethane/methanol (9:1) on

silica yielded in 72% of the 1,6- and 1,7-dibromo-perylene diimide crude product. To obtain the pure 1,7-regioisomer **42**, the commonly known repetitive crystallization method was changed. The isolated solid was dissolved in dichloromethane and methanol was added to yield in a 2:1-mixture of dichloromethane and methanol. This solution was concentrated under reduced pressure until the a precipitate started to form. The solution was then put in the refrigerator overnight to ensure a complete crystallization. The precipitate was again filtered off and the purity concerning the ratio of the regioisomers was checked by NMR-spectroscopy. The procedure was repeated when the yield needed to be enhanced or when the 1,6-regioisomer was still present, but in four out of five times this rerun was not necessary. With this very facile and fast method, 66% of the pure 1,7-dibromo-perylene-diimide **42** could be obtained which is significantly higher than the comparable yield of the established recrystalization route of 31%. One additional feature is the fact, that this step can be done at the rotating evaporator in a very time efficient manner and does not need two weeks bench time as described in the initial paper.

The synthesis of the morpholino-PDI **41** was also based on the instructions found in literature.[57] The dibromo-PDI **42** was mixed with morpholine and heated to 70°C for three days. Instead of pouring the mixture into 10% HCl for workup, morpholine was removed under reduced pressure to maintain the Boc-protecting group. The remaining solid was purified by normal phase column chromatography using 100% dichloromethane, which gave a mixture of different crude products. Therefore the solvent was changed to dichloromethane/tetrahydofurane (85:15) and with this solvent mixture it became obvious that crude product was a mixture of four substances which differ in color and retention factor. The second column chromatography resulted in a very pure green solid (**41**) in a yield of 73%.

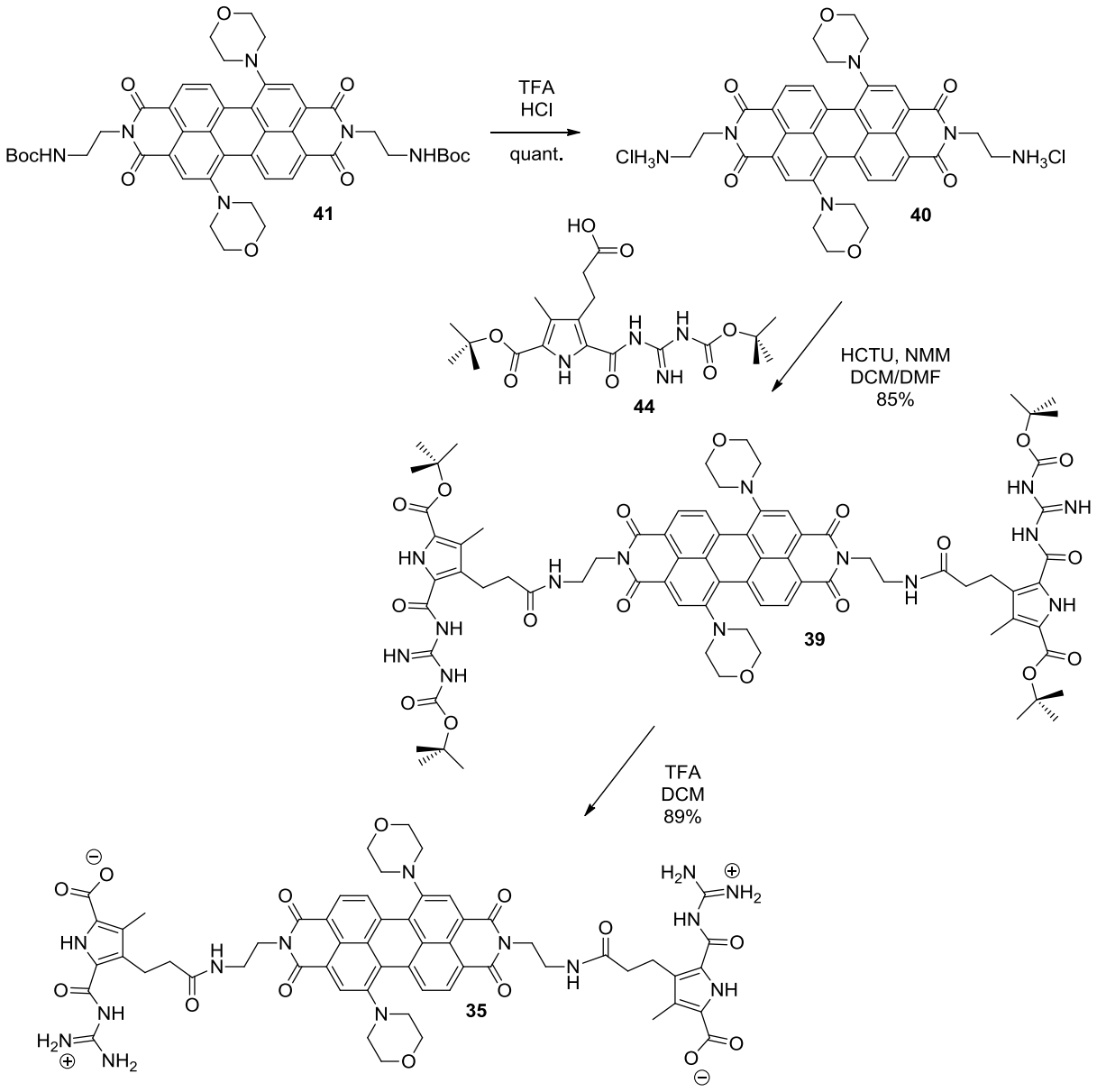

Figure 56: Synthesis of imide linked Module **35**.

In the next step, the morpholino-PDI **41** was deprotected with trifluoro acetic acid (TFA). Therefore the solid was mixed with TFA and stirred for several hours. The TFA was removed under reduced pressure, subsequently followed by the addition of 0.1 mM hydrochloric acid solution and the lyophilization of the suspension to give the hydrochloride salt **40** of the morpholino-PDI. For the coupling of the GCP-precursor **44** with the morpholino-PDI **40**, coupling conditions as known from literature were chosen for the GCP-precursor which used HCTU and NMM as coupling agents. The mixture was stirred over night and the crude product purified by column chromatography with ethyl acetate/cyclohexane (4:1) as solvent to yield in 85% of a dark green solid (**39**).

The morpholino-PDI-GCP-precursor **39** was deprotected analogue to literature which is known for the formation of the zwitterionic GCP-unit. After several steps, which included deprotection with trifluoric acid, lyophilization after the addition of 0.1 mM hydrochlorid acid solution and filtration of the crude product, the crude product was dissolved in 1 mM sodium hydroxide solution and the pH adjusted to 5.88 with 0.1 mM hydrochloride acid solution to give the desired imide linked Module **35**. The formed precipitate was again filtered to give a dark green amorphous solid (**35**) in a 89% yield.

4.2.2 Core linked Module

To obtain the ditopic Module with the binding axis along the core axis, a similar retrosynthetic route compared to the previous molecule was chosen. The synthetic pathway is depicted below.

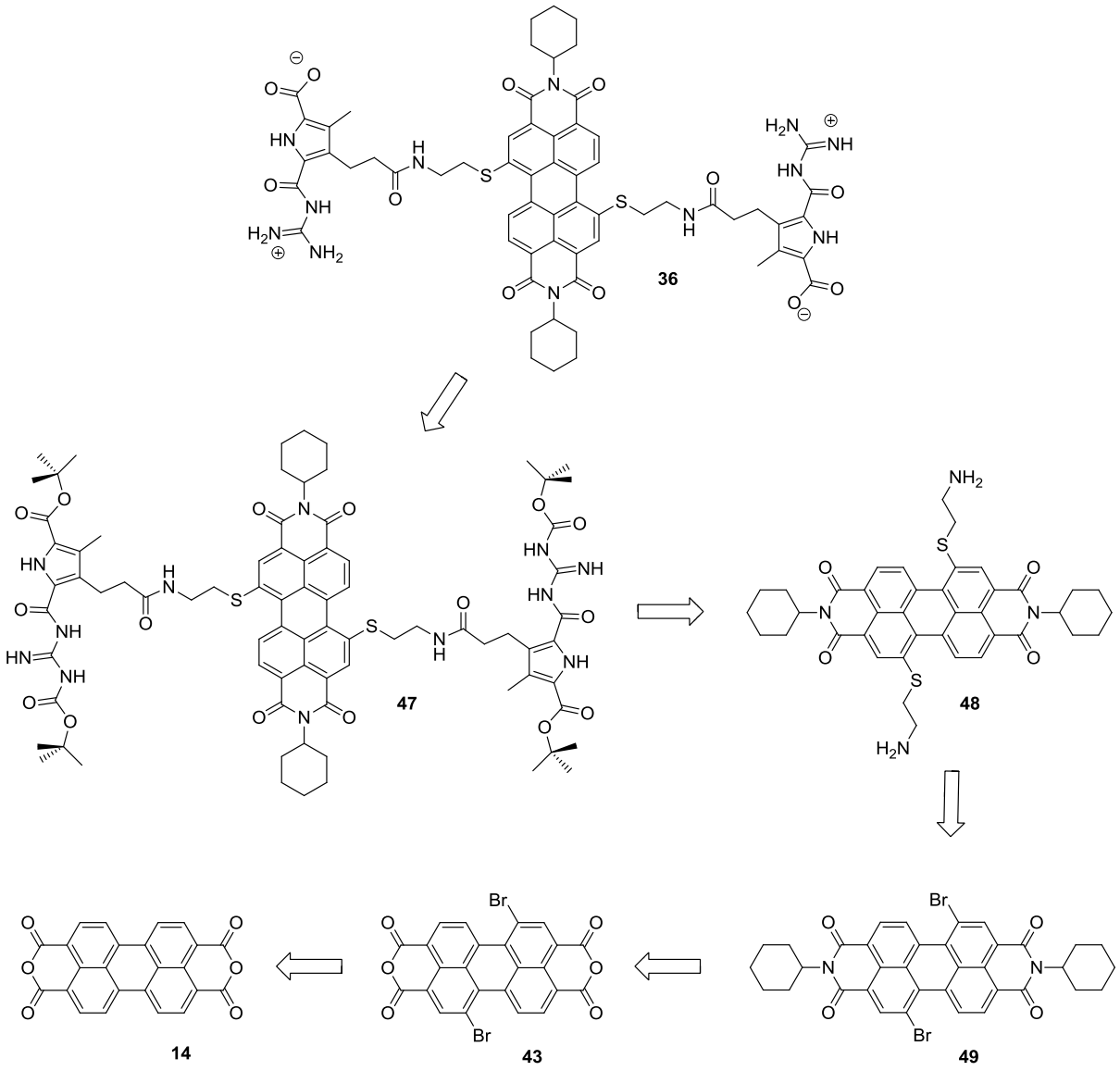

Figure 57: Retrosynthesis of the core linked Module **36**.

For the second molecule, a 1,7-substitution at the core position was also chosen to preserve the aggregation ability of the PDI. To obtain two molecules which are comparable in size, the imidization was performed with a cyclohexylamine. An amide functionality was introduced through a flexible cysteamine linker, which has been introduced by Santosh and coworkers.[58] This cysteamine linker makes a synthetic route with protecting group at the amine position unnecessary since the reaction is very selective even with a free amine group. Subsequently, the GCP-precursor was coupled with the

PDI diamine and deprotected afterwards to obtain the ditopic Module with binding axis along the core position.

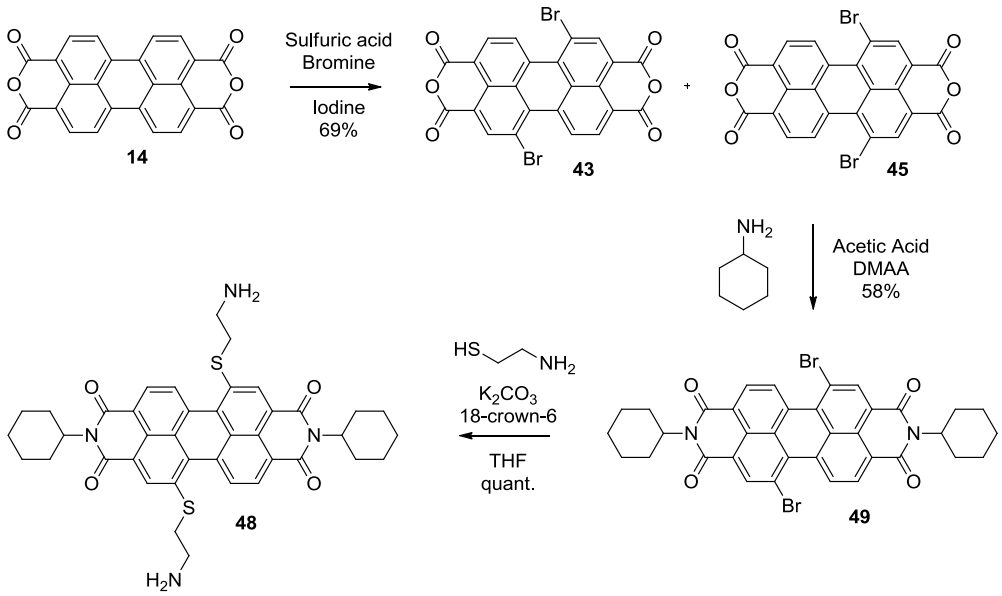

Figure 58: Synthesis of the cysteamine-PDI precursor **48**.

Since the synthesis of the dibromo-perylene has already been mentioned before, the mixture of 1,6- and 1,7-dibromoperylene **43** and **45** will act as starting material for this part. The synthesis of the perylene-cyclohexyldiimide **49** is also literature known and it was prepared accordingly.[54] The only step which was altered, was again the recrystallization as described above to yield in 58% of pure 1,7-dibromo-perylenediimide after only one recrystallization step. Compared to the reported yield in the literature of 31%, the actually synthesized yield is comparatively high, therefore it can be pointed out that the newly introduced recrystallization is significantly more efficient.

The functionalization with the cysteamine has been reported of Santosh et al. for a monotopic derivatization of the perylene core. Two obtain the ditopic cysteamine-PDI **48**, 1,7-dibromo-perylenediimide **49** was dissolved in tetrahydrofuran and potassium carbonate as well as 18-crown-6 ether were added. This was followed by the addition of cysteamine after a few minutes which resulted in a direct color change from an orange to a red solution. The slurry was stirred for 2 hours after which water was added and the mixture was extracted with dichloromethane. The solvent was removed under reduced pressure to give a quantitative yield of a shiny red substance. The ditopic cysteamine-PDI **48** has to be reacted further in a timely manner since the diamine is not stable for a long time.

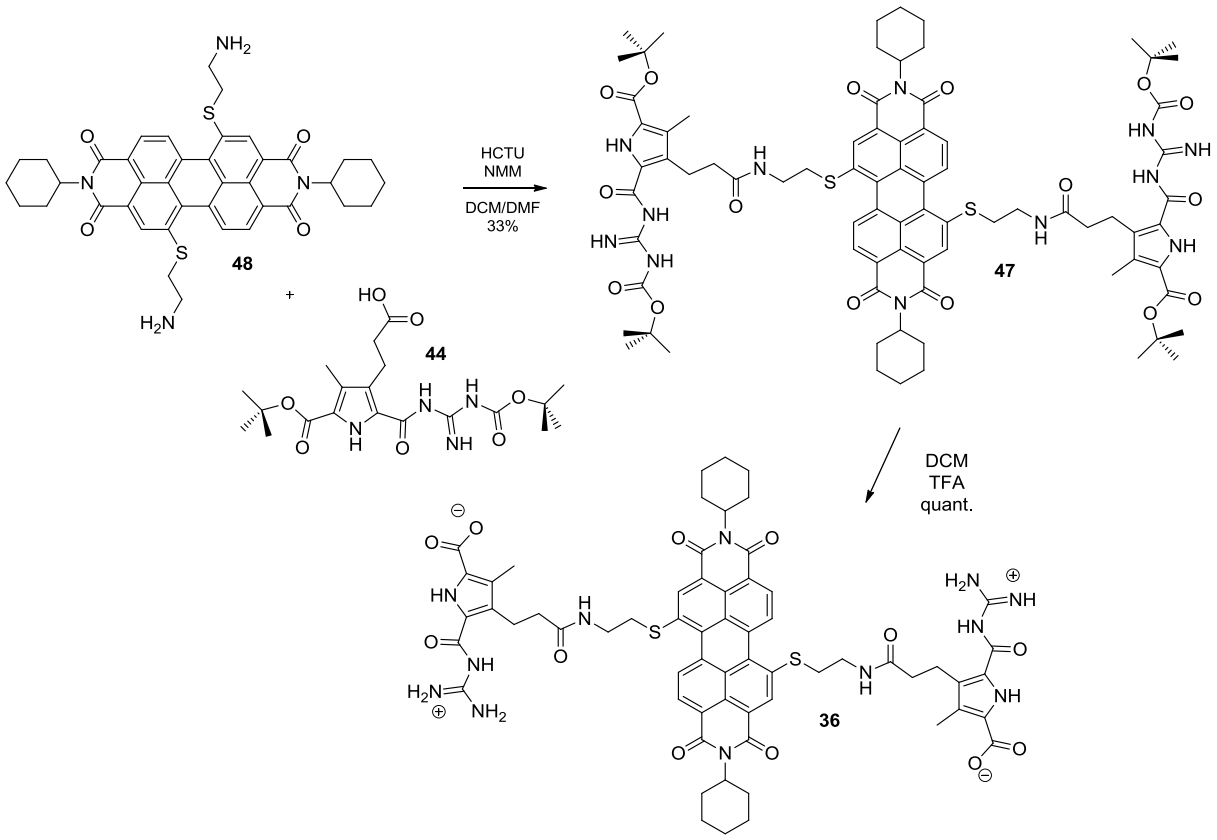

Figure 59: Synthesis of the core linked Module **36**.

The following steps were based on literature and performed the same way as for the imide linked Module **35**. For the coupling of the GCP-precursor **44** with the cysteamine-PDI **48**, also HCTU and NMM were used as coupling agents. The mixture was stirred over night and the crude product purified by column chromatography with dichloromethane/methanol (9:1) as solvent to yield in 33% of a dark red solid (**47**). The yield of the coupling of **48** with **44** is significantly lower than the yield of the imide linked Module **35**, whereby this can have different reasons. One possibility might be, that the starting material was no hydrochloride salt of the amine, because similar coupling reactions have higher yields when using the hydrochloride salt of the amine instead of the free amine. A second more plausible explanation is, that the reaction conditions lead to a side reaction of the cysteamine linker. The deprotonation of the amine can cause an intra- or intermolecular nucleophilic substitution at the perylene with the result that the amine is not accessible for the coupling any more. The next step is then the deprotection of the cysteamine-GCP-PDI-precursor **47** also analogue to the deprotection of the imide linked Module **35**, after which the core linked Module **36** could be obtained as a dark red amorphous solid in a quantitative yield.

The first goal of this thesis could be achieved by the synthesis of both ditopic Modules. It was possible to synthesize two different PDI-derivatives which are comparable in size and functional groups. The

zwitterionic GCP units are attached at the core and at the imide position to give access to different binding axes. Therefore existing PDI chemistry was altered and adapted to fit the new functional systems. The overall yield of 25% over six steps for the imide linked Module **35** and of 13% over five steps for the core linked Module **36** is also quite good compared to other PDI-derivatives. The next chapter will now investigate the supramolecular assembly behavior of both dyes.

4.3 Aggregation behavior

With the successful synthesis of both ditopic Modules the first step towards a new supramolecular system was accomplished. The following part of this chapter will now highlight the investigation of the aggregation behavior of these two molecules. Since the Modules showed only solubility in DMSO and no other solvents, all measurements were performed in DMSO and the solvent therefore will not be mentioned again each time. To dissolve the solid in DMSO, the solution had to be treated in an ultrasonic bath for one hour to achieve a complete dissolution of the Module.

4.3.1 Spectroscopy

As discussed in the conceptional part of this thesis, UV/vis spectrometry can be used to get an insight into the spectral properties of both ditopic Modules and thus in the molecular properties and aggregation behavior. Therefore various UV/vis measurements were performed to investigate their self-assembly of the ditopic Modules. For the imide linked Module an absorption maximum of 639 nm is observed in the UV/vis spectra of a 1.0 mM solution. This bathochromic shift compared to an unsubstituted perylene diimide derives from the amine substitution at the core and the electronic influence of the nitrogen. This behavior is typical for a nitrogen substituent as discussed in the conceptional part of this thesis. Since the shift of the absorption is proportional to the π-donor strength of the substituent, a strong bathochromic shift is visible in the absorption spectrum, caused by a quadrupolar charge transfer from the nitrogen to the perylene. Due to the distortion of the aromatic perylene system upon substitution as well as the strong π-donor strength of the imide linked Module, no vibronic fine structure can be observed in the UV/vis curve. The additional absorption band at 432 nm is furthermore characteristic for the $S_0 \rightarrow S_2$ transition of the dye.

The corresponding UV/vis spectrum of the core linked Module at 1.0 mM is completely different. Opposite to the nitrogen substituted PDI derivative, the spectrum of the sulfur substituted core linked Module shows an absorption maximum at 535 nm. The spectrum exhibits a slight vibronic fine structure, which is also described for other perylene diimides with sulfur at the 1,7-core positions. Shahar et al. for example reported a sulfur substituted perylene diimide derivative with an absorption maximum at 528 nm in chloroform at 0.1 mM, whereby the sulfur substituent was attached at both sides of the 1,7-PDI.[59] Since the π-donor strength of the sulfur is lower than the one of nitrogen the effect on the spectrum is also less significant with nearly no bathochromic shift of the absorption maximum compared to an unsubstituted perylene diimide. The less significant vibronic fine structure is

also a result of the substitution and not only dependent on the twisting of the perylene core but also correlates with the π-donor strength of the substituent. Therefore the $S_0 \rightarrow S_1$ transition is still clearly visible accompanied by the absorption band at 429 nm characterizing the $S_0 \rightarrow S_2$ transition.

What is rather unusual for the UV/vis spectra of the two ditopic Modules is the "monomeric" type of spectrum in both cases even though the spectra were measured at comparably high concentrations of 1.0 mM. The observed absorption maxima appear where other perylene diimides exist in their monomeric form without interactions between assembled molecules like excitonic coupling which shifts the absorption bands. Also a vibronic fine structure is still observed for the core linked Module which is usually lost upon aggregation. Furthermore the spectra were measured in polar medium for which a vibronic fine structure is highly uncommon and has only been reported for PDIs with a shielding of the perylene core by polar substituents.[60] To obtain a detailed insight into the assembly behavior of the ditopic Modules and possibly give an explanation for the observed absorption bands, concentration dependent UV/vis studies were made that are shown in Figure 60.

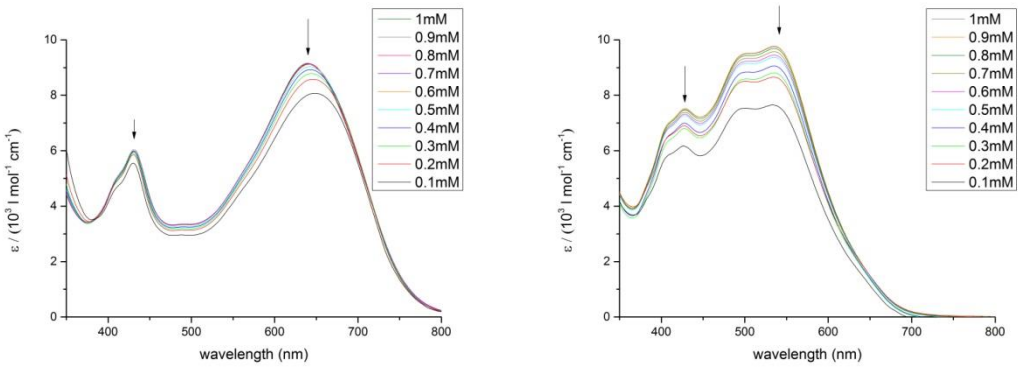

Figure 60: Left: Concentration dependent UV/vis measurements of the imide linked Module in a concentration range from 1.0 mM to 0.1 mM; Right: Concentration dependent UV/vis measurements of the core linked Module in a concentration range from 1.0 mM to 0.1 mM. The arrows indicate the spectral changes with decreasing concentration. Solvent is for both cases DMSO.

A 1.0 mM solution was diluted with DMSO to obtain various concentrations down to 2.5 µM. To cross check the results of this dilution experiment, various concentrations were obtained by direct dissolution of the respective ditopic Modules. These two approaches gave the same curves in UV/vis and therefore only the results of the dilution experiments are shown here. The dilution series from 1mM to 0.1 mM is shown in Figure 60, whereby the arrows indicate the spectral changes with decreasing concentration. Despite the difference in their original spectra, the behavior of the two ditopic Modules is very similar upon dilution. With decreasing concentration also a decrease in extinction coefficient can be observed. The absorption curve additionally shows the same shape as well as the same absorption bands upon dilution compared to the solution at 1.0 mM. A further decrease in

concentration gives the same results as in the range from 1.0 mM to 0.1 mM and is therefore not depicted.

The findings of the dilution series are rather unusual for perylene diimide assemblies. Not only the lack of a different absorption band at lower concentrations is an unexpected result, but also the decrease in extinction coefficient itself. Concentration dependent UV/vis measurements of PDI dyes normally result in an increase of extinction coefficient upon dilution. At higher concentrations, aggregated systems are the predominant species while at lower concentration, a less aggregated and therefore monomeric species is predominant. An excitonic coupling between π-systems of aggregated perylenes leads normally to a lower extinction coefficient for the aggregated species at higher concentrations. In the case of the ditopic Modules the opposite is evident, thus no decrease of extinction coefficient at higher concentrations can be observed. Additionally the lack of a new absorption band at lower respectively higher concentrations is apparent. As introduced in the conceptional part, the assembly of perylene diimides results in a change of the absorption spectrum due to the π-π-stacking of the perylene core units depending on the aggregation type. While a J-type stacking leads to a bathochromic shift, an H-type stacking of the perylene diimides results in a hypsochromic shift of the absorption bands. A possible explanation for the lack of an additional absorption band as well as the decrease of extinction coefficient upon dilution might be, that the ditopic molecules do not form assemblies at the reported concentration range. This explanation is not very plausible though, since the large aromatic core of the perylene diimide is not stabilized in the polar environment and therefore has a high tendency to aggregate due to a solvophobic interaction. The absence of a new absorption band could also be explained by the lack of a direct perylene-perylene contact and therefore a lack of π-π-stacking in the assembly. This leads to the conclusion, that the aggregation is somehow different to previously reported PDI assemblies. It may further be noted that temperature dependent UV/vis measurements give the same results as concentration dependent measurements.

To identify the principal aggregation mechanism, an analysis of the concentration dependent UV/vis measurements was performed according to the theory described in the conceptional part of this thesis. This analysis is based on the values of the extinction coefficient of the maximum absorption band for both ditopic Modules at 639 nm respectively 535 nm. These values were plotted as a function of the dimensionless concentration as explained in the conceptional part of this thesis and then fitted by a nonlinear regression analysis according to equation (4) which is shown in Figure 61.

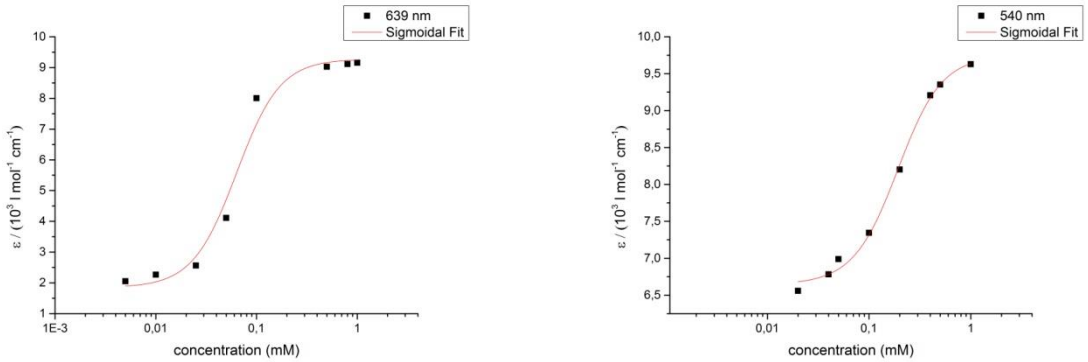

Figure 61: Extinction coefficients of the maximum absorption band upon dilution plotted as a function of the dimensionless concentration. Left: Curve for the imide linked Module with a maximum absorption band at 639 nm; Left: Curve for the core linked Module with a maximum absorption band at 540 nm.

The data points can be perfectly fitted by equation (4), so an isodesmic aggregation mechanism can be stated. The fitting curves of both ditopic Modules furthermore look very much alike. This means, that even though the decrease in extinction coefficient itself is unusual for PDI assemblies, the isodesmic aggregation mechanism is also known for other PDI assemblies. Also the principal shape and the maximum absorption bands of the ditopic Modules are similar to reported PDI assemblies.

4.3.2 Microscopy

To get further insight into the aggregation behavior of the two ditopic Modules, AFM measurements were performed at different concentrations. Therefore solutions with different concentrations were spin coated at 60 rps for 1 min onto a freshly cleaved mica surface. The AFM measurements of the imide linked Module will be discussed first, since the principle molecular build-up is more comparable with conventional PDI-derivatives with additional binding motifs which were designed to form supramolecular assemblies.[36, 38] The AFM images for the imide linked Module at higher concentrations show a complete surface coverage. Since these images do not allow to draw any conclusions regarding the aggregation behavior, they are not depicted below. Therefore lower concentrations of the Module were investigated which are shown in Figure 62.

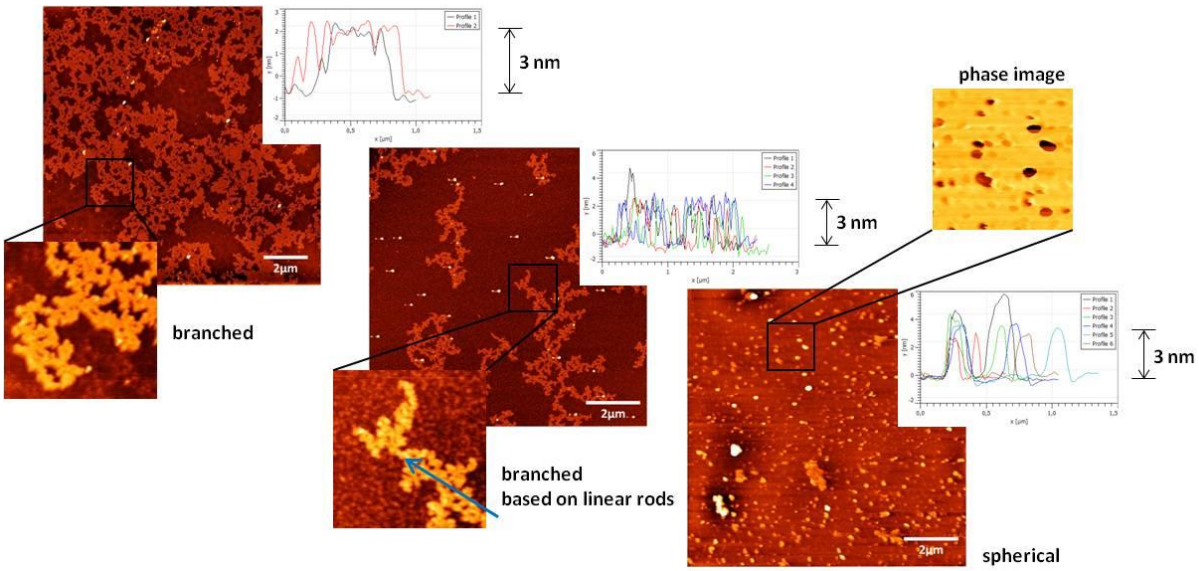

Figure 62: AFM height measurements of the imide linked Module at various concentrations in DMSO and the respective height profiles. The magnified parts also show height measurements unless otherwise mentioned. Left: Concentration of 0.5mM; Middle: Concentration of 0.25mM; Right: Concentration of 0.1mM, the magnification depicts the phase image of the respective AFM measurement.

To distinguish between background and aggregate in the pictures of the AFM measurement, it shall be mentioned that the surface is colored dark red while the aggregates are light red to orange. The left height image in Figure 62 shows the AFM measurement at a concentration of 0.5 mM. A sponge like structure can be observed on the surface. Magnification further reveals a branched aggregate with a height of about 3 nm. This principle structure can also be found at lower concentrations of 0.25 mM which is depicted in the middle of figure. The surface is not as crowded as at 0.5 mM, but the branched, network like structure can also be observed. The magnification reveals that these interlinked structures are based on a linear motif. Since the images do not reveal straight or rigid strings, a flexible assembly can be anticipated that might also coil on the surface. Assuming that the imide linked Module builds up polymeric aggregates, these structures can be explained by an interlacing of these linear strands to form a entangled network at the measured concentration. The height profile of the respective AFM images also give a height of 3 nm while the width of the aggregates is decreasing compared to the 0.5 mM solution. If the concentration is lowered even further to 0.1 mM, circular as well as irregular aggregates can be observed in the AFM height image. These irregular aggregates look like agglomerates of spherical particles. The average height of the aggregates is also 3 nm. The AFM phase image of the 0.1 mM solution does not give a hint on a vesicle formation, since no corona can be observed around the circular aggregate in the AFM of the imide linked Module. Due to the small size of the circular aggregate compared to other literature known PDI assemblies, it is most likely that the aggregates are build-up in a micellar fashion. It can

furthermore be mentioned that it is likely that the assemblies at different concentrations have the same principle build-up, since they exhibit a similar height at all investigated concentration.

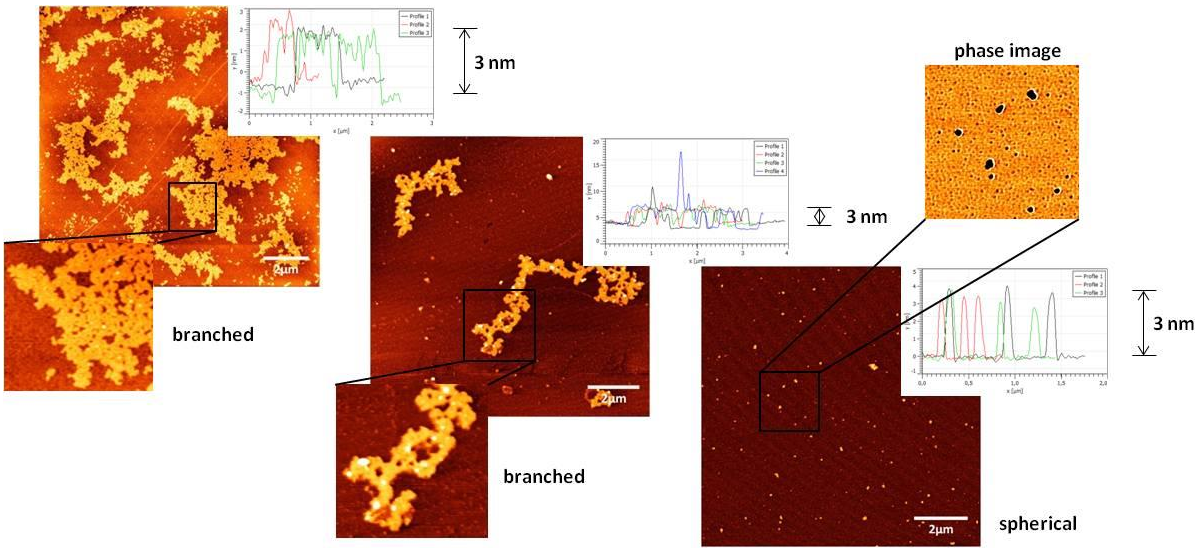

Figure 63: AFM height measurements of the core linked Module at various concentrations in DMSO and the respective height profiles. The magnified parts also show height measurements unless otherwise mentioned. Left: Concentration of 0.5mM; Middle: Concentration of 0.25mM; Right: Concentration of 0.1mM, the magnification depicts the phase image of the respective AFM measurement.

In comparison to the imide linked Module, the AFM measurements of the core linked Module look very much alike at first sight. At a concentration of 0.5 mM also sponge or network like structures can be observed. The branching cannot be observed as clearly as for the imide linked Module, since the aggregates look far more compact. It seems like the aggregates have the same principal structure but with a tighter packing of the main aggregate leading to denser assemblies. An additional similarity of the two Modules is the height of the aggregates of about 3 nm at a concentration of 0.5 mM. These branched aggregates are also found at lower concentrations of 0.25 mM. Opposite to the AFM image of imide linked Module at 0.25 mM, a basic linear motif is not clearly visible for the core linked Module. A possible explanation might be a tighter packing of a possible polymeric basic motif as already mentioned above or the formation of three dimensional polymers. The height profile gives also an average height of 3 nm. At a concentration of 0.1 mM, the assembly also changes into circular aggregates. Due to height profiles in which only sharp peaks could be observed for each sphere and the lack of a shoulder which is usually attributed to a vesicle formation, it can be stated that micelles are formed. The height profiles further show a similar height for the aggregates of approximately 3 nm.

In summary, both ditopic Modules form similar assemblies which look like network like structures and are probably based on a linear motif. This would indicate that both Modules form a polymeric assembly as basic assembly motif. The size of the aggregate additionally suggests that the

assemblies of both Modules have a similar build-up. This is a very crucial result of this work because it gives a hint on the influence of the binding axis in PDI assemblies. These findings indicate that both binding axes are equally suitable to build up supramolecular assemblies and that the built up aggregate is not dependent on the binding axis.

All reported assemblies were found on mica, which is a layered silicate that has a charged surface. To investigate if the aggregates also form on a neutral surface and are not only a result of a charge induced arrangement on the surface, measurements on silicon surfaces were performed. To obtain a better resolution than with AFM, helium ion microscopy (HIM) was used to investigate the aggregates. The measurements were performed by Henning Vieker, with a Carl Zeiss Orion Plus ®. The helium ion beam was operated between 36 kV and 37.4 kV acceleration voltage at currents below 0.5 pA. Secondary electrons were collected by an Everhart-Thornley detector at 500 V grid voltage. Working distances of 7-8 mm were used. To obtain the samples for HIM, a 0.25 mM solution of each Module was spin coated at 60 rps for 1 min onto a freshly cleaned silicon surface. The results of the measurements are shown in Figure 64.

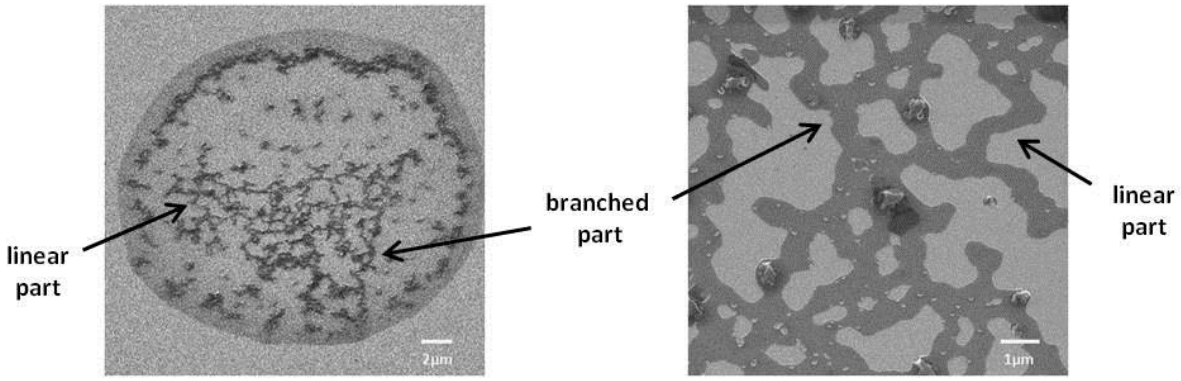

Figure 64: HIM measurements of the ditopic Modules at 0.25 mM in DMSO. Left: Imide linked Module; Right: Core linked Module.

The left picture for the imide linked Module is depicted to give an overview while the right image for core linked Module shows the detailed image. In the HIM pictures, the background is colored in grey while they aggregates are black or dark grey. On the image of the imide linked Module, a round shape can be observed on the surface whereby the black aggregate is found within that space. These circular spots were found in all HIM measurements of the ditopic Modules. The shape derives from the formation of small droplets on the silicon surface that are anticipated to form due to repulsion of the DMSO solvent and the unpolar surface. After evaporation of the solvent, circular spots remain on the surface. The aggregates within these spots show branched structures for both Modules, whereby the assembly is clearly based on linear aggregates. In the right image of core linked Module, linear

strands are clearly visible, which was not that explicitly observable in the AFM images. Since the height of the aggregates is not distinguishable in HIM measurements, no comparison can be made with the AFM measurements. In principal similar assemblies can be observed for both Modules with different microscopic methods. Thus it could be shown, that the formation of the assemblies is not dependent on the surface.

4.3.3 Assembly mode

In the following part, the basic aggregation mode will be discussed to distinguish which assembly is formed by the Modules. Summarizing the previous parts of this chapter, some results can be highlighted. The measured UV/vis spectra as well as the position of the absorption bands of both Modules are in good accordance with literature known PDI derivatives with nitrogen respectively sulfur at the core. The curves show in both cases a "monomeric" spectral shape even though they were measured at comparably high concentrations of 1 mM. Additionally, no shift of the main absorption band and an unusual decrease in extinction coefficient can be observed upon dilution. Microscopic measurements further reveal that assemblies are formed even at lower concentration than 1 mM. The lead aggregate that was be clearly observed in the range between 0.2 and 0.7 mM is a branched structure which is based on a linear motif. All reported assemblies were found to be 3 nm in height and the aggregates were furthermore very similar for both Modules.

Now the question arises, how the results of the measurements can be underlined with a theoretical model. As pointed out in the conceptional part of this thesis, PDI assemblies are mainly based on the π-π-interaction between perylene cores, leading to a linear elongation along the z-axis. This π-π-stacking may be prevented by large substituents, but for both ditopic Modules, no sterical hinderance is anticipated. With the involvement of a binding motif, the aggregation was reported to additionally elongate along the axis of the binding motif. So in summary, an assembly along the x- and z-axis may be expected for our created system which is depicted as a model in Figure 65. Therefore a calculation of a test system regarding the elongation in x- and z-axis was made. A chain of 3 core linked Modules was stacked 4 times to yield in an assembly of 12 molecules. All calculations were performed by Willi Sicking from our working group with Maestro V 9.3 and minimized with MacroModel V 9.9. The conformation analysis with 1000 cycles was calculated with a OPLS_2005 force field and water as solvent.

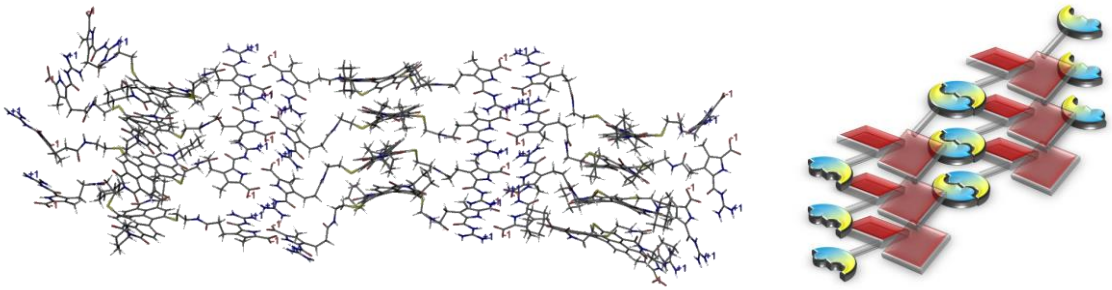

Figure 65: Left: MM-calculation of the homotopic assembly of 12 molecules of the core linked Module; Right: Model for the homotopic assembly with 6 molecules of the core linked Module.

As a result from the calculation of the "conventional" PDI assembly, it can be stated that the formation of the assembly is possible in principle. The calculation in Figure 65 shows a tightly packed assembly which elongates in two dimensions. The assembly is 2 nm in width and of unknown dimension in the other two dimension. The width is thereby not in good agreement with the height profiles of the AFM measurements which showed a height of about 3 nm. If the elongation of the aggregation is somehow limited in the dimension of the PDI-PDI stacking, it still might be possible that an aggregate of 3 nm in height would be formed. What is more important, is that this kind of assembly does not explain the behavior in UV/vis based on literature data of related PDI derivatives. The π-π-stacking between the Modules in the proposed assembly should result in an increase of extinction coefficient upon dilution and in a shift of the absorption band upon deaggregation. Since this behavior is not reflected by the measurements, it would strongly argue against the formation of this assembly.

In the next step it shall be discussed, if an assembly can be found, that explains all results of the measurements up to this point. It was reported in the previous chapter, that the zwitterionic dimer can also aggregate by π-π-stacking to form extensive linear assemblies.[22] Due to the planar nature of the zwitterionic dimer, it might be possible that PDI core and zwitterionic dimer could interact by π-π-stacking. The principle question that therefore has to be raised is concerning the stacking mode of both subunits and if a heterotopic stacking of the electron deficient perylene and the electron rich zwitterionic dimer can take place. Looking at literature known examples on the assembly of mixtures of electron deficient PDIs and other electron rich units, normally a self sorting into the homotopic assembled nanostructure is predominant. For example Meijer mixed a perylene diimide and a Oligo(*p*-phenylene vinylene) (OPV) to observe a self sorting process into separate homotopic aggregates for both molecules.[61] These nanostructures showed no alternating order of the electron rich and electron deficient unit. It is possible though, that such homo-aggregates can further assemble to form ordered structures of electron rich and electron deficient nanostructures.[62, 63] Therefore the stacking of perylene and zwitterion dimer seems unlikely at first sight.

Since the UV/vis measurements give a hint that no perylene π-π-stacking is involved in the assembly, it strongly argues towards an involvement of the zwitterionic dimer in the assembly. Merschky proposed an alternating stacking of PDI and GCP zwitterion dimer in his dissertation.[53] Based on the different behavior in temperature dependent UV/vis studies in neutral and anionic state of the investigated molecule, he stated an alternating stacking of perylene core with zwitterionic dimer. He based his assumptions on the results of the UV/vis measurements where the anionic version of the molecule - in which the zwitterionic dimer is not assembled - showed temperature dependent changes in UV/vis. The neutral and therefore aggregated molecule showed nearly no change in UV/vis which points to an involvement of the zwitterion dimer in the stacking. This lead to the conclusion that the GCP zwitterion dimer is stacked between two perylene subunits.

To check whether it is possible in principle to form a heterotopic aggregate of perylene diimide and zwitterion dimer, a control experiment was carried out. For that purpose, the assembly of two model substances was investigated. Therefore the behavior of both substances was studied separately and then in a mixture. The perylene diimide model substance is molecule **50**, which has been synthesized according to the synthesis of the core linked Module. For the GCP model substance, a precursor molecule from the synthesis of the GCP was deprotected to form the zwitterionic version **51**.

Figure 66: AFM height measurements of the respective molecules at 0.25 mM in DMSO. Left: Molecule **50**, Middle: Combination of **50** and **51** in a 1:1 ratio; Right: Molecule **51**.

The AFM measurements of molecule **50** reveal the formation of linear aggregates at 0.25 mM in DMSO. These strings look a lot like the structures found for the imide linked Module. **51** on the other side forms predominantly spherical aggregates in DMSO, whereby also some irregular aggregates can be found. The AFM height image of the 1:1 mixture of both molecules is distinctively different to the separately observed aggregates. Neither linear nor spherical aggregates can be found in the measurements of the mixture. The images show the formation of discrete discoid structures that are evenly distributed on the surface. These results show that it is indeed possible to form co-aggregates

of the electron deficient perylene diimide and the electron rich zwitterion dimer and that not always a self-sorting into the homotopic aggregate occurs.

As a starting point for further discussion, the most probable structure for one ditopic molecule was calculated. The structure was minimized and at the energetic minimum an intramolecular zwitterion-dimer with a loop like structure was formed as expected. Within this monomer, the intramolecularly formed zwitterion-dimer stacks on top of a perylene core. In the following two of these monomeric loops where stacked onto each other with zwitterion dimer-perylene contact and MM calculations were performed for both Modules.

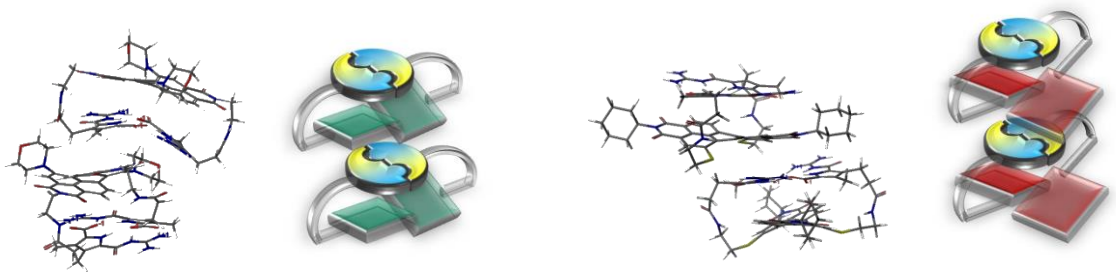

Figure 67: Left: MM-calculation and model of the heterotopic assembly of two imide linked Modules; Right: MM-calculation and model of the heterotopic assembly of two core linked Modules

This calculation leads to two stable dimers which give a ABAB-type of aggregation with an alternating arrangement of perylene and zwitterion dimer depicted in Figure 67, whereby A stands for the zwitterion dimer and B stands for the perylene. A stacking of several of these monomers in a AB-contact manner leads to a linear aggregate, whereby perylene and zwitterion-dimer are arranged in an alternating manner. This kind of assembly results in an isolated PDI core which is stacked between two zwitterionic dimers. Due to the lack of a π-π-stacking between the perylene cores, no shift in the spectral curves would be anticipated upon dilution. Additionally this kind of assembly can explain the vibronic structure in the UV/vis spectrum of the core linked Module due to the isolated perylene core. The π-π-stacking of the perylene core with the zwitterionic dimer might furthermore lead to a charge transfer interaction between both units which could explain the unusual decrease in absorption upon dilution.

The width of the calculated assembly is 1.5 nm for both ditopic Modules. Recalling the results of the AFM measurement that gave a height of about 3 nm, a double string of the heterotopic linear assembly could explain this value. A possible point to enable the interaction of two strings is the amide functionality of the linker moieties that connect GCP and perylene core. The formation of H-bonds between two linker moieties of adjacent rods can then lead to the assembly of a double string. In

principal it is possible that more than two strings assemble, since the linker moieties are located at both sides of the molecule. The circumstance that only a double string is formed needs therefore further evaluation.

Even if this assembly is not based on a direct PDI-PDI interaction, the usual PDI stacking modes observed in other systems shall be used for descriptional purposes, since also a π-π-stacking of perylene and zwitterion dimer takes place. Therefore the arrangement of the ditopic Modules can be described as J-like aggregates, since only one half of the perylene core is involved in the π-π-stacking with the adjacent zwitterion dimer. Looking at both PDIs of the formed dimers, they are arranged in an H-type position relative to each other, but with a significant offset. Though this arrangement, two sides can be distinguished in this heterotopic aggregate. On one side, the linker moieties which contain the amide functionalities are in near vicinity to each other while on the other side linker moieties are far apart. When stacking more of these dimers on top of each other, an alternating arrangement of the units can be seen.

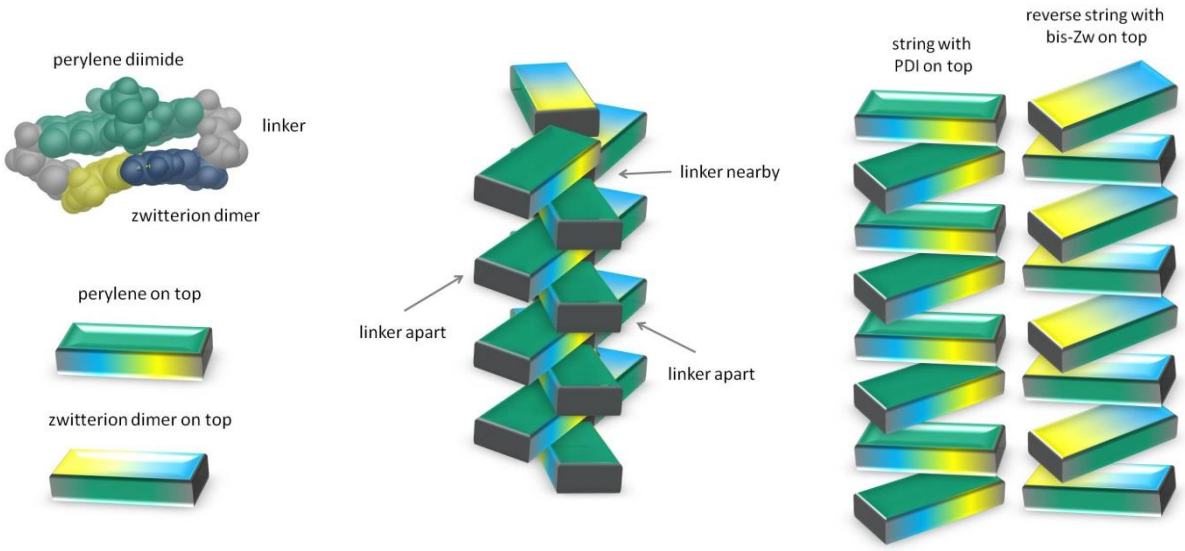

Figure 68: Schematic representation of the formed double string. The ditopic Modules form an intramolecular loop (left scheme: perylene diimide marked in green, zwitterion dimer marked in yellow-blue, linker moiety marked in grey) that further aggregates in a way similar to an H-type stacking. The loops are not stacked in the middle of the molecule like similar PDI assembly, but with a significant offset. Caused by this offset, one side of the heterotopic aggregate has the linker moieties, which are able to form H-bonds with another linker moiety, nearby while the other side has the linker moieties apart (scheme in the middle). Two strings where the linker moieties are oriented nearby can then form a double string. This only only possible though when one of the strings is oriented upside down compared to the other one, so the linker moieties are arranged in the right manner (right scheme). The green surface means that the loop is arranged so the perylene diimide subunit is on top while the yellow-blue surface means that the zwitterionic dimer is on top.

When arranging two of these strings, whereby the first polymer is arranged bottom up and the second polymer the other way around, a double strand can be formed. This arrangement is necessary, because the inside amides are facing in the same direction and can form hydrogen bonds with the adjacent amides of the second string since the linker units are in near vicinity. The amides on the other side of the string are too far apart to form H-bonds with a second string though. This proposed assembly is shown in Figure 68. To check whether this model is a sufficient explanation for the assembly of the Modules, MakroModel calculations were performed.

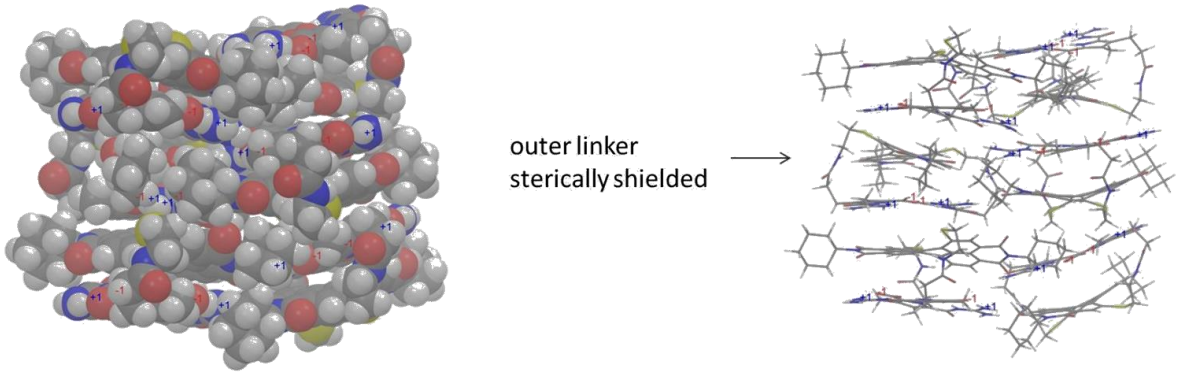

Figure 69: MakroModel calculation of the core linked Module, whereby 6 molecules are arranged to form a double string (left:: stick and ball, right: molecular representation). The outer linkers are thereby sterically shielded by neighbored cyclohexyl groups of the next molecule whereby the inner linkers form H-bonds with the adjacent string.

The core linked Module was arranged in the proposed manner and indeed forms a double string which is shown in Figure 69. The calculations reveal a stable formation of a double string whereby the outer linker is sterically shielded by adjacent cyclohexyl groups of the next molecule. Therefore it is unlikely that a further aggregation with another string takes place. Nonetheless it is possible that an intramolecular interaction comparable to protein folding takes place, which would explain the coiled structures on the mica surface since the other amide functionalities face outwards. The calculated aggregate has a width of 3 nm, so the measured height of 3 nm in AFM can be explained by two assembled strings. Therefore the proposed aggregation would be in good accordance with the AFM measurements.

In summary, the alternating stacking of perylene and zwitterion dimer for the ditopic Modules explains all results found in the measurements and can therefore be stated as principle aggregation mode for both ditopic Modules. The position of the perylene, isolated between two zwitterion dimer, leads to a "monomeric" UV/vis spectrum with a lack of spectral changes upon concentration variation. Since the principal structure is a rod formed by two assembled strings, the linear structures found in AFM are also explained by this model. What is remarkable though, is that both Modules form the same type of

assembly even though the binding motifs are attached at different positions in the molecule. This is an important result since it shows that the assembly of the investigation systems is independent of the position of the binding motif. The anticipated elongation along the y-axis, which was proposed in the conceptional part of this thesis, could not be obtained. This is due to the stacking of the binding motif in between two perylene cores that yielded in a sole elongation along the z-axis. This heterotopic assembly is unique to the reported ditopic Modules and has not been reported for other perylene diimide systems yet.

4.3.4 Aging of the core linked Module

During the investigation of the aggregation behavior of the ditopic Modules some unexpected observations were made for the core linked Module were made. Since UV/vis and AFM measurements were rechecked at least twice to be sure that the reported findings can be reproduced, all measurements were repeated after one week with the same solution from the previous week as well as a fresh solution. In the case of the imide linked Module no differences could be observed, whereas the investigation of the core linked Module gave surprising results. While the fresh solution gave the same results as one week before, the aged solution showed a completely different behavior. Therefore the next part of this chapter will describe the aging behavior of the core linked Module.

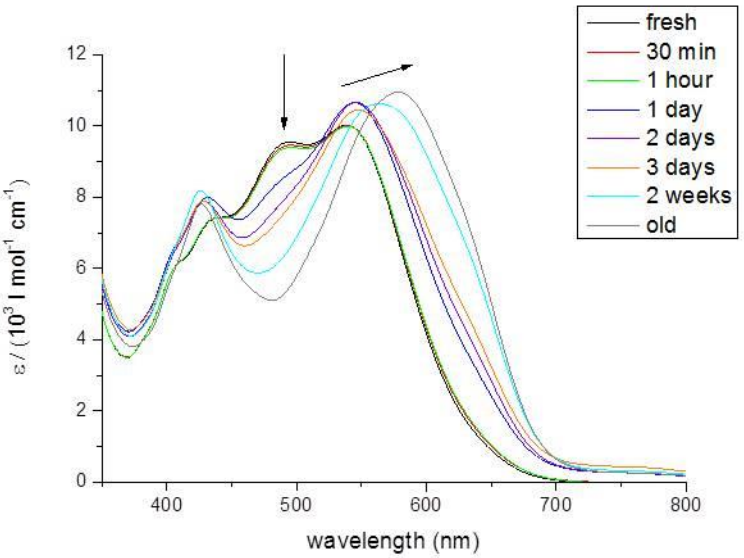

Figure 70: UV/vis spectra of the core linked Module at 0.25mM in DMSO after different time periods.

To investigate the change upon aging, time dependent UV/vis measurements were made. Therefore the same solution was measured after different time periods. A bathochromic shift of the maximum absorption band from 535 nm to 578 nm is observed with increasing time span. The vibronic fine structure is also vanishing with increasing time, which means that the band at 495 nm is decreasing. The shift of an absorption band as well as the loss of vibronic structure indicates a change in aggregation with involvement of the perylene core upon aging. As mentioned earlier, a significant vibronic structure in the UV/vis spectrum is acquainted with a monomeric, not aggregated PDI unit. If a change in the UV is observed, it can be probably connected to a change in aggregation of the PDI units. The maximum absorption band will shift, depending on the aggregation type. Keeping these arguments in mind, the bathochromic shift of the maximum absorption band indicates the formation of a J-aggregates for the aged core linked Module.

Sharar et al. investigated the aggregation behavior of a bis-mercaptopropionic acid derivative of perylene diimide **52** (bis-MPA-PDI).[59] They reported a solvent dependent UV/vis measurement, which was performed in chloroform and water. The spectrum which was measured in chloroform shows a distinct vibronic fine structure, which is completely lost in the case of the measurement in water. They assumed that the spectrum of the bis-MPA-PDI in chloroform reflects the disaggregated state, while the spectrum in water reflects the aggregated state of the bis-MPA-PDI.

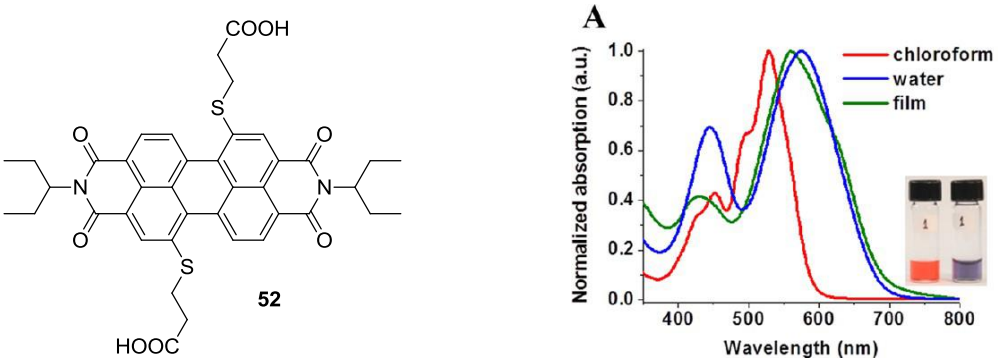

Figure 71: UV/vis spectra of PDI **52** in aggregated (aqueous media) and disaggregated (chloroform) state at 0.1mM. Reprinted with persmission of C. Shahar, J. Baram, Y. Tidhar, H. Weissman, S. R. Cohen, I. Pinkas, B. Rybtchinski, ACS Nano **2013**, *Vol. 7, No. 4*, 3547-3556.[59]

When the time dependent spectra of the core linked Module and the solvent dependent spectra of the bis-MPA-PDI are compared, it is obvious that they correlate very well. Since the principal aggregate of the core linked Module has a kind of monomeric assembly because of the alternating stacking of PDI and Zw-Dimer unit, it might be possible that this assembly somehow changes during time to yield in an assembly where perylene cores have direct contact to each other. To investigate the change in aggregation further, AFM images were measured of 0.25mM solutions after different time spans. The measurements shown in Figure 72 were made with the same solution which was kept over that time period, but measurements with different solutions which were kept the same time span the gave same results.

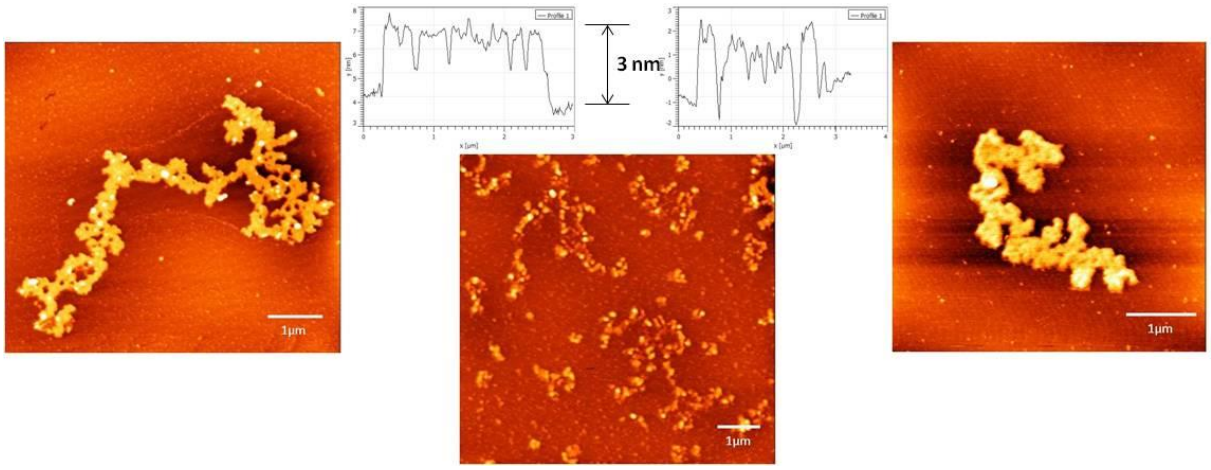

Figure 72: AFM height images and height profiles of the core linked Module at 0.25mM in DMSO. Left: Fresh solution; Middle: same solution after 1 week; Right: same solution after 1 month. The height profile on the left belongs to the fresh solution while the height profile on the right belongs to the aged solution. Both show a height of 3 nm.

The AFM images depict different aggregates at different time periods. The fresh solution shows branched structures based on linear as already reported in the previous part of this chapter. After one week a change into disordered structures that look like agglomerates of spherical particles can be observed. The AFM measurements of the 1 month old solution show again details of branched and linear and therefore similar aggregates like in the fresh solution. The height profile of AFM picture of a fresh solution shows aggregates that are 3 nm in height while the height of the aggregates in the aged solution is also about 3 nm. This means that not only the AFM images of the aged solution are similar to those of the fresh solution, but also the height profiles with a height of approx. 3 nm are comparable. Therefore it can be assumed, that the aggregates are built up in similar way. This assumption would also predict the formation of linear aggregates for the aged core linked Module. Furthermore the measurements show a distinct change in aggregation from the fresh solution to the one week old solution and from the one week old solution to the one month old solution which hint to a rearrangement of the aggregates.

In principal, there are different possibilities to arrange two core linked Module monomers. The basic aggregation mode of the core linked Module was already reported earlier. In this case, the perylene-core and the zwitterionic GCP-dimer are stacked in an alternating manner to give a polymeric strand. This heterotopic assembly can be designated as ABAB-assembly. The second possibility to arrange the two dimer is a ABBA-alignment. Each perylene core is then stacked on top of a second perylene core and the zwitterionic GCP-dimers face outwards. A linear aggregation of the assembly also includes a BAAB-alignment where two zwitterion dimers are in direct contact to each other. This rearrangement would lead to a homotopic assembly.

To evaluate, if this homotopic assembly can explain the results of the measurements, MakroModel calculations were made for all aggregation possibilities. For the calculation of the ABBA-assembly both stacking possibilities need to be accounted for, the perylene/perylene contact (ABBA) as well as the zwitterion dimer/zwitterion dimer contact (BAAB).

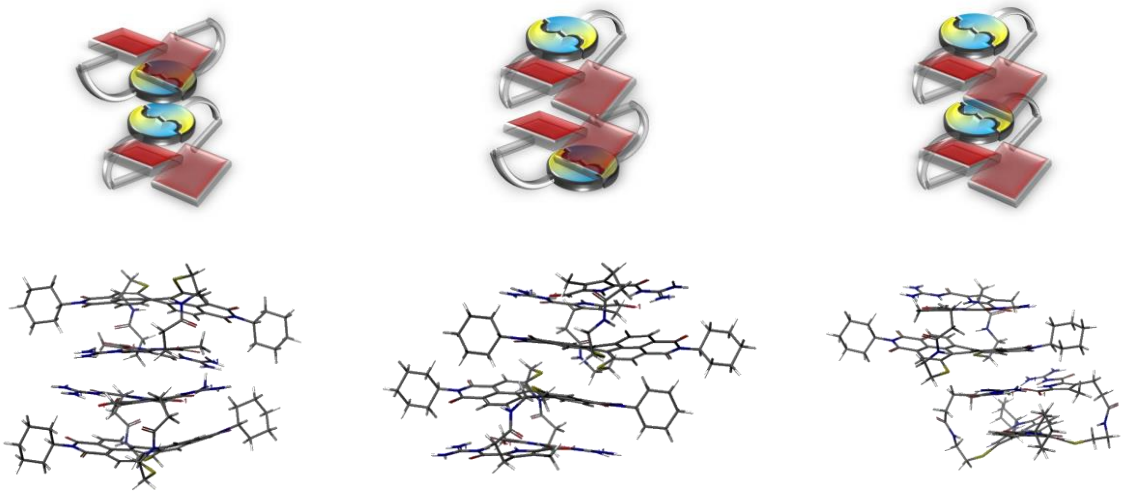

Figure 73: Models and MM-calculation of different respective arrangements with: Left: zwitterion dimer/zwitterion dimer contact (BAAB); Middle: perylene/perylene contact (ABBA); Right : zwitterion dimer/perylene contact (ABAB).

The different possibilities are shown in Figure 73. MakroModel calculations with the focus on the zwitterion dimer/zwitterion dimer contact give the energetically least stable conformation. Compared to that, the conformation with perylene/perylene contact is significantly more stable with an energetic difference of - 45.04 kJ/mol. The alternating aggregation structure is with - 10.23 kJ/mol energetically less stable than the conformation with perylene/perylene contact but still more stable than conformation with the zwitterion dimer/zwitterion dimer contact. This means that the zwitterion dimer/zwitterion dimer-assembly (AA) is slightly disfavored compared to the zwitterion dimer/perylene-assembly (AB) while the perylene/perylene-assembly (BB) is significantly more stable.

For a theoretical comparison of these values in the next step, a trimer is considered. If this trimer would be composed of Modules in an alternating arrangement, the double value of the zwitterion dimer/perylene stacking would be - 20.46 kJ/mol. Compared to that the combination of perylene/perylene and zwitterion dimer/zwitterion dimer contact - to yield in a type of homo-assembly - would give a value of - 45.05 kJ/mol and therefore be more stable than the hetero-assembly. The realistic energetic values would of course differ to those just mentioned, but this theoretical consideration gives a first hint which assembly version is the most stable for the Modules.

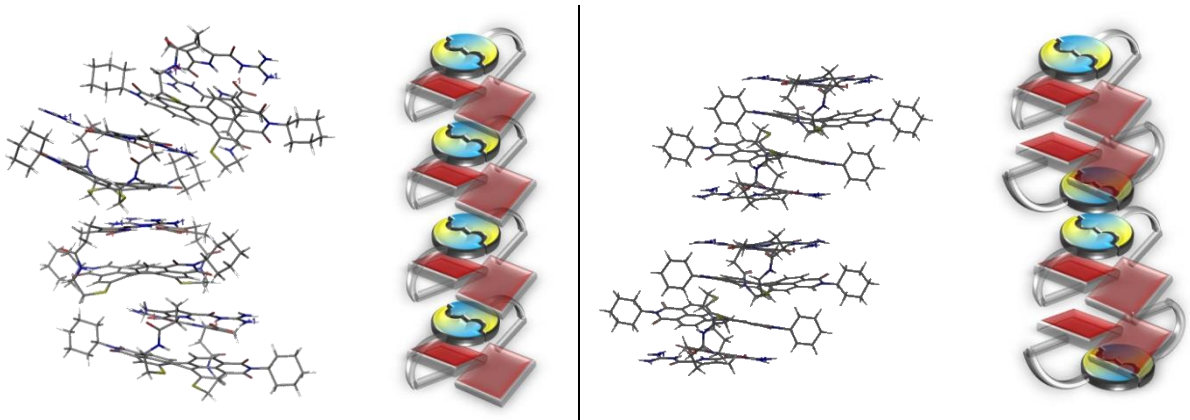

Figure 74: MM-calculation and models of: Left: heterotopic ABABABAB-assembly; Right: homotopic ABBAABBA-assembly; for the core linked Module.

The calculation of four subunits shown in Figure 74 gives a further insight and a more solid basis to compare both assemblies. The MM-calculation of the ABABABAB-assembly gives the energetically less stable structure. Opposite to that, the calculation of the ABBAABBA-assembly gives an energetic difference of - 60.13 kJ/mol. These results lead to the conclusion that an aggregate in the heterotopic assembly mode is less stable then the homotopic assembly. The side view of the ABBAABBA-assembly reveals an offset of both perylene units with partial overlap of the aromatic core. This is commonly known as formation of a J-type aggregate, which explains the bathochromic shift of the aging core linked Module. To change from the ABAB to the ABBA-assembly, the subunits would have to rearrange, causing a transition state where no clear assembly could be observed in AFM. The width of the calculated homotopic aggregates is also 1.5 nm, which explains the structures found in AFM also with the formation of a double string.

Since the ABABABAB-assembly does not form the most stable aggregate, it is assumed to be the kinetically controlled aggregation. The ABBAABBA-structure on the other side does form the most stable aggregate according to MM calculations, probably because of the stabilizing contribution of the perylene-perylene interaction which overweighs the destabilizing contribution of the zwitterion dimer/zwitterion dimer-stacking. With these two assumptions in mind, the change in UV/vis and AFM measurements upon aging can be explained by the transition from the kinetically controlled to the thermodynamically controlled assembly. This kind of time dependent change in aggregation is a highly unique feature of the Module introduced in this thesis. A possible explanation for the initial formation of the kinetically controlled aggregate is the repulsion of the zwitterionic dimer units upon aggregation. As reported earlier, the zwitterion dimer/zwitterion dimer interaction is the least stable one and will not form preferential. If the two units approach in an unfavorable way, an electrostatic repulsion of the

units might add to the already disfavored assembly and push them away from each other. When this repulsion additionally overweighs the stabilizing contribution of the perylene-perylene-assembly, this can lead to the kinetically favored formation of an ABAB-aggregate.

While the core linked Module showed remarkable changes over time, the imide linked Module did not exhibit such behavior. To clarify the question, why no aging behavior was observed for the imide linked Module, the same calculations as for the core linked Module were made. Therefore two Modules were again stacked in three possible arrangements: zwitterion dimer/zwitterion dimer-contact, perylene/zwitterion dimer-contact and perylene/perylene-contact.

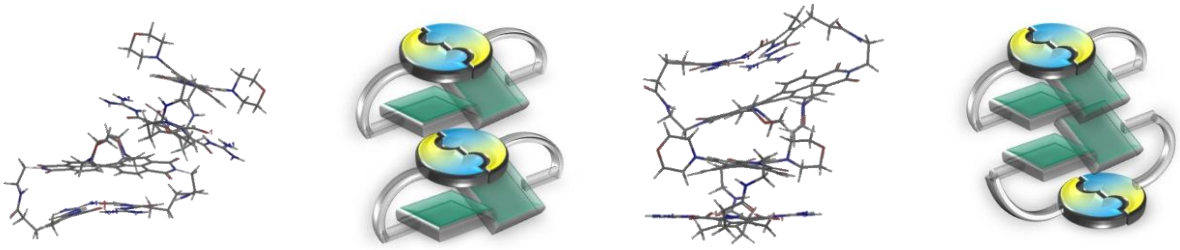

Figure 75: Models and MM-calculation of different respective arrangements with: Left: zwitterion dimer/perylene contact (ABAB); Right: perylene/perylene contact (ABBA).

The first possibility with zwitterion dimer/zwitterion dimer-contact surprisingly converted into perylene/zwitterion dimer upon conformational minimization. Therefore it is safe to state, that this arrangement is the least stable one. Comparing the other two arrangements, the one with perylene/zwitterion dimer-contact is more stable than the one with perylene/perylene-contact. It can therefore be concluded that an alternating arrangement is more stable for the imide linked Module and hence the thermodynamically formed assembly. This additionally indicates that no rearrangement is needed since the most stable arrangement is already formed from the beginning.

4.4 Switching ability

While the previous part of this chapter concentrated on the principal aggregation type, this part will highlight the switching ability of the Modules. As mentioned in the conceptional part of this thesis, the principal idea of this thesis is the creation of switchable supramolecular systems. Therefore different stimuli should be applied to the synthesized Modules to see if changes of the assembly occur. In the last chapter, concentration dependent changes were already observed for both Modules. For the core linked Module additionally a very unusual time dependent change of the aggregation mode was investigated. While concentration dependent changes are generally known for supramolecular systems, this thesis wants to apply other stimuli to specifically target the two functional units in the Modules, GCP and PDI. The zwitterionic GPC unit is prone to a switching of the formed assembly with acid and base. The addition of acid protonates the carboxylic acid while the addition of base leads to a deprotonation of the guanidinium unit, both resulting in a loss of the dimeric GCP assembly. As second switchable motif, perylene diimide is incorporated in the Modules. While the conventional change in assembly for perylenes is controlled by concentration, temperature or solvent polarity, a novel switching was reported by Baram and coworkers.[50] The addition of sodium dithionite leads to a formation of a radical anionic species of the perylene accompanied by a loss of the initial assembly. A more detailed description of both switching possibilities for GCP and PDI was given in the conceptional part of this thesis. This thesis will now investigate the aggregation behavior with addition of acid, base and sodium dithionite.

4.4.1 Acid and Base

In the first part, the switching of the ditopic Modules with acid and base will be investigated. As well as in the previous part of this chapter, the first step of investigation will be the measurement of UV/vis-spectra to have a detailed insight into the switching ability of the Modules. Therefore a 0.25 mM solution of both Modules was treated with varying amounts of acid and base. To enable also AFM measurements which can be related to the corresponding results in UV/vis, the measurements were performed with TFA and TEA instead of the commonly used hydrochloric acid (HCl) and sodium hydroxide (NaOH). In earlier trials with HCl and NaOH, AFM measurements were significantly influenced by salt formation where only salt crystals could be found in the images instead of actual aggregates of the substance.

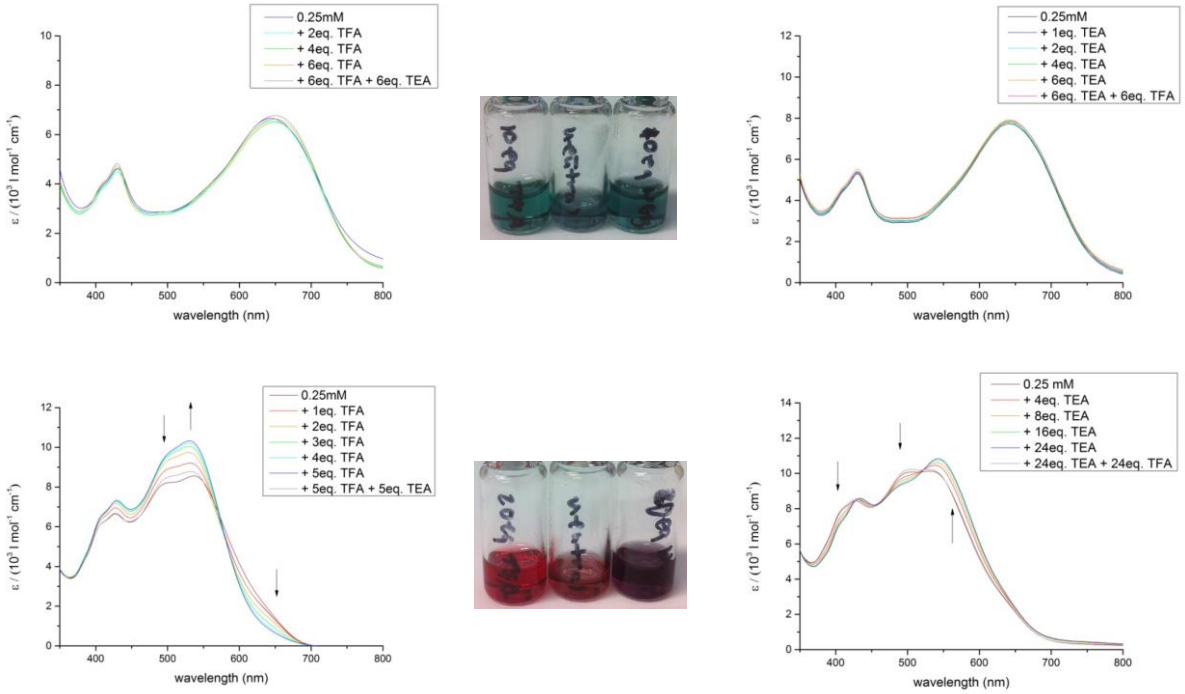

Figure 76: UV/vis spectra of the imide linked Module (above) and the core linked Module (below) with acid and base and pictures of color change with addition of acid and base at 0.25 mM in DMSO. Above left: Measurements with acid; Middle: Pictures of the neutral solution (middle) and with addition of acid (left, 10 eq. TFA) and base (right, 10 eq. TEA); Right: measurements with base. Below left: Measurements with acid, Middle: Pictures of the neutral solution (middle) and with addition of acid (left, 20 eq. TFA) and base (right, 20 eq. TEA); Right: Measurements with base.

At first sight, it is obvious that both Modules behave differently upon addition of acid and base. Whereas the UV/vis bands of the imide linked Module show no change, the bands of the core linked Module are significantly altered. This corresponds with the results of the aging investigation, when the imide linked Module also did not exhibit any change in UV/vis. So, either no change in assembly is occurring for the imide linked Module upon addition of acid and base or a possible change in aggregation does not lead to spectral changes.

As just mentioned, the core linked Module exhibits spectral changes upon addition of acid and base. With the addition of acid, the color of the solution turns into a light red, whereby the maximum absorption band reveals a loss of vibronic fine structure as well as a slight hypsochromic shift from 535 nm to 530 nm. These results suggest the formation of an H-aggregate in the acidic solution. Upon addition of base, the color of the solution turns into a more purple shade, which is comparable with the color of the aged solution of the core linked Module. This color change is attributed to a bathochromic shift in the UV/vis with an absorption maximum at 543 nm. This spectral change could be attributed to a formation of a J-aggregate in basic solution. The initial absorption band is reformed upon addition of

the respective amount of acid or base, therefore it can be concluded that the switching of the Module is reversible.

To take a closer look into the aggregation behavior upon switching, AFM measurements were performed. Therefore solutions with a concentrations of 0.25 mM were treated with 10 equivalents of TFA respectively TEA and then spin coated at 60 rps for 1 min onto a freshly cleaved mica surface.

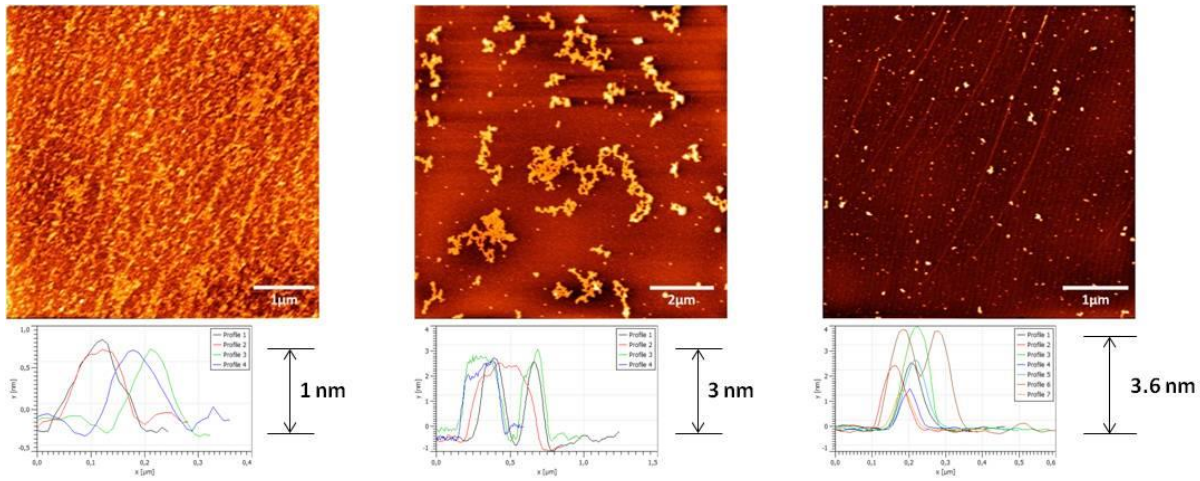

Figure 77: Aggregation behavior of the imide linked Module in DMSO upon addition of acid and base at 0.25mM. Left: Addition of 10 equivalents TFA; Middle: Addition of 10 equivalents TFA and 10 equivalents TEA afterwards to restore the zwitterionic dimer; Right: Addition of 10 equivalents TEA.

Opposite to the behavior in UV/vis, the AFM height image of the imide linked Module exhibit a change in aggregation upon addition of acid and base. In principal, a rearrangement to circular aggregates can be observed for both cationic and anionic imide linked Module in Figure 77. The AFM images presumably depict micelles, because no hint of vesicle formation can be found in the phase images of the corresponding measurement. The AFM measurements of the acidic solution shows a nearly complete surface coverage whereby the particles are evenly distributed. The height profiles of the cationic imide linked Module reveal assemblies that are 1 nm in height, whereby the actual height is anticipated to be slightly higher since particles might lie in the void in between two other particles due to the high surface coverage. For the basic solution of the Module, isolated spherical particles can be observed in the AFM images. The height profiles of the anionic Module give a size of the aggregate of a multiple of 1.2 nm, respectively 2.4 nm and 3.6 nm.

To investigate, if the switching process is reversible, the ionic solutions were brought to pH 6.58 again. A reformation of the initial branched assembly can be observed upon addition of same equivalents base to the cationic Module. The same applies for the anionic imide linked Module upon addition of acid, which means that two statements can be made after the AFM measurements. First of all, a

change in assembly upon addition of acid and base is clearly visible in the microscopical images opposite to the UV/vis measurements. Secondly, the switching process is found to be reversible for the imide linked Module. The AFM images of the core linked Module shown in Figure 78 reflect the results of the UV/vis measurements.

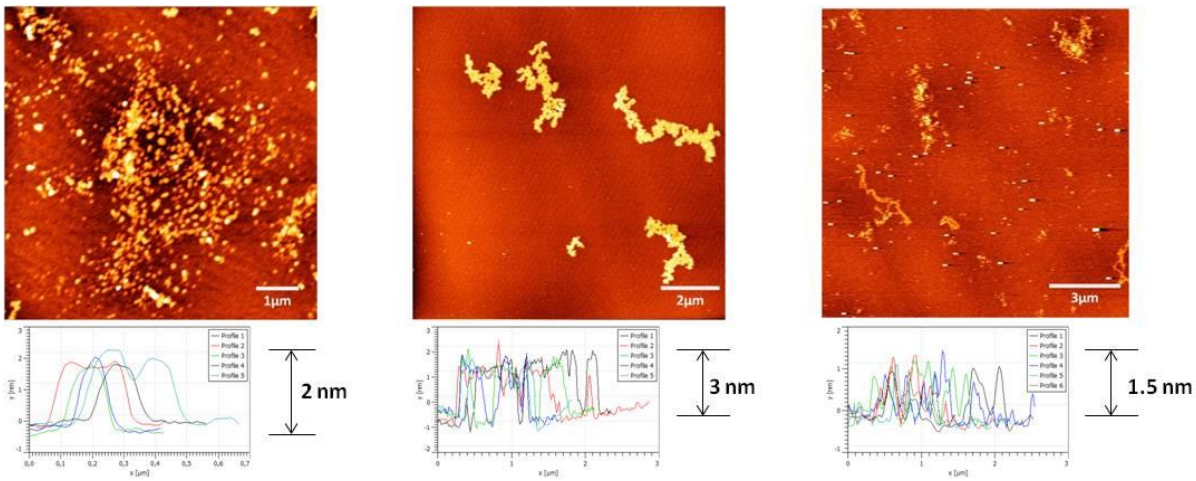

Figure 78: Aggregation behavior of the core linked Module in DMSO upon addition of acid and base at 0.25mM. Left: Addition of 10 equivalents TFA; Middle: Addition of 10 equivalents TFA and 10 equivalents TEA afterwards to restore the zwitterionic dimer; Right: Addition of 10 equivalents TEA.

Similar to the results of the imide linked Module, a rearrangement into circular aggregates can be observed upon addition of acid or base. The phase images of the same measurements give also no hint of a vesicle formation, so it is safe to assume that a micellar assembly is formed. The height profiles of the measurements show aggregates in an acidic milieu that are about 2 nm in height and aggregates in an alkaline milieu that are about 1.6 nm in height. The different height of the aggregates would suggest the formation of different aggregates for the basic case like the results of the UV/vis measurements hinted. Thereby the formation of an H-aggregate for the cationic Module and a J-aggregate for anionic core linked Module was implied. Upon addition of the respective amount of acid or base, the initial assembly is restored, so a reversible switching can be stated.

As well as in the general aggregation studies, HIM measurements were performed to investigate the aggregate formation on a neutral silicon surface. These measurements are depicted in Figure 79.

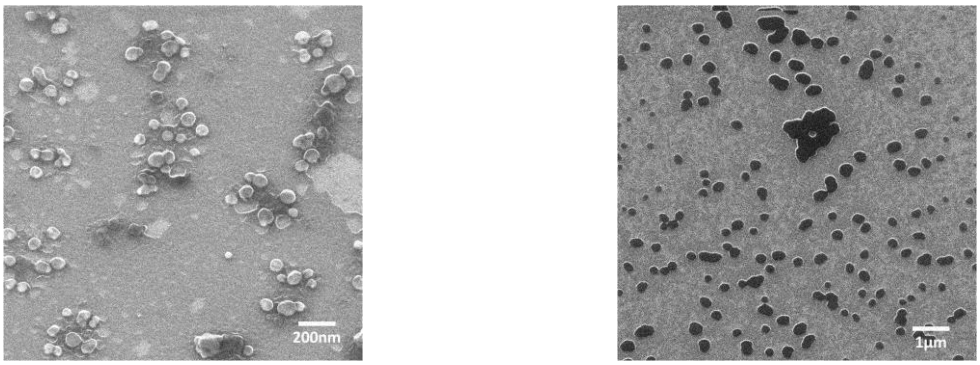

Figure 79: HIM pictures of the imide linked Module (left) and the core linked Module (right) at 0.25 mM in DMSO with 10 equivalents TFA.

Both measurements were performed of the acidic solution of the Module at a concentration of 0.25 mM. In the left image of the imide linked Module, white dots can be observed. These spots are probably salts and the dark spots of the measurement are the aggregates. The HIM pictures show circular aggregates in both cases. It is obvious that the core linked Module forms more distinctive aggregates upon addition of acid which correlates with the AFM measurements. Again it was observed that the two Modules form similar aggregates.

Up to this point, it can be stated that both Modules show similarities upon addition of acid or base as well as some differences. The microscopic images depict circular aggregates for all switching possibilities while the height profiles and images themselves do not match. Results of the UV/vis studies further highlight the difference between both Modules. While the core linked Module shows a significant spectral change upon addition of acid and base, the imide linked Module does not show any spectral change upon switching. Now the question arises how these findings can be explained.

For the core linked Module the shift in absorbance can be explained best by π-π-stacking in the newly formed aggregate which requires a direct perylene-perylene contact in the assembly. The protonation respectively deprotonation of the Module gives two GCP units with the same charge which are in near vicinity due to the alternating arrangement of perylene and zwitterion dimer in the initial assembly. The repulsion of the nearby charges leads to a rearrangement so that the charged pyrrole groups point outside of the assembly enabling a π-π-stacking of the perylene cores. Since the charges are located in different parts of the GCP molecule, a repulsion can result in different arrangements of the Modules and therefore a different aggregation type. Recalling the results of the UV/vis measurements, the spectral changes implicate the formation of an H-aggregate for the cationic core linked Module due to a hypsochromic shift of the maximum absorption bands and a bathochromic shift for the anionic core linked Module suggesting the formation of a J-aggregate. A model of the two assembly types is shown in Figure 80.

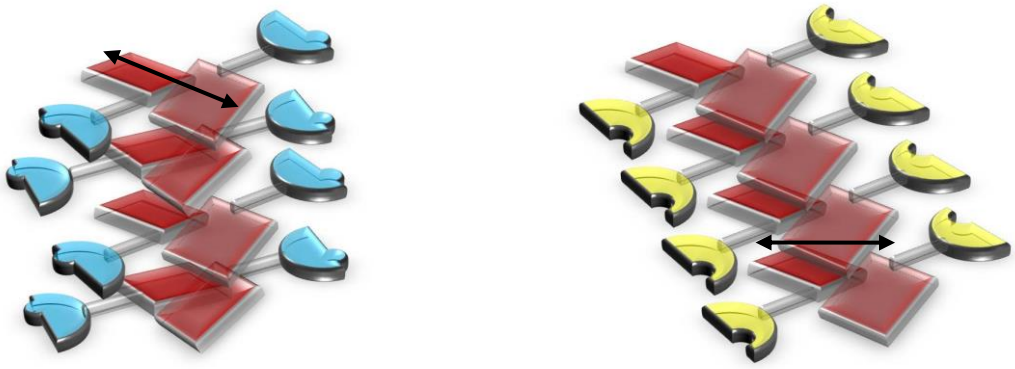

Figure 80: Left: Cationic core linked Module that is anticipated to form an H-aggregate; Right: Anionic core linked Module that is anticipated to form a J-aggregate.

To find out if the measures of the molecule in the respective aggregate can be brought in agreement with the AFM measurements, MM-calculations were performed. The calculation of a dimer of the cationic core linked Module is shown in Figure 81 and reveals the measures of the molecule in x- and y-axis. The H-aggregate is 3 nm in length along the y-axis from GCP to GCP-unit and 2 nm in width along the x-axis from cyclohexyl to cyclohexyl. The calculated size of 2 nm in the x-axis fits the height of the assemblies in the AFM measurements perfectly when a micellar build up is assumed. Since the J-aggregate is arranged offset, the overall width is not characterized by the distance from cyclohexyl to cyclohexyl but in a diagonal fashion like shown in Figure 80. This can explain the smaller height of the formed aggregates when also micelles are formed. With a stacking distance of 3.9 Å for the H-aggregate and 3.8 Å for the J-aggregate, the distance between the perylene cores is relatively large. Due to this large stacking distance, only slight changes in absorption occur upon π-π-stacking which is in good accordance with the UV/vis measurements.

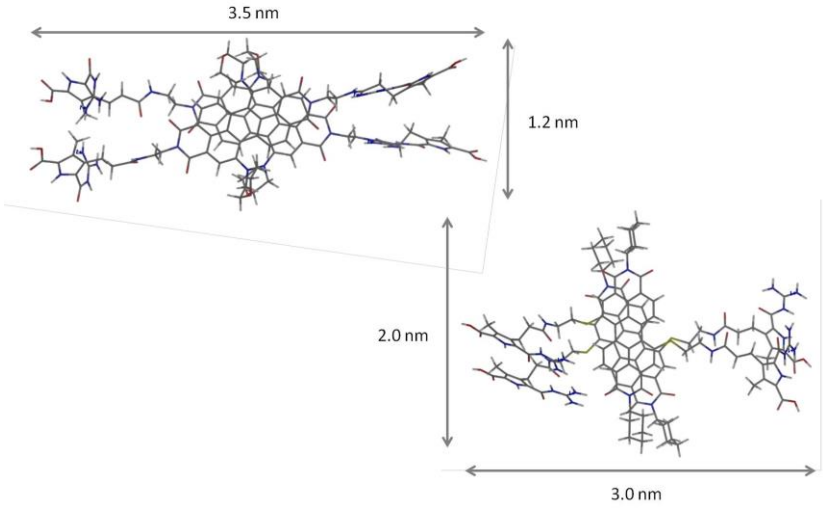

Figure 81: MM-calculation of the cationic imide linked Module (left) and the cationic core linked Module (right) with dimensions.

After it has been clarified which type of assembly is formed by the core linked Module upon switching of the GCP unit, the imide linked Module will be highlighted in detail. Opposite to the distinct spectral changes of the core linked Module upon addition of acid and base, the UV/vis measurements of the imide linked Module did not reveal any changes. The results therefore do not give a hint, if a switching is possible for the Module and furthermore if a different assembly is being formed. The AFM images in contrast reveal the formation of spherical assemblies and therefore a significant change upon switching. The height profile further show that the assemblies themselves are significantly smaller then for the other Module. The question now arises how to reconcile these results. Like for the core linked Module, MM-calculations were performed with a straight alignment of the Module shown in Figure 81.

This calculation reveals that the distance between the outmost point of the two opposite morpholine groups is 1.2 nm. With that width in mind, the microscopical measurements can be explained by the formation of micelles in the acidic case and spherical multilayer aggregates in the basic case. From the explanations regarding the aggregate formation of the ionic core linked Module, the same conclusions may be drawn to explain the aggregation behavior of the imide linked Module upon switching. The MM-calculations reveal two cationic Modules that are stacked with a rotational offset which is known for an H-type stacking. Since an H-aggregate is stacked without longitudinal offset, the width of the aggregate is in agreement with the width of the stacked molecule. Therefore it is anticipated that the imide linked Module does also form H-aggregates in the acidic case. The AFM height profiles in the basic case show aggregates that are multiple of 1.2 nm in height and therefore also match the calculated width. Thus, the relative height of the aggregate compared to the calculated width differs from the results of the core linked Module, where the height of the J-aggregate was smaller than of the H-aggregate. This can be explained best by the different molecular build-up of both Modules. In principal a longitudinal offset in a J-aggregate means an offset of the perylene cores along the x-axis. For the core linked Module, the width along x-axis determines size of aggregate, therefore an offset along this axis causes the size of the aggregate to change. In the imide linked Module, the width along the y-axis responsible for size of aggregate and an offset does thereby not affect the width.

Getting back to the previously raised question, the lack of a change in UV/vis for the imide linked still needs to be explained. A look into a MM-calculation with stacked imide linked Modules reveals the sterical demand of the morpholine side groups leading to a sterical crowding in between the stacks. This sterical crowding is responsible for larger π-π-distance with an average stacking distance of about 4.3 Å. The distance is probably too large for spectral changes in UV/vis upon aggregation. For other assembled perylene diimide systems no examples for a larger stacking distance than 4 Å could

be found in a thorough screening of the accessible literature that resulted in a shift of the absorption bands upon aggregation. The usual stacking distance found in literature is about 3.8 Å for twisted perylene diimides. It therefore seems that the stacking distance of about 4 Å is the threshold for a spectral change upon assembly, which explains the "monomeric" spectrum for the imide linked Module.

In summary it can be stated that a reversible switching with acid and base is possible for both Modules. In both cases micellar assemblies are being formed in the ionic version. H-aggregates are formed upon assembly in the acidic solution, whereby J-aggregates are formed in basic solution. An extraordinary result is that both Modules form micelles that assemble perpendicular to the binding axis and that again both Modules form the same kind of assembly despite their difference in binding axis.

4.4.2 Reduction

As mentioned abvoe, one goal of this thesis was the exploration of different switching possibilities for the ditopic Modules. Other than the switching with acid and base, a novel switching with sodium dithionite was introduced by Baram and coworkers.[50] Opposite to the ionic switches, this reversible switching process is based on a redox-reaction which targets the perylene core and not the zwitterionic GCP unit. As reported in the conceptional part of this thesis, the reduced state of the PDI core is only stable in the absence of oxygen while the initial state can be restored with air oxidation. This novel switching with sodium dithionite shall be investigated for both Modules in this part of the chapter.

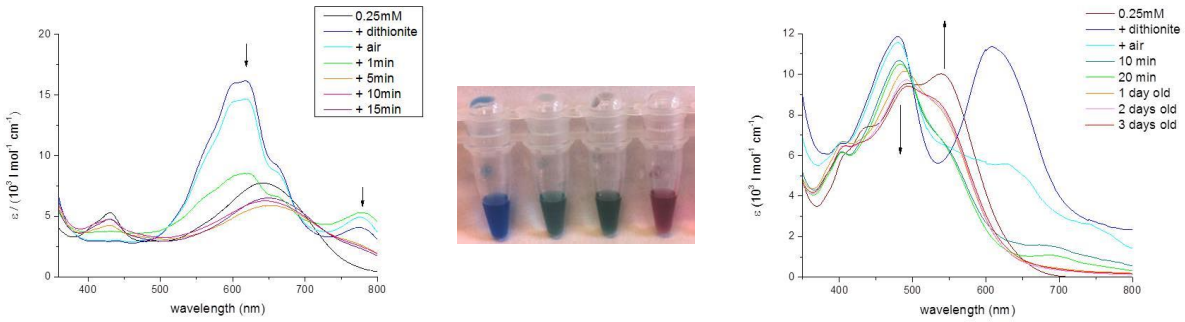

Figure 82: UV/vis spectra of the imide linked Module (left) and the core linked Module (right) after addition of $Na_2S_2O_4$ and oxidation with air at 0.25 mM in DMSO. Middle: Photographs of the respective solutions, from left to right: imide linked Module + $Na_2S_2O_4$, imide linked Module, core linked Module + $Na_2S_2O_4$, core linked Module

Since sodium dithionite is not soluble in DMSO, switching was performed with 3 µL of an 1M aqueous sodium dithionite solution. Control experiments where only 3 µL water were added to the solutions of

the Modules did not show a spectral change in the UV/vis, so the following measurements can be completely attributed to the effect of sodium dithionite. Since the reduced state is only stable without oxygen, the spectra were measured in the absence of air in a closed vial. The vial was then opened to allow a reoxidation in the presence of air. Spectra were then measured every 5 minutes after opening of the vial.

For both Modules, a significant change in UV/vis can be observed upon addition of sodium dithionite. Also both UV/vis measurements show broad absorption band around 600 nm that is attributed to the reduced state of the PDI core. The other results upon reduction differ for both Modules and will therefore discussed separately. For the imide linked Module, a color change to deep blue can be observed upon addition of sodium dithionite. Besides the absorption band around 600 nm, a second absorption band at 775 nm can be observed. This bathochromic spectral shift relative to the maximum absorption band of the initial Module might suggest the formation of a J-aggregate. A fast reformation of the initial absorption band can be further observed after oxidation. For the core linked Module a color change to turquoise is evident after the addition of sodium dithionite. In this case, also a second absorption band forms in the reduced state. The band at 480 nm suggests, that an H-aggregate is formed. Opposite to the imide linked Module, no complete reformation of initial absorption bands could be observed.

AFM measurements were performed for both Modules to see whether the switching can be monitored by microscopy measurements. The reduced solution of the Modules was spin coated onto the mica surface under argon atmosphere to ensure that indeed the reduced state of the Module is measured.

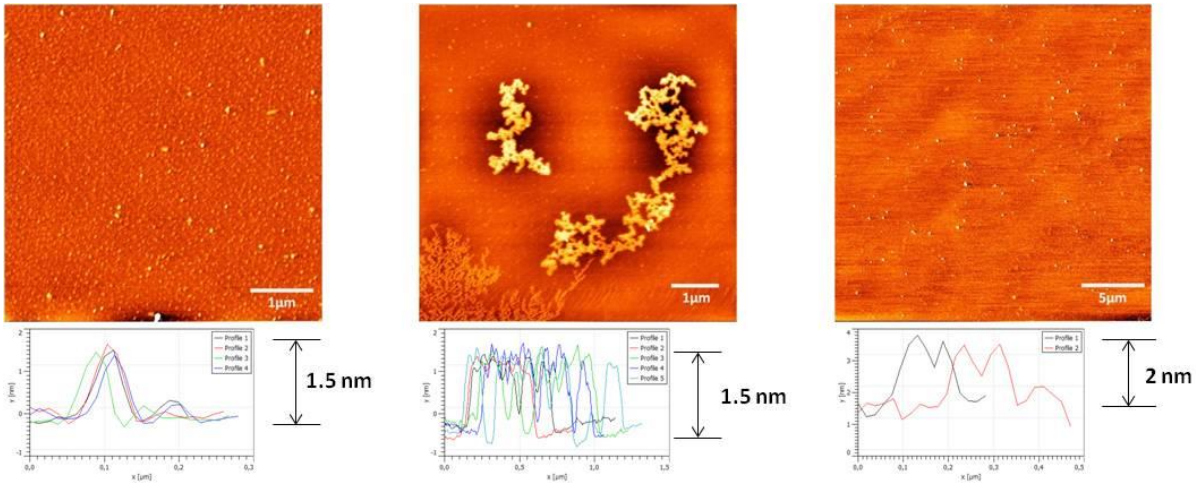

Figure 83: AFM images and height profiles of 0.25 mM solutions of the respective Module upon reduction with sodium dithionite respectively reoxidation with oxygen. Left: imide linked Module upon addition of sodium dithionite; Middle: core linked Module upon addition of sodium dithionite followed by the reoxidation with oxygen; Right: core linked Module upon addition of sodium dithionite.

Like for the switching studies with acid and base, circular aggregates form upon addition of sodium dithionite. The AFM phase images show also no vesicle formation in both cases. For the imide linked Module isolated spherical structures with a height of 1.5 nm were recorded. The AFM images of the core linked Module showed also spherical structures that are 2 nm in height. A reformation of the initially reported branched structures is evident after one day for both Modules. The assemblies of the imide linked Module thereby showed again the initially reported height of 3 nm, whereby the structures of the oxidized core linked Module were only 1.5 nm in height.

It is important to note that these were the first measurement, where both Modules exhibited a spectral change upon switching. Now, the assembly model of the Modules upon reduction will be highlighted in detail. Since the dimeric zwitterion remains unchanged by the switching, the loop like structure of the Module stays intact. The reduction of the perylene causes a rearrangement of the Module that leads to a significant spectral change. Taking the bathochromic shift into account, it is expected that a J-aggregate is formed of the reduced imide linked Module. MM-calculations of the Module lead to a J-aggregate which reveals outer measures of a formed dimer of 1.5 nm in two dimensions. These values are in good agreement with the AFM measurements of the reduced Module. Upon oxidation the reformation of initial absorption band could be observed. This can be explained by the reformation of the initial heterotopic assembly structure with alternating arrangement of zwitterion dimer and perylene core which is the most stable aggregate for the Module.

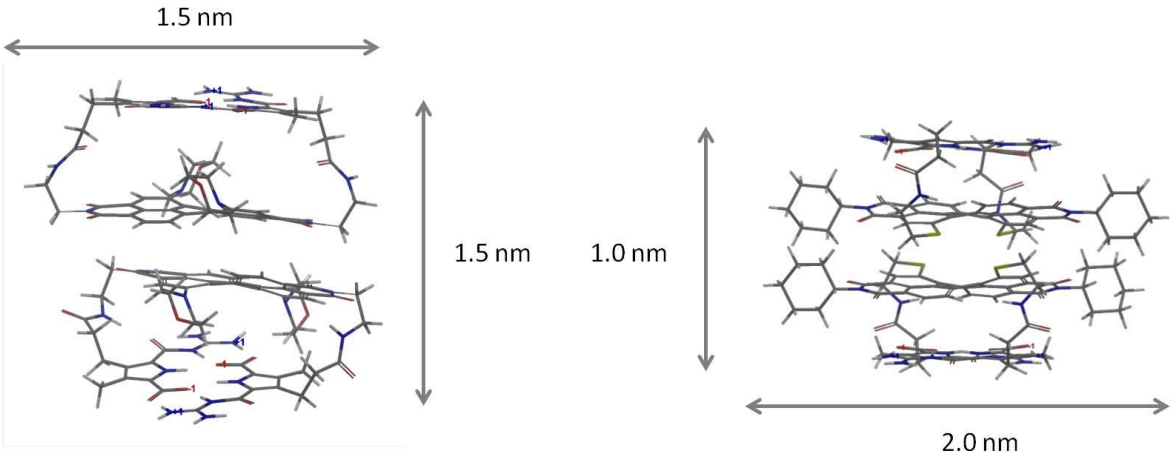

Figure 84: MM-calculations of the respective Module with external dimensions. Left: Imide linked Module that is anticipated to form a J-aggregate; Right: Core linked Module that is anticipated to form an H-aggregate

For the reduced core linked Module, the hypsochromic shift indicates the formation of an H-aggregate. The MM-calculation shows indeed a J-aggregate that is 1 nm along the z-axis, 2 nm along the x-axis and 1.5 nm along the y-axis. The height in AFM can therefore be explained by the measure in x-axis.

Upon oxidation a branched structure forms, but the reformed branched assembly is only 1.5 nm in height. This means that only a single strand is formed after switching and not the initial double string. Responsible for this unexpected behavior might be a kinetic trapping of the H-aggregate. Since the respective energy of the H-aggregate is lower than the initial alternating assembly, it is not stable enough to re-form. Therefore no complete reformation of the initial absorption band can be observed. The aging behavior of the Module was driven by the formation of the thermodynamically stable J-aggregate. The energetic difference between the H- and J-aggregate is too small though to cause a rearrangement. Therefore no aging behavior is observable after switching with sodium dithionite.

This part of the chapter proved that a reversible switching with more than one stimuli only possible for imide linked Module. The core linked Module is reversibly switchable with acid and base, but the switching with sodium dithionite leads to a kinetic trapping.

4.5 Summary

This chapter showed the successful combination of zwitterionic binding motif with a perylene diimide. It was possible to synthesize and investigate molecules with a different binding axis. The two presented molecules formed polymers in an alternating stacking behavior between perylene core and intramolecular zwitterion dimer. A difference in aggregated structure of the two molecules which form assemblies based on different binding axes could not be observed. This enables new possibilities for functionalization of PDIs, since the experiment lead to the conclusion that the formed aggregates are not dependent on the binding axis.

The assembly with the core binding axis exhibited an interesting aging behavior. The kinetically stable alternating polymer transforms into a thermodynamically stable ABBA assembly over time. It is not possible for the molecule with imide binding axis, because the bulky morpholino-groups hinder a tight perylene-perylene stacking. The investigated systems are furthermore all reversibly switchable in acid, base and dithionite.

5. Monotopic Modules

5.1 Concept

This chapter of the thesis will investigate the supramolecular behavior of two monotopic Modules. Like for the ditopic Modules, the core motif is the functional chromphore perylene. To obtain a monotopic Module, only one GCP unit will be attached to the peryene while the other side will be substituted with a polyethylene glycol chain to enhance the solubility in polar media. To accomplish that, the monotopic Modules shown in Figure 85 were created.

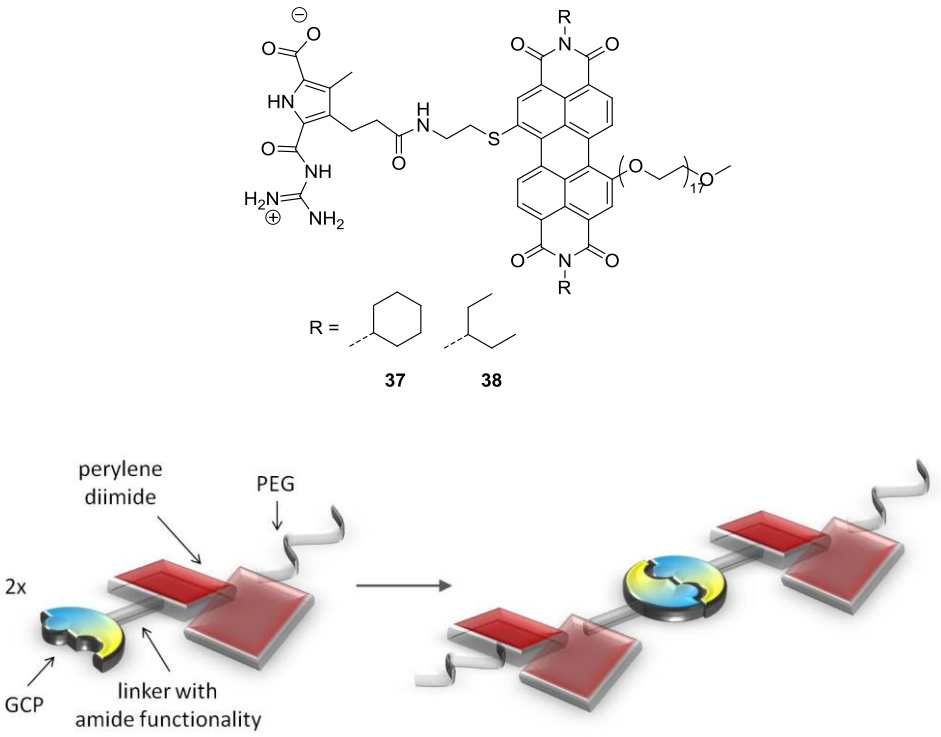

Figure 85: Above: Monotopic Modules 37 (cyclohexylamine substituted) and 38 (3-pentylamine substituted) . Below: Schematic representation of the monotopic Module and dimerization through the zwitterionic GCP unit.

To obtain these monotopic Modules, an unsymmetrical attachment of both substituents to the core is needed. The methyl capped polyethylene glycol chain can be directly attached to the core. The GCP unit on the other side was attached via a cysteamine linker like it was done for the core linked Module. To investigate the influence of the side chain at the imide position on the aggregation behavior, two different monotopic Modules were created. Therefore molecule **37** was synthesized with

a closed cyclohexyl side chain at the imide position (cyclohexyl Module), while molecule **38** was utilized with a flexible 3-pentyl side chain (3-pentyl Module).

After the assembly of the zwitterionic GCP unit of two molecules, a dimer forms which is structurally similar to molecules presented by the working group of Rybtchinski. The working group showed several examples in which two perylene units were connected with a linker in between. Recalling the example of Krieg and coworkes,[51] it might also be possible to form a supramolecular gel with the monotopic Modules. This gel would then not onyl be switchable with the switches presented in that paper but additionally with acid and/or base due to the zwitterionic GCP unit.

In principle two different aggregation types are possible for a formed zwitterion dimer which are depicted in Figure 86.

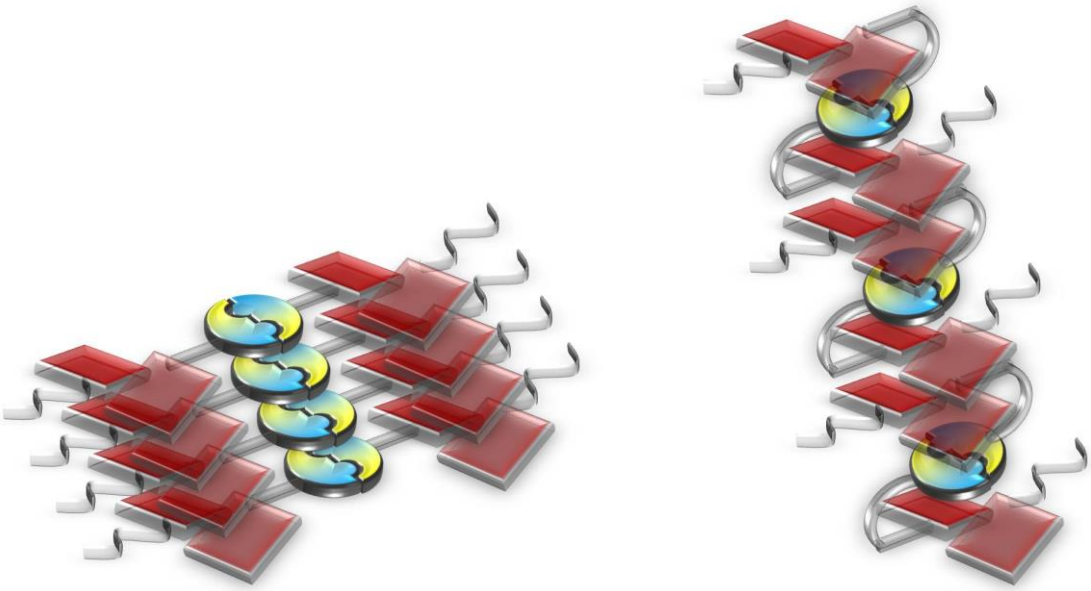

Figure 86: Schematic presentation of the possible aggregation types of the monotopic Modules. Left: homotopic stacking; Right: heterotopic stacking.

The first aggregation type is a homotopic stacking of a straight dimer of the monotopic Module. The assembly of this version is like systems of the working group of Rybtchinski, based on a π-π-stacking of perylene dyes. In this aggregate all perylene subunits would stack onto each other and all zwitterion dimers would also stack on top of a second zwitterion dimer due to their planar nature. This aggregation type is additionally supported by a hydrogen bond between the linker moieties. The elongation of the assembly is possible along several axes depending on the Modules. The elongation along the z-axis is driven by the π-π-stacking of perylene and zwitterion dimer. The assembly along the x-axis is only possible through the interlinking of 3-pentyl chains, which means that the cyclohexyl

Module should not be able to elongate along that axis. An aggregation though an interpenetration of PEG chains would lead to an elongation along the y-axis, even though it is not anticipated to be a directed assembly but an irregular entanglement of the chains. If the growth of the assembly along the z-axis is limited for the 3-pentyl Module, a formation of segmented fibers is possible. Lacking the interpenetration possibility, it is not expected that the cyclohexyl Module assembles into segmented fibers. In principal, it is anticipated that the cyclohexyl Module forms one or two dimensional assemblies through an elongation along the z-axis respectively y-axis while the 3-pentyl Module forms one, two or three dimensional aggregates along all axes possible.

The second assembly type is a heterotopic stacking. Based on the results of the last chapter, in which an intercalation of the zwitterionic dimers between two perylene units was reported, a BABBAB-stacking could be possible, whereby A stands for the zwitterion dimer and B stands for the perylene. The principal aggregation elongates along the z-axis, which nevertheless means that an assembly along the other axes is still possible. Like for the homotopic stacking, an elongation along the x-axis is possible through an interlinking of the 3-pentyl chain and along the y-axis is possible through an interpenetration of PEG chains. Again it is anticipated that the cyclohexyl Module forms one or two dimensional assemblies through an elongation the z-axis respectively y-axis, while the 3-pentyl Module forms one, two or three dimensional along all axes possible. In principal it can be noted that manifold assembly possibilities for both aggregation types exist. The further part of this chapter will now outline the synthetic procedures as well as the investigation of the aggregation behavior of the monotopic Modules.

5.2 Retrosynthesis

5.2.1 3-Pentyl Module

Depending on the substituent at the imide position, different synthetic routes were chosen. The synthesis of the 3-pentyl Module will be described in the next part of this chapter. The retrosynthetic route is shown in Figure 87.

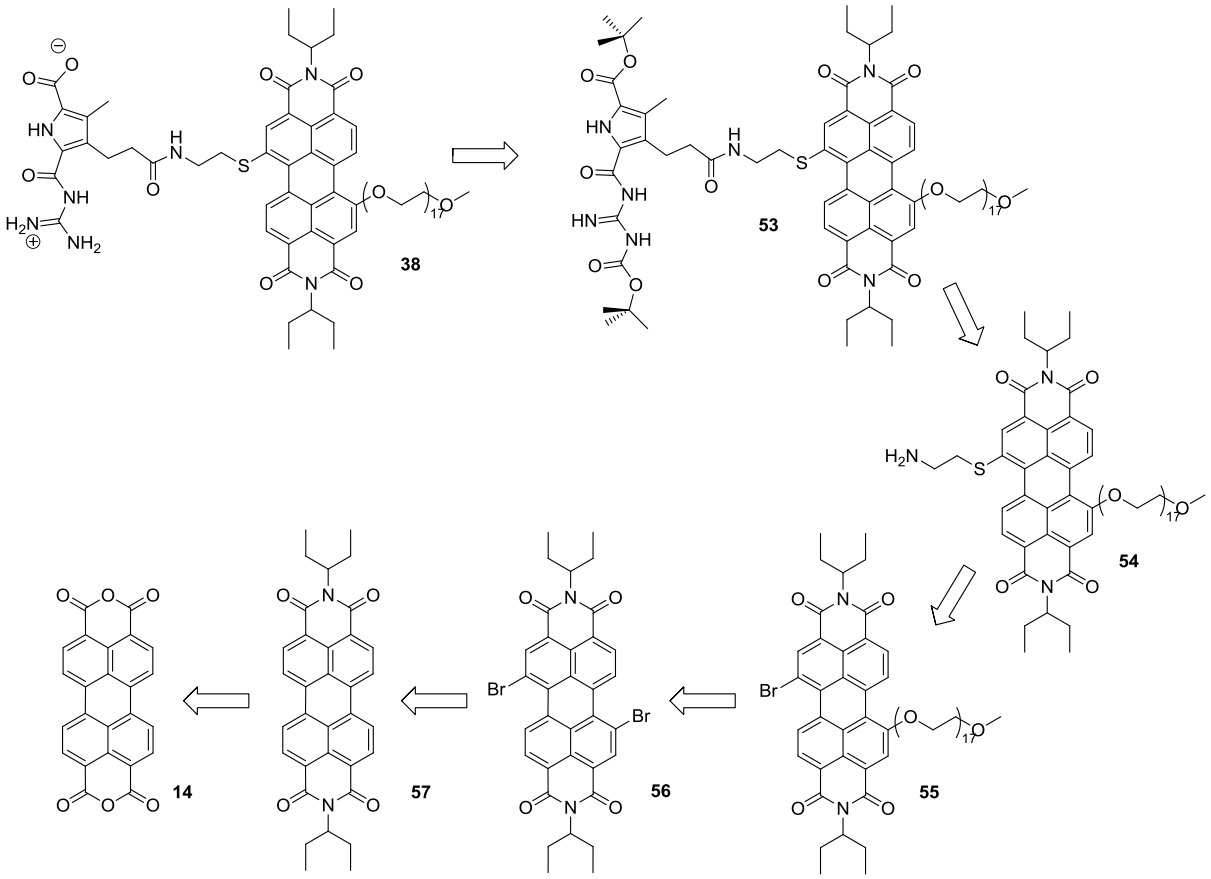

Figure 87: Retrosynthesis of the 3-pentyl Module **38**.

Like for the ditopic Modules, the reaction also starts with PTCDA **14**, which is the perfect precursor to attach all kinds of functional groups to the perylene. The anhydride is not functionalized at the core in the first step, but directly converted into the imide with 3-pentylamine. The bromination is then accomplished with a newly introduced procedure by Rajasingh and coworkers,[64] which gives a higher yield and an easier experimental procedure as the conventional bromination reported by Würthner.[54] To attach the PEG chain at only one side of the perylene core, the synthesis is performed in an altered way compared to the literature procedure.[50] On the other side of the core, functionalization is made with cysteamine as introduced in the last chapter, to provide a free amine position which will be used

for the coupling of the GCP precursor. Afterwards the GPC subunit is deprotected to give the final molecule **38**.

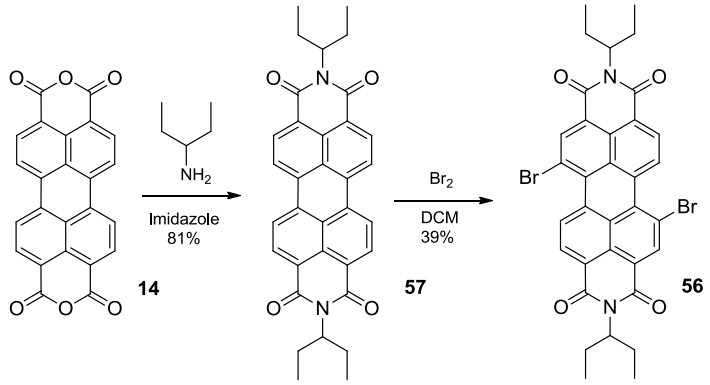

Figure 88: Synthesis of dibrominated PDI **56**.

57 and **56** were synthesized according to literature.[65,64] In the first step PTCDA **14**, imidazole and 3-pentylamine were mixed, heated to 140 °C and stirred for 24 hours. After cooling of the slurry, methanol and 0.1 M HCl were added and the precipitate was filtered off. The resulting crude product was purified by column chromatography with dichloromethane as eluent to obtain **57** in 81% yield. **57** was then dissolved in dichloromethane and heated to reflux for 72 hours after the addition of bromine. After removal of dichloromethane and excess bromine, the regioisomeric mixture of the 1,6- and 1,7-bromo PDI was purified by column chromatography with dichloromethane as eluent. The altered recrystalisation method, which was introduced in the last chapter, was also performed with dichloromethane and n-hexane. The isolated solid was dissolved in dichloromethane and n-hexane was added to yield in a 2:1-mixture of dichloromethane and n-hexane. This solution was concentrated under reduced pressure until the a precipitate started to form. The solution was then put in the refrigerator overnight to ensure a complete crystallization. The precipitate was again filtered off and the purity concerning the ratio of the regioisomers was checked by NMR-spectroscopy. The pure 1,7-regioisomer of **56** was obtained in 39% yield after one recrystallisation step. Compared to the calculated overall yield of the literature procedure of 36%, the yields with the altered recrystallization step is slightly higher.

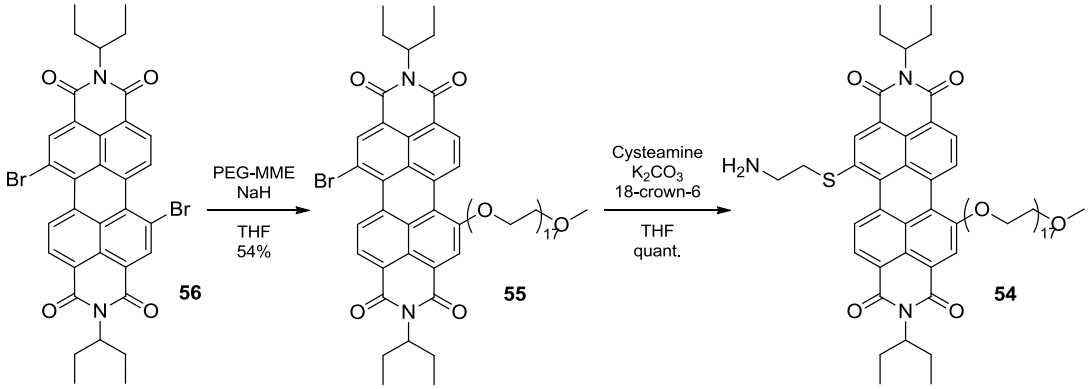

Figure 89: Synthesis of the cysteamine precursor **54** of the 3-pentyl Module.

To obtain the asymmetrically substituted perylene, the literature known synthesis was altered. In the literature procedure, all components seem to be added at the same time which yielded in an inseparable mixture of the mono- and the ditopic PEG-PDI.[50] In the modified version, **56** and polyethylene glycol monomethyl ether (PEG-MME, 750 Dalton) were mixed in dry THF under argon and stirred for 5 minutes after which NaH was added. The solvent was removed after 24 hours and the crude product purified by column chromatography with dichloromethane/methanol (19:1). The purple wax **55** could be obtained in 54% yield. Analogue to the procedure introduced in the previous chapter, cysteamine, 18-crown-6 and K_2CO_3 were mixed in THF and **55** was added after 5 minutes. The dark red solution was stirred for 2 hours, followed by an addition of water and extraction with DCM, until the water phase remained nearly colorless. The solvent was evaporated after drying of the DCM phase to obtain **54** in nearly quantitative yield.

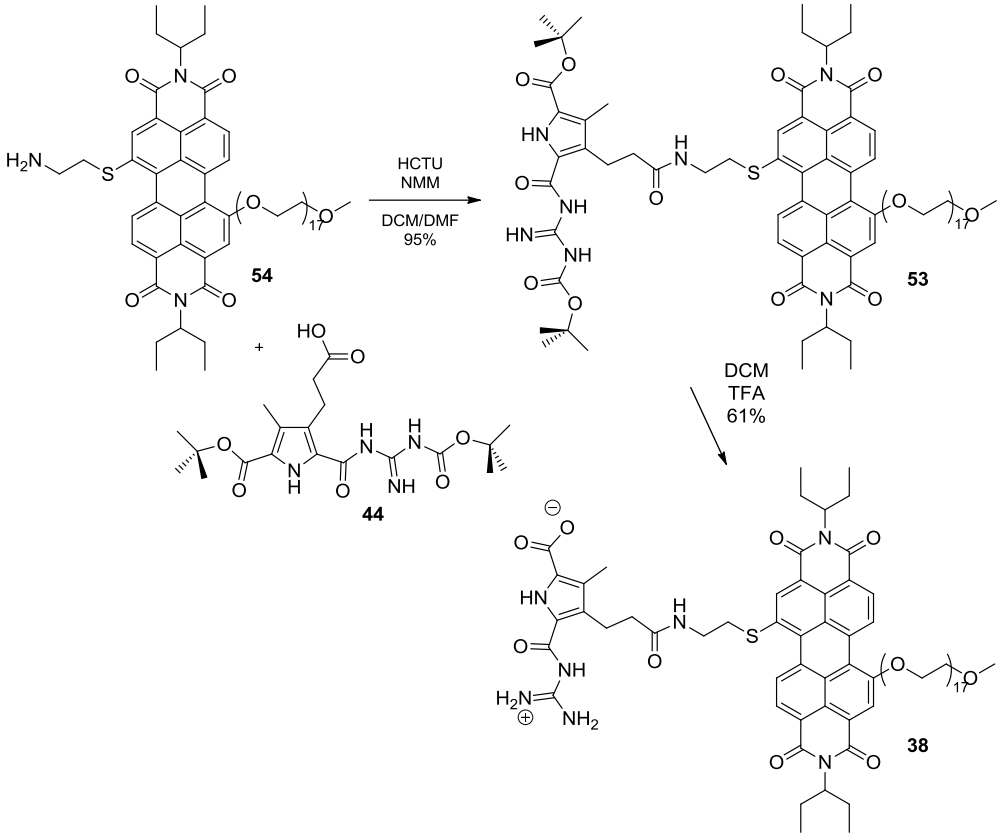

Figure 90: Synthesis of 3-pentyl Module **38**.

In the next step, **54**, **44**, HCTU and NMM were mixed in DCM/DMF and stirred for 24 hours. Since some starting material could still be observed by TLC after that time span, an additional portion of HCTU was added and the mixture was again stirred for 24 hours. DCM was removed after completion of the reaction and water added to the solution. The formed precipitate was filtered off and purified by column chromatography with dichloromethane/methanol (9:1) as eluent to obtain **53** in 95% yield. The dark pink wax was dissolved in DCM/TFA (5:1) and stirred for 24 hours. DCM was evaporated afterwards, followed by the addition of 0.1M HCl to lyophilize the solution afterwards. To deprotect the GCP unit, **53** was dissolved in 1 M NaOH and 0.1 M HCl was added until pH=5.68 was reached. The solution was filtered to remove precipitated salts and the filtrate, which contained the 3-pentyl Module, was again lyophilized. The dark purple wax was dissolved in THF and filtered off again to remove remaining salts. This step had to be performed several times to completely remove all salts. After evaporation of the solvent, a yield of 61% of the 3-pentyl Module **38** could be obtained.

5.2.2 Cyclohexyl Module

The retrosynthesis of the cyclohexyl Module **37** contains basically the same steps as the synthesis of the 3-pentyl Module **38**. The only difference lies in the different starting material due to the different substitute at the imide position.

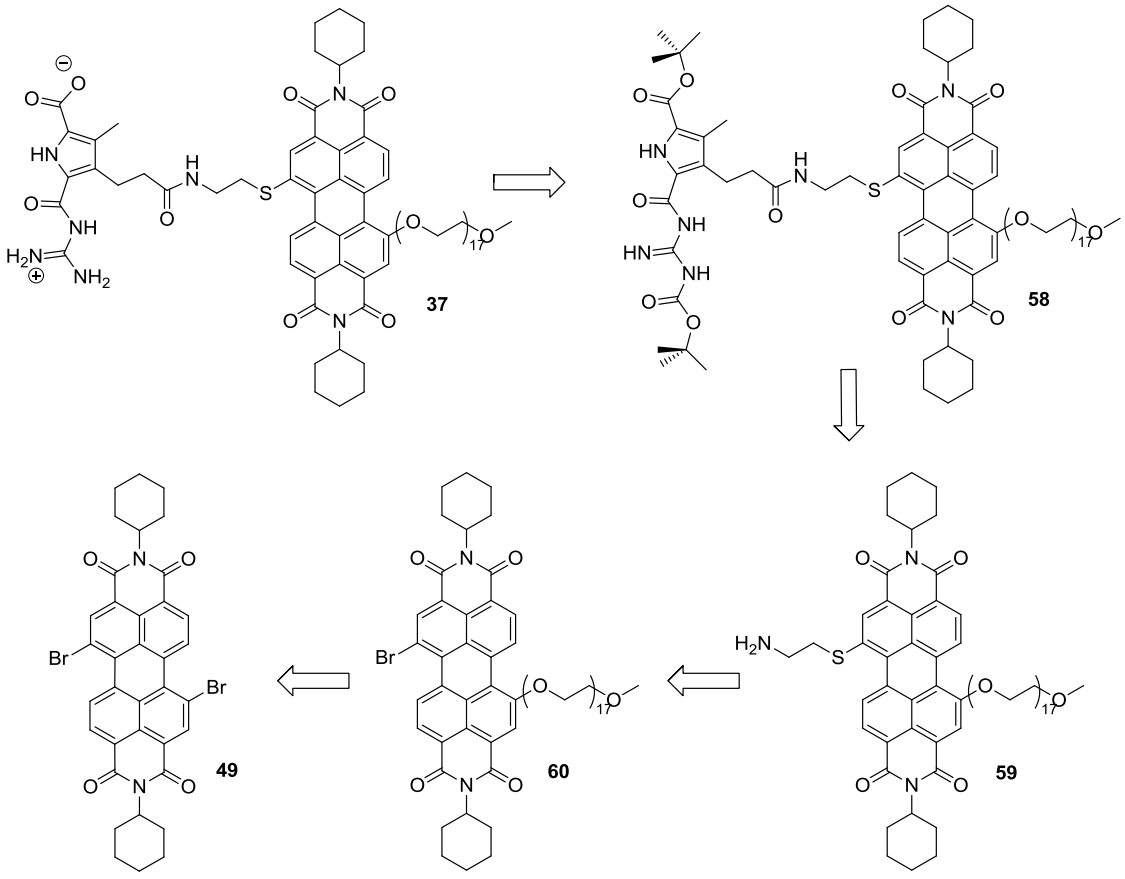

Figure 91: Retrosynthesis of the cyclohexyl Module **37**.

As starting point for the synthesis, **49** was chosen. This synthesis has been outlined in the previous chapter. As well as for the 3-pentyl Module, the monotopic PEG attachment takes place first, followed by the reaction with cysteamine to obtain a free amine. After the coupling with the GCP precursor unit and its deprotection, the cyclohexyl Module can be obtained. The following part will therefore highlight the differences in synthesis between both Modules.

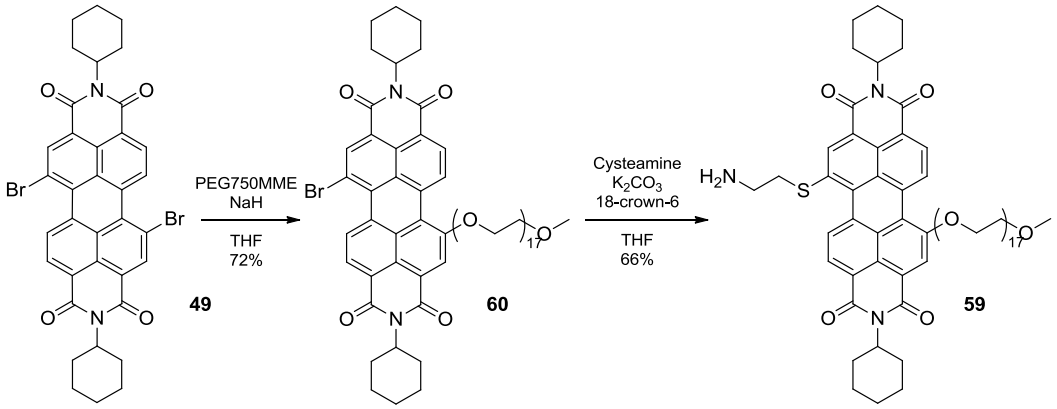

Figure 92: Synthesis of the cysteamine precursor **59** of the cyclohexyl Module.

In the first step, the same conditions as for **55** gave a better yield of 72% for **60** compared to 54 % for **55**. This is probably due to a better separation from side products during column chromatography of the reaction compared to the 3-pentyl Module. Upon reaction with cysteamine, a poorer yield of 66% could be obtain which can be explained by the shorter reaction time of **59**. Unfortunately the reaction time could not be extended very well, since a lot of side products or decomposition products are formed during the elongated time. Why this fast decomposition only occured for **59** was not investigated further though.

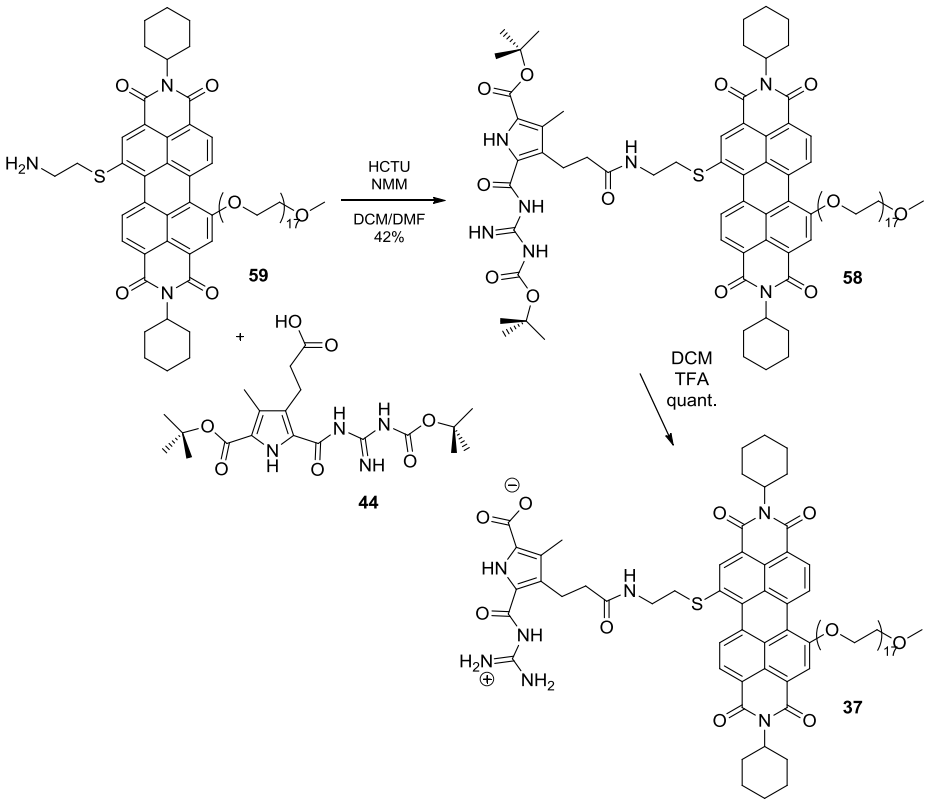

Figure 93: Synthesis of the cyclohexyl Module **37**.

The solubility of **59** in DCM/DMF was not ideal in the next coupling step with **44**, which resulted in a lower yield of 42% compared to **53**. However, since the obtained amount of the substance was sufficient for further investigation, the synthesic step was not optimized. Opposite to the 3-pentyl Module **38**, the cyclohexyl Module **37** was not soluble at pH=5.8 after deprotection but formed a precipitate when becoming zwitterionic. After the filtration of the precipitate, a quantitative yield could be obtained. Since the filtration had not to be repeated several times to remove the salts, the yield was significantly better for the cyclohexyl Module.

Both retrosynthetic routes have 6 steps and an overall yield of 10% for the 3-pentyl Module **38** respectively 8 % for the cyclohexyl Module **37**. Therefore it can be stated, that the synthesis of both Modules could be achieved successfully.

5.3 Aggregation behavior

After the synthesis of both monotopic Modules, the aggregation behavior of both compounds was investigated. But before going into detail about the aggregation, a few words will be said about the solubility of the Modules. Both molecules were perfectly soluble in THF as well as DCM, but unfortunately the cyclohexyl Module was not completely soluble in water. Therefore the aggregation behavior was first investigated in THF as a basis for further measurements.

5.3.1 Spectroscopy

As a first insight into the behavior of the monotopic Modules, UV/vis measurements were carried out. The spectra of both Modules in THF are similar in regard to the maximum absorption bands and the vibronic fine structure. The monotopic Modules show a monomeric spectrum similar to what was reported for the ditopic Modules and for other PDI systems in THF. The 3-pentyl Module shows a maximum absorption band at 560 nm with a second band at 522 nm, which correspond to the electronic $S_0 \rightarrow S_1$ transition. The vibronic 0 → 0 transition appears around 560 nm, while the vibronic 0 → 1 transition appears as a shoulder around 522 nm. The electronic $S_0 \rightarrow S_2$ transition occurs around 399 nm. Compared to the spectrum of the 3-pentyl Module, the spectral curve of the cyclohexyl Module is very similar. The extinction coefficient of the cyclohexyl Module is slightly higher than of the 3-pentyl Module, but otherwise the curves show the same features. The maximum absorption band is at 562 nm and second band at 524 nm, so the transitions from the ground to the first excited state are shifted only 2 nm compared to the 3-pentyl Module. The transition from the ground to the second excited state occurs at 391 nm. To take a deeper look into the aggregation behavior, concentration dependent UV/vis measurements were performed.

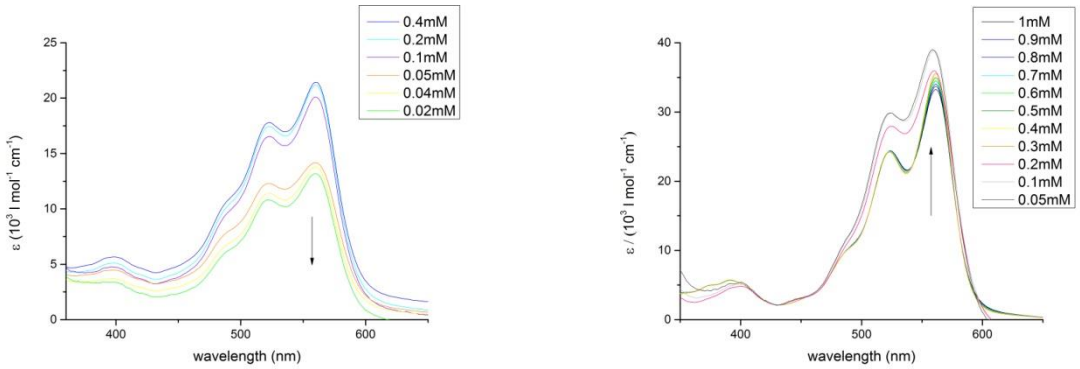

Figure 94: Left: Concentration dependent UV/vis measurements of the 3-pentyl Module in a concentration range from 0.4 mM to 0.02 mM; Right: Concentration dependent UV/vis measurements of the cyclohexyl Module in a concentration range from 1.0 mM to 0.05 mM. The arrows indicate the spectral changes with decreasing concentration. Solvent for both cases is THF.

For both Modules a change in extinction coefficient occurs upon dilution whereby no shift of the maximum absorption bands is observable. In the case of the 3-pentyl Module a decrease in extinction coefficient can be seen. This behavior is similar to the investigated change of the ditopic Modules, whereby the decrease was anticipated to be caused by the interaction between perylene and zwitterionic dimer which are stacked onto each other. This hints that for the 3-pentyl Module a similar assembly might form. For the cyclohexyl Module the opposite is evident. In similar cases in the literature always an increase in extinction coefficient is observed when an aggregated PDI assembly is diluted. This means that the cyclohexyl Module is the only ditopic Module studied in this thesis that behaves like literature known PDI aggregates upon dilution whilst all other synthesized Modules show the opposite behavior. Furthermore a monomeric spectrum is also observed at higher concentrations for both monotopic Modules. For the ditopic Modules this monomeric spectrum is attributed to an isolated PDI due to alternating arrangement of zwitterion dimer and perylene unit. This possibility however does not exist for the monotopic Modules, since the heterotopic stacking as well as the homotopic stacking would result in a direct perylene-perylene contact in the assembly. In similar systems known from literature, a monomeric spectrum in THF is attributed to a deaggregated molecule, which means that for these cases no assembly is being formed in THF.[59] Assuming that the Modules would not form an assembly in THF, the electronic spectrum would consequently not show a change in extinction coefficient upon dilution, since the extinction coefficient is independent of the concentration. For both Modules a change in extinction coefficient can be observed upon dilution though. Therefore it is justified to assume for the further investigation that the Modules form assemblies in THF, unless the opposite is proven.

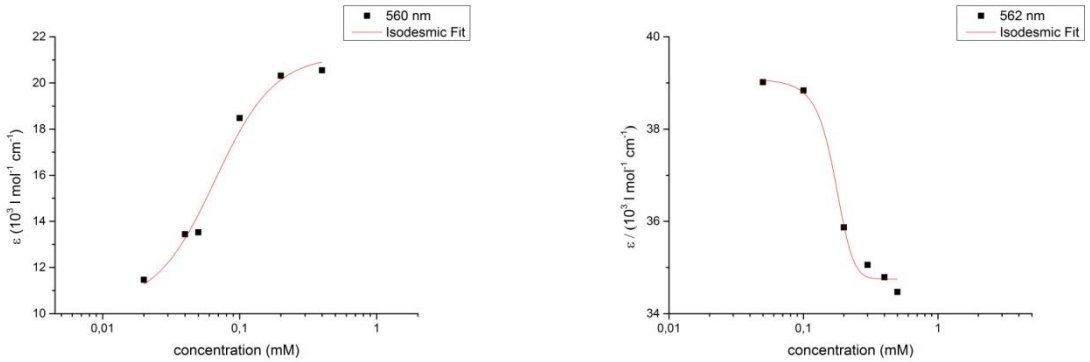

Figure 95 Extinction coefficients of the maximum absorption band upon dilution plotted as a function of the dimensionless concentration. Left: 3-pentyl Module with a maximum absorption band at 560 nm , Right: cyclohexyl Module with a maximum absorption band at 562 nm.

To get an idea about the principle aggregation mechanism, the extinction coefficient at 560 nm for the 3-pentyl Module, respectively 562 nm for the cyclohexyl Module was plotted against the dimensionless

concentration. The resulting data points were then fitted with equation (4). The fit reveals an isodesmic aggregation behavior in both cases which is typical for PDI assemblies like reported before. The gradient of the curve is different for both Modules though. While the 3-pentyl Module has a flat gradient like observed for the ditopic Modules, the cyclohexyl Module shows a steeper curve. This is the second indication that both Modules form different assemblies and that the assembly of the 3-pentyl Module is somehow similar to those of the ditopic Modules.

Additional to the concentration dependent studies, temperature dependent UV/vis measurements were made for both monotopic Modules in THF to check whether the change in extinction coefficient can be also observed with a change in temperature.

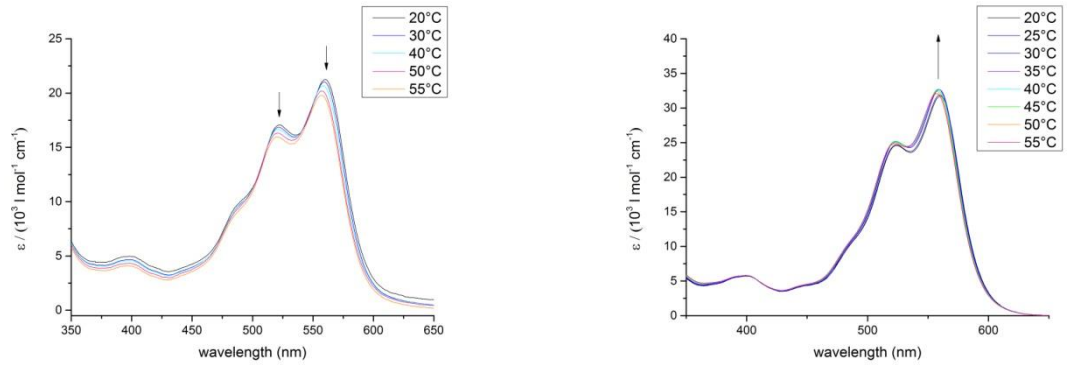

Figure 96: Temperature dependent UV/vis studies of the monotopic Modules at 0.1 mM in THF. Left: Measurements of the 3-pentyl Module in a temperature range from 20°C to 55°C; Right: Measurements of the cyclohexyl Module in a temperature range from 20°C to 55°C. The arrows indicate the spectral changes with increasing temperature .

As shown in Figure 96, the temperature dependent measurements confirm the behavior of the ditopic Modules in the concentration dependent measurement. Like for the dilution experiments, no shift of the maximum absorption is observed. The same absorption bands remain upon increase of the temperature and only a change of the extinction coefficient occurs. Again as in the concentration dependent measurements, the 3-pentyl Module shows a decrease of the extinction coefficient, while the cyclohexyl Module shows an increase. With these results of the UV/vis measurements, the question arises how the aggregates of the 3-pentyl Module and the cyclohexyl Module differ and if the difference can be attributed to the existence of the 3-pentyl group. Additionally it is important to ask whether the 3-pentyl Module forms somehow similar to aggregates like the ditopic Modules, since the monotopic Module shows also a decrease of extinction coefficient in UV/vis upon dilution.

5.3.2 Microscopy

To further evaluate, if an assembly is formed for the monotopic Modules in THF, AFM measurements were carried out. Therefore different concentrations of the two molecules were investigated. All AFM measurements of were made on mica, whereby the respective solution was spin coated onto the target at 60 rps for 1 minute. The measurements shown in Figure 97 and Figure 98 indeed reveal, that an aggregation takes place for both monotopic Modules in THF.

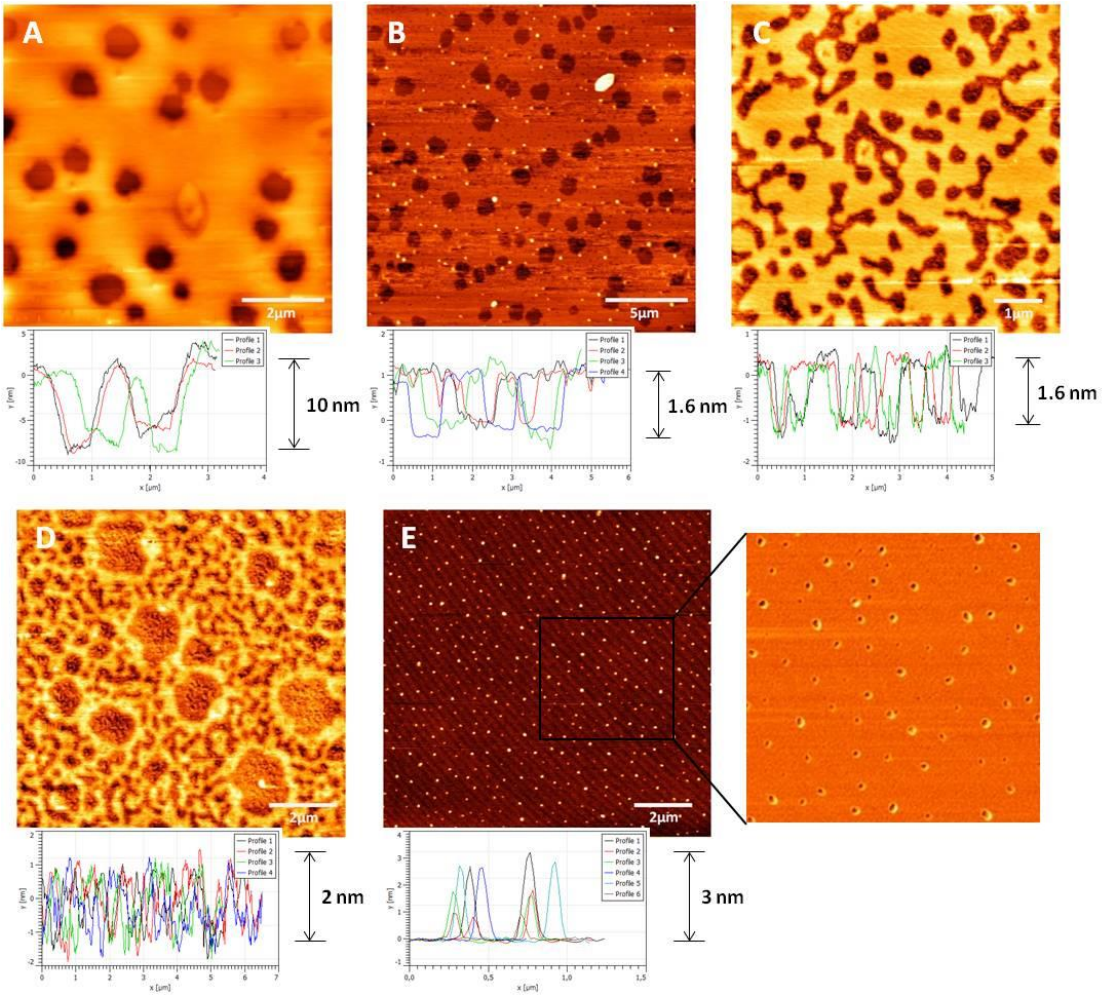

Figure 97: AFM height measurements of the 3-pentyl Module at various concentrations in THF and the respective height profiles. A: Concentration of 0.8 mM, B: Concentration of 0.5 mM, C: Concentration of 0.2 mM, D: Concentration of 0.1 mM, E: Concentration of 0.05 mM, the magnification depicts the phase image of the respective AFM measurement.

The AFM height images of the 3-pentyl Module show layer like aggregates in a concentration range from 0.2 mM up to 1.0 mM, whereby the lighter yellow to orange parts of the image resemble the layer while the holes are colored deep red. The AFM phase images of the higher concentration ranges are not shown, because they give no hint about the aggregation behavior due to a complete surface coverage. The thickness of the layer at a concentration of 0.8 mM is about 8 to 10 nm. If the

concentration is lowered to 0.5 mM, the thickness of the layer decreases to about 1.6 nm. At 0.2 mM bigger voids can be observed in the layer while the height is the same as for 0.5 mM. The AFM height images of a 0.1 mM solution of the 3-pentyl Module show a change to linear aggregates. Thereby the branched strands are colored yellow while the surface is characterized by a dark red color. Opposite to the linear aggregates found for the ditopic Modules, the aggregates are distributed evenly on the surface and not condensed at several spots. Around the bigger voids in between the aggregates it looks like the linear strings fuse together to form again a layered aggregate, which might give a hint on the build-up of the layered aggregate itself. The height of the strings is about 2 nm. If the concentration is decreased further to 0.05 mM, spherical particles with varying heights of multiple of about 1 nm can be observed. The AFM phase image of the same measurement reveals a vesicular structure of these spherical particles as indicated by the yellow corona around the particle.

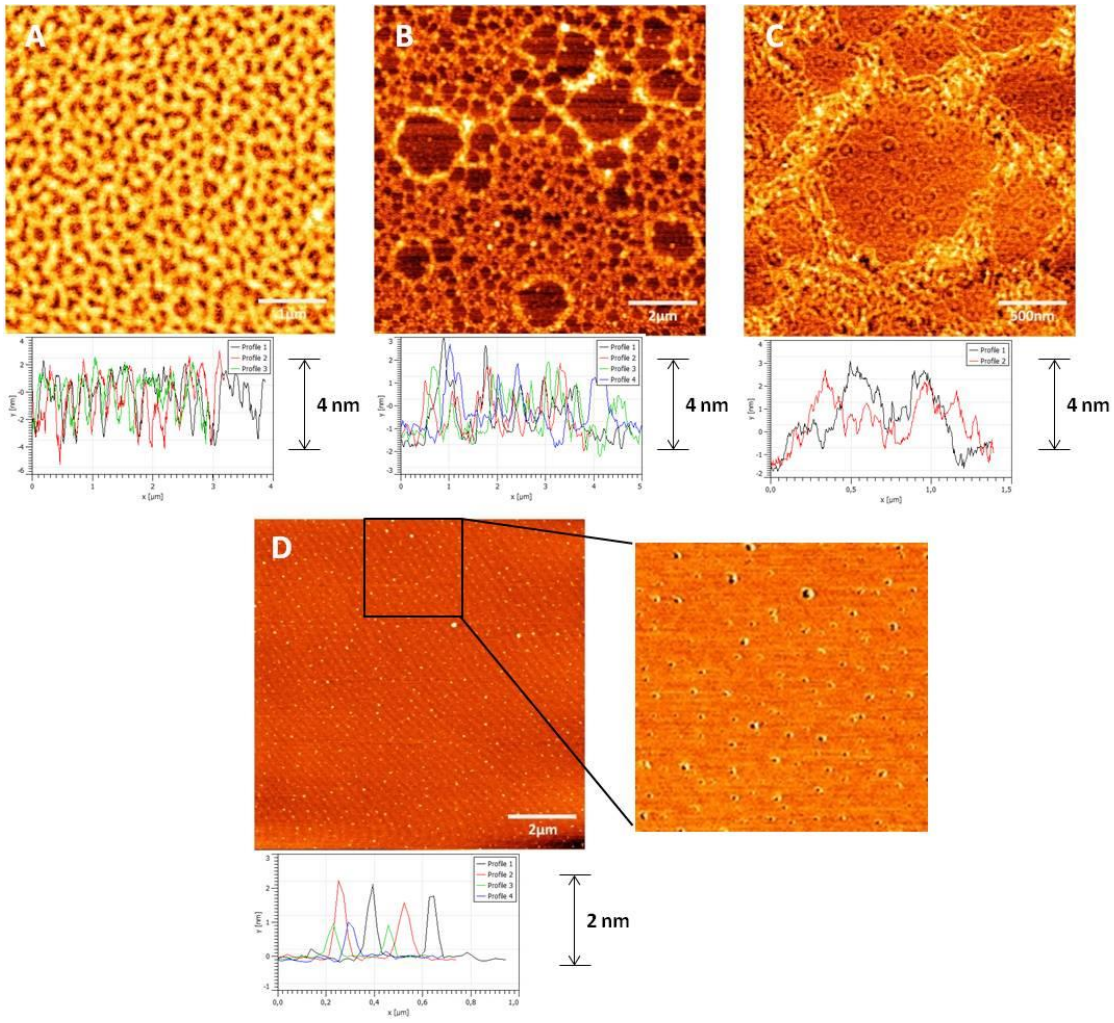

Figure 98: AFM height measurements of the cyclohexyl Module at various concentrations in THF and the respective height profiles unless otherwise specified. A: Concentration of 1.0 mM, B: Concentration of 0.5 mM, C: Phase image at a concentration of 0.5 mM, D: Concentration of 0.1 mM, the magnification depicts the phase image of the respective AFM measurement.

Opposite to the aggregation behavior of the 3-pentyl Module, the cyclohexyl Module does not form layer like structures at higher concentrations but linear ones. At 1.0 mM these strands are about 4 nm in height which is about two times bigger than the linear aggregates of the 3-pentyl Module. Like for the ditopic Modules, a branching of the linear strands is also visible even though an evenly distribution of the aggregates on the surface can be observed. Looking at the AFM phase images of a 0.5 mM solution of the cyclohexyl Module, the aggregates are still linear, whereby separated fibers can be observed. At higher magnification it becomes obvious that the linear strands are double walled and look like tubular structures. Within this measurement, two size distributions can be distinguished. The smaller structures are about 1 nm in height whereas the bigger structures have a height of about 4 nm. Besides the linear strands, also vesicular aggregates can be observed at 0.5 mM. Withdecreasing concentration, spherical particles are seen in the images. The AFM phase image of the 0.1 mM solution sample reveals again spherical structures for the spherical particles at 0.1mM with a height of 1 and 2 nm due to the corona around the circular particle.

These measurements prove that the Modules form assemblies in THF, although a monomeric spectrum was observed in UV/vis. Like in the UV/vis measurements, different results were obtained for the 3-pentyl Module and the cyclohexyl Module in the microscopic studies. While the spectral changes can only be attributed to an unlike behavior of both Modules, the differences in aggregation of the 3-pentyl Module and the cyclohexyl Module found with AFM might directly be linked to the substitution at the imide position. The predominant assembly form of the 3-pentyl Module is a layer, which is assumingly built-up by linear strings.Tthe cyclohexyl Module however forms linear aggregates at various concentrations that do not fuse into layered aggregates. Opposite to the cyclohexyl Module, the 3-pentyl Module has an open and therefore flexible alkyl side chain at the imide position which enables the interaction of two molecules of the same type by interlinking of the alkyl chain. the cyclohexyl Module, lacking that interlinking possibility due to the more rigid cyclohexyl side chain at the imide position, shows a one dimensional aggregation which leads to the formation of a linear assembly. The 3-pentyl Module on the other side forms a two dimensional aggregate, because the aggregation is not only evolving in the z-direction of the PDI by π-π-stacking, but also in x-direction via the imide position.

To get a further look into the aggregation behavior of both Modules, HIM measurements were made to investigate how an unpolar surface influences the assembly. The samples of both Modules were spin coated onto a silicon surface with the same conditions as for the AFM measurements.

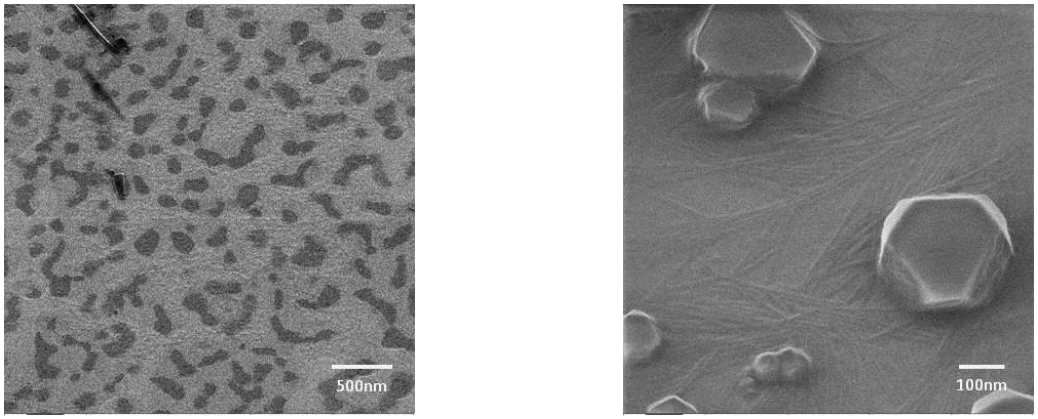

Figure 99: HIM measurements of the 3-pentyl Module in THF. Left: 1mM, right: 0.1mM.

The 1 mM sample of the 3-pentyl Module reveals a smooth regular coverage of the surface with dark spots in between. Like in the AFM measurement, a layered assembly is observed, whereby the dark spots resemble the holes in the layer. At concentrations of 0.1 mM, thin needle like aggregates can be observed. As well as the measurement at higher concentrations, the aggregates are very evenly formed, with a uniform size distribution. The rods are straight and not randomly twisted or oriented in contrast to the linear aggregates found in the AFM measurements.

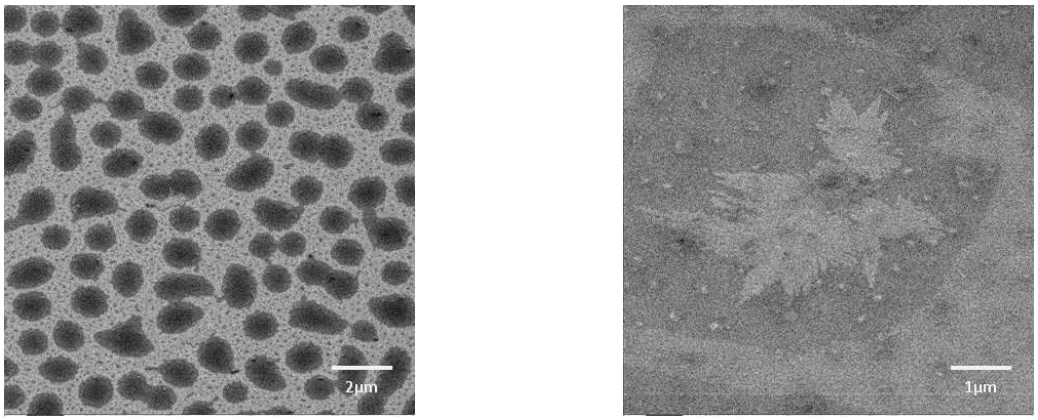

Figure 100: HIM measurements of the cyclohexyl Module in THF. Left: 1mM, right: 0.1mM

At first sight, the assemblies of the cyclohexyl Module and the 3-pentyl Module at 1 mM look very much alike, except for the shape of the dark spots in the layer. For the cyclohexyl Module, these are larger and more regular than the case of the 3-pentyl Module. At a closer look, tiny spaces in the layers can be observed. The distribution of these voids is very evenly and comparable to those found in AFM. It looks like spaces which form when linear aggregates are tightly packed together, but do not interlink. Therefore it can be assumed, that opposite to the layered aggregate of the 3-pentyl Module linear aggregates are formed by the cyclohexyl Module. These are also obtained at measurements with lower concentrations. It may be noted, that the aggregates obtained at 0.1mM from AFM and HIM

measurements do not match. As described in the previous chapter, the surface of the silicon waver is not wetted completely, but droplets of solution are formed on the surface. After evaporation of the solvent, circular spots are formed which leads to a locally higher concentration at evaporation as well as a denser distribution of aggregates which is a possible explanation for the differing results of the measurements.

5.3.3 Assembly mode

At this point two results can be noted. The first result is that both monotopic Modules indeed form assemblies despite their monomeric UV/vis spectra in THF. The second result is the difference in the assemblies of both Modules found with AFM and HIM, which is assumingly attributed to the different substitution at the imide postition. Recalling the two suggested assembly possiblities from the beginning of this chapter, these differed significantly in their build-up and possibility to elongate along various axes for the two monotopic Modules. To see if the aggregation can be explained by one of these models, they will be used as a basis for further discussion. To clarify which of the initially suggested assemblies is the most probable and if the models are in agreement with the recorded measurements, MM-calculations were made. The dimer of the respective monotopic Module with already assembled zwitterionic GCP units was stacked in two different versions in these calculations. In the homotopic assembly, a stacking of straight dimers occurs whereby each perylene core is stacked onto the respective perylene core of the next dimer and each zwitterion dimer onto the next zwitterion dimer. In the heterotopic stacking a folding of the dimeric Module takes place which causes an intercalation of the zwitterion dimer between the two perylene subunits. The outer perylene units are then further stacked to form an assembly in an ABAABA way. To obtain comparable structures, 4 dimeric Modules were stacked in the respective manner and the energetic minimum was calculated. All calculations were performed by Willi Sicking with Maestro V 9.3 and minimized with MacroModel V 9.9. The conformation analysis with 1000 cycles was calculated with a OPLS_2005 force field and water as solvent. The calculations were made with a short glycol chain, since the large polyethylene glycole chains cause convergence problems upon minimization.

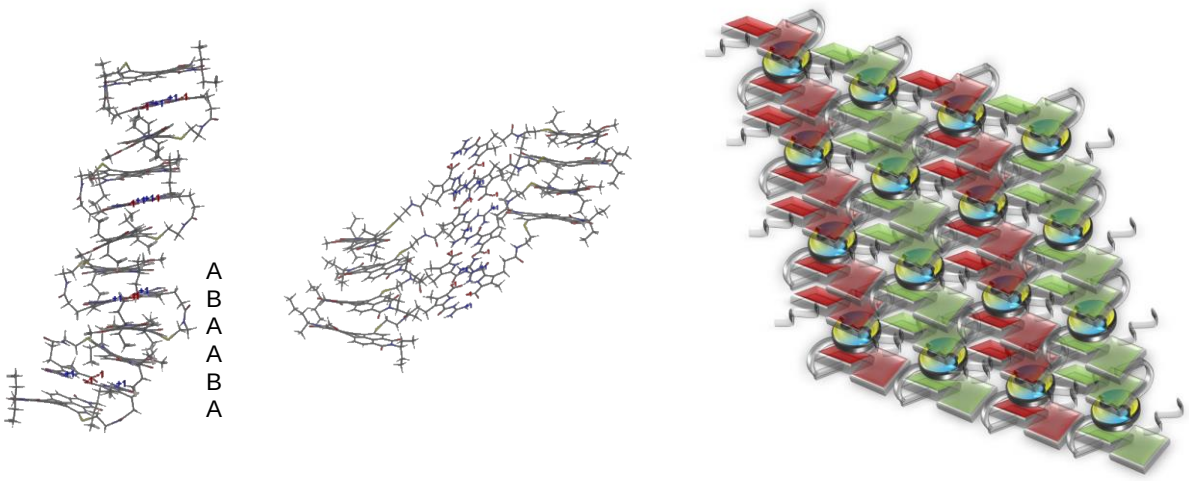

ΔG = - 62.84 kJ/mol ΔG = 0 kJ/mol

Figure 101: MM-calculations of 4 dimeric 3-pentyl Modules (8 molecules, dimierized through the zwitterionic GCP unit) with ΔG values. Left: heteroptopic ABAABA stacking; Middle: homotopic $(A)_n(B)_n(A)_n$ stacking. Left: Schematic representation of the proposed layered aggregation.The different heterotopically stacked strings are marked in different colors.

The different calculated structures of the 3-pentyl Module are depicted in Figure 101. The energetic minimization lead to an energetic difference of ΔG = - 62.84 kJ/mol for the heterotopic compared to the homotopic assembly. The results of the MM-calculations suggest that for the 3-pentyl Module, the heterotopic assembly is the most stable. The height of the calculated aggregate is 3.8 nm for the homotopic and 1.6 nm for the heterotopic assembly. Recalling the results of the AFM measurement, the aggregate of the 3-pentyl Module at 0.5 mM was about 1.6 nm in height. The homotopic assembly would be significantly too large, while the heterotopic assembly matches the results of the AFM measurements very well. This further suggest that the principal assembly mode for the 3-pentyl Module is the intercalated assembly similar to the ditopic Modules. The 3-pentyl chains in the aggregate further enable an interlinking of separate strings. When these strings fuse, a layered aggregate can be formed, which is in accordance with the structures observed in the microscopic images. A schematic representation of this assembly is also shown in Figure 101. The polyethylene glycol chains that were neglected in the calculation will wrap around both sides of the layer in the proposed assembly. When the chains are arranged flat on the respective surface, they would not add significantly onto the height of the aggregate, also explaining the smooth unstructured surface in AFM and HIM

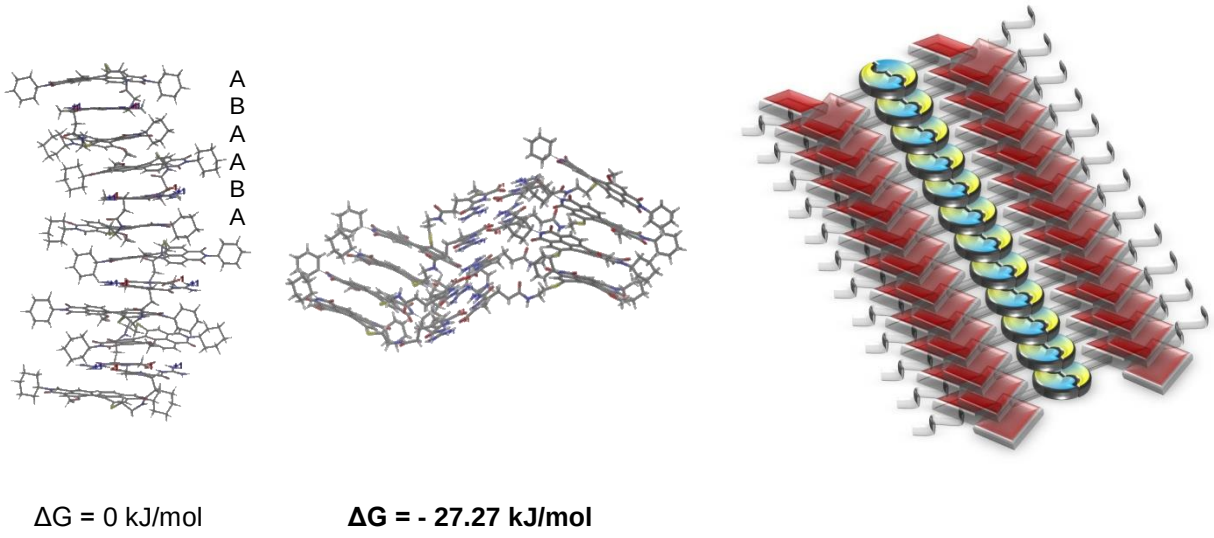

ΔG = 0 kJ/mol **ΔG = - 27.27 kJ/mol**

Figure 102: MM-calculations of 4 dimeric cyclohexyl Modules (8 molecules, dimierized through the zwitterionic GCP unit) with ΔG values. Left: heteroptopic ABAABA stacking; Middle: homotopic $(A)_n(B)_n(A)_n$ stacking. Left: Schematic representation of the proposed homotopic linear aggregation.

The calculated assemblies of the cyclohexyl Module are shown in Figure 102. The energetic minimization resulted in an energetic difference of ΔG = - 27.27 kJ/mol for the homotopic assembly compared to the heterotopic. This suggests that for the cyclohexyl Module the most stable aggregate is the homotopic assembly. Comparing the energetic difference to the value found for the 3-pentyl Module, the difference is not as significant though. The height of the aggregate for the calculated molecules is 3.8 nm for the homotopic type and 2.0 nm for the heterotopic. Since the AFM measurement of the cyclohexyl Module at 0.5 mM revealed an assembly that was about 4 nm in height, both assembly types could explain the height. The sides feasible for the formation of H-bonds in the heterotopic assembly are shielded by the PEG chains though, assumingly inhibiting the aggregation into a double string. This means that the formation of a homotopic assembly is more probable. In the AFM measurements of the 0.5 mM solution also aggregates with a height of about 1 nm were reported, which furthermore matches the homotopic assembly. The polyethylene glycol chains would face outside in the proposed assembly and wrap around the linear aggregate, also not contributing significantly to the overall height of the molecule.

The calculations show that the microscopic results can be explained with these models. The question is now, if the assembly models can also elucidate the results of the UV/vis measurements. The cyclohexyl Module showed an increase in extinction coefficient with decreasing concentration, which was in good accordance with literature known aggregation behavior of other PDI systems, while the 3-pentyl Module did show an unusual decrease in extinction coefficient with decreasing concentration. If the cyclohexyl Module aggregates as suggested by the MM calculation, only the PDI-PDI

deaggregation influences the spectral part from 400 - 600 nm. The deaggregation leads to a weaker charge transfer between the perylenes which causes an increase of the extinction coefficient upon dilution. In contrast to this homotopic deaggregation, the 3-pentyl Module would aggregate in a heterotopic manner with zwitterionic dimers intercalating between two PDI-subunits and therefore influencing the deaggregation behavior significantly. As mentioned previously this behavior is also observed for the ditopic Modules. They also aggregate in a heterotopic manner with an intercalation of zwitterionic dimers between the PDI units which assumingly leads to a charge transfer causing the decrease in extinction coefficient upon dilution. This different aggregation would also explain the difference in overall extinction coefficient between the cyclohexyl Module and the 3-pentyl Module. The interaction between perylene and zwitterionic dimer could lead to an intramolecular charge transfer for the 3-pentyl Module that causes a lower overall extinction coefficient.

The last result which is still unclear in this context is the existence of the monomeric spectral curve in UV/vis in THF for both Modules even though an assembly is being formed. The stacking distance of the perylenes subunits in the MM-calculatiosn of the monotopic Modules is 3.8 Å for both Modules. The calculation was performed with water as solvent as reported above. For less polar solvents a larger distance between the perylene subunits is anticipated, since the solvophobic effect on the aggregate is significantly lower. MM-calculations with octanol as solvent for example gave a stacking distance of about 5 Å for the Modules. It was suggested in the last chapter that a stacking distance of more than 4 Å does not result in a spectral change upon aggregation. Taking these considerations into account, both assemblies probably crossed this distance in THF and therefore show a monomeric spectrum in UV/vis even though they are forming aggregates at this concentration. Zhang et. al recently reported a series of perylene diimides where also monomeric spectrum was observed for aggregates dyes.[66] The assembly of molecule **61** was investigated in DCM and EtOH, whereby DCM is normally attributed to a disaggregated PDI and EtOH to an aggregated PDI. The PDI was dissolved in different ratios of the two solvents so the solvent influence changed from aprotic to protic with a change in polarity.

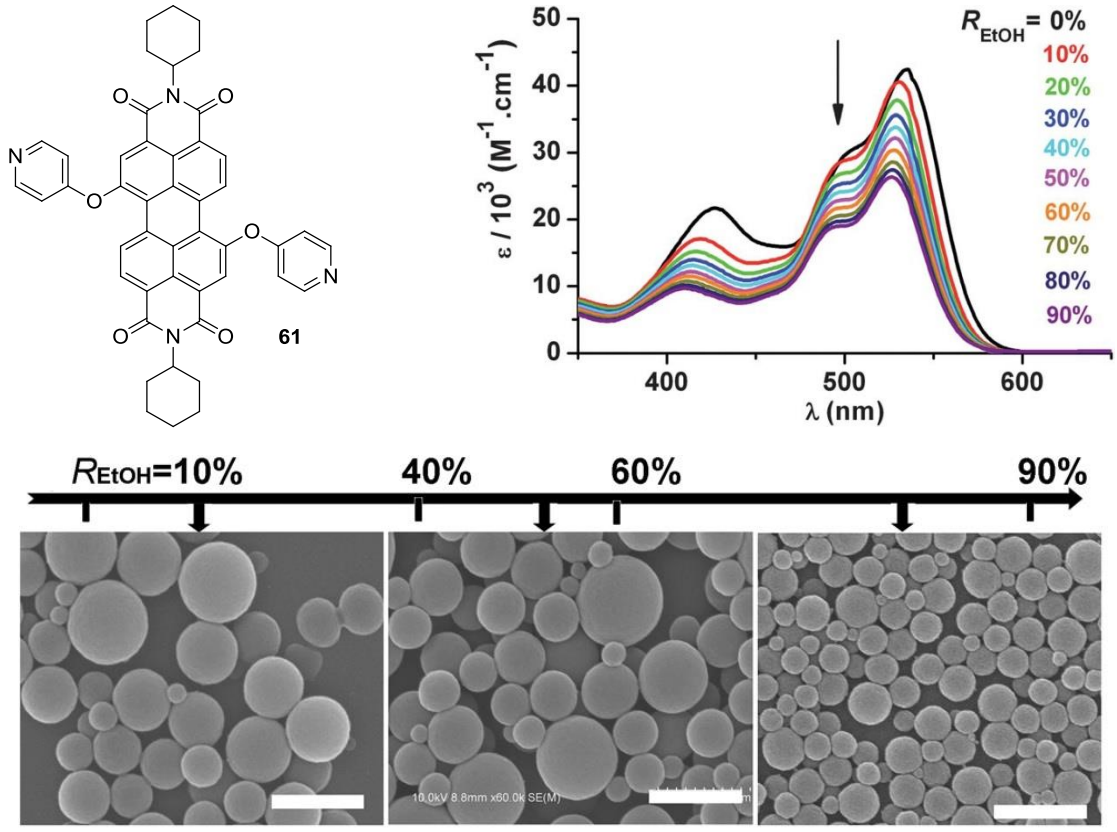

Figure 103: Above right: Absorption spectra of molecule **61** measured in DCM-EtOH mixtures with R_{EtOH} = 0, 10, 20, 30, 40, 50, 60, 70, 80 and 90%. Below: SEM images of the final nanomorphologies of molecule x formed from DCM-EtOH mixtures. The unlabelled scale bars are 500 nm. For all samples, concentration is 1 mM. Reproduced from Z. Zhang, X. Zhang, C. Zhan, Z. Lu, X. Ding, S. He, J. Yao, Soft Matter, 2013, 9, 3089-3097 with permission of The Royal Society of Chemistry. [66]

The spectrum with absorption maxima at 490 nm and 540 nm for the excitation from ground to first state and a second band at 410 nm for the excitation from ground to second state is very similar to the one found for the monotopic Modules. Even though a monomeric spectrum is recorded, the PDI **61** forms circular aggregates that were observed with SEM. The stacking distance of 4 Å between the perylene units in this bilayered aggregate was determined with XRD. This further underlines the initial suggestion that the threshold to cause a change in UV/vis for the stacking distance of PDIs is about 4 Å, explaining the monomeric spectra for both Modules.

5.4 Switching ability

While the previous part of the chapter introduced the two monotopic Modules and gave insight into the aggregation behavior in THF, this part will outline the switching ability of the systems. As mentioned in the conceptional part of this thesis, the principal idea of this thesis is the creation of switchable supramolecular systems. Therefore different stimuli should be applied to the monotopic Modules to see if changes of the assembly occur. In the last part, concentration and temperature dependent changes were already observed for both Modules. While concentration dependent changes are generally known for supramolecular systems, this thesis wants to apply other stimuli to specifically target the two functional units in the Modules, GCP and PDI. As introduced earlier, the zwitterionic GPC unit is prone to a switching with acid and base while the perylene diimide can be switched upon addition of sodium dithionite. As the two Modules form different assemblies, also a different behavior upon switching is anticipated.

5.4.1 Acid and base

To investigate the switching ability with acid and base, UV/vis measurements of both Modules were performed with varying amounts of TFA and TEA.

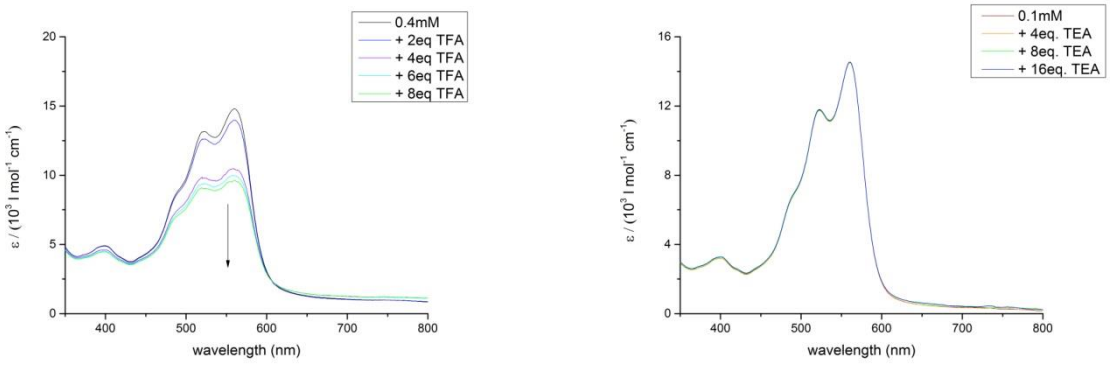

Figure 104: UV/vis measurements of the 3-pentyl Module at 0.1 mM with varying amounts of TFA/TEA in THF. Left: Measurements with acid, Right: Measurements with base.

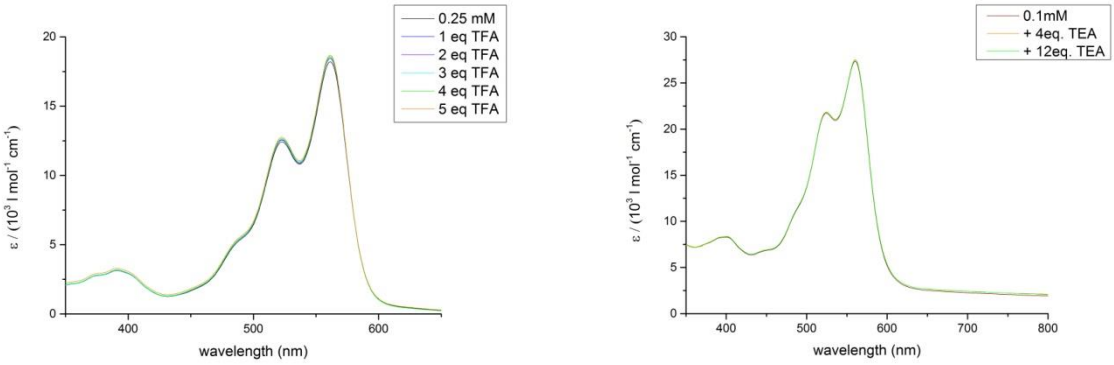

Figure 105: UV/vis measurements of the cyclohexyl Module at 0.1 mM with varying amounts of TFA/TEA in THF, Left: Measurements with acid, Right: Measurements with base.

Most recorded UV/vis measurements of the monotopic Modules surprisingly show the same behavior upon addition of acid and base. The spectral curves do not change upon addition of the stimuli, which can be observed for the switching of the 3-pentyl Module with base and all investigated solutions of the cyclohexyl Module. The only case where a change in UV/vis upon addition of the stimulus occurred, is the switching of the 3-pentyl Module with acid. Upon addition of TFA, a decrease in extinction coefficient can be observed. Therefore the question arises, if only the 3-pentyl Module can be switched with acid and no switching is possible for the cyclohexyl Module.

To check whether a switching can be observed in microscopic images, AFM measurements were made with a 1 mM solution and a corresponding solution with 5 eq. of acid or base.

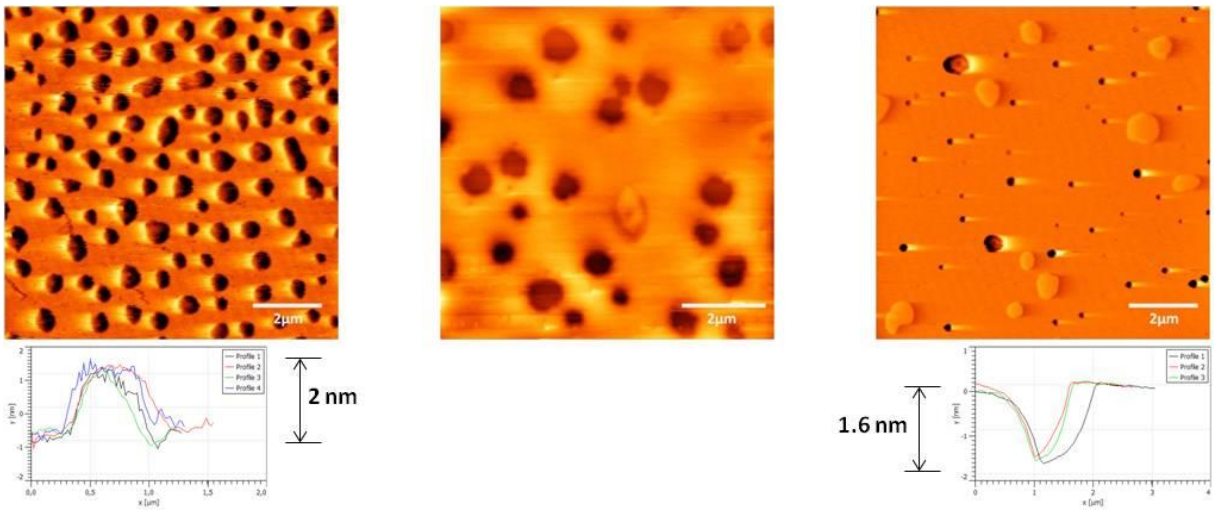

Figure 106: AFM height images and height profiles of the 3-pentyl Module upon addition of acid and base at 1 mM in THF. Left: Addition of 5 equivalents TFA; Middle: Reference image of the 1 mM solution of the neutral 3-pentyl Module in THF; Right: Addition of 5 equivalents TEA.

In the case of the 3-pentyl Module, a change can only be observed in the acidic case. The addition of the acid leads to the formation of large sheet like aggregates, which are irregularly formed. The height of these aggregates is about 2 nm. This is in good agreement with the previously reported heterotopic aggregate. A possible explanation is that the aggregate itself is not completely rearranged, but only cut off at the end to form smaller sheets which would also explain the irregular shape of the aggregates. With addition of base to the acidic solution, the initial assembly can be restored. Upon addition of base, the AFM images do not exhibit any change in aggregation. The height image still shows a layered aggregate with a height of about 1.6 nm. This means that the layered structure is still prevailing for the alkaline state.

A possible explanation for this behavior lies in shielding of the zwitterion dimer that is not easily accessible for base as shown in Figure 107.

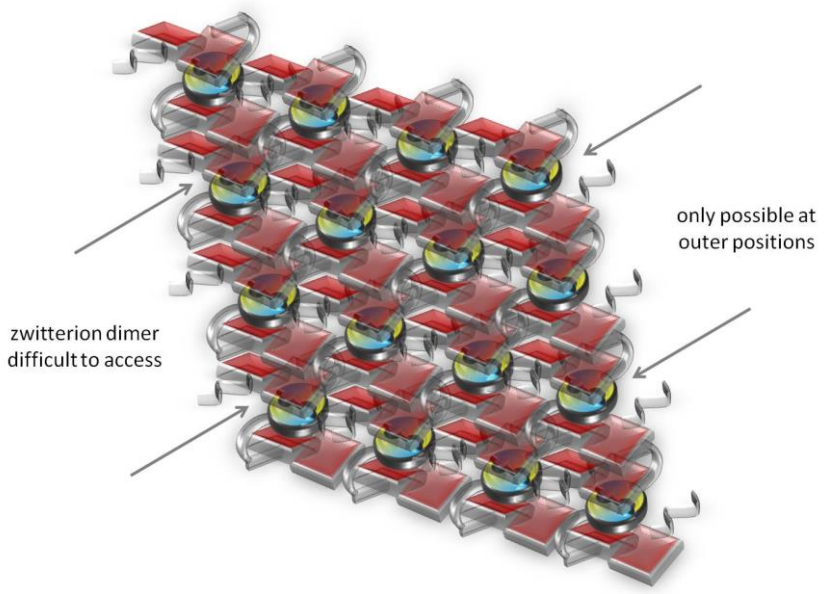

Figure 107: Schematic representation of the previously proposed layered aggregate of the 3-pentyl Module and accessible points for approach of acid and base.

The 3-pentyl groups interlink in this assembly to form a stable two dimensional aggregate, while the PEG side chain wraps around the back and the front of the assembly. This leads to a good shielding of the zwitterion dimer by the perylene core because of the sandwich position. With such kind of tightly packed arrangement, the approach of acid or base towards the switchable zwitterionic unit is sterically hindered. This can explain the formation of the small sheets for the acidic case, because only the zwitterion dimer at outer positions of the layered aggregate are accessible for a protonation. Since the zwitterion dimer is then not stacked onto the perylene unit, at least at the edges of the aggregate, the

larger influence of the PDI-PDI stacking on UV/vis leads to a decrease in extinction coefficient. The intercalation can further explain the different behavior upon addition of acid and base. In the case of the acid, the proton is small enough to reach the switchable zwitterionic unit. TEA in the basic solution is a lot bigger compared to the proton, so the approach is sterically disfavored compared to the acid.

The AFM measurements of the cyclohexyl-Module show a completely different behavior upon addition of acid and base. A change in aggregation can be observed clearly in the AFM height images.

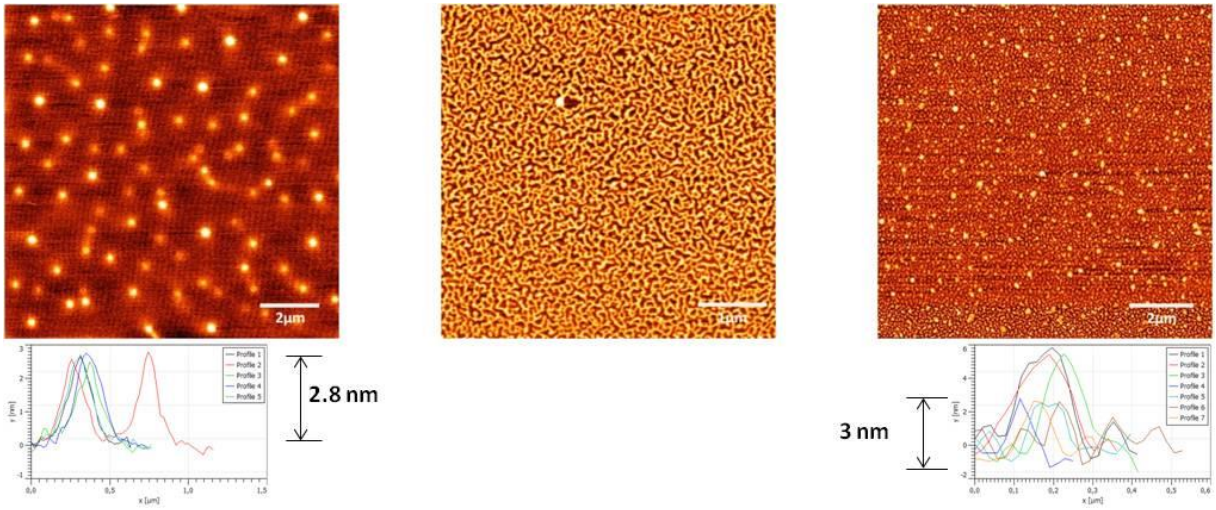

Figure 108: AFM height images and height profiles of the cyclohexyl Module upon addition of acid and base at 1 mM in THF. Left: Addition of 5 equivalents TFA. Middle: Reference image of the 1 mM solution of the neutral 3-pentyl Module. Right: Addition of 5 equivalents TEA.

With addition of acid, a change in aggregation to circular aggregates can be seen. The phase images reveal the formation of solid particles. The height of the aggregate is about 2.8 nm. Upon addition of base the switching is as distinctive as in the acidic case. The images show the beginning formation of circular aggregates, while the phase images also reveal the formation of solid particles. The height profiles of the anionic Module give a height for the aggregates of about 3 nm and 6 nm. Therefore it can be stated that a switching is indeed possible for the cyclohexyl-Module. Upon neutralisation with the respective amount of acid and base, the initial assemblies can be restored, which means that also a reversible switching is possible.

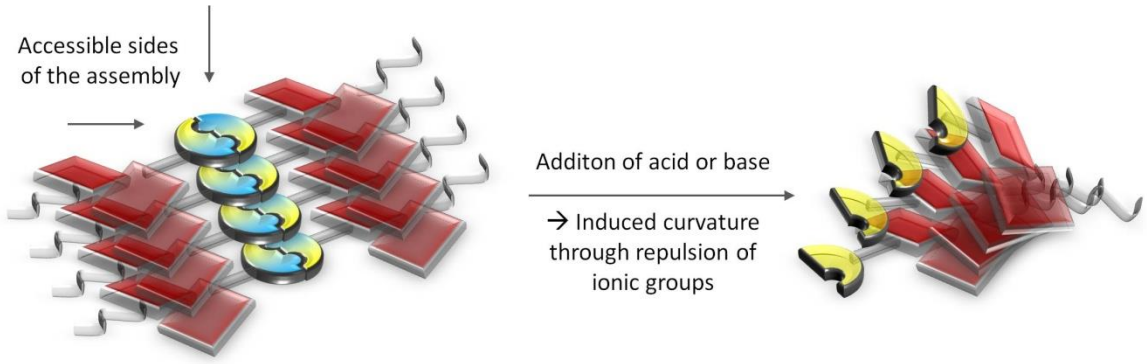

Figure 109: Schematic representation of the previously proposed layered aggregate of the cyclohexyl Module and accessible points for approach of acid and base. The protonation respectively deprotonation of the zwitterionic GCP unit induces a curvature through the repulsion of the ionic groups which is shown on the right side.

The build-up of the straight assembly leaves two sides of the molecule "unshielded" and therefore accessible for the stimuli. Acid or base can easily reach the zwitterion dimer to enable a switching of the aggregate. The aggregate is then cut off in the middle of the molecule at the GCP units, which assumingly results in similar aggregates for the cationic and anionic Module. The repulsion of the ionic groups in anticipated to induce a curvature of the assembly. If the PEG chains coil in the middle of the spherical aggregate, the expected size is bigger than only half of the initially calculated molecule, since the PEG chains were neglected in the calculation of the neutral assembly. This means that the size of the aggregate is in accordance with the height of 3 nm found in AFM. While the cationic Module forms micellar aggregates, the anionic Module simultaneously builds up single and double walled aggregates, explaining the size of 3 and 6 nm. The slight variation in size between the cationic and anionic Module might derive from different respective arrangement of the perylene units like reported for the ditopic Modules. For this case, it is not easy to distinguish though, since no change in UV/vis occurs that could give a hint on the respective orientation of the perylene units. The lacking change in the spectral curves can be explained by the straight assembly of the dimeric Module in the neutral assembly. A switching would therefore not result in a rearrangement of the PDI dyes, because the pyrrole subunits already face in the same direction in the initial assembly.

5.4.2 Sodium Dithionite

The switching with sodium dithionite was not possible in THF. The addition of an aqueous solution of sodium dithionite led to two phases which did not mix. At the interphase between the aqueous and THF phase, a slight blue line was observed that might give a hint that indeed a switching is possible. The addition of solid sodium dithionite to the THF solution of the Modules did also not result in a change.

5.5 Assembly in water

As mentioned previously, one goal of this part of the thesis was the achievement of a better solubility in water compared to the ditopic Modules. Therefore one PEG chain was attached at the core of each monotopic Module. This chapter will outline the behavior of both Modules in aqueous medium. As already discussed in the previous part of this chapter which dealt with the synthesis of both Modules, the 3-pentyl Module is completely soluble in water while the cyclohexyl Module is only soluble in mixtures with THF. Therefore the next part will focus primarily on the investigation of the 3-pentyl Module in water.

5.5.1 3-Pentyl Module

To investigate the assembly, temperature dependent UV/vis measurements of the 3-pentyl Module were carried out and compared with the results of the measurements in THF.

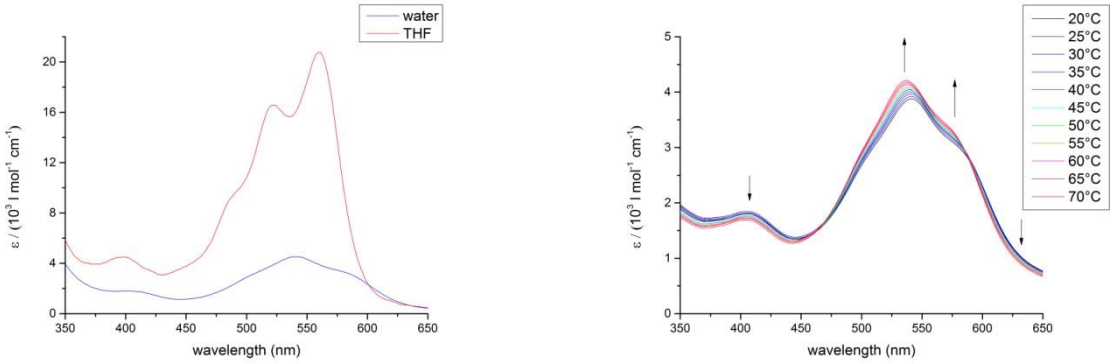

Figure 110: Left: UV/vis spectrum of the 3-pentyl Module in water (blue curve) compared to THF (red curve); Right: Temperature dependent UV/vis spectrum of the 3-pentyl Module in water in a termperature range of 20°C to 70°C. Arrows indicate the spectral change upon increasing temperature. All measurements were performed at a concentration of 0.1 mM.

The UV/vis measurement of a 0.1 mM solution of the 3-pentyl Module in water shows an "aggregated" spectrum accompanied with a loss of fine structure. The extinction coefficient is significantly lower compared to the spectrum in THF, whereby the shape of the spectrum itself is similar to those reported by Rybtchinski or Würthner. The absorption maximum undergoes a hypsochromic shift to 540 nm, which indicates the formation of an H-aggregate. The temperature dependent measurement reveals an increase of the extinction coefficient at higher temperatures for the maximum absorption band. At about 460 nm and 585 nm, an isosbestic point can be observed which usually indicates a change in assembly. This behavior is different to the temperature dependent measurements in THF,

but this does not necessarily mean that a different assembly is being formed in water. Recalling the discussion about the stacking distance in THF in the previous part of this chapter, the results of the UV/vis measurements might hint that the hydrophobic interaction indeed leads to tighter π-π-stacking within the aggregate. The driving force would be a minimization of the exposed surface in aqueous medium. A tighter stacking of the perylene subunits further results in a shift in absorption due to the interaction of the perylenes as well as an increase in extinction coefficient upon deaggregation. The results of the UV/vis measurement can therefore be explained solely by a change in the π-π-stacking distance. To investigate if this argumentation is valid and indeed the same aggregate is being formed in water or if change in aggregation occurs due to the polar environment, AFM measurements were performed.

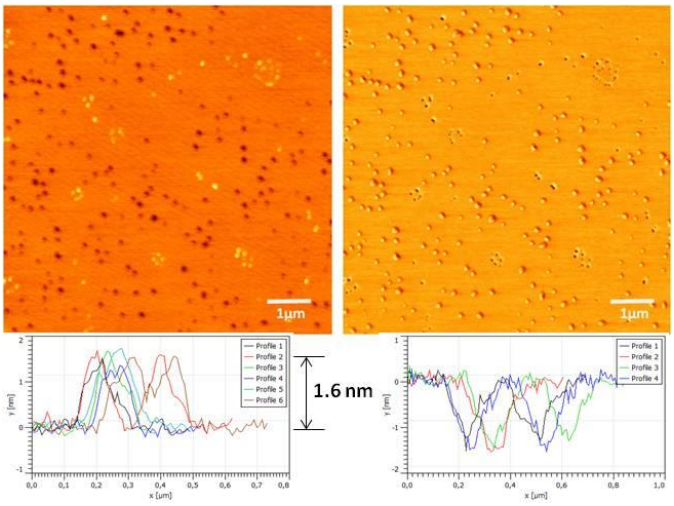

Figure 111: AFM measurements of the 3-pentyl Module in water at a concentration of 1 mM. Left: Height image; Right: Phase image; Below: Height profiles of the aggregates on the layer (left) as well as the holes in the layer (right).

The images of the 3-pentyl Module at 1 mM show a smooth layer which is even smoother as the measurements in THF showed. The dark spots in the measurements are holes in the layered structure of the 3-pentyl Module. The phase images reveal the formation of vesicles on top of the layer which are displayed in the height image as light yellow spots. The height of the layer is 1.6 nm and therefore in agreement with the AFM measurements in THF.

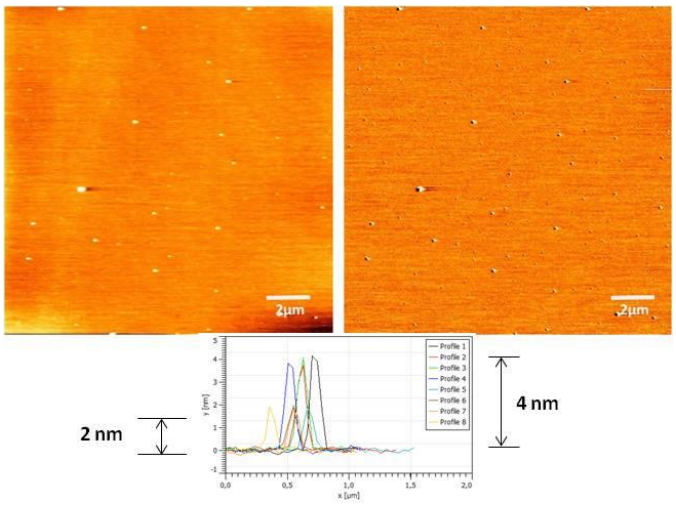

Figure 112: AFM measurements of the 3-pentyl Module in water at a concentration of 0.1 mM. Left: Height image; Right: Phase image; Below: Height profile of the aggregates.

At lower concentration of 0.5 mM, circular aggregates can be observed. The phase image as well as the height profile point to a simultaneous formation of vesicles and micelles. The smaller aggregates show a height of about 2 nm and do not exhibit a significant corona in the phase image, therefore it can be assumed that micelles are being formed. The bigger aggregates have a height of about 4 nm and show a clear corona in the phase image which is attributed to a vesicle formation. Linear assemblies could not be observed with AFM, therefore it can be stated that the principle aggregation type in water is still a layered structure at higher concentrations.

Additionally, HIM high resolution measurements were performed to see, if this method can give more detail on the aggregation behavior of the 3-pentyl Module in water. Therefore a 1.0 mM solution of the 3-pentyl Module was investigated. The sample was prepared as previously reported by spin coating of the respective solution onto a silicon target.

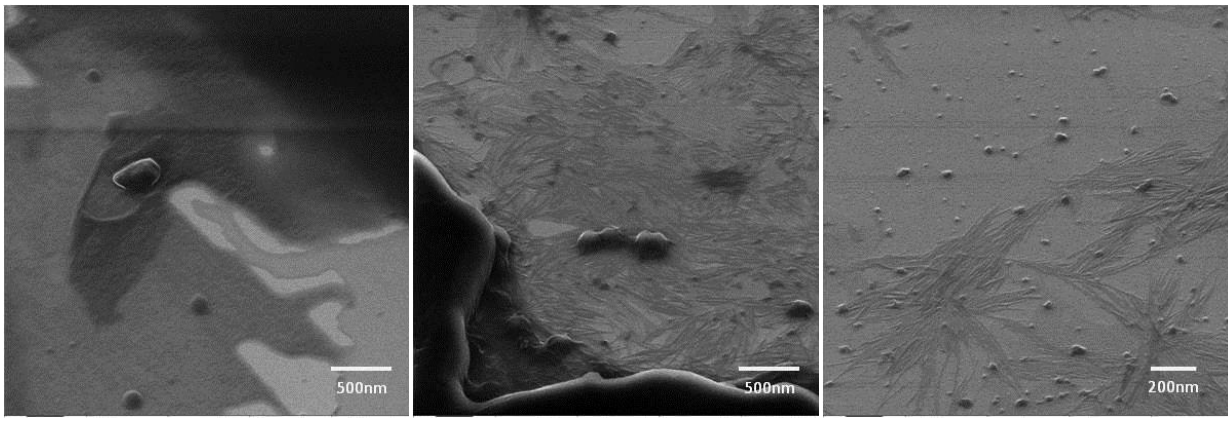

Figure 113: HIM measurements of the 3-pentyl Module in water at a concentration of 1.0 mM; different spots and magnifications.

The HIM pictures at 1.0 mM depicted in Figure 113 show a layered assembly with a smooth even surface. The magnification reveals that several layers are stacked onto each other. This means that the 3-pentyl Module forms large layered aggregates on the silicon surface. Further magnification reveals that linear aggregates are formed beneath the layered assembly. The strings are straight and slightly bended, but not randomly twisted or oriented like observed in the AFM measurements. Thereby several packs of strings are stacked onto each other. At the interphase of both aggregates, it looks like strings and layers fuse together. Therefore it can be assumed that the layered aggregate is regularly build up by the linear strings. The same behavior was earlier reported for the assembly of the 3-pentyl Module in THF and suggests that the same assembly is being formed in aqueous solution which would also be in accordance with the UV/vis measurements.

5.5.2 Cyclohexyl Module

Even though the cyclohexyl Module is not completely soluble in water, it shall nonetheless be investigated how the Module assembles in aqueous mixtures of THF. The maximum amount of water that could be added to a solution of the cyclohexyl Module without causing a precipitation of the substance, was 50% at concentrations between 10 µm and 1 mM. Therefore AFM measurements were made in H_2O/THF (1:1).

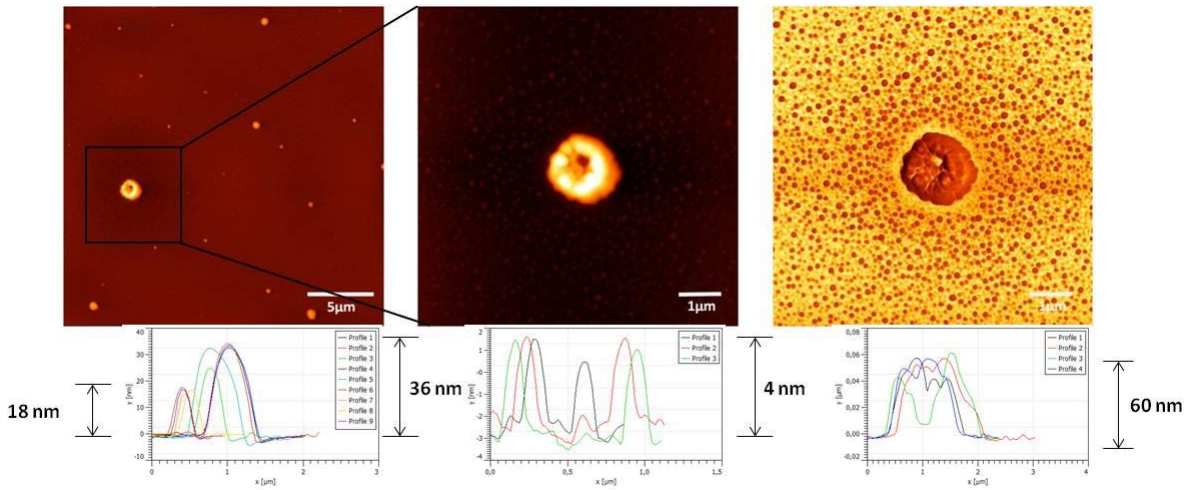

Figure 114: AFM measurements of the cyclohexyl Module in water/THF (1:1 ratio) at a concentration of 0.5 mM. Left: Height image; Middle: Magnification of a distinctive aggregate on the height image; Left: Phase image of the magnified aggregate. Below: Height profiles of the different aggregates found in the AFM measurement. Right: bigger particles in the height image on the left; Middle: Smaller particles of the height image in the middle. Left:Ddistinctive aggregate of the height image in the middle.

The images of a 0.5 mM solution of the cyclohexyl Module reveal the formation of spherical particles as well as larger circular aggregates. The phase images give no hint about a vesicle formation, so it is

safe to state, that solid spheres are formed upon addition of water. Whereas the bigger particles have a height of about 18 and 36 nm, the smaller aggregates show a height of about 4 nm. The smaller aggregates are assumingly micelles with the according height of the homotopic assembly found for the cyclohexyl Module in THF. This suggests that the same assembly type is still prevailing in aqueous mixtures. The middle sized aggregates may furthermore be build-up by micelles or short stacks with the same height, which would explain the size that is divisible by 4 nm. These aggregates can be formed by an interpenetration of the PEG chains which face outwards of the assembly. In the AFM image of one of the larger aggregates, it looks like an agglomerate of the middle sized particles is being formed.

Since methods where aggregates are investigated on a surface do not always reflect the actual assembly situation in solution, cryo-TEM measurements were performed by Haim Weissman. The measurements investigate the time dependent formation of aggregates in solution.

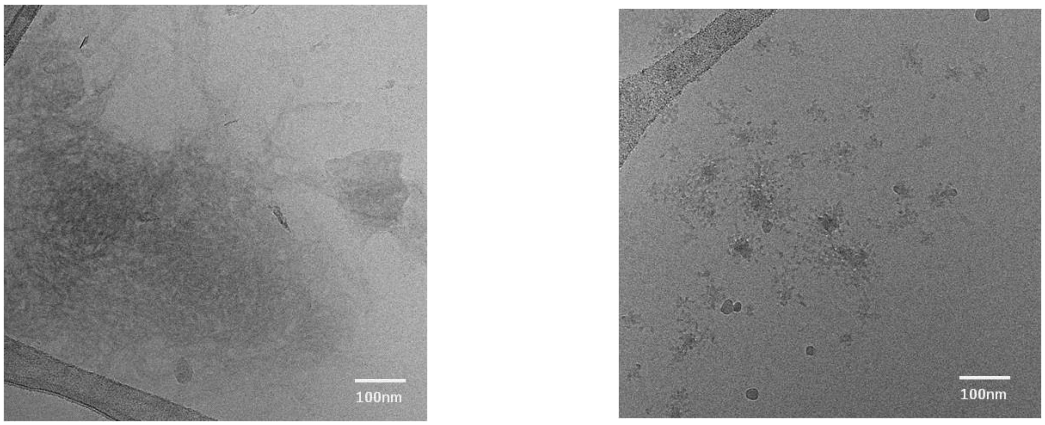

Figure 115: Cryo-TEM images of the cyclohexyl Module in water/THF (1:1 ratio) at a concentration of 0.5 mM. Left: measurement after 5 hours; Right: measurement after 24 days.

Two measurements were made after different time spans; one after 5 hours and one after 24 days. To enable a comparison between both methods, AFM measurement were also performed after each time period, but they did not show any difference to the assemblies reported above. The cryo-TEM measurement after 5 hours shows long linear fibers that are entangled, coiled and overlap significantly. The size of the fibers could not be distinguished due to large overlap of the strings. After 24 days, no long linear strands were observed in the measurement. Instead, only short linear strings and spherical particles were found in solution. It looks like these short linear strands fuse together to form the spherical particles. A likely explanation for this behavior is the formation of primary stacks which condense into larger globular aggregates like explained in the conceptional part of this thesis.[48] When these kinds of aggregates themselves assemble again, a larger agglomerate can result.

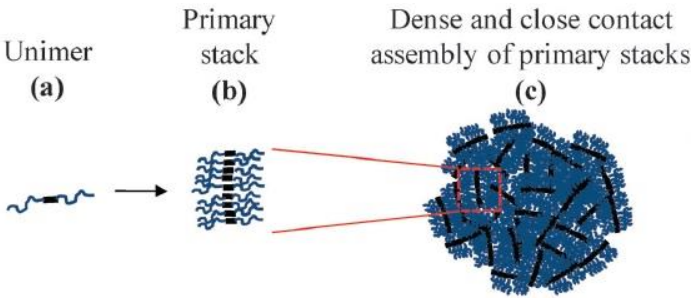

Figure 116: Schematic representation of the proposed aggregation mode of cyclohexyl Module in water/THF mixtures analogue to the example of Jouault and coworkers.[48]

This gives a good idea about the principal build-up of the spherical particles. The cryo-TEM measurements further underline the difference between solution based and surface based microscopic methods. The influence of the (charged) surface or evaporation effects can highly impact the aggregation. For the cyclohexyl Module it could be shown that the labile strings condense in aqueous solution to form solid sphere particles. Hereby the driving force is probably the reduction of the exposed surface to the polar solvent.

5.6 Gel formation

The last goal of this thesis was the formation of switchable supramolecular gels with the monotopic Modules. Therefore different pathways were investigated to achieve a gel formation.

First of all, a solution with a concentration of 50 mM was made of both monotopic Modules in THF. These solutions did not show any significant change in viscosity compared to pure THF, judging from the outside. The first conditions to form a gel which were chosen, are described in the paper of Krieg and coworkers.[51] Therefore a 50 mM solution was treated with the tenfold amount of water under vigorous shaking. In the case of the 3-pentyl Module, the solvents simply mixed to yield a purple solution of the Module, while in the case of the cyclohexyl Module a precipitate formed. The method was repeated several times with different concentrations (0.1 mM - 100 mM) and amounts of water (10% - 100%), but each time no gel was formed.

Subsequently heating experiments were made with the precipitated solution of the cyclohexyl Module in all variations. Unfortunately, no gel formation could be observed even after 15 minutes of heating and cooling down again. Samples of the 3-pentyl Module in water at varying concentrations were also heated for several minutes, again with no change in viscosity or any hint of a gel formation, even at lower concentrations, where a rod assembly was observed in AFM and HIM.

The lacking gel formation for the 3-pentyl Module is not overly surprising, since the Module forms layers in water. With this kind of assembly, no separate fibers exist, that can entangle to form a gel. Even with the heating of the Module, the interlinking between the strings via the 3-pentyl-chain is maintained. The cyclohexyl Module on the other hand does form separated fibers but it is too insoluble in water and precipitates upon addition of water. It might be possible to form gels with different solvent mixtures, but this thesis did not evaluate these possibilities further. So unfortunately it was not possible to form a supramolecular gel with one of the monotopic Modules.

5.7 Summary

This chapter showed the successful monotopic attachment of the zwitterionic binding motif to a perylene diimide. It was possible to synthesize and investigate molecules with different substitution at the imide position. Due to this different substitution, the two presented molecules formed different assemblies in THF. While the 3-pentyl Module layered assembly through a heterotopic stacking of the subunits, the cyclohexyl Module built up a linear aggregate by a homotopic stacking.

Both Modules are reversibly switchable, but only the cyclohexyl Module could be switched with acid and base. The 3-pentyl Module was only switchable with acid due to the tight assembly that inhibited the switching with base. The solubility of both monotopic Modules was investigated in water, whereby only the 3-pentyl Module was water soluble. The principle sheet like heterotopic assembly of the Module was maintained even in highly polar solution. The cyclohexyl Module was not soluble in water but mixtures with THF whereby globular aggregates are formed which are based on the linear homotopic aggregate. A gel could unfortunately not be formed due to the layered aggregation of the 3-pentyl Module and due to the bad solubility of the cyclohexyl Module. The creaction of these Module enables manifold possibilities to adjust the molecule to achieve a gel formation though.

6. Summary

The goal of this thesis was the creation of bi-functional supramolecular systems which exhibit a manifold switching ability based on the known stimuli for the underlying functional units. The supramolecular systems should furthermore form aggregates that are stable in polar media. Starting point for this development were two different functional units shown in Figure 117.

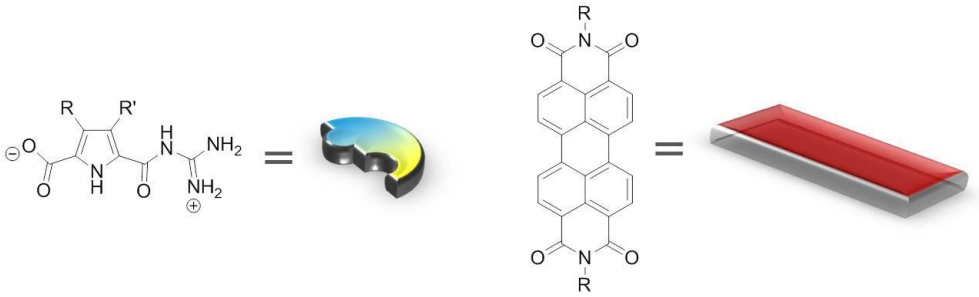

Figure 117: Exemplary structural formula and schematic representation of the two functional units used in this thesis. Left: Zwitterionic GCP, Right: Perylene diimide.

As core unit, perylene diimide was chosen because of its interesting optical properties as well as its tendency to form supramolecular aggregates through π-π-stacking of the large aromatic core. Besides the principal switching ability of the PDI aggregate through a change in concentration or temperature, a novel reversible switching method with sodium dithionite was investigated. The zwitterionic GCP unit was attached to this core as binding motif to enable further aggregation. This self-complementary unit forms extremely stable dimeric aggregates in polar solutions due to a feasible combination of ionic interactions and H-bonds. Since the ionic interaction plays a significant role in the assembly, the aggregates formed by the zwitterionic GCP unit are reversibly switchable upon addition of acid and base.

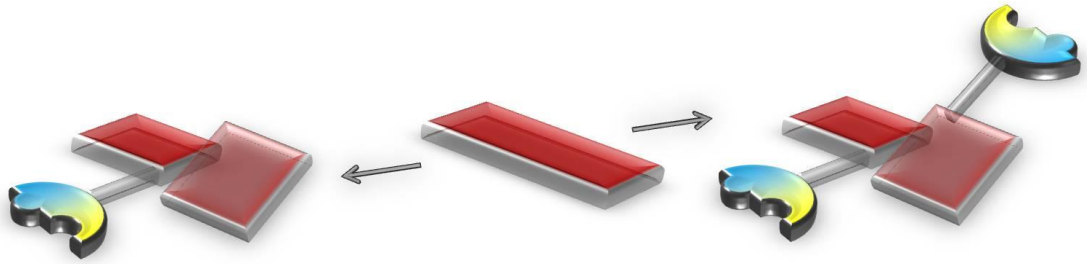

Figure 118: Schematic representation of the monotopic (right) and the ditopic (right) attachment of the GCP binding motif to the perylene core. The tilted red rectangles shall represent the twisting of the core upon substitution.

Binding motifs can in principal be attached to various positions at the perylene diimide. Most examples have the binding motifs attached on either one or two sides though. Therefore this thesis has investigated a monotopic as well as a ditopic attachment of the zwitterionic GCP unit to the perylene diimide core. The schematic representation of the monotopic and ditopic Modules is depicted in Figure 118. After successful synthesis of these new bi-functional Modules, the resulting two ditopic and two monotopic Modules were analyzed. The investigation of the principal properties of the perylene diimide - GCP zwitterion - Modules focused especially on the self-assembly of the Modules as well as switching behavior upon addition of different stimuli.

6.1 Ditopic Modules

This thesis showed a successful ditopic attachment of the GCP binding motif to the perylene core which resulted in the creation of two different Modules. In the **imide linked Module** the binding motif is attached at the imide position of the PDI while the binding motif in the **core linked Module** is attached at the core position of the PDI. This attachment at two different positions enabled a comparison of two different binding axes for the final molecules. For all Modules an elongation along the z-axis through π-π-stacking of the perylene cores is anticipated. Through an additional elongation along the x-axis for the imide linked Module and along the y-axis for the core linked Module through the bindings motifs a layered assembly was expected for both Modules originally.

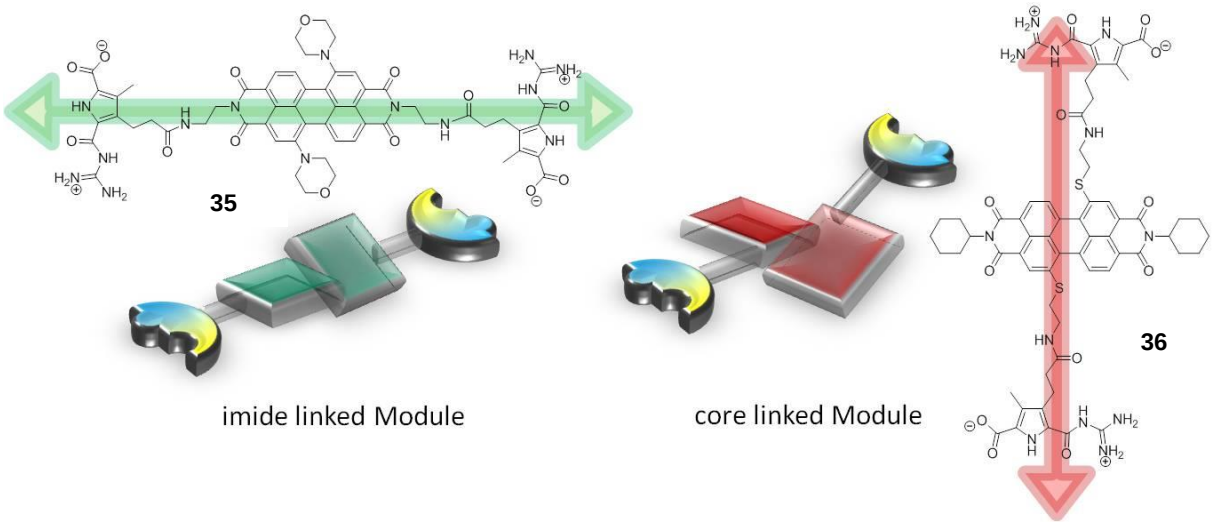

Figure 119: Imide linked Module **35** and core linked Module **36**: Structural formula and schematic representation. The arrow along the molecules shall illustrate the aspired binding axis.

The synthesis based on literature known procedures yielded in two Modules that are stable and soluble in DMSO. First measurements showed some conflicting results compared to literature known PDI system that have additional binding motifs while others revealed a similar behavior as already reported in literature. The spectral investigation with UV/vis showed a "monomeric" spectral curve for both ditopic Modules and a very unusual decrease in extinction coefficient upon dilution, which is not known for other PDI assemblies, while the analysis of the principal aggregation mechanism showed an isodesmic aggregation for both Modules which is typical for PDI assemblies. Opposite to the originally suggested layered assembly, both Modules formed network like assemblies. These branched aggregates are based on linear strands which could both be observed on a charged surface with AFM and on a neutral surface with HIM. MM-calculations revealed surprisingly no homotopic aggregates like found for comparable PDI systems, but a heterotopic assembly with an alternating arrangement of PDI and zwitterion dimer like shown in Figure 120.

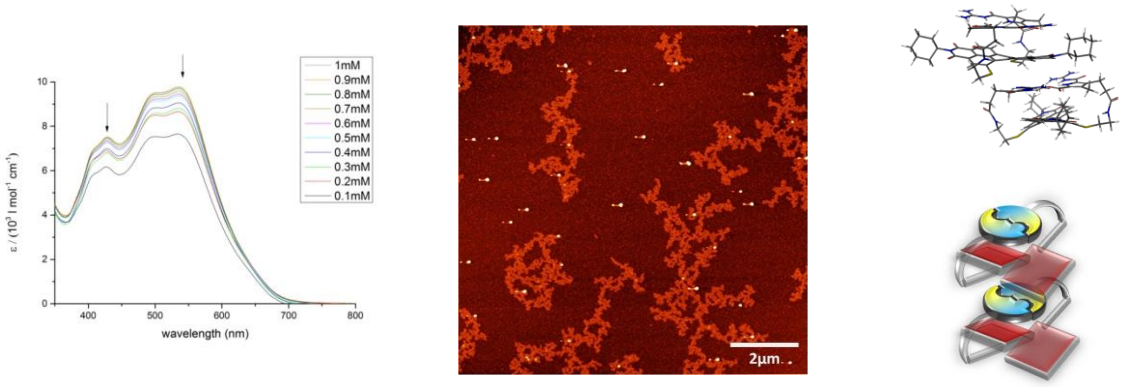

Figure 120: Left: Concentration dependent UV/vis measurements of the core linked Module in a concentration range from 1.0 mM to 0.1 mM in DMSO. The arrows indicate the spectral changes with decreasing concentration; Middle: AFM height measurements of the imide linked Module at a concentration of 0.25 mM in DMSO; Right: MM-calculation and model of the heterotopic assembly of two core linked Modules.

This heterotopic (ABAB) stacking leads to the formation of polymeric assemblies, which then further entangle to form the branched assembly observed in the microscopic measurement. The position of the perylene, isolated between two zwitterionic dimers, leads to a "monomeric" UV/vis spectrum with a lack of spectral changes upon concentration variation, explaining the results of the spectral investigation. The decrease in extinction coefficient can furthermore be explained by a possible charge transfer between the electron-rich zwitterion dimer and the electron-poor perylene diimide. The aggregate is build up by a π-π-stacking of the intramolecularly dimerized Modules, which is an aggregation analogue to literature known PDI-systems, explaining the isodesmic aggregation mechanism. What is remarkable though, is that both Modules form the same type of assembly even though the binding motifs are attached at different positions in the molecule. This is an important result

since it shows that the assembly of the investigated systems is independent of the position of the binding motif. The anticipated elongation along the y-axis could not be obtained due to the stacking of the binding motif in between two perylene cores that yielded in a sole elongation along the z-axis. This heterotopic assembly is unique to the reported ditopic Modules and has not been reported for other perylene diimide systems yet.

One exceptional feature of the core linked Module, was a time dependent aggregation change. Upon increasing time span, both spectral and microscopic measurements revealed differences in aggregation. A bathochromic shift of the maximum absorption band from 535 nm to 578 nm was observed in UV/vis with increasing time span. The vibronic fine structure also vanished with increasing time, which means that the band at 495 nm is decreasing. The shift of an absorption band as well as the loss of vibronic structure indicated the formation of a J-aggregate for the aged core linked Module.

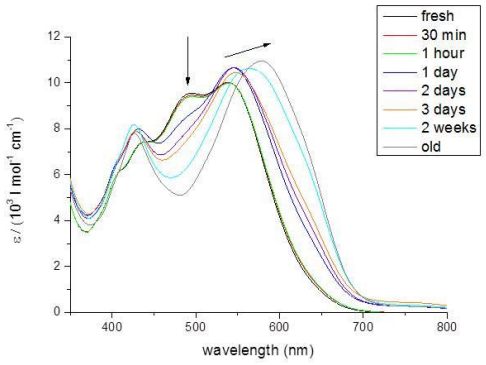

Figure 121: UV/vis spectra of the core linked Module at 0.25mM in DMSO after different time periods.

A rearrangement was clearly visible in AFM measurement. While the fresh solution of the core linked Module showed the linear aggregates, the assembly changed into a disordered structure after one week, only to reassemble into the same linear structure after one month. MM-calculations revealed a rearrangement of the hetero-assembled Module with alternating arrangement of perylene diimide and zwitterionic dimer into an energetically most favorable homo-assembled Module in an ABBAABBA-type whereby perylene diimide stacks onto perylene diimide and zwitterionic dimer stacks onto zwitterionic dimer. This means, that in principal a time dependent change from kinetically controlled to the thermodynamically controlled assembly occurred for the core linked Module.

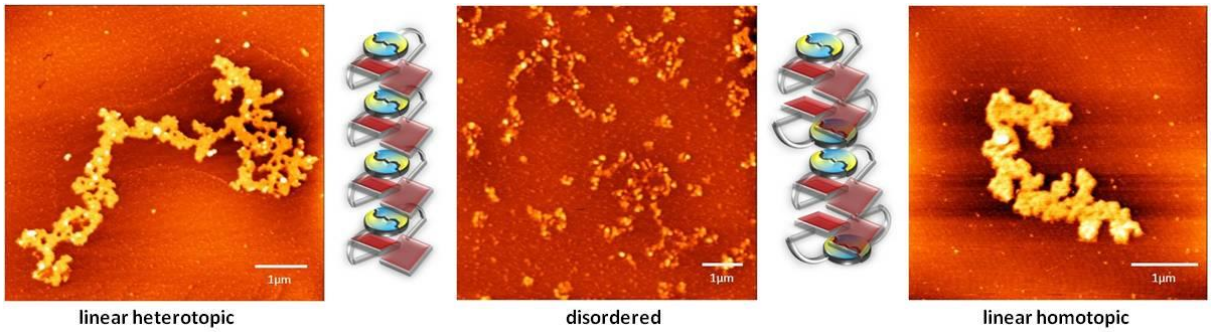

Figure 122: AFM height images and height profiles of the core linked Module at 0.25mM in DMSO. Left: Fresh solution; Middle: same solution after 1 week; Right: same solution after 1 month. The aggregation model on the left belongs to the fresh solution while the aggregation model on the right belongs to the aged solution.

The initial polymeric assembly is restored after rearrangement into the homotopic assembly, explaining the matching microscopic measurements for the fresh and the aged solution of the Module. The PDI units form a J-aggregate in the homotopic assembly causing a bathochromic shift which was observed in the UV/vis measurements. This time dependent change in assembly is an outstanding feature of the ditopic Module since such complete time dpendent rearrangement of the aggregation has not been reported yet in literature. A rearrangement could not be observed for the imide linked Module though since the heterotopic arrangement is already the thermodynamically stable assembly.

Since one goal of this thesis was the investigation of the tuning ability of the supramolecular assemblies, switching experiments were performed with acid/base and with dithionite targeting the zwitterionic dimer respectively the perylene diimide. The switching of the ditopic Modules with acid and base led to the formation of spherical aggregates in both cases. The protonation respectively deprotonation of the Module gives two GCP units with the same charge which are in near vicinity due to the alternating arrangement of perylene and zwitterion dimer in the initial assembly, causing a rearrangement so that the charged pyrrole groups point outside of the assembly enabling a π-π-stacking of the perylene cores. Recalling the results of the UV/vis measurements, the spectral changes implicate the formation of an H-aggregate for the cationic core linked Module due to a hypsochromic shift of the maximum absorption bands and a bathochromic shift for the anionic core linked Module suggesting the formation of a J-aggregate. A model of the two assembly modes is shown in Figure 123.

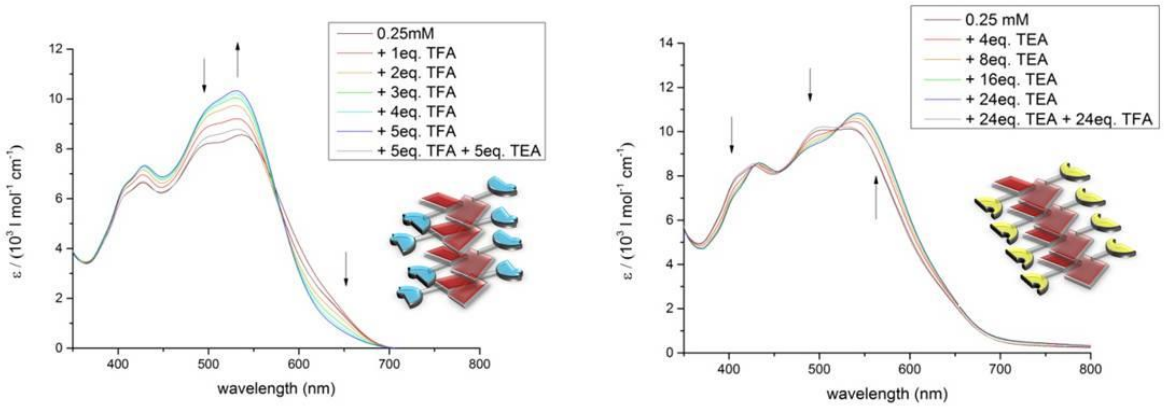

Figure 123: UV/vis spectra of the the core linked Module with addition of acid and base at 0.25 mM in DMSO. Left: measurements with acid. Right: measurements with base. Inset left: cationic core linked Module which is anticipated to form an H-aggregate. Inset right: anionic core linked Module which is anticipated to form a J-aggregate.

For the imide linked Module the same aggregation is anticipated, only the size of the aggregates is different compared to the core linked Module. This can be explained best by the different molecular build-up of both Modules due to the different position of the binding motifs at the perylene diimide. This furthermore shows that the assembly of the cationic and anionic Modules is also independent of the position of the binding motif. It could be furthermore shown that a reversible switching is possible both with acid/base since the initial assembly reformed upon neutralization.

The switching with sodium dithionite also led to a change in arrangement into spherical aggregates. Upon reduction of the perylene diimide, a rearrangement into homotopic stacks occurs which was underlined by MM-calculation. For imide linked Module a J-aggregate is being formed while the core linked Module preferentially forms an H-aggregate explaining the different spectral shift in UV/vis. It has to be noted that these are the first measurement were the two ditopic Modules form different assemblies. It is not clear though, if the different aggregation is caused by difference in attachment of the binding motif or if the bulky morpholine group at the core of the imide linked has a more significant influence on the assembly.

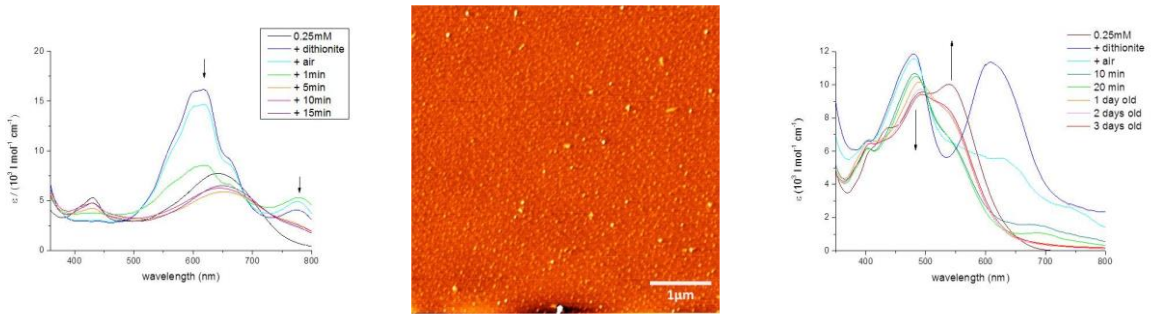

Figure 124: UV/vis spectra of the imide linked Module (left) and the core linked Module (right) after addition of $Na_2S_2O_4$ and oxidation with air at 0.25 mM in DMSO. Middle: AFM height image of the imide linked Module after addition of $Na_2S_2O_4$ at 0.25 mM in DMSO.

The initial assembly is restored after reoxidation only for imide linked Module. The core linked Module does not re-form the initial assembly probably due to a kinetic trapping of the H-aggregate that prohibits the re-formation of the alternating stacking or the change into the thermodynamically stable J-aggregate that was reported after aging. The energetic difference between the H- and J-aggregate is assumingly too small to cause a rearrangement explaining also the lack in aging behavior after switching with sodium dithionite.

6.2 Monotopic Modules

Opposite to the ditopic attachment, also one binding motif was introduced to the perylene core in this thesis to have the possibility to attach other substituents at the other side. For a good solubility in water PEG chains were connected to the perylene core, which were also supposed to add an additional supramolecular interaction through an interpenetration of adjacent PEG chains. Two molecules were successfully synthesized to study the principal assembly and investigate the possibility of a gel formation. Furthermore this thesis focused on the influence of a 3-pentyl-chain at the imide position that principally enables an interlinking of adjacent molecules that also have 3-pentyl groups at the imide position. Therefore one Module with 3-pentyl chains at the imide positions was synthesized (**3-pentyl Module**) while the comparable molecule has a closed cyclohexyl chain at the imide position (**cyclohexyl Module**), inhibiting the interlinking possibility in this case.

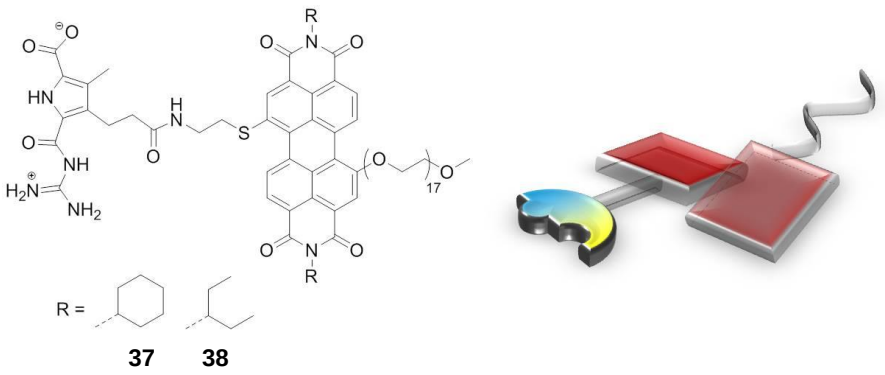

Figure 125: Monotopic Modules **37** (cyclohexylamine substituted) and **38** (3-pentylamine substituted): Structural formula and schematic representation.

The monotopic Modules shown in Figure 125 were expected to form dimers through the self-complementary zwitterionic interaction of the GCP binding motif. This self-assembled dimer is similar to various molecules reported by the working group of Rybtchinski and was expected to form similar assemblies. Like for the ditopic Modules some measurements showed conflicting results compared to literature known PDI system that have additional binding motifs while others revealed a similar behavior as already reported in literature. Both monotopic Modules exhibited a "monomeric" spectrum in THF, which was attributed to a deaggregated molecule in similar systems. The observed increase in extinction coefficient upon dilution for the cyclohexyl Module is also not surprising while the decrease for the 3-pentyl Module was more similar to the behavior of the ditopic Modules. Opposite to the initial assumption that the Modules might not form assemblies in THF, the microscopic studies indeed revealed aggregates. While the 3-pentyl Module formed layers at various concentrations, the cyclohexyl Module formed linear strings.

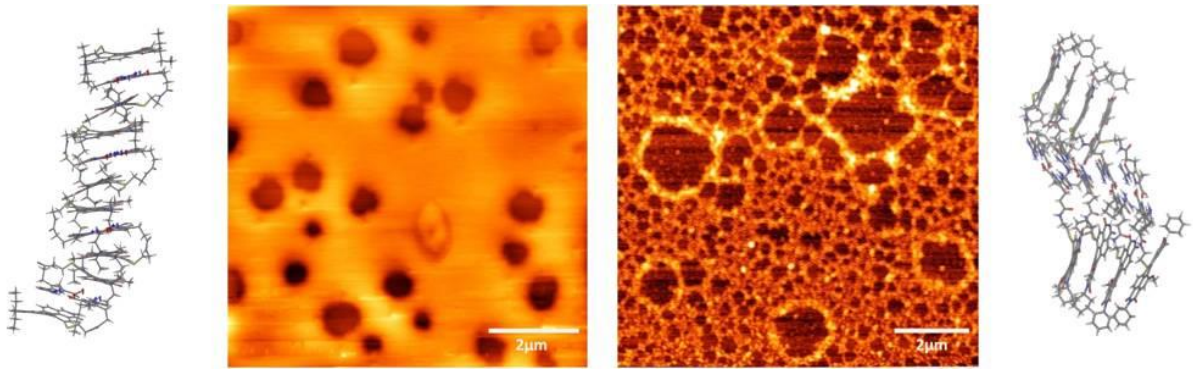

Figure 126: Left: Schematic representation of the proposed heterotopic aggregation of the 3-pentyl Module. Middle left: AFM height measurement of the 3-pentyl Module at 0.8 mM in THF. Middle right: AFM height measurement of the cyclohexyl Module at 0.5 mM in THF Right: Schematic representation of the proposed homotopic aggregation of the cyclohexyl Module.

MM-calculation revealed that the stable aggregation for 3-pentyl Module is an alternating stacking (ABAABA) similar to the ditopic Modules which leads to a rod formation which then further interlink to

form sheets. This similar build-up compared to the ditopic Modules also explained the decrease in extinction coefficient upon dilution. The MM-calculation for the cyclohexyl Module showed a homotopic stacking as the most stable confirmation like originally suggested for all Modules. This arrangement is in good accordance with the other results also since it was the only Module that showed an increase of extinction coefficient upon decrease of the concentration like conventional PDI systems. Considering the assembly which includes a direct perylene-perylene contact for both monotopic Modules, the "monomeric" spectral curve rather unusual though and can only be explained by a large stacking distance of the subunits in THF.

One goal of this thesis was the evaluation of the switching possibilities for both monotopic Modules. For the 3-pentyl Module, only a switching with acid was possible which lead to the formation of large irregularly formed aggregates. The aggregate itself was probably not completely rearranged compared to the zwitterionic assembly, but only cut off at the end to form smaller sheets which would also explain the irregular shape of the aggregates as shown in Figure 127. With addition of base to the acidic solution, the initial assembly can be restored.

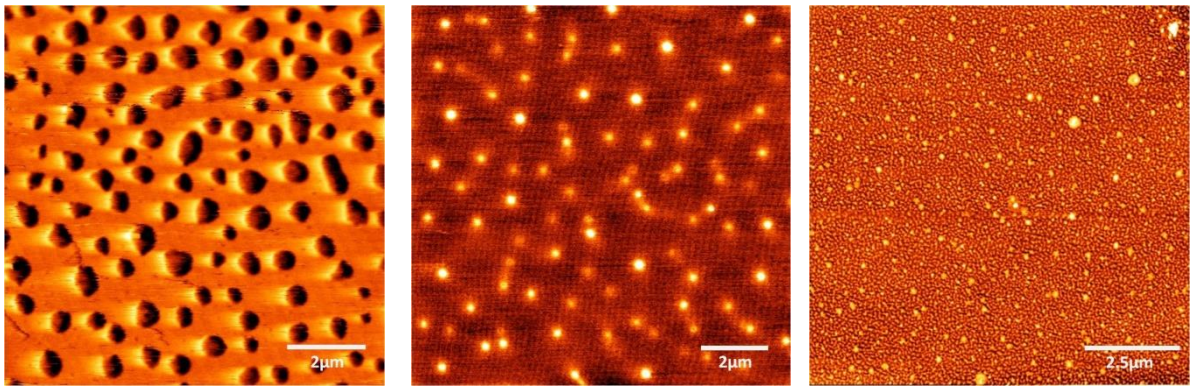

Figure 127: Left: AFM height image of the 3-pentyl Module upon addition of 5 equivalents TFA at 1 mM in THF. Middle: AFM height image of the cyclohexyl Module upon addition of 5 equivalents TFA at 1 mM in THF. Right: AFM height image of the cyclohexyl Module upon addition of 5 equivalents TEA at 1 mM in THF.

The switching was not possible with base though. A possible explanation for this behavior lies in shielding of the zwitterion dimer that is not easily accessible for base. In this tightly packed arrangement, the approach of acid or base towards the switchable zwitterionic unit is sterically hindered. In the case of the acid, the proton is small enough to reach the switchable zwitterionic unit. TEA in the basic solution is a lot bigger compared to the proton, so the approach is sterically disfavored compared to the acid which therefore prohibits the switching with base. For the cyclohexyl Module both acid and base lead to the formation of spherical aggregates. The zwitterionic dimer in this case is easier to access due to the homotopic stacking of the Module. The aggregate can be cut off in

the middle to yield in the switched assembly and also explaining the height for the cationic and anionic cyclohexyl Module. A repulsion of the ionic groups at the sides of the assembly induces a curvature that leads to the formation of spherical aggregates.

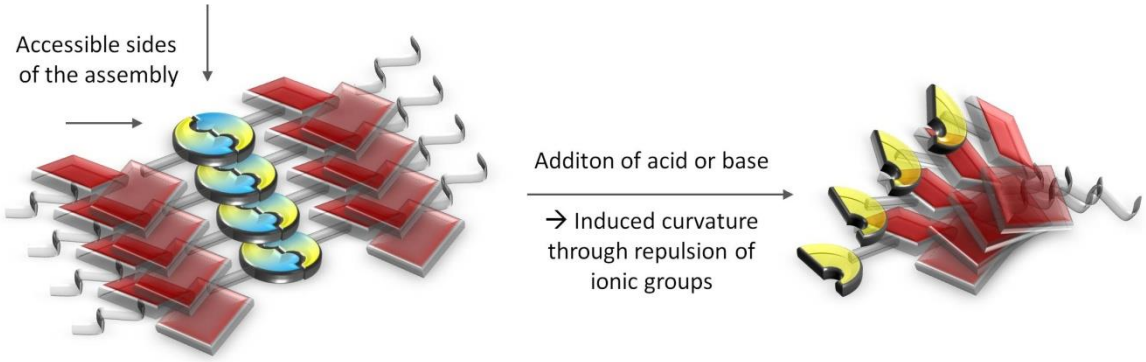

Figure 128: Schematic representation of the previously proposed layered aggregate of the cyclohexyl Module and accessible points for approach of acid and base. The protonation respectively deprotonation of the zwitterionic GCP unit induces a curvature through the repulsion of the ionic groups which is shown on the right side.

The attachment of the PEG chains should lead to a better solubility in water as mentioned above, so also the assembly in aqueous medium was investigated. The 3-pentyl Module was found to be completely soluble in water exhibiting a significant hypsochromic shift in UV/vis indicating the formation of an H-aggregate. The predominant aggregate was still a layered assembly, whereby HIM measurements revealed that the layered aggregate is regularly build up by the linear strings. This further supported the previously proposed assembly mode in which the alternating stacking (ABAABA) similar to the ditopic Modules lead to a rod and further interlinking of the 3-pentyl groups to a layer formation.

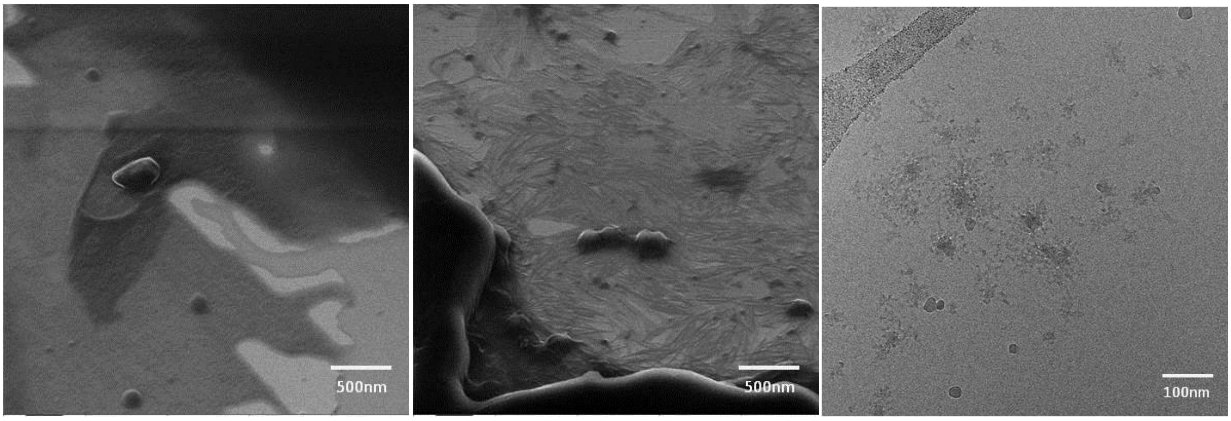

Figure 129: Left and middle: HIM measurements of the 3-pentyl Module in water at a concentration of 1.0 mM; Right: Cryo-TEM image of the cyclohexyl Module in water/THF (1:1 ratio) at a concentration of 0.5 mM after 24 days.

The cyclohexyl Module was not found to be soluble in water, but only water THF mixture up to a 1:1 mixture of both solvents. Microscopic measurements revealed the formation of circular aggregates, whereby time resolved cryo-TEM measurements showed that initially linear string are formed that fuse together over time to form the spherical particles. A likely explanation for this behavior is the formation of primary stacks which condense into larger globular aggregates, which also means that the principal aggregation mode is maintained in the aqueous solution.

A gel could unfortunately not be formed due to the layered aggregation of the 3-pentyl Module and due to the bad solubility of the cyclohexyl Module. The build-up of these Module enables manifold possibilities to achieve a gel formation through a change of the molecule though. With an asymmetrical molecule with a cyclohexyl at one side of the perylene and a 3-pentyl chain at the other side, it is conceivable that a Gel could be formed.

In summary, this thesis showed that it is possible to create perylene diimide - GCP zwitterion - Modules that build up complex supramolecular systems. Both monotopic and ditopic Modules could be synthesized and investigated. The found assembly mode for both ditopic Modules and for the 3-pentyl Module is not comparable to any reported assembly for other PDIs due to the exceptional heterotopic stacking. The core linked Module showed furthermore an extraordinary time dependent aggregation change which is also not known for other PDI assemblies. All assemblies are reversibly switchable with multiple stimuli and stable in polar medium. In total, the combination of perylene diimides and the zwitterionic GCP binding motif created exceptional bi-functional supramolecular systems. It is fair to state though that few results of this thesis have been reported for other PDI assemblies before, underlining the statement of J. R. R. Tolkien: "You certainly usually find something, if you look, but it is not always quite the something you were after."[67]

6. Zusammenfassung

Das Ziel dieser Dissertation war die Entwicklung bifunktioneller supramolekularer Systeme, welche - basierend auf den bekannten Stimuli der verwendeten funktionellen Einheiten - eine vielfältige Schaltbarkeit aufweist. Diese supramolekularen Systeme sollten zusätzlich in polarer Umgebung stabile Aggregate ausbilden. Startpunkt für die Entwicklung dieser Systeme waren die beiden funktionellen Einheiten, die in Abbildung 117 dargestellt sind.

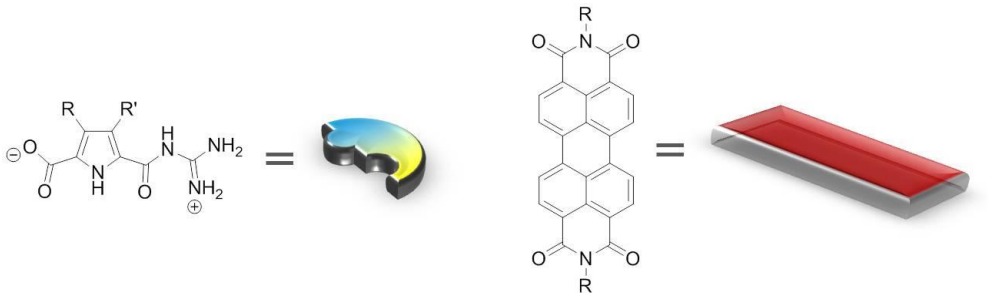

Abbildung 117: Exemplarische Strukturformel und schematische Darstellung der beiden funktionellen Einheiten dieser Dissertation. Links: Zwitterionische GCP Einheit, Rechts: Perylendiimid.

Das Perylendiimid wurde aufgrund seiner interessanten optischen Eigenschaften sowie seiner Tendenz, supramolekulare Aggregate durch π-π-Stapelung des aromatischen Kerns auszubilden, als Kerneinheit ausgewählt. Zusätzlich können die supramolekularen Aggregate des Farbstoffs nicht nur durch die Variation von Konzentration oder Temperatur geschaltet werden, sondern auch durch die Zugabe von Natriumdithionit. Die zwitterionische GCP Einheit wurde an diesen Kern angebunden, um eine weitere Aggregation fernab der π-π-Stapelung zu ermöglichen. Dieses selbstkomplementäre Bindungsmotiv bildet durch eine Kombination von ionischen Wechselwirkungen und Wasserstoffbrückenbindungen extrem stabile dimere Aggregate in polarer Umgebung aus. Da die ionischen Wechselwirkungen einen signifikanten Anteil an der Assemblierung haben, kann die Aggregatbildung reversibel durch die Zugabe von Säure oder Base geschaltet werden.

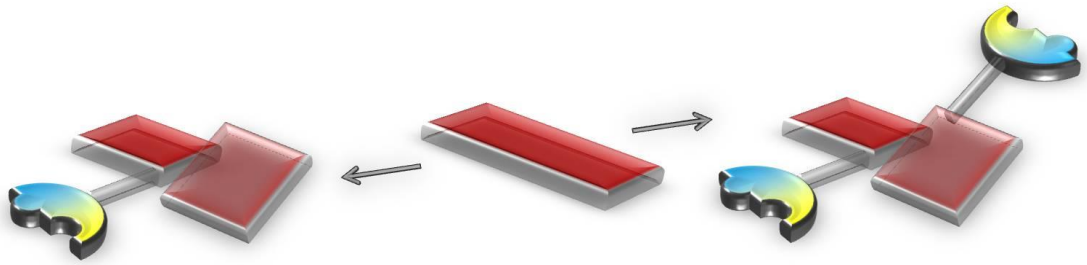

Abbildung 118: Schematische Darstellung der monotopischen und der ditopischen Anbindung des GCP Bindungsmotivs an den Perylenkern. Die versetzt zueinander angeordneten Rechtecke sollen dabei die Verdrehung des Kerns nach der Substitution darstellen.

Bindungsmotive können prinzipiell an verschiedenen Positionen des Perylendiimids angebunden werden. Die meisten Beispiele aus der Literatur beschreiben jedoch eine Anbindung von entweder einem oder zwei Bindungsmotiven an den Kern. Aus diesem Grund hat diese Arbeit sowohl die Anbindung von einem GCP Bindungsmotiv (monotopische Anbindung) als auch von zwei GCP Bindungsmotiven (ditopische Anbindung) an einen Perylendiimidkern untersucht. Eine schematische Darstellung der monotopischen und ditopischen Module aus Perylendiimid und GCP Zwitterion findet sich in Abbildung 118. Nach der erfolgreichen Synthese dieser neuen bifunktionellen Module wurden die monotopischen und ditopischen Module untersucht. Dabei fokussierte sich die Untersuchung der Perylendiimid - GCP Zwitterion - Module speziell auf die Selbstassemblierung sowie die Schaltbarkeit nach Zugabe verschiedener Stimuli.

6.1 Ditopische Module

Diese Arbeit zeigte eine erfolgreiche ditopische Anbindung der GCP Bindungsmotivs an den Perylenkern, woraus zwei neue Module entstanden. Bei dem **Imid verlinkten Modul** wurde das Bindungsmotiv über die Imidposition des Perylendiimids eingeführt, während das Bindungsmotiv bei dem **Kern verlinkten Modul** an den aromatischen Kern des PDIs gebunden wurde. Diese unterschiedliche Anbindung des Bindungsmotivs ermöglicht einen Vergleich von zwei unterschiedlichen Bindungsachsen bei der Assemblierung. Durch die π-π-Stapelung des Perylenkerns wird für alle Module eine Verlängerung der Aggregation entlang der z-Achse erwartet. Durch das zusätzliche GCP Bindungsmotiv wird nun die Aggregation entlang einer weiteren Achse für die unterschiedlichen Module ermöglicht. Dabei soll das Imid verlinkte Modul zusätzlich entlang der x-Achse assemblieren während das Kern verlinkte Modul entlang der y-Achse assemblieren soll.

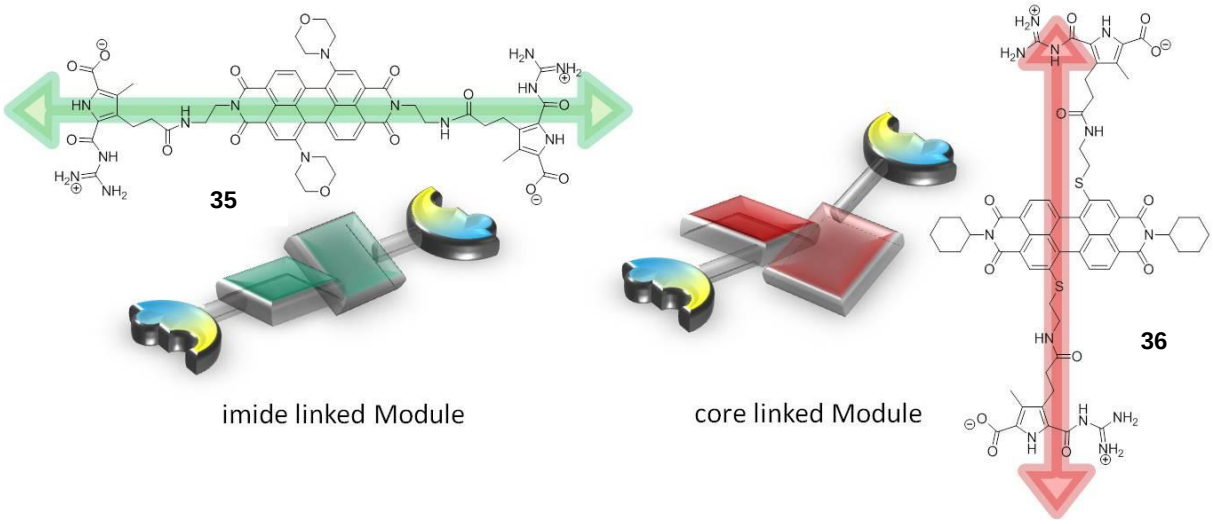

Abbildung 119: Imid verlinktes Modul **35** und Kern verlinktes Modul **36**: Strukturformel und schematische Darstellung. Der Pfeil soll die Assemblierung entlang der zusätzlichen Bindungsachse veranschaulichen.

Die Synthese, welche angelehnt an literaturbekannte Vorschriften durchgeführt wurde, ergab zwei bifunktionelle Module. Diese ditopischen Module waren sowohl löslich also auch stabil in DMSO. Verglichen mit literaturbekannten Perylendiimid-Systemen, welche ebenfalls zusätzliche Bindungsmotive hatten, zeigten die ersten Messungen sowohl ähnliche Ergebnisse als auch einige widersprüchliche Ergebnisse. Die UV/vis Messungen der beiden ditopischen Module wiesen eine "monomere" Kurve des Spektrums auf, was in Anbetracht des polaren Lösungsmittels sehr ungewöhnlich ist. Zusätzlich zeigte sich bei den Kurven der Verdünnungsreihe eine Abnahme des Extinktionskoeffizienten wohingegen bei vergleichbaren Perylendiimid-Systemen in der Literatur eine Zunahme des Extinktionskoeffizienten beschrieben wird. Der prinzipielle Aggregationsmechanismus, bei dem eine isodesmische Aggregation festgestellt werden konnte, hingegen korreliert wieder mit dem Verhalten von literaturbekannten Systemen. Die mikroskopische Untersuchung der Aggregation zeigte nicht die ursprünglich vorgeschlagene Schichtaggregation sondern eine netzwerkartige Assemblierung bei beiden Modulen. Diese verzweigten Aggregate basieren auf linearen Strängen, die sowohl auf der geladenen mica Oberfläche in AFM Messungen als auch auf der neutralen Siliziumoberfläche in HIM Messungen nachgewiesen werden konnten. MM-Rechnungen zeigten, dass nicht wie im Konzeptteil vorgeschlagen homotopische Aggregate gebildet werden, sondern für beide ditopische Module heterotopische Aggregate energetisch günstiger sind, in denen sich Perylendiimid und GCP Zwitterion alternierend zueinander anordnen. Die Messungen des Kern verlinkten Moduls sowie die Ergebnisse der MM-Rechnungen sind in Abbildung 120 dargestellt.

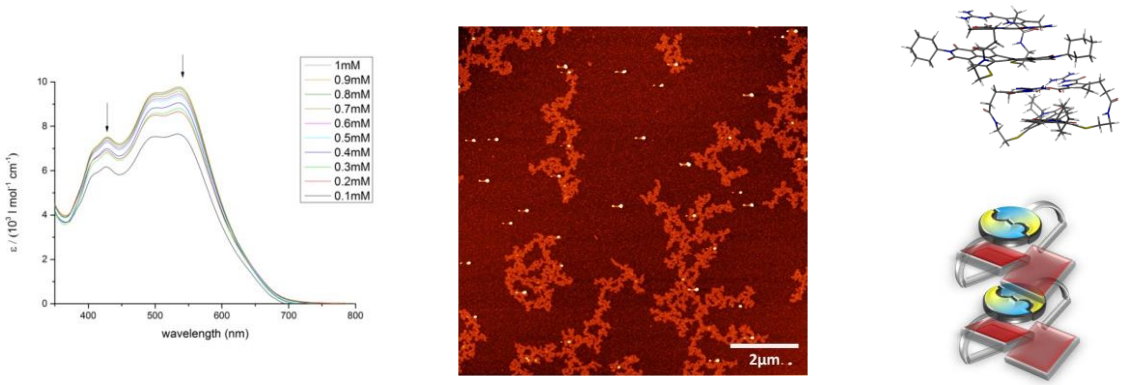

Abbildung 120: Links: Konzentrationsabhängige UV/vis Messungen des Kern verlinkten Moduls in einem Konzentrationsbereich von 1.0 mM bis 0.1 mM in DMSO. Die Pfeile beschreiben die spektrale Änderung bei abnehmender Konzentration. Mitte: AFM Höhenbilder des Kern verlinkten Moduls bei einer Konzentration von 0.25 mM in DMSO; Rechts: MM-Rechnung und Modell der heterotopischen Assemblierung des Kern verlinkten Moduls.

Diese heterotopische (ABAB) Stapelung führt zur Bildung polymerer Aggregate, welche sich dann umeinander wickeln, was dann in den mikroskopischen Messungen wie ein Netzwerk aussieht. Die isolierte Anordnung des Perylens zwischen den beiden assemblierten zwitterionischen Dimeren führt zu dem "monomeren" Spektrum der UV/vis Messungen sowie dem gleichbleibenden Spektrum in der Verdünnungsreihe. Durch einen möglichen Ladungstransfer zwischen dem elektronenrechen zwitterionischen Dimer und dem elektronenarmen Perylendiimid kann zusätzlich die Abnahme des Extinktionskoeffizienten erklärt werden. Das Aggregat wird über eine π-π-Stapelung der einzelnen Module gebildet, also eine Aggregation analog zu anderen literaturbekannten Perylendiimid Systemen, was sich auch im isodesmischen Aggregationsmechanismus widerspiegelt. Was jedoch besonders hervorzuheben ist, ist die Tatsache, dass beide Module den gleichen Aggregattyp bilden unabhängig von der Position des Bindungsmotivs. Dies ist ein wichtiges Resultat dieser Arbeit, da es zeigt, dass die Aggregate der untersuchten ditopischen Module unabhängig von der Bindungsachse der angebrachten Bindungsmotive gebildet werden. Die erwartete Verlängerung entlang der y- oder x-Achse wurde jedoch nicht erreicht. Durch die Stapelung des assemblierten Bindungsmotives zwischen zwei Peryleneinheiten konnte einzig ein Aggregatwachstum entlang der z-Achse gefunden werden. Eine solche heterotopische Stapelung wurde bisher noch nicht für Perylendiimid Systeme berichtet und ist einzigartig für die ditopischen Module.

Eine außergewöhnliche Eigenschaft des Kern verlinkten Modul ist eine zeitabhängige Änderung der Aggregation. Mit größer werdender Zeitdauer weisen sowohl die AFM als auch die UV/vis Messungen Unterschiede im Gegensatz zur Untersuchung der frischen Lösung des Kern verlinkten Moduls auf. Im UV/vis Spektrum konnte man eine bathochrome Verschiebung der maximalen Absorptionsbande von 535 nm zu 578 nm beobachten. Zusätzlich verschwand die vibronische Feinstruktur was zusammen

mit der Verschiebung der Absorptionsbande auf eine Aggregation, speziell die Bildung eines J-Aggregates, hinweist.

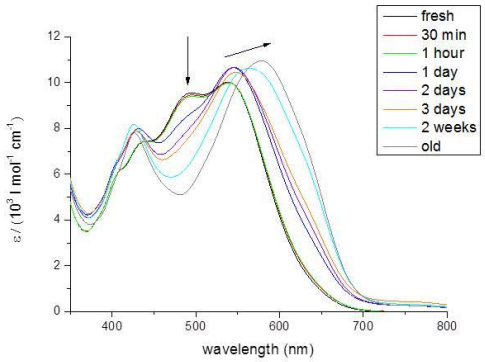

Abbildung 121: UV/vis Spektrum des Kern verlinkten Moduls bei 0.25mM in DMSO zu verschiedenen Zeitpunkten.

In den AFM Messungen ist eine Umlagerung der Aggregate klar erkennbar. Während die frische Lösung lineare Aggregate bildet, ändert sich die Assemblierung nach einer Woche in ungeordnete Strukturen, nur um nach einem Monat wieder lineare Strukturen auszubilden. MM-Rechnungen zeigen eine Umlagerung des heterotopischen Aggregates in ein homotopisches Aggregat in dem Perylen auf Perylen und GCP Dimer auf GCP Dimer gestapelt ist. Da dieses homotopische Aggregat für das Kern verlinkte Modul energetisch günstiger ist als die heterotopische Anordnung, kann die zeitabhängige Änderung der Aggregation als Umlagerung vom kinetisch kontrollierten zum thermodynamisch kontrollierten Aggregat angesehen werden.

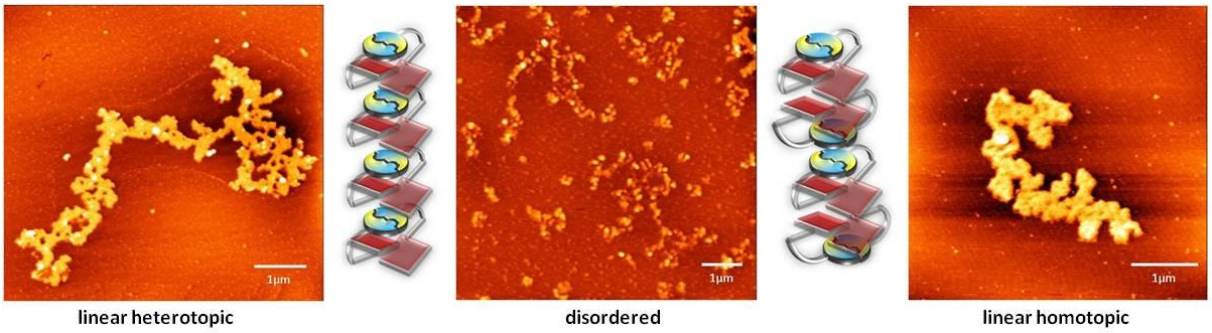

Abbildung 122: AFM Höhenbild des Kern verlinkten Moduls bei 0.25 mM in DMSO. Links: Frische Lösung; Mitte: gleiche Lösung nach 1 Woche; Rechts: gleiche Lösung nach 1 Monat. Das Modell des Aggregation auf der linken Seite (heterotopische Stapelung) gehört zur frischen Lösung während das Modell rechts (homotopische Stapelung) zur gealterten Lösung gehört.

Die ursprüngliche polymere Anordnung der Module wird nach der Umlagerung zum homotopischen Aggregat wieder hergestellt, was die übereinstimmenden Höhenprofile der frischen und gealterten Lösung erklärt. Die Peryleneinheiten bilden dabei ein J-Aggregat in der homotopischen Anordnung was die bathochrome Verschiebung der maximalen Absorptionsbande verursacht. Da eine solche

komplette zeitabhängige Umlagerung bisher noch in keiner Veröffentlichung erwähnt wurde, stellt diese zeitabhängige Aggregationsänderung eine herausragende Eigenschaft des Kern verlinkten Moduls dar. Eine Umlagerung des Imid verlinkten Moduls hingegen wurde nicht beobachtet, da aus MM-Rechnungen hervorgeht, dass bei diesem Modul die heterotopische Stapelung bereits die thermodynamisch stabilere ist.

Wie zuvor erwähnt war ein Ziel dieser Arbeit die Untersuchung der Schaltbarkeit der supramolekularen Systeme. Daher wurde das Verhalten der Aggregate nach Zugabe von Säure/Base - um die Assemblierung des zwitterionischen GCP Dimers aufzuheben - und Natriumdithionit - um die Assemblierung des Perylenkerns aufzuheben - beobachtet. Nach Zugabe von Säure und Base zu den ditopischen Modulen entstanden in beiden Fällen sphärische Partikel, die mit AFM Messungen nachgewiesen wurden. Ebenfalls zeigte sich für das Kern verlinkte Modul eine Änderung der Absorptionsbanden, wobei im kationischen Fall eine hypsochrome Verschiebung und im basischen Fall eine bathochrome Verschiebung zu beobachten war. Die Protonierung bzw. Deprotonierung der Module ergibt geladene Bindungsmotive, wobei die Abstoßung der gleich geladenen Einheiten zu einer Umlagerung führt nach der die GCP Einheiten nach außen zeigen und so eine direkte π-π-Stapelung der Perylenkerne ermöglichen. Bezieht man dies auf die UV/vis Messungen kann davon ausgegangen werden, dass das kationische Kern verlinkte Modul ein H-Aggregate bildet, während das basische Kern verlinkte Modul ein J-Aggregate ausbildet. Ein Modell dieser beiden Aggregate ist in Abbildung 123 dargestellt.

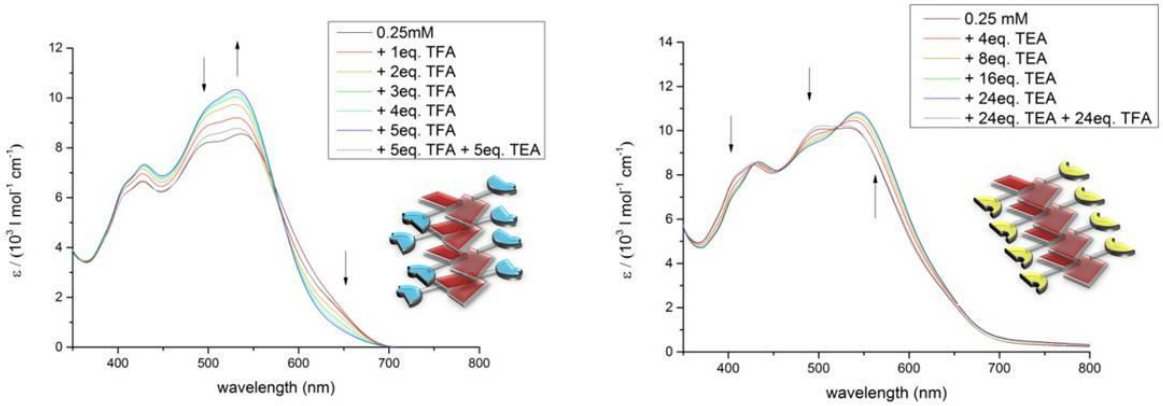

Abbildung 123: UV/vis Spektren des Kern verlinkten Moduls nach Zugabe von Säure und Base bei 0.25 mM in DMSO. Links: Säure; Rechts: Messungen mit Base. Einschub links: Modell des vorgeschlagenen H-Aggregats; Einschub rechts: Modell des vorgeschlagenen J-Aggregats.

Die gleiche Aggregationsweise wird auch für das Imid verlinkte Modul erwartet, wobei die Größe der Aggregate welche im AFM gefunden wurden, verglichen mit dem Kern verlinkten Modul, anders ist.

Dies kann durch den unterschiedlichen molekularen Aufbau der beiden Module durch die unterschiedliche Anbindung des Bindungsmotives am Perylenkern erklärt werden. Weiterhin zeigt die prinzipielle Art der Aggregation der geschalteten Module dass die Bindungsachse, an der die Bindungsmotive angebracht sind, auch hier nicht von Relevanz bei der Assemblierung ist. Es konnte außerdem gezeigt werden, dass die Schaltbarkeit der Module reversibel ist. Dbei wurden die ursprünglichen linearen Aggregate nach der Wiederherstellung des zwitterionischen Zustandes, also der Neutralisierung, wieder ausgebildet.

Die Schaltung der ditopischen Module mit Natriumdithionit führte ebenfalls zu einer Bildung von sphärischen Aggregaten. Durch die Reduktion des Perylenkerns kommt es zu einer Umlagerung in homotopische Stapel was durch MM-Rechnungen unterstrichen wurde. Dabei entstehen beim Imid verlinkten Modul bevorzugt J-Aggregate während beim Kern verlinkten Modul präferiert H-Aggregate gebildet werden. Dies erklärt die unterschiedlichen Verschiebungen der Absorptionsbanden der ditopischen Module in den UV/vis Messungen. Bei der Reduktion mit Natriumdithionit entstehen auch das erste Mal unterschiedliche Aggregate für die beiden ditopischen Module. Es ist jedoch nicht ganz klar, ob die unterschiedliche Aggregation durch die unterschiedliche Anbindung der Bindungsmotive bedingt wird oder ob der sterische Anspruch der Morpholingruppen einen größeren Einfluss auf die Aggregation hat.

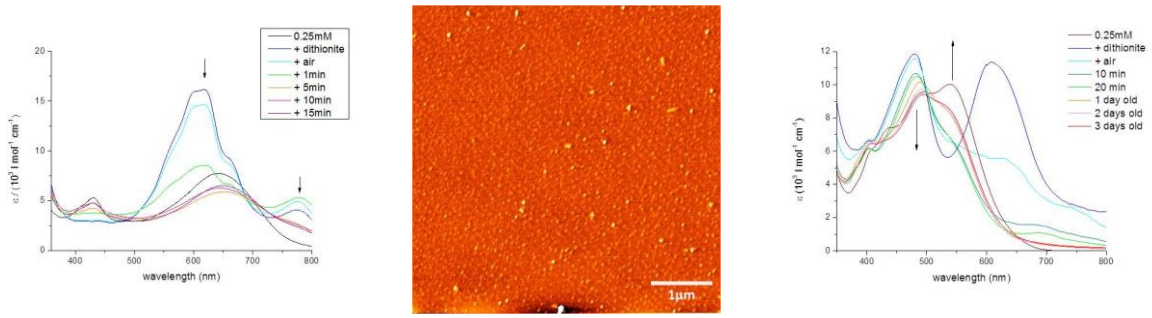

Abbildung 124: UV/vis Spektren des Imid verlinkten Moduls (links) und des Kern verlinkten Moduls (rechts) nach Zugabe von $Na_2S_2O_4$ und Reoxidation mit Luftsauerstoff bei 0.25 mM in DMSO. Mitte: AFM Höhenbild des Imid verlinkten nach Zugabe von $Na_2S_2O_4$ bei 0.25 mM in DMSO.

Das ursprüngliche Aggregat wird nach der Reoxidation auch nur für das Imid verlinkte Modul wieder hergestellt. Das Kern verlinkte Modul bildet nach der Reduktion nicht mehr das ursprüngliche Aggregat aus, was vermutlich auf ein kinetisches Einfrieren des homotopischen H-Aggregats zurückzuführen ist und die Wiederherstellung der alternierenden, heterotopischen Stapelung oder auch die thermodynamisch stabilere homotopische J-Aggregatbildung verhindert. Der energetische Unterschied zwischen homotopischen H- und J-Aggregat ist mutmaßlich ebenfalls zu klein um noch

eine zeitabhängige Umlagerung zu bewirken, was das Fehlen des zeitabhängigen Aggregatbildung nach dem Schalten mit Natriumdithionit erklärt.

6.2 Monotopische Module

Außer der diotopischen Anbindung des Bindungsmotivs, wurde in dieser Arbeit auch eine monotopische Anbindung untersucht, um die Möglichkeit zu haben auf der anderen Seite des Perylens noch andere Substituenten einzuführen. Für eine bessere Löslichkeit in wässrigem Medium wurde der Perylenkern deswegen mit PEG Seitenketten versehen, welche weitere supramolekulare Wechselwirkungen durch die Verdrillung benachbarter PEG Gruppen ermöglichen. Ein Fokus dieser Arbeit war außerdem die Untersuchung des Einflusses einer 3-pentyl Gruppe an der Imidposition des Perylendiimids, welche eine Verzahnung mit Molekülen die ebenfalls eine 3-pentyl Gruppe besitzen zulässt. Um die prinzipielle Assemblierung sowie eine mögliche Gelbildung zu untersuchen, wurden zwei monotopische Moleküle erfolgreich synthetisiert. Die beiden Moleküle unterscheiden sich in der Substitution an der Imidposition. Während das **3-pentyl Modul** eine 3-pentyl Gruppe an der Imidposition aufweist, wurde das zweite ein Molekül mit einer geschlossenen cyclohexyl Gruppe an der Imidposition (**cyclohexyl Modul**) versehen welche die Verzahnungsmöglichkeit in diesem Fall verhindert.

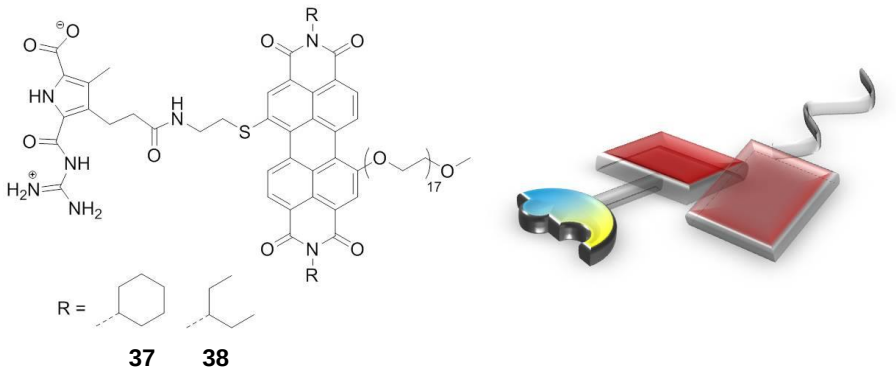

37 **38**

Abbildung 125: Monotopische Module **37** (Cyclohexylamine substituiert) and **38** (3-Pentylamine substituiert): StruKturformel und schematische Darstellung.

Es wurde gezeigt, dass die monotopischen Module in Abbildung 125 durch die Wechselwirkung der selbstkomplementären zwitterionischen GCP Bindungsmotive dimerisieren. Wie schon bei den ditopischen Modulen zeigten einige Messungen widersprüchliche Messungen im Vergleich zu literaturbekannten Perylendiimid Systemen. Während beide monotopischen Module wie die

ditopischen Module ein „monomeres“ Spektrum in THF aufwiesen, wurde nur für das 3-pentyl Modul eine Abnahme des Extinktionskoeffizienten bei der Verdünnung beobachtet. Das cyclohexyl Modul wies, wie bei ähnlichen Perylendiimid Systemen, eine Zunahme des Extinktionskoeffizienten bei der Verdünnung der Lösung auf. Die Vermutung lag also nahe, dass beide monotopische Module unterschiedliche Aggregate ausbilden, was auch in AFM Messungen gezeigt werden konnte. Das 3-pentyl Modul wies dabei eine schichtartige Aggregation bei verschiedenen Konzentrationen auf, wohingegen das cyclohexyl Modul lineare Stränge ausbildet.

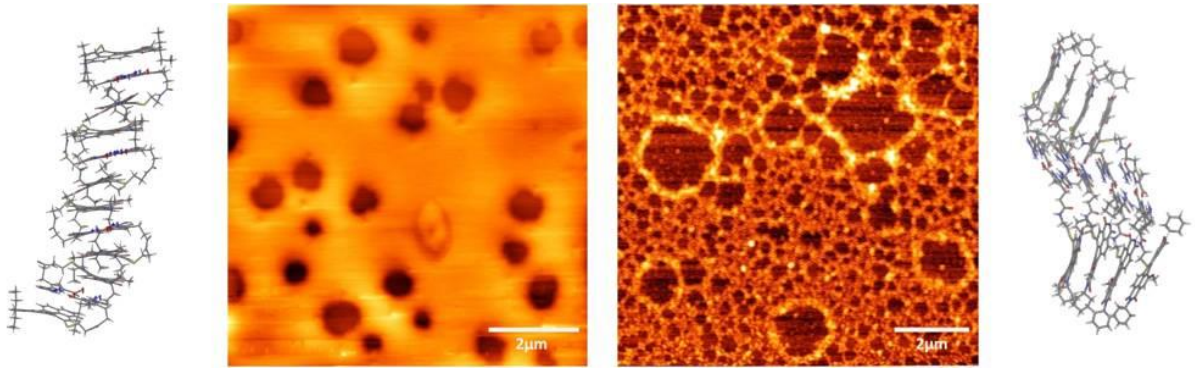

Abbildung 126: Links: Schematische Darstellung des vorgeschlagenen heterotopischen Aggregats des 3-pentyl Moduls. Mitte links: AFM Höhenbild des 3-pentyl Moduls bei 0.8 mM in THF. Mitte rechts: AFM Höhenbild des cyclohexyl Module bei 0.5 mM in THF. Rechts: Schematische Darstellung des vorgeschlagenen homotopischen Aggregats des cyclohexyl Moduls.

MM-Rechnungen zeigten, dass sich die Aggregationsart der beiden monotopischen Module signifikant voneinander unterscheidet. Dabei bildet das 3-pentyl Modul ein alternierendes, also heterotopisches Aggregat (ABAABA) ähnlich der Aggregate der ditopischen Module aus. Dies führt zu linearen Aggregaten, die dann allerdings durch die 3-pentyl Gruppen benachbarter Stränge miteinander verzahnen um schichtartige Aggregate auszubilden. Dieser ähnliche Aufbau verglichen mit den ditopischen Modulen erklärt auch die Abnahme des Extinktionskoeffizienten bei der Verdünnung. Die MM-Rechnung des cyclohexyl Moduls hingegen zeigte eine homotopische Stapelung der assemblierten Dimere was ursprünglich für alle Module vorgeschlagen wurde. Diese Anordnung spiegelt auch alle anderen Resultate wie beispielsweise die Zunahme des Extinktionskoeffizienten bei Verdünnung wider. Das für beide monotopische Module ein "monomeres" Spektrum beobachtet wurde, obwohl in beiden Aggregaten ein direkter Perylen-Perylen Kontakt vorliegt, kann einzig auf eine große Distanz in der Stapelung in THF zurückgeführt werden.

Ein Ziel dieser Arbeit war die Evaluierung der Schaltungsmöglichkeiten der Aggregate welche die monotopischen Module ausbilden. Das 3-pentyl Modul konnte erfolgreich mit Säure geschaltet werden, wobei es ungleichmäßig geformte Aggregate ausbildete. Diese unregelmäßige Form kann dadurch erklärt werden, dass das Aggregat des kationischen Moduls wahrscheinlich nicht komplett

umgeordnet, sondern das ursprüngliche Schichtaggregat nur an einigen Stellen abgeschnitten wurde um kleinere Schichten zu bilden. Das ursprüngliche Aggregat konnte nach Zugabe von Base wiederhergestellt werden, wonach auf ein reversibles Schalten geschlossen werden kann.

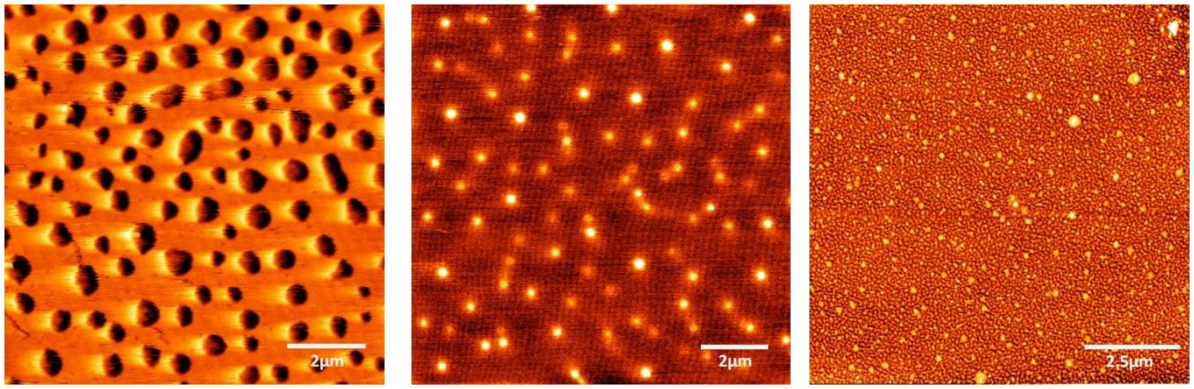

Abbildung 127: Links: AFM Höhenbild des 3-pentyl Moduls nach Zugabe von 5 Äquivalenten TFA bei 1 mM in THF. Middle: AFM Höhenbild des cyclohexyl Moduls nach Zugabe von 5 ÄquivalentenTFA bei 1 mM in THF. Right: AFM Höhenbild des cyclohexyl Moduls nach Zugabe von 5 Äquivalenten TEA bei 1 mM in THF.

Eine Schaltung mit Base war für das 3-pentyl Modul nicht möglich, was durch die gute Abschirmung des zwitterionischen Dimers erklärt werden kann, was eine Annäherung der sterisch anspruchsvolleren Base deutlich erschwert. Das Aggregat des cyclohexyl Moduls konnte sowohl durch Säure als auch Base verändert werden, wobei im AFM sphärische Aggregate erkennbar waren. Das zwitterionische GCP Dimer ist in der homotopischen Stapelung deutlich besser zu erreichen, was die Veränderung mit beiden Stimuli erklärt. Das ursprüngliche Aggregat wird dabei in der Mitte zerschnitten, wobei die Abstoßung der gleich geladenen ionischen Gruppen eine Krümmung des Aggregates induziert. Die Neutralisierung der jeweiligen Stimuli führt zu einer Wiederherstellung des linearen Aggregats, was bedeutet, dass auch diese Schaltung reversibel ist.

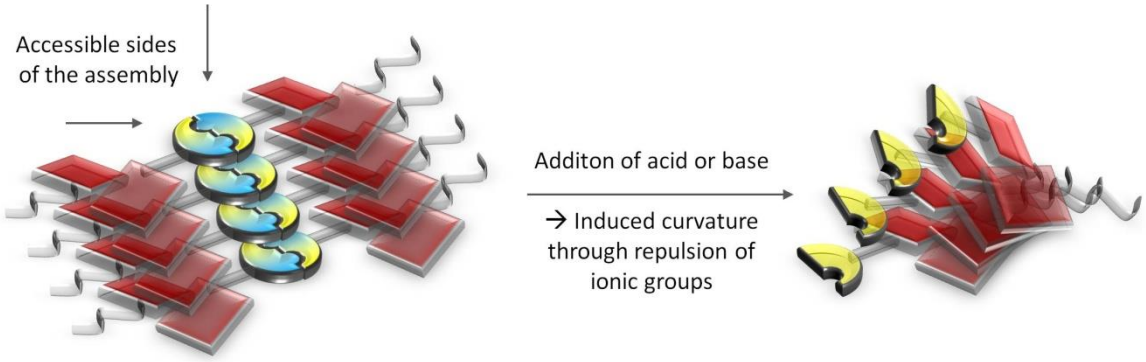

Abbildung 128: Schematische Darstellung des Aggregats des cyclohexyl Moduls und die zugänglichen Punkte für einen Angriff mit Säure und Base (links). Die Protonierung bzw. Deprotonierung des zwitterionischen GCPs induziert eine Krümmung durch die Abstoßung der gleich geladenen ionischen Gruppen auf einer Seite (rechts).

Die Anbindung der PEG Gruppen sollte wie zuvor erwähnt eine bessere Löslichkeit der Module in Wasser bewirken, weswegen ebenfalls die Assemblierung in wässrigem Medium untersucht wurde. Die Löslichkeitsuntersuchungen zeigten allerdings, dass nur das 3-pentyl Modul komplett wasserlöslich war. In UV/vis Messungen zeigte das Modul einen signifikanten hypsochromen Shift der maximalen Absorptionsbande, was sich auf die Bildung eines H-Aggregats zurückführen lässt. Wie auch in THF konnte in den AFM Messungen ein schichtförmiges Aggregat gefunden werden. Aus hochaufgelösten HIM Messungen geht weiter hervor, dass dieses Schichtaggregat aus linearen Strängen aufgebaut ist. Dies unterstützt zusätzlich die Annahme, dass ein alternierendes Aggregat gebildet wird, was durch die Verzahnung der 3-pentyl Gruppen eine Schicht bildet.

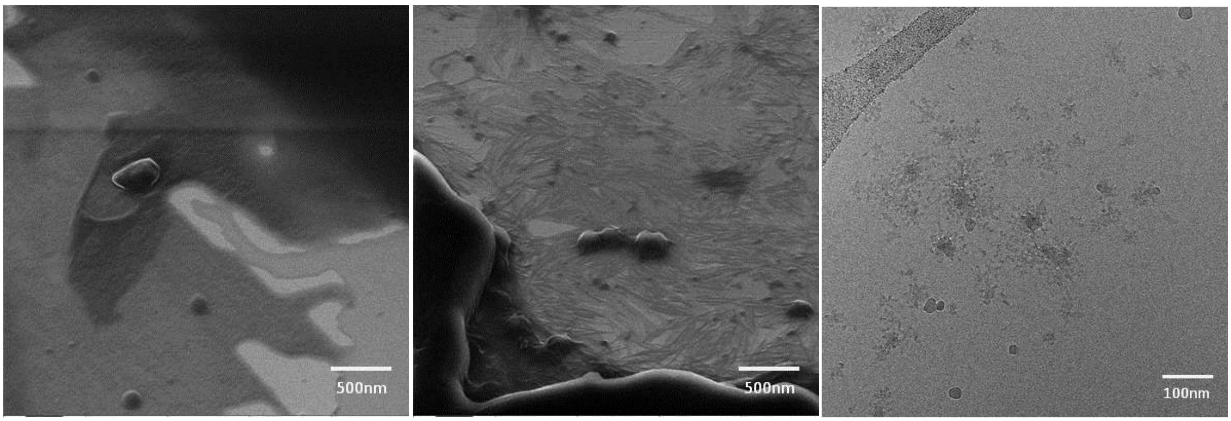

Abbildung 129: Links und Mitte: HIM Messungen des 3-pentyl Moduls in Wasser bei einer Konzentration von 1.0 mM; Rechts: Cryo-TEM Bild des cyclohexyl Moduls in Wasser/THF (1:1) bei einer Konzentration von 0.5 mM nach 24 Tagen.

Das cyclohexyl Modul war nicht in Wasser, sondern nur in einer Mischung mit THF bis zu einem Mischverhältnis von 1:1 Wasser/THF löslich. Mikroskopische Messungen zeigten dabei, dass sich in

dieser Mischung sphärische Aggregate bilden. In zeitabhängigen cryo-TEM Messungen war außerdem zu erkennen, dass sich ursprünglich gebildete lineare Aggregate nach und nach in sphärische Partikel umwandeln. Eine mögliche Erklärung für dieses Verhalten ist die Kondensierung der linearen Stränge in größere globulare Aggregate was schon für andere Perylendiimid Systeme berichtet wurde. Dies bedeutet aber gleichzeitig, dass auch hier die prinzipielle homotopische Stapelung in wässrigem Medium beibehalten wird. Ein Gel konnte leider mit den monotopischen Modulen nicht gebildet werden, was der schichtförmigen Aggregation des 3-pentyl Moduls und der schlechten Löslichkeit des cyclohexyl Moduls geschuldet ist. Der Aufbau der Module ermöglicht jedoch noch einige Möglichkeiten um durch eine Veränderung eine Gelbildung zu erreichen. Würde man beispielsweise ein asymmetrisches Molekül schaffen, was auf der einen Seite einen cyclohexyl Rest und auf der anderen einen 3-pentyl Rest enthält, wäre es denkbar dass dieses dann ein Gel bildet.

Zusammenfassend hat diese Arbeit gezeigt, dass es möglich ist Perylendiimid - GCP Zwitterion - Module zu schaffen, welche komplexe supramolekulare Systeme aufbauen. Es konnten sowohl ditopische als auch monotopische Module erfolgreich hergestellt und untersucht werden. Der gefundene heterotopische Aggregationsmodus der ditopischen sowie des 3-pentyl Moduls sind nicht vergleichbar mit bisher bekannten Perylendiimidsystemen und stellt aus diesem Grund ein herausragendes Resultat dieser Arbeit dar. Das Kern verlinkte Modul zeigt außerdem eine ungewöhnliche zeitabhängige Aggregationsänderung, die in dieser Art bisher auch noch nicht berichtet wurde. Alle gefundenen Aggregate sind reversibel schaltbar mit mehreren Stimuli und zusätzlich stabil in polarem Medium. Man kann also sagen, dass die Kombination von Perylendiimiden und dem zwitterionischen GCP Bindungsmotivs außergewöhnliche supramolekulare Systeme geschaffen hat. Ebenfalls kann man aber auch unterstreichen, dass wenige Ergebnisse dieser Arbeit bisher für andere Perylendiimid Systeme berichtet wurden, was die Aussage von J. R. R. Tolkien Tolkien unterstreicht: "Es geht nichts über das Suchen, wenn man etwas finden will. Zwar findet man bestimmt etwas, aber gewöhnlich ist es durchaus nicht das, was man gesucht hat. ".[68]

7. Experimental Part

Solvents and Chemicals

All solvents were dried according to literature procedures. Diethyl ether and tetrahydrofurane were distilled from sodium with benzophenone as indicator. Water for chromatographic and spectroscopic measurements was purified with a *TKA MicroPure* ultrapure water system. All other commercial reagents were purchased and used as received unless otherwise specified.

Inert Gas

Reactions with inert gas were carried out under technical argon from *Air Liquide* (99.996 % purity), which was dried with orange gel and calcium chloride.

Lyophilisation

All samples were freeze dried with a *Christ* Alpha 1-4 LD plus freeze dryer.

Melting Point (mp)

The melting points were determined on a *Reichert Thermovar* type 300429 Kofler hot stage melting plate. As Cryostatic Temperature Regulator Equipment, Julabo F12; ED was used.

Thin Layer Chromatography (TLC) and Column Chromatography (CC)

Thin Layer Chromatography reaction control was performed with *Macherey-Nagel* POLYGRAM SIL/UV254 TLC precoated silica gel plates. The TLC elution mixtures are reported in volume percent (v/v).

Column chromatography was performed with silica gel MN Kieselgel 60M, 0.04–0.063 mm, 230–400 mesh from *Macherey Nagel* in glass columns of various diameter and length. The CC elution mixtures are also reported in volume percent (v/v).

Nuclear Magnetic Resonance Spectrometry (NMR)

- *Bruker* DMX 300 (^{1}H: 300 MHz; ^{13}C: 75 MHz)
- *Bruker* DRX 500 (^{1}H: 500 MHz; ^{13}C: 126 MHz)
- *Bruker* Avance III HD 600 (^{1}H: 600 MHz; ^{13}C: 151 MHz)

All measurements were performed at room temperature, using varying solvents. The chemical shifts were measured against the solvent signal and are reported in ppm from TMS (*d* scale). The coupling constants are given in Hertz. The following abbreviations for the description of the fine structure were used: s = singlet, bs = broad singlet, d = doublet, t = triplet, q = quartet, m = multiplet, br = broad signal.

High Resolution Mass Spectrometry (HR-MS)

- *Bruker* amaZon SL (ESI, APCI)
- *Bruker* maXis 4G (ESI)
- *Bruke*r autoFlex Speed (MALDI)

The ESI and APCI samples were measured at a concentration of 10^{-5} M and introduced into the ionization chamber via liquid injection. For MALDI, the samples were mixed with the DCTB-matrix solution in a ratio of 1:3 (sample/matrix) and added drop wise (0.5µL) onto the target plate.

Fourier Transform Infrared Spectroscopy (FT-IR)

- *Jasco* FT-IR 430 spectrophotometer

The compounds were measured in pure form with the *Pike Miracle* or *JASCO* ATR-500M unit. The maxima are classified in four intensities: s (strong), m (middle), w (weak), br (broad) and are reported in cm^{-1}.

UV-Spectroscopy (UV/vis)

- *Jasco* V-660 UV-spectrometer

All UV/vis-spectra were measured at 25°C in a 10mm or 2mm 114-QS quartz cuvette from *Helma*

Atomic Force Microscopy (AFM)

- *Veeco* Innova Scanning Probe Microscope
- *Veeco* NanoDrive Controller
- *HALCYONICS* Micro 40 active vibration isolation unit
- AC 160TS *OLYMPUS* cantilever

Software: Gwyddion-2.18

6µL of the sample solutions were spin coated (60 rps) on a freshly cleaved mica surface. All AFM measurements were performed in tapping mode.

Molecular Modelling (MM)

Software: Schrödinger Maestro, MacroModel V. 9.6

The structure calculations with MacroModel were performed based on the forcefield OPLS 2005 and water as solvent.

7.1 GCP and other precursor molecules

Substance 46

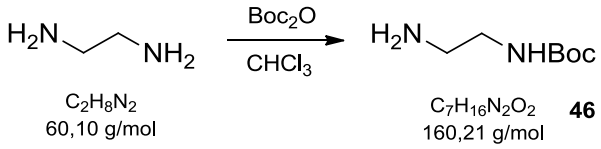

Ethylene diamine (1.32 g, 22 mmol, 5 eq.) was dissolved in chloroform (50 mL) and the mixture was cooled to 0°C. A solution of di-*tert*-butyldicarbonate (960 mg, 4.4 mmo, 1 eq.) in chloroform (25 mL) was added drop wise. The solution was stirred for 3h and the precipitate was subsequently filtered off. Afterwards the filtrate was concentrated and ethyl acetate (30 mL) was added to the remaining oil. The solution was washed with brine (2 x 25 mL) and the combined aqueous phase extracted with ethyl acetate (25 mL). After drying with $MgSO_4$ the solvent was removed under reduced pressure to give a yellow oil (693 mg, 4.33 mmol, 98% yield)

Soluble $CHCl_3$, EtAc

Insoluble H_2O

R_f 0.5 (SiO_2: MeOH/NEt_3 (99:1))

MP -

^{1}H NMR (300 MHz, CHLOROFORM-*d*) δ = 1.45 (s, 9 H, CH_3), 1.57 (br. s., 2 H, NH_2), 2.81 (t, ^3J=5.94 Hz, 2 H, CH_2), 3.18 (q, ^3J=5.94 Hz, 2 H, CH_2), 4.90 (br. s., 1 H, NH)

^{13}C NMR (126 MHz, CHLOROFORM-*d*) δ = 28.40 (CH_3), 41.83 (CH_2), 147.46 (C_q), 156.21 (CO)

HR-MS (ESI pos.) m/z = calculated 161.1245, measured 161.1299 for M + H^+

FT-IR v [cm^{-1}] = 3355 (w), 2980 (w), 2865 (w), 1680 (s), 1530 (s), 1365 (s), 1250 (s), 1160 (s), 880 (w)

Substance 62

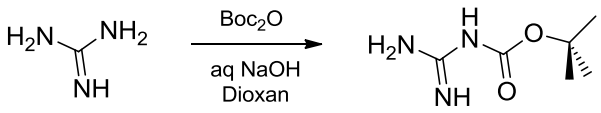

CH_5N_3
59,07 g/mol

$C_6H_{13}N_3O_2$ **62**
159,19 g/mol

A solution of di-*tert*-butyldicarbonate (12 g, 55 mmol, 1 eq.) in dioxane (100 mL) was filled in a precision dropping funnel and added drop wise to a solution of guanidinium chloride (26.50 g, 227 mmol, 4.1 eq.) and NaOH (12.1 g, 303 mmol, 5.5 eq.) in water (50 mL) over a period of 8h at 0°C. The suspension was extracted with 3 x 100 mL ethyl acetate and the combined organic phases were dried with $MgSO_4$. The solvent was removed under reduced pressure to give a white solid (7.96 g, 50 mmol, 91% yield).

Soluble DCM, $CHCl_3$, EtAc

Insoluble H_2O

R_f 0.3 (SiO_2: DCM/MeOH (5:1) + 1% NEt_3)

MP > 200°C

^{1}H NMR (300 MHz, CHLOROFORM-*d*) δ = 1.34 (s, 9 H, CH_3), 6.73 (br. s., 4 H, NH)

^{13}C NMR (151 MHz, DMSO-d_6) δ = 28.25 (CH_3), 75.46 (C_q), 162.68, 163.45 (CO, CN)

HR-MS (ESI pos.) m/z = calculated 160.1081, measured 160.1094 for $M + H^+$

FT-IR v [cm^{-1}] = 3420 (w), 3320 (w), 2975 (w), 2860 (w), 1655 (m), 1595 (s), 1535 (s), 1360 (m), 1300 (s), 1120 (s), 1055 (s), 865 (s), 800 (s)

Substance 63

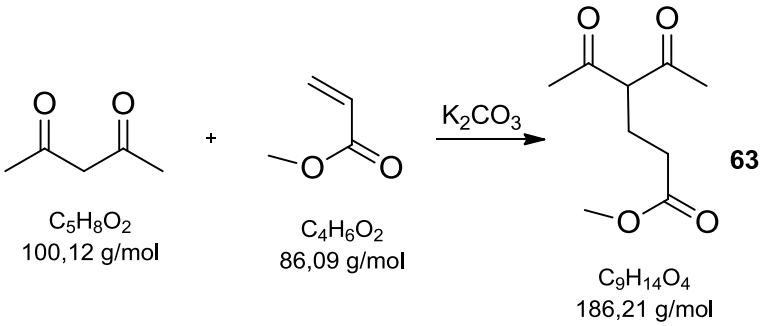

Acetyl acetone (112 g, 1.13 mol, 3.2 eq.), acrylic acid methyl ester (30.2 g, 350 mmol, 1 eq.) and K_2CO_3 (48.1 g, 348 mmol, 0.99 eq.) were stirred at 37°C overnight. The slurry was filtered and the precipitate was washed with chloroform (4 x 100mL). The filtrate was reduced under vacuum and the remaining liquid was distilled to obtain a yellow oil (54.67 g, 293.6 mmol, 84% yield).

Soluble	DCM, $CHCl_3$
Insoluble	H_2O, MeOH
R_f	0.67 (SiO_2: CyHex/EtAc (1:1))
BP	103 °C at 0.37 mbar
^{1}H NMR	(300 MHz, CHLOROFORM-*d*) δ = 1.97 - 2.01 (m, 6 H), 2.06 (s, 6 H, CH_3), 2.16 (t, ^3J=6.8 Hz, 2 H, CH_2), 2.26 (m, 1 H, CH_2), 2.45 (m, 1 H, CH_2), 3.51 (s, 3 H, CH_3), 3.53 (s, 1 H, CH), 3.61 (t, ^3J=6.8 Hz, 1 H, CH) Please note, that there is a second signal set observed due to the keto-enol tautomerism of the product.
^{13}C NMR	(75 MHz, CHLOROFORM-*d*) δ = 22.5 (CH_2), 22.6 (CH_3), 22.7 (CH_2), 29.0 (CH_3), 31.1, 34.3 (CH_2), 51.4 (CH_3), 66.6 (CH), 108.4, 172.6, 172.7, 191.0, 203.6 (C_q)
HR-MS	(ESI pos.) m/z = calculated 209.0784, measured 209.0827 for M + Na^+
FT-IR	v [cm^{-1}] = 2955 (w), 1730 (s), 1700 (s), 1440 (m), 1355 (s), 1255 (m), 1150 (s), 990 (m)

Substance 64

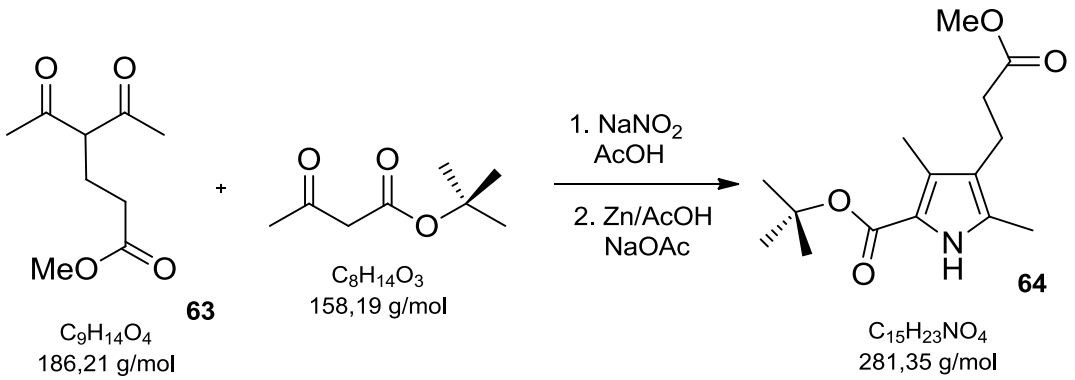

A solution of *tert*-butylacetoacetate (45.60 g, 289.20 mmol, 1 eq.) in acetic acid (84 mL) was cooled to 5°C and a solution of $NaNO_2$ (19.92 g, 239 mmol, 0.83 eq.) in H_2O (72 mL) was added slowly. The mixture was stirred for 3h at 5°C, to give the intermediate oxime. In a second flask NaOAc, zink, **63** and AcOH were mixed swiftly and the oxime solution was added slowly to the toughening suspension, so that the temperature of the reaction mixture didn't exceed 60°C. After completion of the addition, the mixture was heated to 65°C and stirred overnight. The yellow slurry was poured into a water-ice mixture (2 L) and the precipitate was filtered. The solid was dissolved in warm ethanol (250 mL) and filtered again to remove zink residues. The solution was concentrated and put kept in the refrigerator overnight to ensure a complete crystallization. The solid was filtered to obtain a yellow crystalline solid (19.36 g, 68.80 mmol, 24% yield)

Soluble	EtOH, DCM, $CHCl_3$
Insoluble	H_2O
R_f	0.26 (SiO_2: CyHex/EtAc (4:1))
MP	99 °C
^{1}H NMR	(300 MHz, CHLOROFORM-*d*) δ = 1.55 (s, 9 H, CH_3), 2.20 (s, 3 H, CH_3), 2.24 (s, 3 H, CH_3), 2.42 (t, ^3J= 8.1 Hz, 2 H, CH_2), 2.67 (t, ^3J= 9.3 Hz, 2 H, CH_2), 3.66 (s, 3 H, CH_3), 8.50 (br. s, 1 H, NH)
^{13}C NMR	(75 MHz, CHLOROFORM-*d*) δ = 10.7, 11.5 (CH_3), 19.8 (CH_2), 28.7 (CH_3), 35.1 (CH_2), 51.7 (CH_3), 80.3, 118.4, 120.0, 126.2, 129.1, 161.3, 173.7 (Cq)
HR-MS	(ESI pos.) m/z = calculated 304.1519, measured 304.1562 for M + Na^+
FT-IR	v [cm^{-1}] = 3305 (m), 2980 (w), 2910 (w), 1730 (s), 1655 (s), 1435 (s), 1275 (s), 1150 (s), 1095 (s), 875 (m), 770 (m)

Substance 65

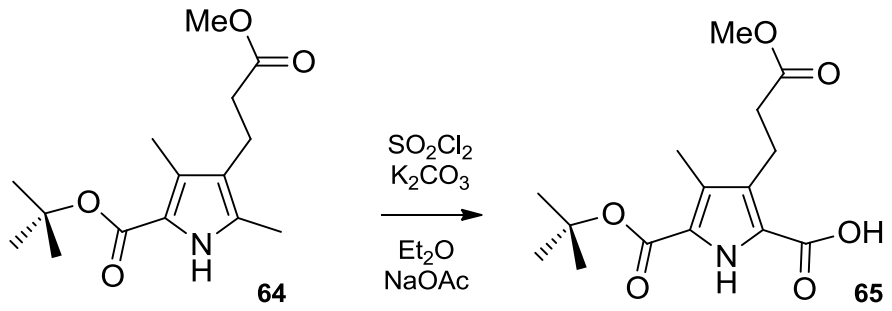

64 (6.00 g, 19.27 mmol, 1 eq.) and dry K_2CO_3 (11.73 g, 77.08 mmol, 4 eq.) were suspended in dry diethyl ether (200 mL) under argon atmosphere and cooled to -25°C with dry ice in acetone. Aluminum foil was wrapped around the flask to avoid light and SO_2Cl_2 (5.91 mL, 68 mmol, 3.5 eq.) was added over a period of 60 min. The cooling was removed and the mixture was refluxed with light exclusion under argon for 3h. The solvent was removed afterwards to give a light yellow substance. NaOAC (18.18 g, 222 mmol, 11.5 eq.), H_2O and dioxane (200 mL each) were added and the solution was stirred overnight. Subsequently the solution was heated to 110°C for 45 min to give a brown solution and brought to pH 2 quickly after cooling. The solution was extracted quickly and carefully with diethyl ether (8 x 100 mL). The diethyl ether fractions were brought to pH 1 separately. The extraction was carried out until no precipitate formed after acidification. The solid was filtered and washed several times with water until the filtrate stayed neutral. The filtered substance was dried in vacuum to give a fluffy white solid (4.35 g, 13.97 mmol, 73% yield)

Soluble	EtAc, DCM, $CHCl_3$
Insoluble	DEE, H_2O
R_f	0.5 (SiO_2: CyHex/EtAc (4:1))
MP	167 °C
^{1}H NMR	(300 MHz, CHLOROFORM-*d*) δ = = 1.58 (s, 9 H, CH_3), 2.27 (s, 3 H, CH_3), 2.56 (t, ^3J= 7.5 Hz, 2 H, CH_2), 3.06 (t, ^3J= 9.0 Hz, 2 H, CH_2), 3.68 (s, 3 H, CH_3), 9.44 (s, 1 H, NH)
^{13}C NMR	(75 MHz, CHLOROFORM-*d*) δ = 10.1 (CH_3), 20.3 (CH_2), 29.9 (CH_3), 34.6 (CH_2), 51.9 (CH_3), 82.2, 120.1, 124.5, 126.4, 131.4, 160.3, 164.5, 173.8 (Cq)
HR-MS	(ESI neg.) m/z = calculated 310.1296, measured 310.1322 for M^-
FT-IR	v [cm^{-1}] = 3005 (w), 2355 (w), 1670 (w), 1270 (w), 1145 (m), 750 (s)

Substance 66

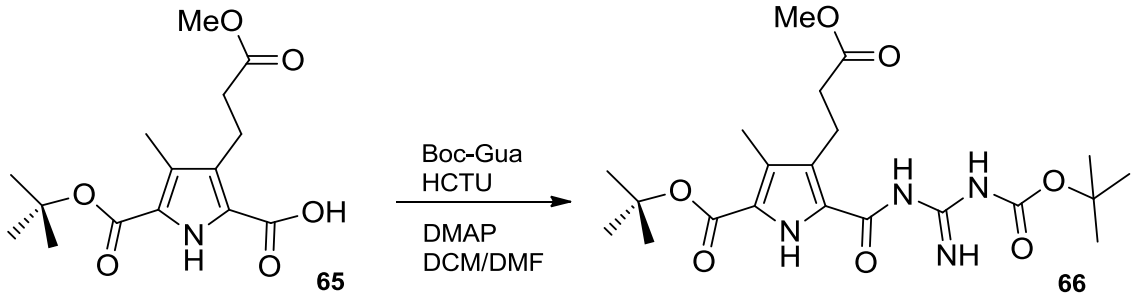

$C_{15}H_{21}NO_6$
311,33 g/mol

$C_{21}H_{32}N_4O_7$
452,50 g/mol

65 (4.20 g, 13.49 mmol, 1 eq.), DMAP (3.46 g, 28.33 mmol, 2.1 eq), HCTU (6.65 g, 16.19 mmol, 1.2 eq) and boc-guanidin **62** (2.57 g, 16.19 mmol, 1.2 eq.) were dissolved in dichloromethane/dimethylformamide (160 mL:30 mL) and the solution was stirred overnight. The DCM was removed under reduced pressure and H_2O (100 mL) was added. The cloudy mixture was extracted with diethyl ether (3x150 mL). Subsequently the organic phases were combined, dried with $MgSO_4$ and concentrated under reduced pressure. The raw product was purified with column chromatography (SiO_2: cyclohexane/ethyl acetate (3:1)) to give a white solid (2.26 g, 5.03 mmol, 38% yield).

Soluble	EtAc, DCM, $CHCl_3$
Insoluble	H_2O, MeOH
R_f	0.3 (SiO_2: CyHex/EtAc (3:1))
MP	70 °C
^{1}H NMR	(300 MHz, CHLOROFORM-*d*) δ = 1.52 (s, 9 H, CH_3), 1.56 (s, 9 H, CH_3), 2.26 (s, 3 H, CH_3), 2.60 (t, ^{3}J= 11.1 Hz, 2 H, CH_2), 3.11 (t, ^{3}J= 9.6 Hz, 2 H, CH_2), 3.7 (s, 3 H, CH_3), 8.38 (s, 1 H, NH), 8.89 (br. s, 2 H, NH), 9.52 (s, 1 H, NH)
^{13}C NMR	(75 MHz, CHLOROFORM-*d*) δ = 10.0 (CH_3), 21.3 (CH_2), 28.0, 28.4 (CH_3), 35.3 (CH_2), 51.6 (CH_3), 81.2, 83.7, 124.1, 125.4, 126.1, 129.5, 153.0, 158.1, 160.6, 174.7 (C_q)
HR-MS	(ESI pos.) m/z = calculated 475.2163 - measured 475.2288 for M + H^+
FT-IR	v [cm^{-1}] = 2980 (w), 2360 (w), 1720 (m), 1630 (m), 1525 (m), 1445 (m), 1265 (s), 1135 (s), 755 (s)

Substance 44

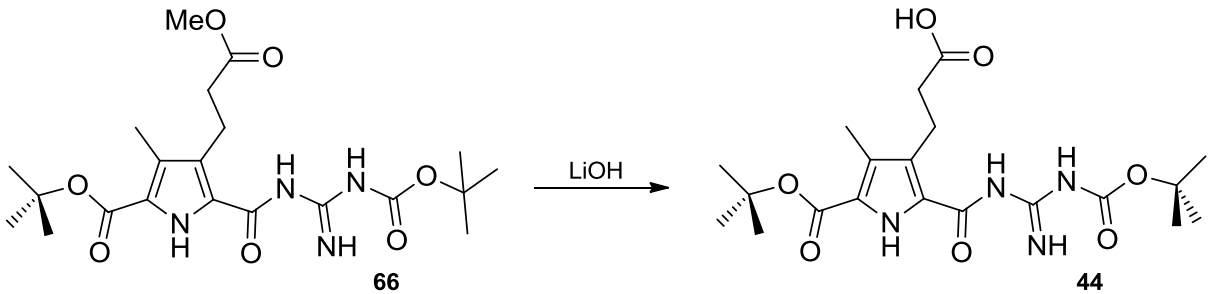

66 (2 g, 4.44 mmol, 1 eq.) was dissolved in THF and mixed with a solution of LiOH*H_2O (372.19 mg, 8.87 mmol, 2 eq.) in H_2O (12 mL). The reaction mixture was stirred at RT overnight. THF was subsequently removed under vacuum and 8 mL H_2O and 20 mL ethyl acetate were added. The clouded mixture was treated with 5%-HCl solution until the clouding disappeared. The clear solution was extracted three times with 40 mL EtAc and the combined organic phases were dried with $MgSO_4$ and filtered. The solvent was removed under reduced pressure to obtain a white fluffy substance (1.757 g, 4 mmol, 90 % yield).

Soluble	EtAc, DCM, $CHCl_3$, THF
Insoluble	H_2O, MeOH
R_f	0.3 (SiO_2: n-Hex/EtAc (2:1) + 1% AcOH)
MP	115 °C
^{1}H NMR	(300 MHz, CHLOROFORM-*d*) δ = 1.54 (s, 9 H, CH_3), 1.60 (s, 9 H, CH_3), 2.27 (s, 3 H, CH_3), 2.62 (t, ^{3}J= 10.2 Hz, 2 H, CH_2), 3.12 (t, ^{3}J= 8.4 Hz, 2 H, CH_2), 9.01 (br. s, 1 H, NH), 10.00 (br. s, 1 H, NH), 10.82 (br. s, 1 H, NH)
^{13}C NMR	(75 MHz, CHLOROFORM-*d*) δ = 10.4 (CH_3), 21.3 (CH_2), 28.5, 28.9 (CH_3), 35.3 (CH_2), 81.7, 82.7, 124.3, 125.5, 126.6, 129.6, 158.0, 161.0, 161.2, 179.3 (C_q)
HR-MS	(ESI pos.) m/z = calculated 461.2007, measured 461.2044 for M + Na^+
FT-IR	v [cm^{-1}] = 3336 (w), 2975 (w), 2930 (w), 1685 (m), 1630 (m), 1456 (m), 1367 (w), 1273 (m), 1245 (m), 1137 (s), 835 (m), 779 (m), 754 (m)

Substance 51

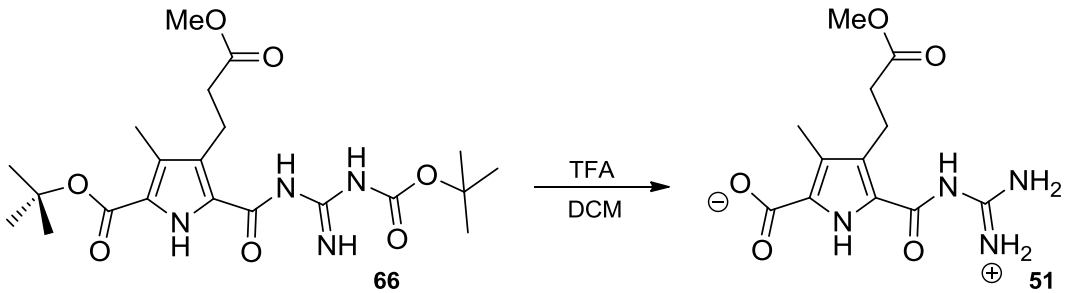

66 (20 mg, 44 µmol) was dissolved in a dichloromethane/TFA-mixture (10 mL:1 mL) and stirred for 24h. After evaporation of the solvent, 0.1M HCl (10 mL) was added and the suspension lyophilized. The remaining solid was dissolved in 0.5M NaOH and the pH was brought to 5.68 with 0.1M HCl. The suspension was stirred for 1h to ensure the complete precipitation of the zwitterion. The precipitate was filtered and washed with water to remove all salts. The substance was dried in vacuum to obtain a beige solid (13 mg, 44 µmol, quant. yield).

Soluble	DMSO
Insoluble	in anything else
R_f	no conditions found
MP	> 200 °C
^{1}H NMR	(300 MHz, DMSO-*d*^{6}) δ = 2.11 - 2.16 (m, 2 H, CH_2), 2.18 (s, 3 H, CH_3), 2.39 - 2.45 (m, 2 H, CH_2), 3.28 (br. s., 3 H, CH_3), 7.94 (br. s., 2 H, NH), 10.10 (br. s., 2 H, NH), 12.66 (br. s., 1 H, NH)
^{13}C NMR	(75 MHz, DMSO-*d*^{6}) δ = 27.40 (CH_3), 30.42, 34.37 (CH_2), 50.38 (CH_3), 124.91 (C_q), 139.18, 151.46 (CN, CO)
HR-MS	(ESI pos.) m/z = calculated 297.1154, measured 297.1184 for M + H^+
FT-IR	v [cm^{-1}] = 3325 (w), 3210 (w), 2920 (s), 2855 (s), 2355 (w), 1695 (s), 1540 (w), 1450 1335 (m), (m), 1275 (s), 1155 (m)

7.2 Ditopic Modules

Substance 43 & 45

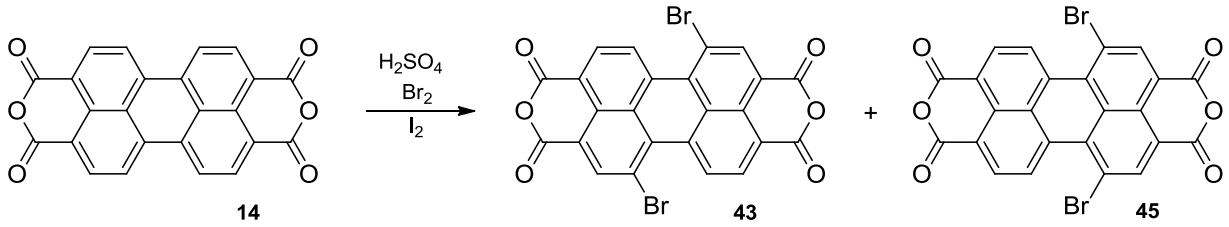

14 **43** **45**

$C_{24}H_8O_6$
392,32 g/mol

$C_{24}H_6Br_2O_6$
550,11 g/mol

A mixture of PTCDA **14** (5.00 g, 12.8 mmol, 1 eq.) and concentrated sulfuric acid (45 mL) were stirred 24h at RT. Then a catalytic amount of iodine (0.12 g, 0.48 mmol, 0.04 eq.) was added. The solution was heated to 85°C and bromine (4.50 g, 28.12 mmol, 2.2 eq.) added drop wise over 1h. After 24h at 85°C the mixture was cooled to RT and the precipitate was filtered and washed with conc. sulfuric acid. The isolated solid was suspended in water and lyophilized to obtain a brick-red solid (4.89 g, 8.89 mmol, 69% yield), which is a mixture of the 1,7-regioisomer **45** and the 1,6-regioisomer **45**.

Soluble	conc. H_2SO_4
Insoluble	anything else
R_f	-
MP	> 200°C
^{1}H NMR	(500 MHz, D_2SO_4) δ = 8.73 - 8.82 (m, 6 H, CH)
^{13}C-NMR	-
HR-MS	(APCI-DIP) m/z = calculated 550.8585, measured 550.8588 for M + H^+
FT-IR	-

Substance 42

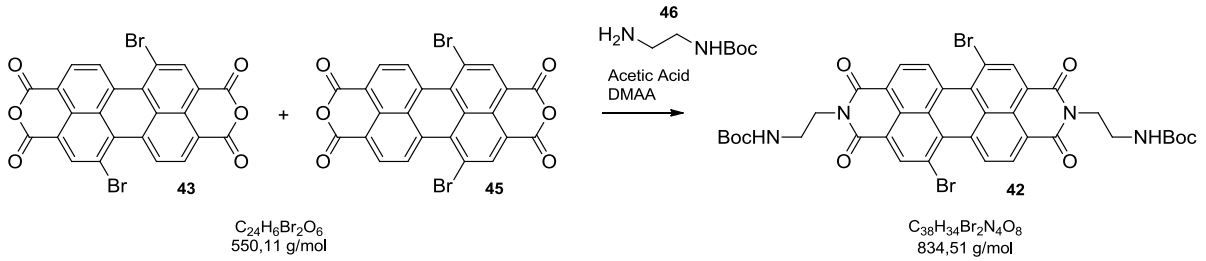

A suspension of the brominated PTCDAs **43** and **45** (1.26 g, 2.29 mmol, 1 eq.) and **46** (1.10 g, 6.87 mmol, 3 eq.) with acetic acid (0.6 ml, 5 eq.) in dimethyl acetamide (23 mL) was stirred 24h at 100°C. After cooling the precipitate was filtered, 15 mL water were added and the suspension was lyophilized. The crude product (72% yield) was purified by column chromatography (SiO_2: methanol/dichloromethane (1:9)). The brick-red substance, which is also a mixture of the 1,7- and 1,6-regioisomer, was dissolved in 100 mL DCM and 50 mL methanol was added. The solvent mixture was slowly reduced under vacuum until a precipitate of the 1,7-regioisomer formed whereby the 1,6-regioisomer stayed in solution. The suspension (ca. 50 mL) was put in the refrigerator overnight and the precipitate was filtered afterwards to obtain the 1,7-regioisomer **42** as a bright red substance (1.27 g, 1.52 mmol, 66% yield).

Soluble	$CHCl_3$, DCM, THF
Insoluble	MeOH, H_2O
R_f	0.5 (SiO_2: DCM/MeOH (9:1))
	0.8 (SiO_2: DCM/MeOH (19:1))
MP	> 200°C
^{1}H NMR	(300 MHz, CHLOROFORM-*d*) δ = 1.30 (s, 18 H, CH_3), 3.58 (m., 4 H, CH_2), 4.35 - 4.47 (t, ^3J=5.00 Hz, 4 H, CH_2), 4.92 (br. s., 2 H, NH), 8.73 (d, ^3J=8.13 Hz, 2 H, CH), 8.95 (s, 2 H, CH), 9.51 (d, ^3J=8.13 Hz, 2 H, CH)
^{13}C NMR	(126 MHz, CHLOROFORM-*d*) δ = 28.22 (CH_3), 39.41, 40.42 (CH_2), 79.30 (C_q), 20.82, 122.57, 122.99, 127.01, 128.12, 128.50, 129.19, 130.17, 132.89, 138.11 (C_q), 156.11, 162.73, 163.24 (CN, CO)
HR-MS	(MALDI) m/z = calculated 857.0616, measured 857.1606 for M + Na^+
FT-IR	v [cm^{-1}] = 3335 (w), 2985 (w), 2355 (w), 1655 (s), 1600 (m), 1515 (m), 1390 (s), 1330 (s), 1245 (s), 1155 (s), 745 (s)

Substance 41

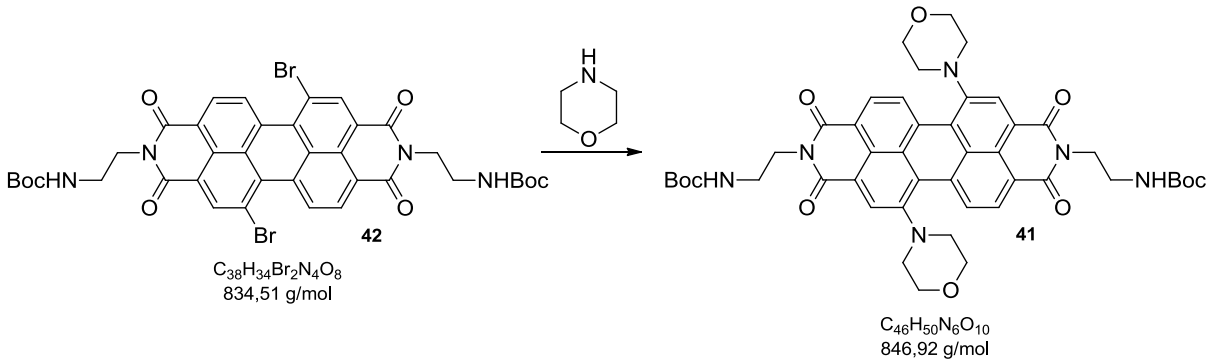

A mixture of **42** (91 mg, 109 µmol, 1 eq.) and morpholine (9 mL, 8.91 g, 0.10 mol) was stirred 72h at 70°C. Afterwards morpholine was removed under reduced pressure and the turquoise crude product was purified by column chromatography (SiO_2: tetrahydrofurane/dichloromethane (1.5:8.5)). The third band (1st = turquoise, 2nd = blue, 3rd = green, 4th = lilac) was collected and after removal of the solvent in vacuum a green solid (70 mg, 83 µmol, 73%) was obtained.

Soluble	$CHCl_3$, DCM, THF
Insoluble	MeOH, H_2O
R_f	0.5 (SiO_2: THF/DCM (1.5:8.5))
MP	168°C
^{1}H NMR	(500 MHz, CHLOROFORM-*d*) δ = 1.33 (br. s., 18 H, CH_3), 2.97 (br. s., 4 H, CH_2), 3.26 (br. s., 4 H, CH_2), 3.56 - 3.63 (m, 4 H, CH_2), 3.87 - 3.96 (m, 8 H, CH_2), 4.40 (br. s., 4 H, CH_2), 5.30 (br. s., 2 H, NH), 8.14 (br. s., 2 H, CH), 8.37 (d, ^3J=7.88 Hz, 2 H, CH), 9.46 - 9.57 (m, 2 H, CH)
^{13}C NMR	(126 MHz, CHLOROFORM-*d*) δ = 28.33 (CH_3), 39.60, 40.62 (CH_2), 66.36, 68.46 (CH_2), 79.06 (C_q), 121.00, 122.27, 122.47, 123.35, 124.14, 128.01, 128.78, 129.33, 130.86, 134.29(C_q), 149.57, 156.21, 163.51 (CN, CO)
HR-MS	(MALDI) m/z = calculated 847.3559, measured 847.6380 for M + H^+
FT-IR	v [cm^{-1}] = 3360 (w), 2930 (w), 2850 (w), 2355 (w), 1685 (m), 1645 (m), 1580 (m), 1410 (m), 1335 (m), 1255 (s), 1010 (m), 755 (s)

Substance 40

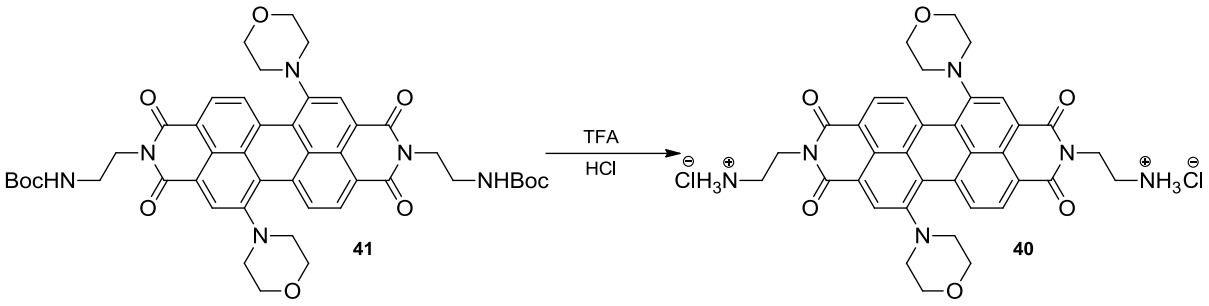

41 (70 mg, 83 µmol, 1 eq.) was treated with TFA (5 mL, 3.36 g, 29 mmol) and stirred for 1h. Subsequently TFA was removed under reduced pressure. The remaining solid was dissolved in 0.1M HCl-solution and lyophilized to obtain the chloride salt as a green solid (60 mg, 83 µmol, quant. yield).

Soluble MeOH, H_2O

Insoluble DCM, $CHCl_3$

R_f 0.4 (SiO_2: DCM/MeOH/NEt_3 (9:1:1))

MP > 200°C

^{1}H-NMR (600 MHz, METHANOL-*d*$_4$) δ = 2.68 (t, ^3J=6.79 Hz, 4 H, CH_2), 3.09 - 3.13 (m, 2 H, CH_2), 3.22 - 3.24 (m, ^3J=6.79 Hz, 4 H, CH_2), 3.30 (t, ^3J =5.69 Hz, 4 H, CH_2), 3.33 - 3.39 (m, 2 H, CH_2), 3.39 - 3.44 (m, 2 H, CH_2), 3.50 - 3.54 (m, 2 H, CH_2), 3.57 - 3.61 (m, 2 H, CH_2), 3.76 - 3.78 (m, 2 H, CH_2), 3.87 (br. s., 4 H, NH_2), 7.99 (br. s., 2 H, CH), 8.37 (d, ^3J=8.44 Hz, 2 H, CH), 9.48 (d, ^3J=8.07 Hz, 2 H, CH)

^{13}C-NMR (151 MHz, METHANOL-*d*$_4$) δ = 40.11, 40.57 (CH_2), 65.11, 67.35, 67.53, 68.52 (CH_2), 80.38 (C_q), 122.13, 123.46, 123.62, 123.79, 125.23, 125.76, 129.63, 130.73, 135.86 (C_q), 151.24, 158.55, 163.45, 165.31, 165.41 (CN, CO)

HR-MS (MALDI) m/z = calculated 647.2573, measured 647.3033 for M - 2x HCl + H^+

FT-IR v [cm^{-1}] = 3390 (w), 2920 (w), 2845 (w), 2355 (w), 1680 (m), 1645 (m), 1575 (m), 1435 (w), 1345 (m), 1260 (m), 1095 (w), 750 (s)

Substance 39

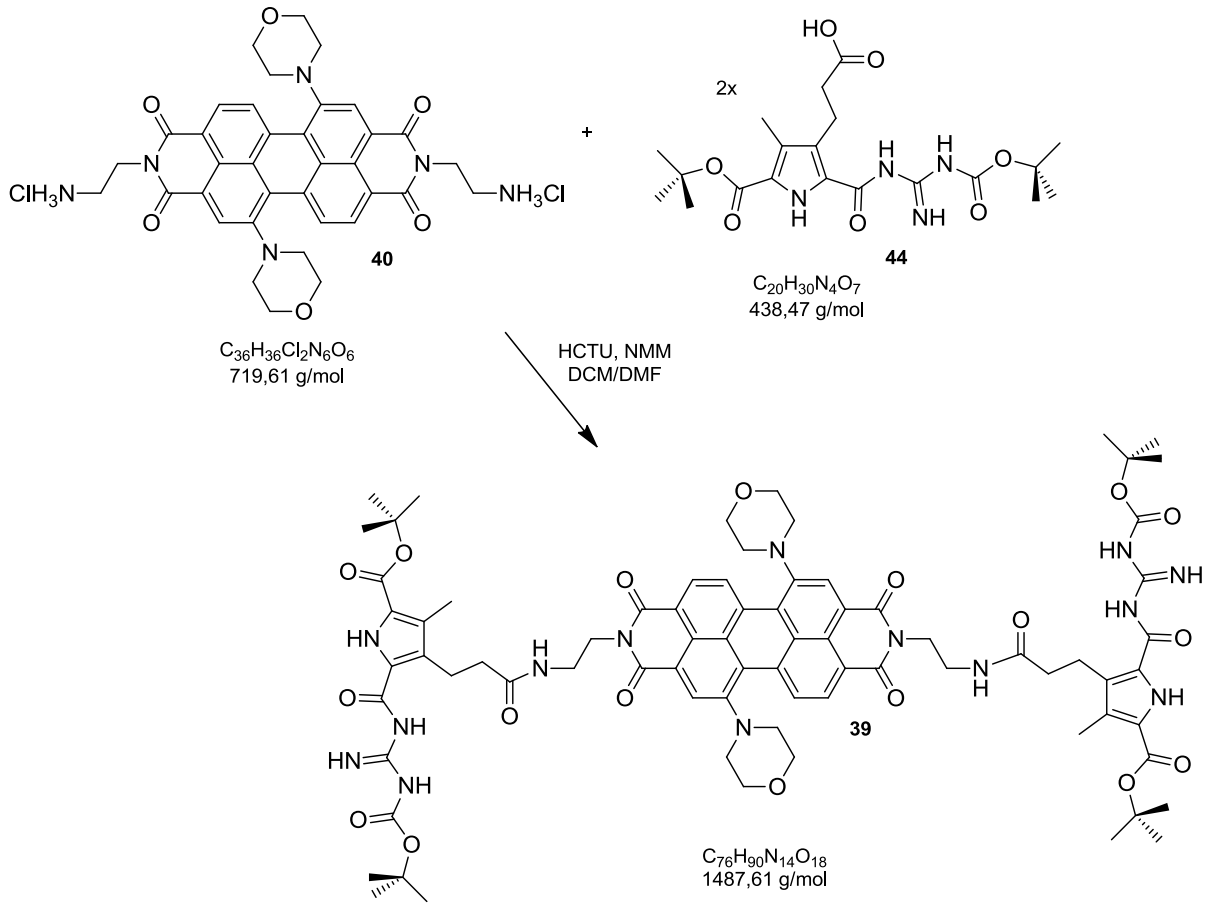

40 $C_{36}H_{36}Cl_2N_6O_6$ 719,61 g/mol

44 $C_{20}H_{30}N_4O_7$ 438,47 g/mol

39 $C_{76}H_{90}N_{14}O_{18}$ 1487,61 g/mol

A mixture of **40** (106 mg, 164 µmol, 1 eq.), **44** (144 mg, 328 µmol, 2 eq.), HCTU (163 mg, 394 µmol, 2.4 eq.) and NMM (96 mg, 104 µL, 946 µmol, 5.8 eq.) in dichloromethane/dimethylformamide (16mL (1:1)) was stirred for 24h at RT. dichloromethane was removed under reduced pressure and 25 mL H_2O were added. The formed precipitate was filtered and subsequently purified by column chromatography (SiO_2: ethyl acetate/cyclohexane (4:1)). After the removal of the solvent, a dark green solid (207 mg, 139 µmol, 85% yield) was isolated.

Soluble THF, DCM, $CHCl_3$

Insoluble H_2O, MeOH

R_f 0.6 (SiO_2: EtAc/CyHex (4:1))

MP > 200°C

^{1}H-NMR (500 MHz, DMSO-d_6) δ = 1.48 (s, 18 H, CH_3 (Py)), 1.53 (s, 18 H, CH_3 (Py)), 2.13 (m, 8 H, CH_2 (Morph)), 2.17 (s, 6 H, CH_3 (Py)), 2.38 (t, ^3J=7.57 Hz, 4 H, CH_2 (Py)), 2.83 (m, 4 H, CH_2 (Linker)), 2.93 (t, ^3J=7.72 Hz, 4 H, CH_2 (Py)), 3.38 (m, 8 H, CH_2 (Morph)), 4.18 (m, 4 H, CH_2 (Linker)), 5.06 (dd, ^2J=19.70, ^3J=6.15 Hz, 2 H, NH (Linker)), 7.91

(br. s., 2 H, CH, (Per)), 8.32 (br. s., 2 H, CH, (Per)), 8.50 (br. s., 2 H, CH, (Per)), 9.39 (br. s., 2 H, NH), 9.67 (br. s., 2 H, NH), 10.09 (br. s., 2 H, NH), 10.78 (br. s., 2 H, NH)

^{13}C-NMR (126 MHz, DMSO-d_6) δ = 9.80 (CH_3), 23.27, 23.54 (CH_3), 28.86, 33.14 (CH_2), 39.76, 39.93 (CH_2-Per), 65.67, 66.59 (CH_2), 80.72, 81.37 (C_q), 97.14, 99.63, 100.47, 105.79, 106.96, 110.89, 113.89, 117.32, 118.97, 121.57, 125.27, 128.61, 134.04, 137.83 (C_q), 160.17, 162.36, 164.77, .169.39, 170.88, 174.16, 174.52 (CN, CO)

HR-MS (ESI pos.) m/z = calculated 1487.6630, measured 1487.6667 M + H^+

FT-IR v [cm^{-1}] = 3385 (w), 2935 (w), 2845 (w), 2340 (w), 1700 (m), 1650 (m), 1580 (m), 1460 (w), 1240 (s), 1135 (s), 750 (s)

Substance 35 (imide linked Module)

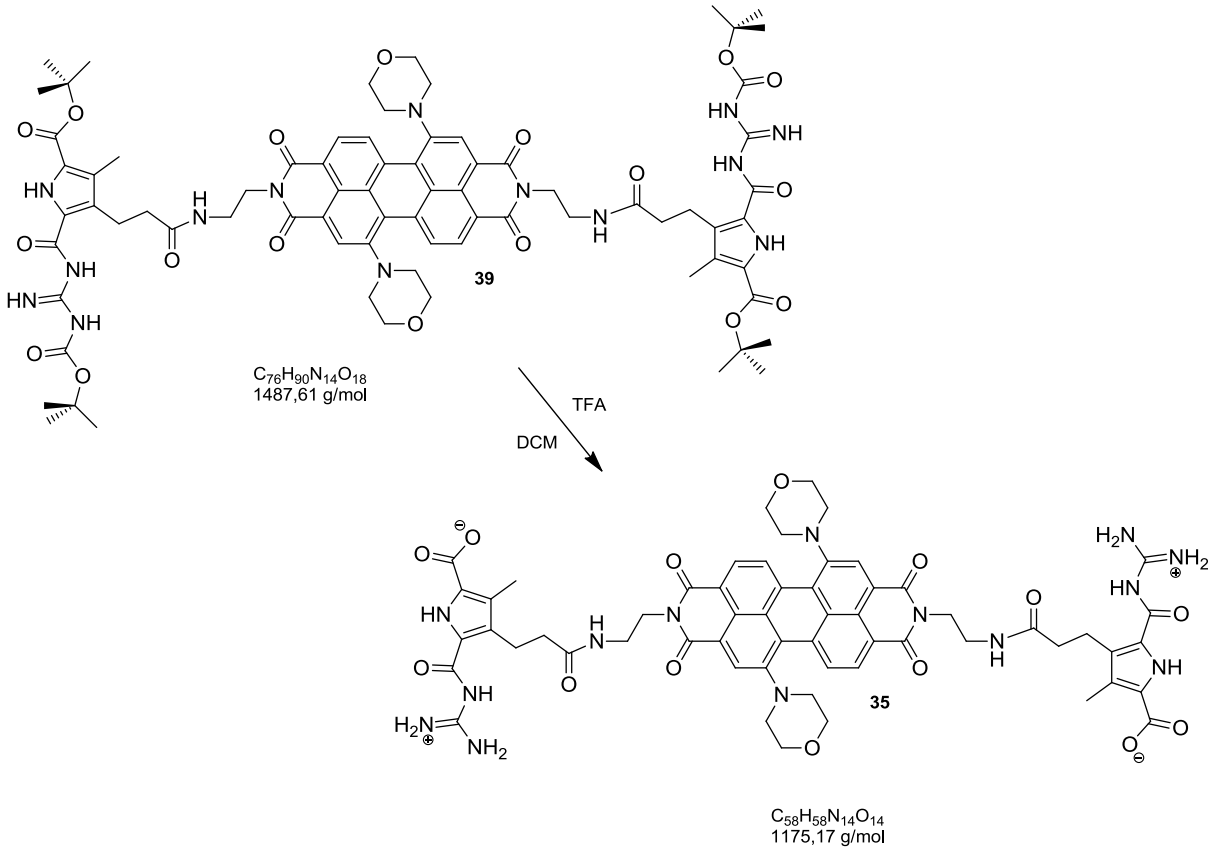

39 (27 mg, 18 µmol) was dissolved in a dichloromethane/TFA-mixture (5 mL:1 mL) and stirred for 5h. After evaporation of the solvent, 0.1M HCl was added and the suspension lyophilized. The remaining solid was dissolved in 1 M NaOH and the pH was adjusted to 5.7 with 0.1 M HCl. The suspension was stirred for 1h to ensure the complete precipitation of the zwitterion. The precipitate was filtered and washed with water to remove all salts. The substance was dried in vacuum to obtain a dark green solid (19 mg, 16 mmol, 89% yield).

Soluble DMSO

Insoluble anything else

R_f no conditions found

MP > 200°C

^{1}H NMR (500 MHz, DMSO-d_6) δ = 2.04 (br. s., 4 H, CH_2 (Py)), 2.18 (br. s., 6 H, CH_3 (Py)), 2.26 (br. s., 4 H, CH_2 (Py)), 2.65 (br. s., 12 H, CH_2 (Morph), CH_2 (Linker)), 3.04 (m, 4 H, CH_2 (Linker)), 3.90 (m, 8 H, CH_2 (Morph)), 4.47 (br. s., 2 H, NH (Linker)), 8.07 (br.s., 2 H, NH (Zw)), 8.57 (s, 2 H, CH (Per)), 9.41 (d, ^3J=7.88 Hz, 2 H, CH (Per)) 9.82 (d,

	^{3}J=8.20 Hz, 2 H, CH (Per)), 10.01 (br.s., 2 H, NH (Zw)), 12.44 (br.s., 1 H, NH (Zw)), 14.6 (br.s., 1 H, NH (Zw))
^{13}C NMR	(126 MHz, DMSO-d_6) δ =28.8, 33.2 (CH_2-Py), 39.7, 40.0 (CH_2-Per), 65. 7, 66.5 (CH_2-Morph), 97.4, 99.6, 100.5, 105. 9, 107.1, 110.9, 114.0, 117.3, 118.9, 121.7, 125.2, 128.6, 134.4, 137.3 (C_q), 160.7, 162.3, 164.7, .169.9, 170.8, 174.4, 174.5 (CN, CO)
HR-MS	(MALDI) m/z = calculated 1175.4290, measured 1175.5794 for M + H^+
FT-IR	v [cm^{-1}] = 3360 (w), 3190 (w), 2950 (w), 2345 (w), 1660 (m), 1550 (m), 1430 (m), 1340 (s), 1270 (s), 1090 (w), 750 (s)

Substance 49

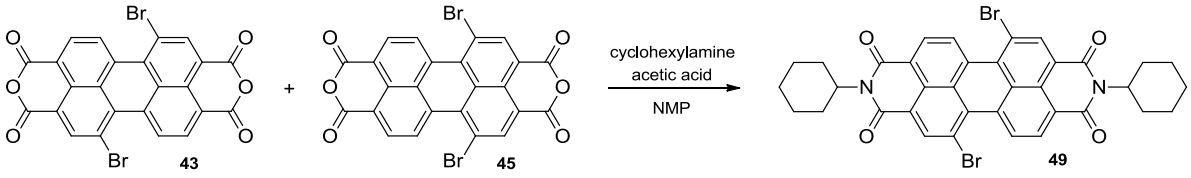

$C_{24}H_6Br_2O_6$
550,11 g/mol

$C_{36}H_{28}Br_2N_2O_4$
712,43 g/mol

A suspension of the brominated PTCDA **43** & **45** (800 mg, 1.4 mmol, 1 eq.) and cyclohexylamine (492 µL, 423 mg, 4.27 mmol, 3 eq.) with acetic acid (0.4 ml, 5 eq.) in NMP (15 mL) was stirred 24h at 100°C. After cooling the precipitate was filtered, 15 mL water were added and the suspension was lyophilized. The crude product (72% yield) was purified by column chromatography (SiO_2: dichloromethane). The brick-red substance was dissolved in 100 mL DCM and 50 mL methanol was added. The solvent mixture was slowly reduced under vacuum until a precipitate of the 1,7-regioisomer formed. The suspension (ca. 50 mL) was put in the refrigerator and the precipitate was filtered afterwards to obtain the 1,7-regioisomer as a bright red substance (581 mg, 0.82 mmol, 58% yield).

Soluble	$CHCl_3$, DCM, THF
Insoluble	MeOH, H_2O
R_f	0.7 (SiO_2: DCM)
MP	> 200°C
^{1}H NMR	(300 MHz, CHLOROFORM-*d*) δ = 1.31 - 1.53 (m, 6 H, CH_2), 1.75 - 1.93 (m, 10 H, CH_2), 2.56 (dq, ^2J=12.35, ^3J=3.28 Hz, 4 H, CH_2), 5.03 (tt, ^2J=12.16, ^3J=3.48 Hz, 2 H, CH), 8.68 (d, ^3J=8.13 Hz, 2 H, CH), 8.89 (s, 2 H, CH), 9.48 (d, ^3J=8.13 Hz, 2 H, CH)
^{13}C NMR	(126MHz ,CHLOROFORM-*d*) δ = 25.5, 26.7, 29.2 (CH_2), 54.4 (CH), 120.9, 123.4, 123.9, 127.2, 128.6, 129.4, 130.1, 132.8, 133.0, 138.1 (C_q), 162.9, 163.5 (CO)
HR-MS	(MALDI) m/z = calculated 712.0395, measured 712.1062 for M
FT-IR	v [cm^{-1}] = 2980 (w), 2355 (w), 1650 (w), 1280 (m), 750 (s),

Substance 48

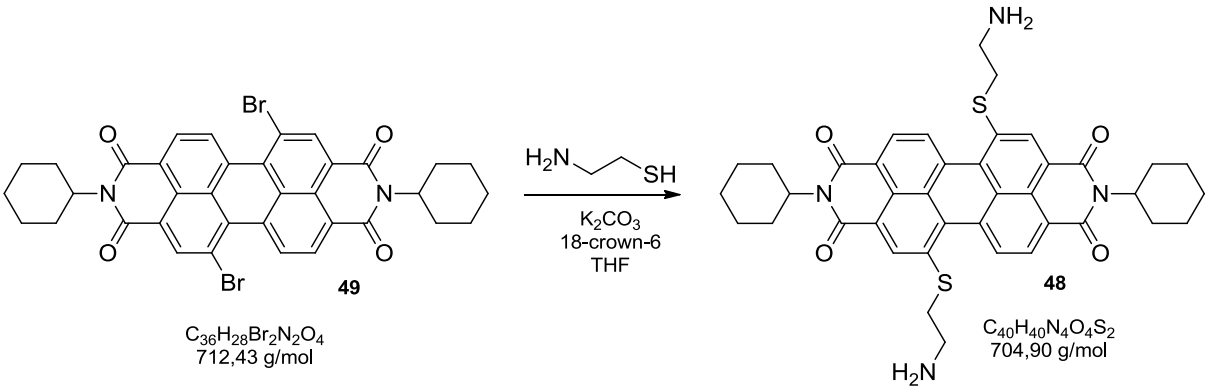

Cysteamine (21 mg, 0.28 mmol, 4 eq.), 18-crown-6 (185 mg, 0.70 mmol, 10 eq.) and K_2CO_3 (97 mg, 0.70 mmol, 10 eq.) were dissolved in THF (15 mL) and **49** (50 mg, 0.07 mmol, 1 eq.) was added after 5 min. An immediate color change occurred from orange to magenta. The starting material was gone after 15 min, but to ensure a complete reaction, the mixture was stirred for additional 2h. After the addition of water (15 mL) the reaction mixture was extracted with dichloromethane until the water phase remained colorless. The combined organic phases were dried with $MgSO_4$, filtered and the solvent removed in vacuum to obtain a magenta solid (49 mg, 0.07 mmol, quant. yield).

Soluble THF, DCM, $CHCl_3$

Insoluble H_2O, MeOH

R_f 0.2 (SiO_2: DCM/MeOH (9:1))

MP > 200°C

^{1}H NMR (300 MHz, CHLOROFORM-*d*) δ = 1.40 - 1.52 (m, 6 H, CH_2), 1.77 - 1.95 (m, 10 H, CH_2), 2.51 - 2.65 (m, 4 H, CH_2), 2.97 (t, ^3J=6.41 Hz, 4 H, CH_2), , 3.31 (t, ^3J =6.41 Hz, 4 H, CH_2), 3.67 (m, 4 H, NH_2), 4.99 - 5.12 (m, 2 H, CH), 8.67 (d, ^3J =8.13 Hz, 2 H, CH), 8.81 (s, 2 H, CH), 8.87 (d, ^3J =8.13 Hz, 2 H, CH)

^{13}C NMR (126 MHz, CHLOROFORM-*d*) δ = 25.4, 26.5, 29.1 (CH_2), 54.1 (CH), 77.2, 78.2 (CH_2), 120.2, 123.4, 126.9, 128.4, 129.2, 131.9, 132.0, 132.7, 132.9, 138.1 (C_q), 162.9, 163.5 (CO)

HR-MS (MALDI) m/z = calculated 705.2525, measured 705.9219 for M + H^+

FT-IR v [cm^{-1}] =2920 (w), 2872 (w), 2365 (w), 1700 (m), 1650 (m), 1590 (m), 1335 (w), 1275 (m), 1095 (m), 960 (w), 750 (s)

Substance 47

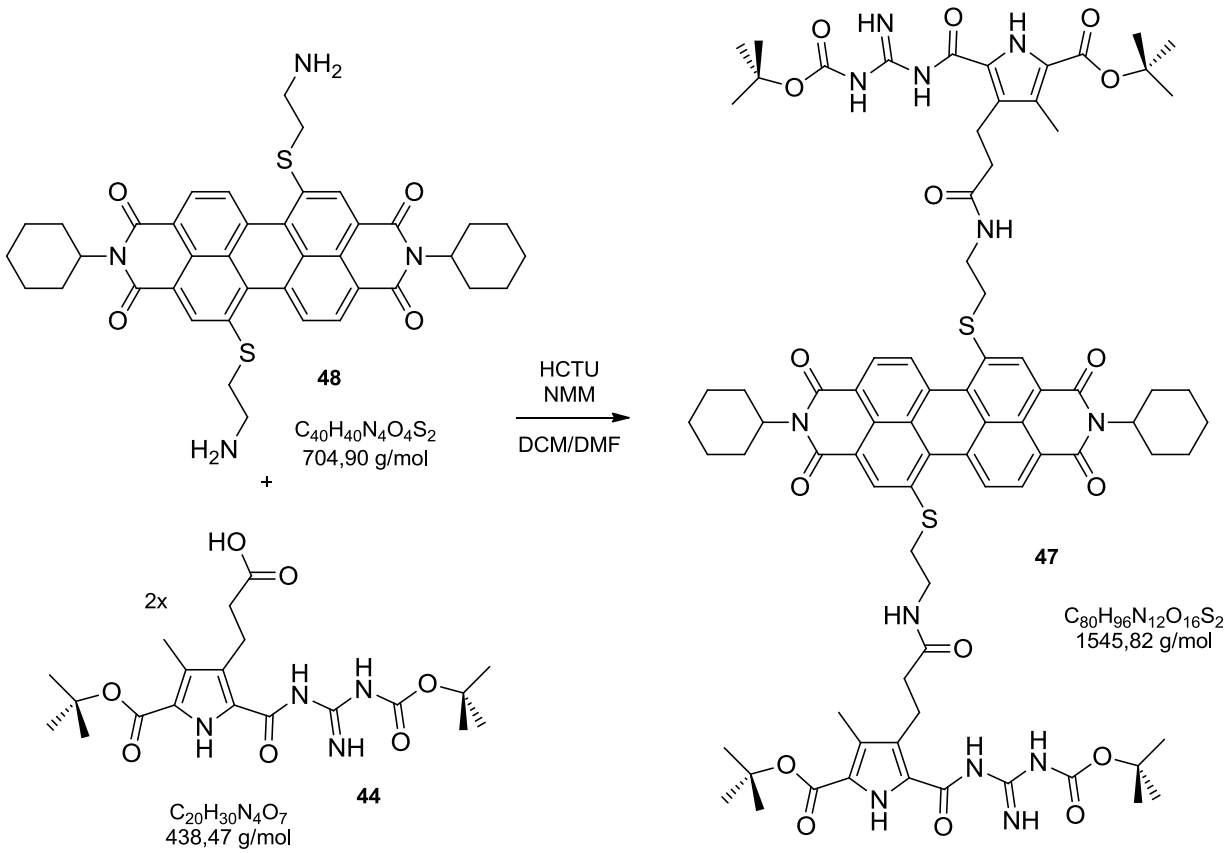

A mixture of 48 (80 mg, 114 µmol, 1 eq.), 44 (150 mg, 342 µmol, 3 eq.), HCTU (170 mg, 410 µmol, 3.6 eq.) and NMM (104 mg, 113 µL, 1.03 mmol, 9 eq.) in dichloromethane/dimethylformamide (20 mL (2:1)) was stirred for 24h at RT. Dichloromethane was removed under reduced pressure and 25 mL H_2O were added. The formed precipitate was filtered and subsequently purified by column chromatography (SiO_2: dichloromethane/methanol (9:1)). After the removal of the solvent, a dark red solid (59 mg, 38 µmol, 33% yield) was isolated.

Soluble THF, DCM, $CHCl_3$

Insoluble H_2O, MeOH

R_f 0.55 (SiO_2: DCM/MeOH (9:1))

MP > 200°C

^{1}H-NMR (500 MHz, DMSO-d_6) δ = 1.23 (br. s., 18 H, CH_3 (Py)), 1.28 (br. s., 18 H, CH_3 (Py)), 1.44 (m, 6 H, CH_2 (CyH)), 1.47 (s, 6 H, CH_3 (Py)), 1.61 - 1.65 (m, 4 H, CH_2 (Linker)), 1.69 - 1.76 (m, 8 H, CH_2 (CyH)), 1.84 - 1.90 (m, 6 H, CH_2 (CyH)), 2.12 - 2.16 (d, ^3J=7.88 Hz, 2 H, CH_2 (Py)), 2.40 - 2.44 (t, ^3J=7.88 Hz, 2 H, CH_2 (Py)), 3.25 - 3.29 (m,

4 H, CH_2 (Py)), 3.36 - 3.41 (m, 4 H, CH_2 (Linker)), 4.10 - 4.16 (m, 2 H, CH (CyH)), 4.89 (br. s., 2 H, NH (Linker)), 8.24 (br. s., 2 H, CH (Per)), 8.58 (br. s., 2 H, CH (Per)), 9.08 (br. s., 2 H, CH (Per)), 9.50 (br. s., 2 H, NH), 10.13 (br. s., 2 H, NH), 10.58 (br. s., 2 H, NH), 11.40 (br. s., 2 H, NH)

^{13}C-NMR (126 MHz, DMSO-d_6) δ = 10.79, 13.88 (CH_3), 21.02, 21.76, 22.39, 23.23, 23.55, 27.60, 28.35, 29.78, 30.41, 34.38, 38.07, 40.42 (CH_2), 66.60, 67.40 (C_q), 68.25 (CH), 105.72, 128.65, 130.76, 131.58, 131.71, 139.18 (C_q), 152.52, 166.97 (CN, CO)

HR-MS (MALDI) m/z = calculated 1342.5304, measured 1342.6719 M - 2x Boc

FT-IR v [cm^{-1}] =2915 (m), 2850 (m), 2365 (w), 1700 (m), 1650 (m), 1455 (m), 1320 (m), 1260 (s), 1140 (s), 755 (s)

Substance 36 (core linked Module)

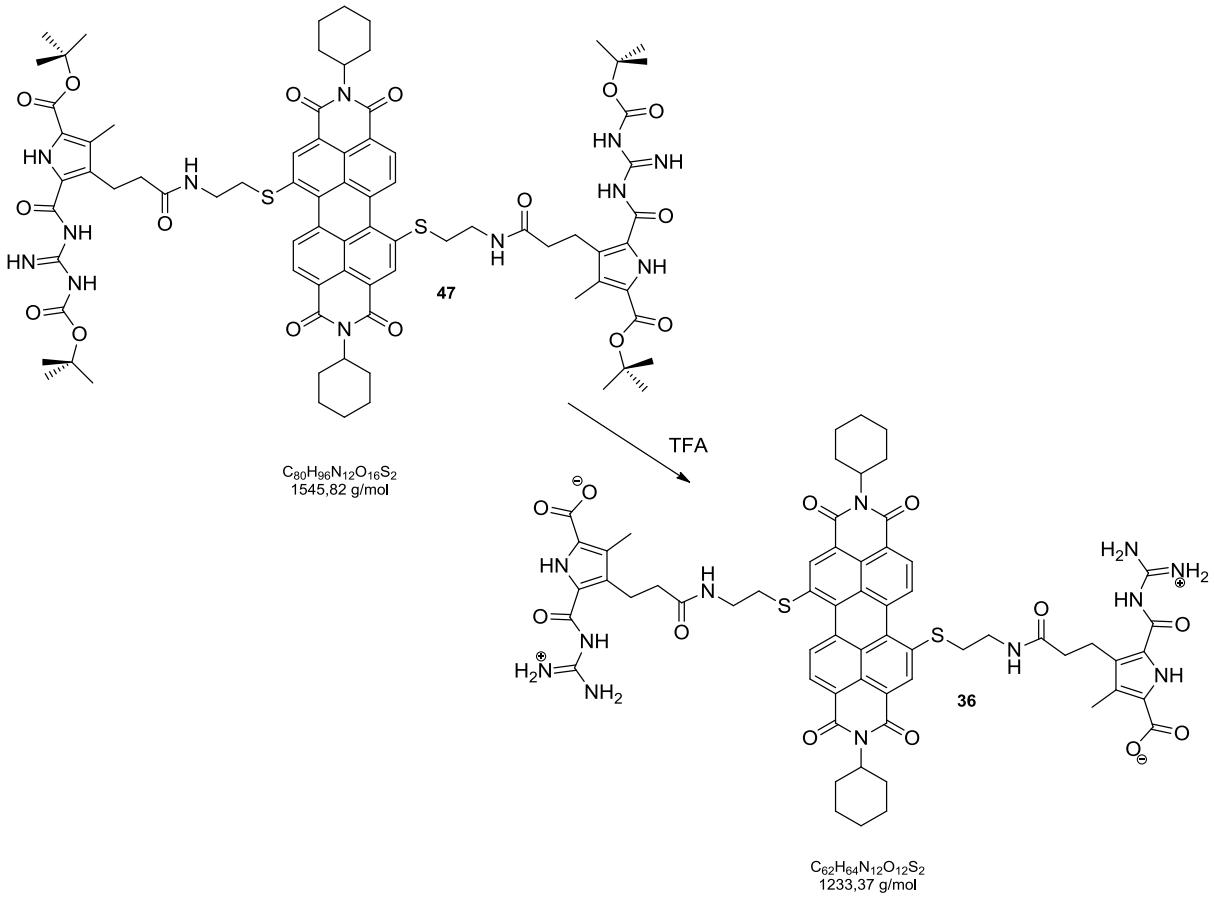

47 (25 mg, 16 µmol) was dissolved in a dichloromethane/TFA-mixture (10 mL:1 mL) and stirred for 24h. After evaporation of the solvent, 0.1 M HCl (10 mL) was added and the suspension lyophilized. The remaining solid was dissolved in 0.5 M NaOH and the pH was brought to 5.68 with 0.1 M HCl. The suspension was stirred for 1h to ensure the complete precipitation of the zwitterion. The precipitate was filtered and washed with water to remove all salts. The substance was dried in vacuum to obtain a dark red solid (20 mg, 16 µmol, quant. yield).

Soluble	DMSO
Insoluble	anything else
MP	> 200°C
R_f	no conditions found
^{1}H NMR	(500 MHz, DMSO-d_6) δ = 1.27 (br. s., 6 H, CH_3 (Py)), 1.60 - 1.64 (m, 4 H, CH_2 (Linker)), 1.71 (m, 6 H, CH_2 (CyH)), 1.92 (m, 6 H, CH_2 (CyH)), 2.04 (m, 8 H, CH_2 (CyH)), 2.44 - 2.52 (m, 4 H, CH_2 (Py)), 3.08 - 3.11 (m, 4 H, CH_2 (Py)), 3.96 - 4.01 (m, 4 H, CH_2 Linker)), 4.09 - 4.16 (m, 2 H, CH (CyH)), 4.85 - 4.96 (m, 2 H, NH (Linker)),

7.20 - 7.23 (br.s., 1 H, NH (Zw), 8.14 (d, J=8.51 Hz, 2 H, CH (Per)), 8.18 (br. s., 2 H, CH (Per)), 8.32 (d, J=8.20 Hz, 2 H, CH (Per)), 11.34 (br. s., 1 H, NH (Zw)), 12.62 (br.s., 1 H, NH (Zw)), 13.61 (br.s., 1 H, NH (Zw))

^{13}C NMR (126 MHz, DMSO-d_6) δ = 22.42, 23.28, 23.77 (CH_2), 28.38 (CH_3), 29.82, 30.28 (CH_2 Linker), 56.48 (CH), 67.45 (CH_2), 128.69, 131.65, 131.73 (C_q), 159.86, 162.18, 167.02 (CO, CN)

HR-MS (MALDI) m/z = calculated 1233.4242, measured 1233.0981 for M + H^+

FT-IR v [cm^{-1}] =3180 (w), 2920 (w), 2855 (w), 2360 (w), 1655 (m), 1540 (m), 1340 (m), 1275 (s), 745 (s)

Reference Substance 50

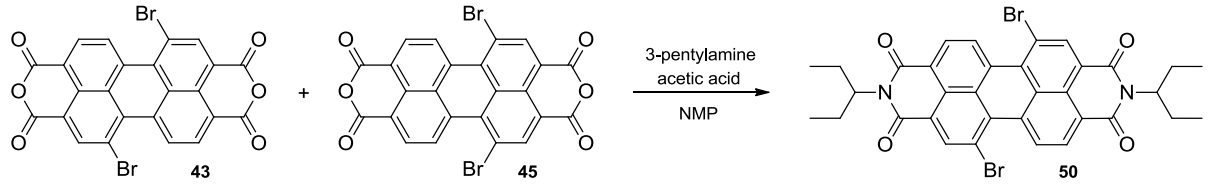

$C_{24}H_6Br_2O_6$
550,11 g/mol

$C_{34}H_{28}Br_2N_2O_4$
688,41 g/mol

A suspension of the brominated PTCDA **43** & **45** (500 mg, 0.9 mmol, 1 eq.) and 3-pentylamine (313 µL, 0.24 g, 2.7 mmol, 3 eq.) with acetic acid (0.25 ml, 5 eq.) in NMP (15 mL) was stirred 24h at 100°C. After cooling the precipitate was filtered, 15 mL water were added and the suspension was lyophilized. The crude product (50% yield) was purified by column chromatography (SiO_2: dichloromethane). The brick-red substance was dissolved in 100 mL DCM and 50 mL n-hexane was added. The solvent mixture was slowly reduced under vacuum until a precipitate of the 1,7-regioisomer formed. The suspension (ca. 50 mL) was put in the refrigerator and the precipitate was filtered afterwards. Since there was still a significant amount of the 1,6-regioisomer present, the recrystalization was repeated several times to obtain the 1,7-regioisomer **50** as an orange-red substance (75 mg, 0.11 mmol, 12% yield).

Soluble $CHCl_3$, DCM, THF

Insoluble MeOH, H_2O

R_f 0.4 (SiO_2: DCM)

MP > 200°C

^{1}H NMR (500 MHz, CHLOROFORM-*d*) δ = 0.93 (t, ^3J=7.41 Hz, 12 H, CH_3), 1.89 - 1.99 (m, 4 H, CH_2), 2.20 - 2.32 (m, 4 H, CH_2), 5.06 (ddd, *J*=9.69, 5.75, 3.78 Hz, 2 H, CH), 8.70 (d, ^3J=8.20 Hz, 2 H, CH), 8.92 (s, 2 H, CH), 9.50 (d, ^3J=7.88 Hz, 2 H, CH)

^{13}C NMR (126 MHz, CHLOROFORM-*d*) δ = 11.27, 11.30, 24.96, 25.02, 57.93, 120.75, 122.94, 123.36, 127.20, 128.08, 128.45, 129.27, 130.10, 130.39, 132.73, 132.88, 138.10, 138.15, 163.41, 163.77

HR-MS (MALDI) m/z = calculated 688.0395, measured 688.0730 for M·

FT-IR v [cm^{-1}] = 2970 (w), 2870 (w), 2355 (w), 1690 (m), 1650 (s), 1585 (s), 1375 (m), 1235 (s), 1085 (m), 810 (m), 750 (s)

7.3 Monotopic Modules

Substance 57

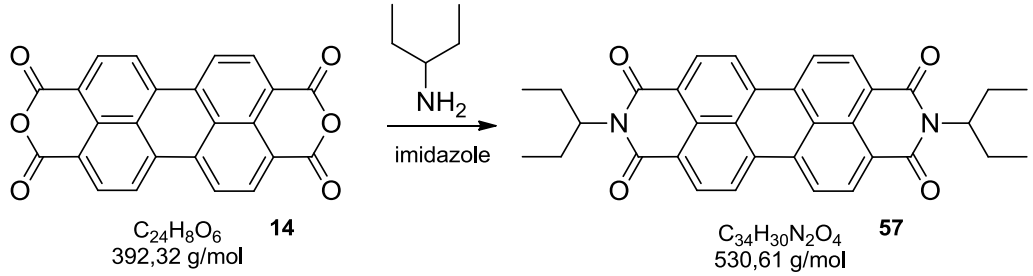

PTCDA **14** (1.00 g, 2.50 mmol, 1 eq.), 3-pentylamine (1.39 mL, 1.05 g, 12.00 mmol, 4.8 eq.) and imidazole (5.00 g, 73 mmol, 29 eq.) were mixed and stirred at 140°C for 12h. The mixture was diluted by the addition of methanol before complete cooling and treated with 1M HCl. The precipitate was filtered and purified by column chromatography (SiO_2: dichloromethane) to give a red crystalline substance (1.07 g, 2.02 mmol, 81% yield).

Soluble	$CHCl_3$, DCM, THF
Insoluble	MeOH, H_2O
R_f	0.1 (SiO_2: DCM)
MP	> 200°C
^{1}H NMR	(500 MHz, CHLOROFORM-*d*) δ = 0.94 (t, ^3J=7.41 Hz, 12 H, CH_3), 1.91 - 2.00 (m, 4 H, CH_2), 2.23 - 2.33 (m, 4 H, CH_2), 5.04 - 5.11 (m, 2 H, CH), 8.61 (d, ^3J=8.20 Hz, 4 H), 8.67 (d, ^3J=8.20 Hz, 4 H)
^{13}C NMR	(126 MHz, CHLOROFORM-*d*) δ = 11.33, 25.01, 57.70, 123.01, 123.49, 126.43, 129.59, 131.47, 134.48, 164.01
HR-MS	(MALDI) m/z = calculated 531.2239, measured 531.1810 for M + H^+
FT-IR	v [cm^{-1}] = 2960 (w), 2870 (w), 2355 (w), 1700 (s), 1645 (s), 1590 (s), 1405 (m), 1335 (s), 1255 (m), 1080 (m), 800 (s), 745 (s)

Substance 56

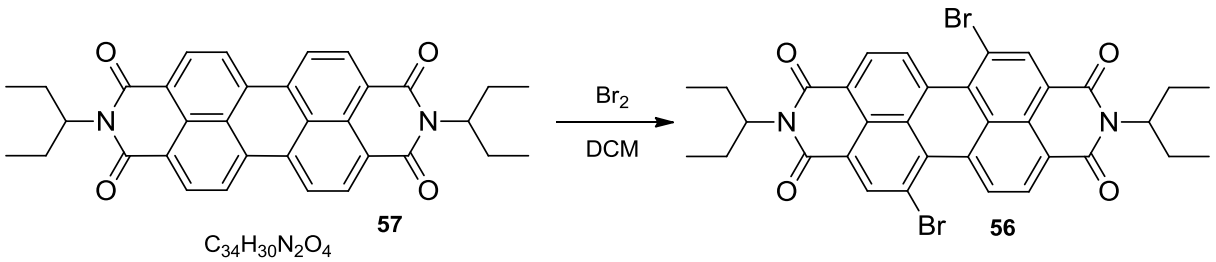

A solution of **57** (500 mg, 0.94 mmol, 1 eq.) and bromine (10.5 g, 66 mmol, 70 eq.) in dichloromethane (60 mL) was heated to reflux for 72h. After cooling the bromine was removed trough air bubbling and the solvent evaporated under reduced pressure. The raw product was purified by column chromatography (SiO_2: dichloromethane) to obtain a mixture of the 1,6- and 1,7-dibromo-regioisomer. To obtain the pure 1,7-regioisomer faster, the commonly known repetitive crystallization was changed. The light red substance was dissolved in 100 mL dichloromethane and 50 mL n-hexane was added. The solvent mixture was slowly reduced under vacuum until a precipitate formed. The precipitate was filtered afterwards and the complete procedure was repeated once again to obtain a orange-red substance (252 mg, 0.37 mmol, 39% yield).

Soluble	$CHCl_3$, DCM, THF
Insoluble	MeOH, H_2O
R_f	0.4 (SiO_2: DCM)
MP	> 200°C
^{1}H NMR	(500 MHz, CHLOROFORM-*d*) δ = 0.93 (t, ^3J=7.41 Hz, 12 H, CH_3), 1.89 - 1.99 (m, 4 H, CH_2), 2.20 - 2.32 (m, 4 H, CH_2), 5.06 (ddd, *J*=9.69, 5.75, 3.78 Hz, 2 H, CH), 8.70 (d, ^3J=8.20 Hz, 2 H, CH), 8.92 (s, 2 H, CH), 9.50 (d, ^3J=7.88 Hz, 2 H, CH)
^{13}C NMR	(126 MHz, CHLOROFORM-*d*) δ = 11.27, 11.30, 24.96, 25.02, 57.93, 120.75, 122.94, 123.36, 127.20, 128.08, 128.45, 129.27, 130.10, 130.39, 132.73, 132.88, 138.10, 138.15, 163.41, 163.77
HR-MS	(MALDI) m/z = calculated 688.0395, measured 688.0730 for M·
FT-IR	v [cm^{-1}] = 2970 (w), 2870 (w), 2355 (w), 1690 (m), 1650 (s), 1585 (s), 1375 (m), 1235 (s), 1085 (m), 810 (m), 750 (s)

Substance 55

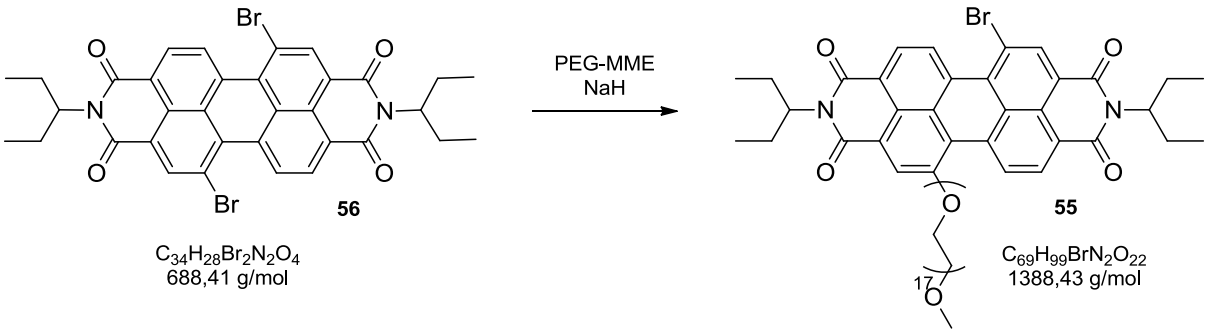

$C_{34}H_{28}Br_2N_2O_4$
688,41 g/mol

$C_{69}H_{99}BrN_2O_{22}$
1388,43 g/mol

Under dry argon atmosphere, **56** (14 mg, 20 µmol, 1 eq.) and polyethylene glycol mono methyl ether (750 Dalton, PEG-MME) (20 mg, 25 µmol, 1.2 eq.) were dissolved in dry tetrahydrofurane and 60% NaH-suspension (1.50 mg, 20 µmol, 1 eq.) was added after 5 min. An instantaneous color change occurred from orange to bright pink. After 24h the solvent was evaporated under reduced pressure and the obtained raw product was purified by column chromatography (SiO_2: dichloromethane/methanol (19:1)). After evaporation of the solvent, a shining magenta substance (15 mg, 11 µmol, 54% yield) could be obtained.

Soluble	THF, DCM, $CHCl_3$
Insoluble	H_2O, MeOH
R_f	0.35 (SiO_2: DCM/MeOH (9.5:0.5))
MP	134°C
^{1}H NMR	(300 MHz, CHLOROFORM-*d*) δ = 0.93 (td, *J*=7.43, 3.28 Hz, 12 H, CH_3), 1.88 - 2.00 (m, 4 H, CH_2), 2.28 (m, 4 H, CH_2), 3.39 (s, 3 H, CH_3), 3.53 - 3.57 (m, 4 H, CH_2), 3.60 - 3.69 (m, 60 H, CH_2), 3.76 - 3.80 (m, 2 H, CH_2), 3.85 (m, 2 H, CH_2), 4.06 - 4.13 (m, 2 H, CH_2), 4.61 - 4.67 (m, 2 H, CH_2), 5.06 (m, 2 H, CH), 8.48 (s, 1 H, CH), 8.56 - 8.70 (m, 2 H, CH), 8.93 (s, 1 H, CH), 9.60 (d, ^3J=7.82 Hz, 2 H, CH)
^{13}C NMR	(126 MHz, CHLOROFORM-*d*) δ = 11.44, 11.46 (CH_3), 25.14, 25.19 (CH_2), 29.84 (CH_3-PEG), 59.18 (CH), 69.52, 69.59, 70.66, 70.71, 70.75, 70.86, 70.98, 71.19, 72.08 (CH_2-PEG), 119.68, 120.77, 123.96, 124.23, 127.71, 128.86, 129.07, 129.46, 129.71, 133.02, 133.56, 134.11, 143.85 (C_q) 157.29 (CO)
HR-MS	(MALDI) m/z = calculated 1392.6695, measured 1392.6217 for M - Br + C_2H_4O + K^+
FT-IR	v [cm^{-1}] = 2935 (m), 2870 (m), 2370 (w), 1700 (s), 1650 (s), 1590 (s), 1400 (m), 1325 (s), 1240 (m), 1080 (s), 810 (s), 750 (s)

Substance 54

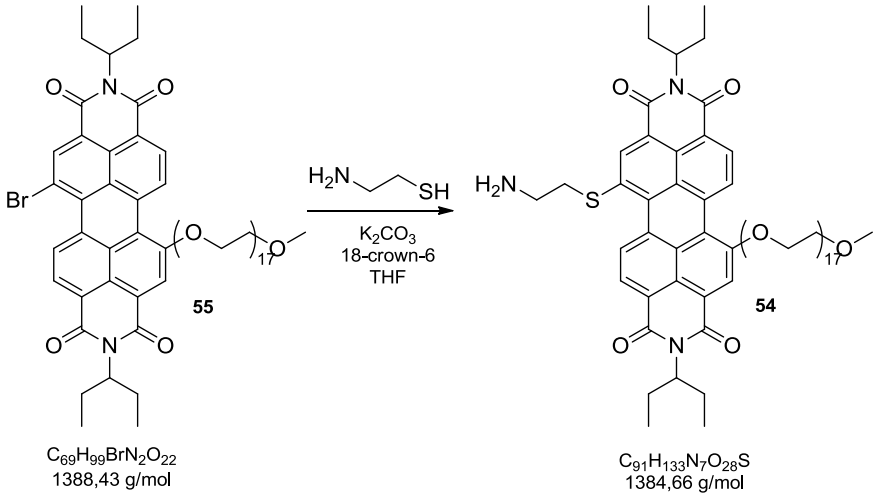

$C_{69}H_{99}BrN_2O_{22}$
1388,43 g/mol

$C_{91}H_{133}N_7O_{28}S$
1384,66 g/mol

Cysteamine (20 mg, 30 µmol, 2 eq.), 18-crown-6 (19 mg, 75 µmol, 5 eq.) and K_2CO_3 (10 mg, 75 µmol, 5 eq.) were dissolved in tetrahydrofurane (10 mL) and **55** (20 mg, 15 µmol, 1 eq.) was added after 5 min. An immediate color change occurred from orange to magenta and the reaction was completed after 2h. After the addition of water (10 mL) the reaction mixture was extracted with dichloromethane until the water phase remained colorless. The combined organic phases were dried with $MgSO_4$, filtered and the solvent removed in vacuum to obtain a magenta solid (20 mg, 15 µmol, quant. yield).

Soluble THF, DCM, $CHCl_3$

Insoluble H_2O, MeOH

R_f 0.4 (SiO_2: DCM/MeOH (9:1))

MP > 200°C

^{1}H NMR (600 MHz, METHANOL-d4) δ = 0.88 - 1.00 (m, 12 H, CH_3), 1.93 - 2.03 (m, 4 H, CH_2), 2.23 - 2.33 (m, 4 H, CH_2), 3.42 (br. s., 3 H, CH_3), 3.51 (m, 4 H, CH_2), 3.53 (m, 4 H, CH_2), 3.54 - 3.65 (m, 54 H, CH_2), 3.81 (m, 2 H, CH_2), 3.88 - 3.92 (m, 2 H, CH_2), 4.12 - 4.16 (m, 2 H, CH_2), 4.23 - 4.31 (m, 2 H, CH_2), 4.56 (dd, J=12.29, 5.69 Hz, 2 H, CH), 4.63 - 4.67 (m, 2 H, CH_2), 5.00 - 5.05 (m, 2 H, NH_2), 8.26 - 8.34 (m, 2 H, CH), 8.35 - 8.43 (m, 2 H, CH), 9.45 - 9.55 (m, 2 H, CH)

^{13}C NMR (151 MHz, METHANOL-d4) δ = 12.11 (CH_3), 23.26, 26.24, 29.98 (CH_2), 52.64 (CH_3), 59.21 (CH), 70.89, 70.93, 70.95, 70.98, 71.05, 71.07, 71.09, 71.12, 71.14, 71.16, 71.21, 71.22, 71.24, 72.59 (CH_2), 74.30, 77.38 (CH_2), 102.05 (C), 117.82, 121.60, 124.39, 127.55, 128.40, 133.05, 136.33, 137.88, 139.02, 139.67, 142.09, 145.94, 153.04 (C_q), 161.63, 170.45 (CO)

HR-MS (MALDI) m/z = calculated 1473.7477, measured 1474.4424 for M + 2x C_2H_4O + H^+

FT-IR v [cm^{-1}] = 3360 (m), 2880 (m), 1695 (m), 1645 (s), 1595 (m), 1420 (m), 1325 (s), 1095 (s), 1035 (m), 850 (m), 615 (m)

Substance 53

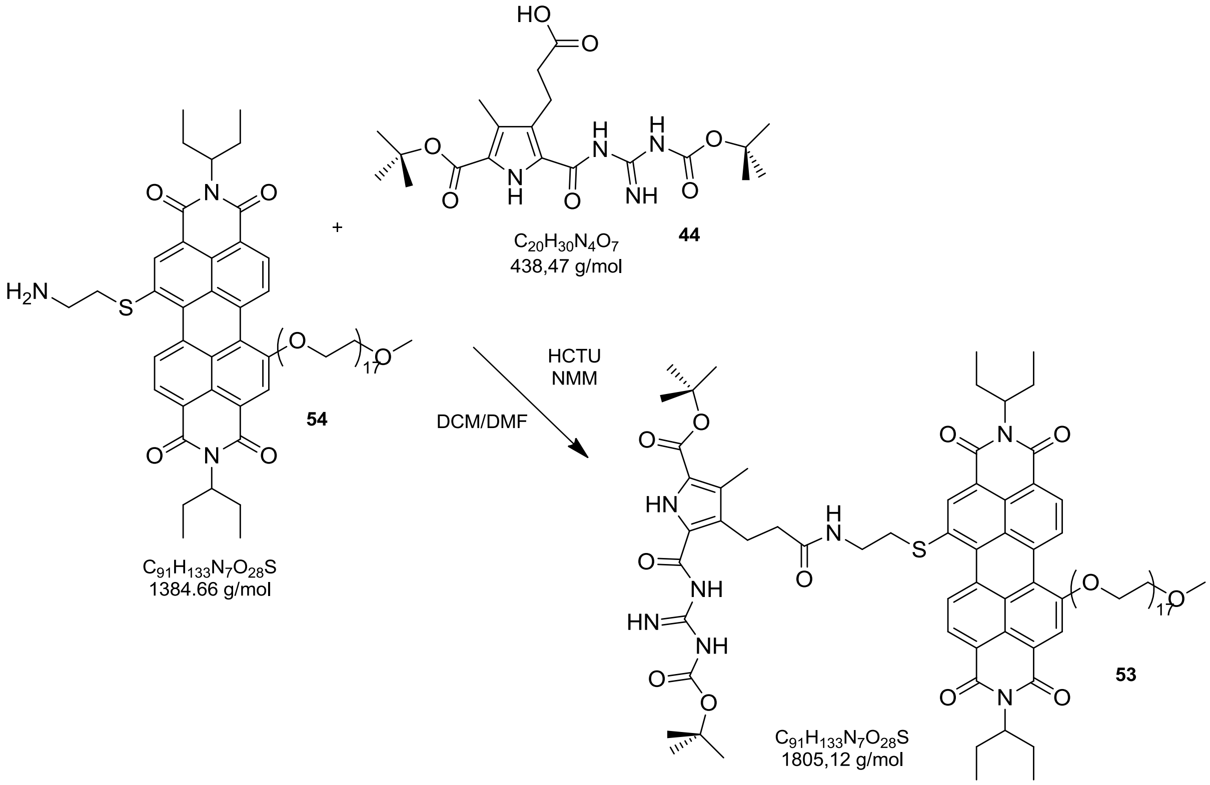

A mixture of **54** (20 mg, 15 µmol, 1 eq.), **44** (13 mg, 30 µmol, 2 eq.), HCTU (15 mg, 36 µmol, 2.4 eq.) and NMM (9 mg, 15 µL, 89 µmol, 6 eq.) in dichloromethane/dimethylformamide (10 mL (2:1)) was stirred for 24h at RT. Since the reaction control still showed spots of the starting material, additional HCTU (13 mg) was added. After 24h dichloromethane was removed under reduced pressure and 25 mL H_2O were added. The formed precipitate was filtered and subsequently purified by column chromatography (SiO_2: dichloromethane/methanol (9:1)). After the removal of the solvent, a dark pink wax (25 mg, 14 µmol, 95% yield) was isolated.

Soluble THF, DCM, $CHCl_3$

Insoluble H_2O, MeOH

R_f 0.5 (SiO_2: DCM/MeOH (9:1))

MP > 200°C

^{1}H-NMR (300 MHz, CHLOROFORM-d) δ = 1.25 (s, 12 H, CH_3 (Pentyl)), 1.50 (s, 9 H, CH_3 (Py)), 1.52 (s, 9 H, CH_3 (Py)), 1.91 - 1.99 (m, 4 H, CH_3 (Pentyl)), 2.24 (s, 3 H, CH_3 (Py)), 2.25 - 2.34 (m, 4 H, CH_3 (Pentyl)), 2.47 - 2.54 (t, ^3J=7.50 Hz, 2 H, CH_2 (Linker)), 2.72 - 2.79 (t, ^3J=6.88 Hz, 2 H, CH_2 (Linker)), 3.08 - 3.15 (m, 2 H, CH_2 (Linker)), 3.37 (s, 3 H, CH_3 (PEG)), 3.40 - 3.45 (m, 2 H, CH_2 (Linker)), 3.63 (s, 60 H, CH_2 (PEG)), 3.75 - 3.80 (m, 2 H, CH_2 (PEG)), 3.83 - 3.88 (m, 2 H, CH_2 (PEG)), 4.11 (m, 2 H, CH_2 (PEG)), 4.64

(m, 2 H, CH_2 (PEG)), 5.00 - 5.11 (m, 2 H, CH), 8.40 (s, 1 H, CH (Per)), 8.60 (d, J=8.76 Hz, 2 H, CH (Per)), 8.64 - 8.70 (m, 1 H, CH (Per)), 8.77 (s, 1 H, CH (Per)), 9.60 (d, J=8.44 Hz, 1 H, CH (Per))

^{13}C-NMR (75 MHz, CHLOROFORM-d) δ = 11.30, 11.35, 14.07 (CH_3), 25.02, 27.98, 28.31, 28.38, 29.65 (CH_2) 38.71 (CH_3), 58.97 (CH), 69.82, 70.42, 70.49, 71.86 (CH_2 (PEG)), 77.21, 77.30 (CH_2) 97.91, 98.64, 112.89, 115.12, 117.92, 126.22, 129.37, 130.84, 131.86, 133.00, 135.15 (C_q), 152.18, 156.95, 158.11, 160.00, 166.02 (CO, CN)

HR-MS (MALDI) m/z = calculated 1846.9108, measured 1847.1198 for M + C_2H_4O - H^+

FT-IR v [cm^{-1}] = 2965 (w), 2920 (w), 2365 (w), 1685 (m), 1620 (m), 1435 (m), 1255 (s), 1080 (s), 1005 (s), 795 (s), 715 (s)

Substance 38

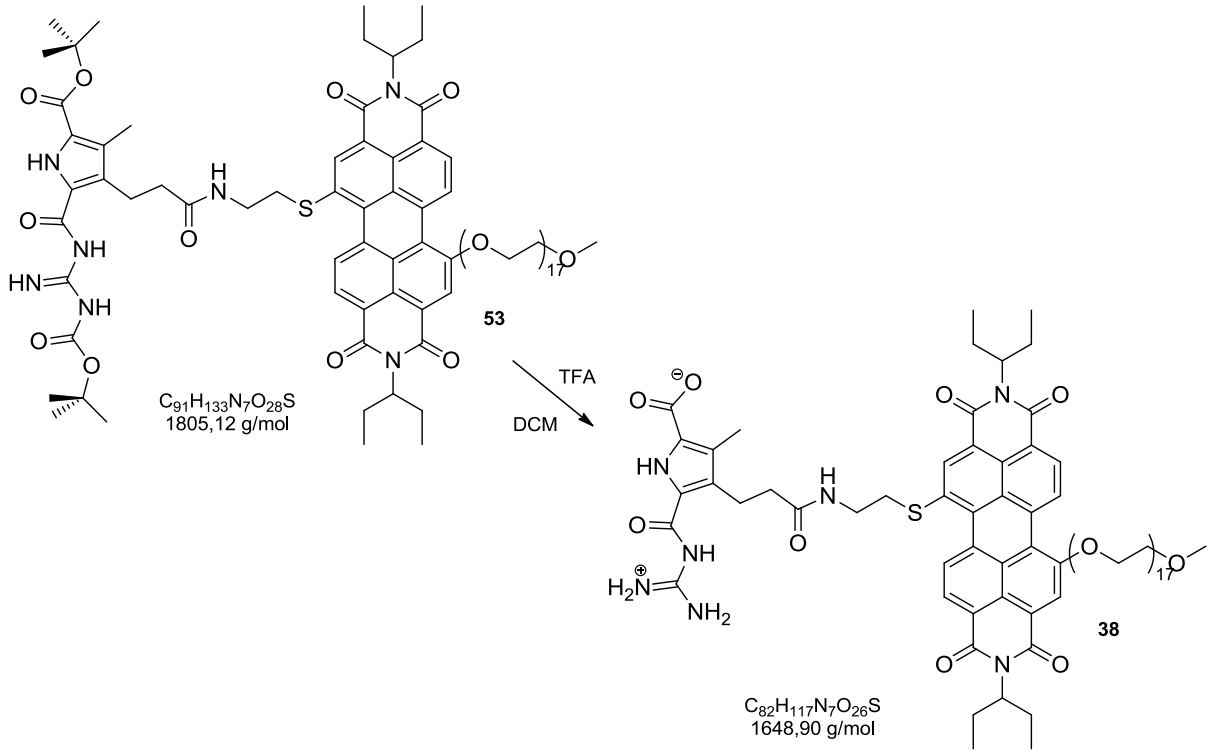

53 (25 mg, 14 µmol) was dissolved in a dichloromethane/TFA-mixture (5 mL:1 mL) and stirred for 24h. After evaporation of the solvent, 0.1M HCl (10 mL) was added and the suspension lyophilized. The remaining solid was dissolved in 0.5M NaOH (5 mL) and the pH was brought to 5.68 with 0.1M HCl. The suspension was stirred for 1h and the precipitate was filtered. The remaining solution which contains IK96 was again lyophilized. To remove all salts, the solid was dissolved in THF and filtered through a nylon membrane filter. The salts were washed with THF and the filtrate was narrowed to its original amount before repeating the procedure. The solvent was removed under reduced pressure to obtain a dark purple wax like substance (14 mg, 8.5 µmol, 61% yield).

Soluble THF, H_2O, DMSO, DCM

Insoluble n-Hex

R_f 0 (SiO_2: DCM/MeOH (9:1))

MP > 200°C

^{1}H NMR (600 MHz, THF-d^8) δ =1.29 (s, 12 H, CH_3 (Pentyl)), 1.39 (s, 3 H, CH_3 (Py)), 1.84 - 1.88 (m, 2 H, CH_2 (Linker)), 1.88 - 1.95 (m, 4 H, CH_2 (Pentyl)), 2.13 - 2.23 (m, 2 H, CH_2 (Linker)), 2.27 - 2.36 (m, 4 H, CH_2 (Pentyl)), 3.27 (s, 3 H, CH_3 (PEG)), 3.40 - 3.45 (m, 4 H, CH_2 (Linker)), 3.50 - 3.56 (m, 58 H, CH_2 (PEG)), 3.62 - 3.64 (m, 2 H, CH_2 (PEG)), 3.73 - 3.76 (m, 2 H, CH_2 (PEG)), 3.82 (m, 2 H, CH_2 (PEG)), 4.08 - 4.11 (m, 2 H, CH_2

(PEG)), 4.68 - 4.71 (m, 2 H, CH_2 (PEG)), 5.02 - 5.12 (m, 2 H, CH), 6.58 (s, 2 H, CH (Per)), 8.55 (br. s., 2 H, CH (Per)), 9.84 (d, ^3J=8.07 Hz, 2 H, CH (Per)), 10.67 (br. s., 1 H, NH), 10.85 (br. s., 1 H, NH)

^{13}C NMR (151 MHz, THF-d^8) δ = 11.67, 14.48 (CH_3), 24.98, 28.71, 29.70, 29.86, 30.69 (CH_2), 35.4230.69 58.98 (CH), 70.44, 70.57, 71.41, 71.51, 71.55, 71.61, 71.82, 71.93, 72.96 (CH_2), 78.31 (CH_2), 122.34, 124.27, 124.91, 130.06, 130.27, 134.48 (C_q), 143.03, 146.32, 147.91, 157.83, 186.84 (CO, CN)

HR-MS (MALDI) m/z = calculated 1670.7662, measured 1670.2423 for M + Na^+

FT-IR v [cm^{-1}] = 2960 (s), 2865 (s), 2355 (w), 1700 (m), 1645 (s), 1460 (m), 1365 (s), 1250 (m), 1155 (m), 1055 (m), 885 (m), 755 (s)

Substance 60

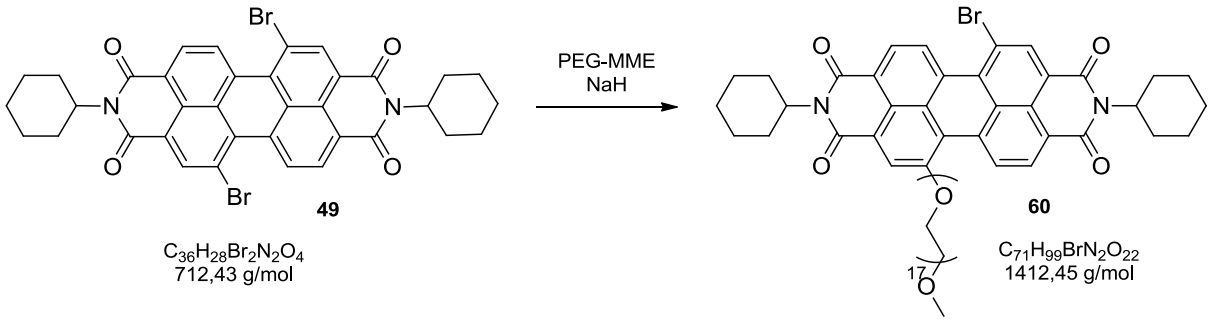

49

$C_{36}H_{28}Br_2N_2O_4$
712,43 g/mol

60

$C_{71}H_{99}BrN_2O_{22}$
1412,45 g/mol

Under dry argon atmosphere, **49** (50 mg, 70 µmol, 1 eq.) and PEG-MME (67 mg, 84 µmol, 1.2 eq.) were dissolved in dry tetrahydrofurane and 60% NaH-suspension (3.5 mg, 70 µmol, 1 eq.) was added after 5 min. An instantaneous color change occurred from orange to bright pink. After 24h the solvent was evaporated under reduced pressure and the obtained raw product was purified by column chromatography (SiO_2: dichloromethane/methanol (19:1)). After evaporation of the solvent, a shining magenta substance (71 mg, 50 µmol, 72% yield) could be obtained.

Soluble THF, DCM, $CHCl_3$

Insoluble H_2O, MeOH

R_f 0.2 (SiO_2: DCM/MeOH (9.5:0.5))

MP 127°C

^{1}H NMR (500 MHz, CHLOROFORM-*d*) δ = 1.74 - 1.81 (m, 10 H, CH_2), 1.92 - 1.94 (m, 6 H, CH_2), 2.58 (ddd, *J*=12.06, 8.12, 3.47 Hz, 4 H, CH_2), 3.62 (s, 3 H, CH_3), 3.65 (m, 48 H, CH_2), 3.70 - 3.71 (m, 4 H, CH_2), 3.79 (dd, *J*=6.15, 3.31 Hz, 4 H, CH_2), 3.85 - 3.88 (m, 4 H, CH_2), 4.09 - 4.13 (m, 4 H, CH_2), 4.61 - 4.65 (m, 4 H, CH_2), 5.05 (m, 2 H, CH), 8.43 - 8.47 (m, 2 H, CH), 8.55 (d, *J*=8.51 Hz, 1 H, CH), 8.57 - 8.64 (m, 2 H, CH) 9.58 (dd, *J*=8.35, 2.68 Hz, 1 H, CH), 9.73 (d, *J*=8.20 Hz, 1 H, CH)

^{13}C NMR (126 MHz, CHLOROFORM-*d*) δ = 25.6, 26.7, 29.3 (CH_2) 53.6 (CH_3) 59.2 (CH) 69.5, 69.6, 70.7, 70.7, 70.7, 70.8, 71.0, 71.2, 72.1 (CH_2), 119.6, 123.7, 127.5, 128.0, 128.8, 129.0, 129.3, 131.4, 132.8, 133.4, 133.9, 137.9 (C_q), 163.2, 163.8 (CO)

HR-MS (MALDI) m/z = calculated 1459.6924, measured 1460.0290 M - Br + K^+

FT-IR v [cm^{-1}] = 2920 (s), 2855 (s), 2355 (w), 1730 (s), 1455 (m), 1375 (m), 1274 (s), 1125 (m), 750 (s)

Substance 59

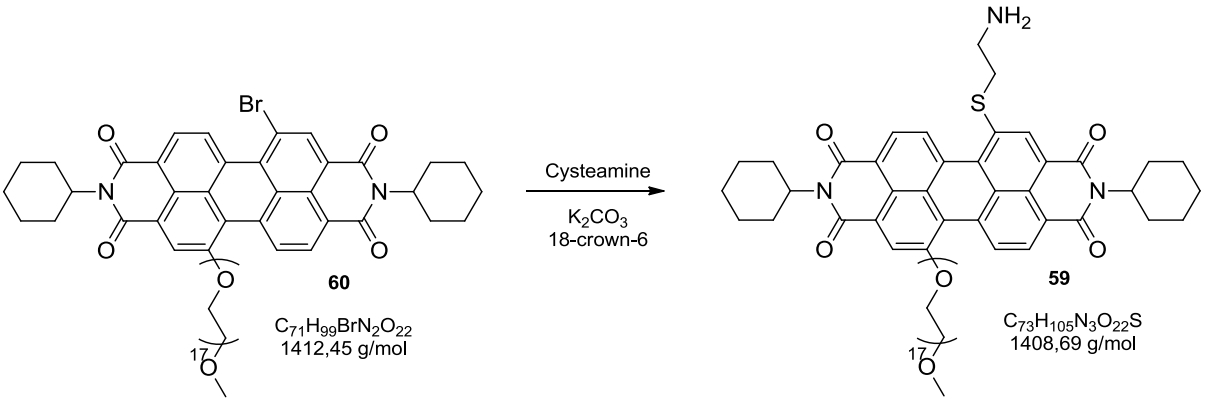

Cysteamine (8 mg, 100 µmol, 2 eq.), 18-crown-6 (66 mg, 250 µmol, 5 eq.) and K_2CO_3 (35 mg, 250 µmol, 5 eq.) were dissolved in tetrahydrofurane (10 mL) and **60** (71 mg, 50 µmol, 1 eq.) was added after 5 min. The reaction mixture was stirred for 30min and after the addition of water (20 mL) the solution was extracted with 4 x 40 mL dichloromethane. The combined organic phases were dried with $MgSO_4$ and the solvent removed in vacuum to obtain a magenta wax like substance (47 mg, 33 µmol, 66% yield).

Soluble THF, DCM, $CHCl_3$

Insoluble H_2O, MeOH

R_f 0.6 (SiO_2: DCM/MeOH (9:1))

MP 140°C

^{1}H NMR (500 MHz, CHLOROFORM-*d*) δ = 1.32 - 1.40 (m, 2 H, CH_2), 1.48 (q, ^3J=12.82 Hz, 4 H, CH_2), 1.80 (d, ^3J=11.66 Hz, 4 H, CH_2), 1.92 - 1.94 (d, ^3J=11.32 Hz, 6 H, CH_2), 2.49 - 2.63 (m, 4 H, CH_2), 3.38 (s, 3 H, CH_3), 3.52 - 3.57 (m, 4 H, CH_2), 3.57 - 3.61 (m, 4 H, CH_2), 3.64 (br. s., 48 H, CH_2), 3.70 - 3.72 (m, 4 H, CH_2), 3.79 (dd, ^3J=5.83, ^4J=3.31 Hz, 4 H, CH_2), 3.86 (dd, ^3J=5.67, ^4J=3.47 Hz, 4 H, CH_2), 4.09 - 4.12 (m, 2 H, CH_2), 4.58 - 4.62 (m, 2 H, CH_2), 4.99 - 5.08 (m, 2 H, CH), 8.40 (s, 2 H, CH), 8.51 (d, ^3J=8.51 Hz, 2 H, CH), 9.67 (d, ^3J=8.51 Hz, 2 H, CH)

^{13}C NMR (126 MHz, CHLOROFORM-*d*) δ = 25.5, 26.5, 29.1 (CH_2), 53.9 (CH_3), 59.0 (CH) 69.2, 69.5, 70.3, 70. 4, 70.5, 70.5, 70.7, 70.8, 70.9, 71.0, 71.9 (CH_2), 77.2, 77.4 (CH_2), 117.3, 121.6, 121.8, 123.7, 123.8, 129.0, 129.1, 129.2, 133.6, 156.4 (C_q), 163.8, 164.0 (CO)

HR-MS (MALDI) m/z = calculated 1408.6944, measured 1408.9483 for M + H^+

FT-IR v [cm^{-1}] = 2920 (m), 2855 (m), 2330 (w), 1695 (m), 1650 (m), 1590 (m), 1335 (m), 1270 (m), 1085 (s), 940 (w), 750 (m)

Substance 58

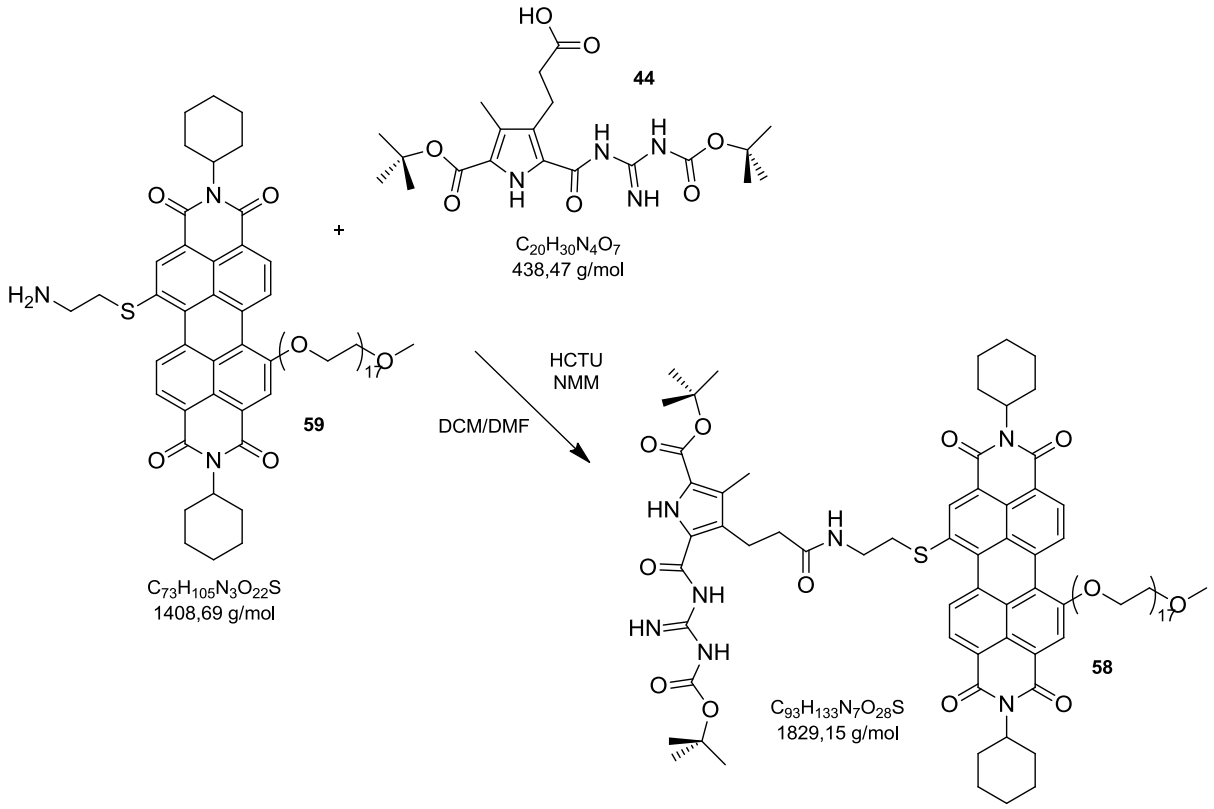

A mixture of **59** (47 mg, 33 µmol, 1 eq.), **44** (29 mg, 66 µmol, 2 eq.), HCTU (33 mg, 79 µmol, 2.4 eq.) and NMM (20 mg, 22 µL, 198 µmol, 6 eq.) in dichloromethane/dimethylformamide (10 mL (2:1)) was stirred for 24h at RT. Afterwards dichloromethane was removed under reduced pressure and 25 mL H_2O were added. The formed precipitate was filtered and subsequently purified by column chromatography (SiO_2: dichloromethane/methanol (9:1)). After the removal of the solvent, a dark pink wax (25 mg, 14 µmol, 42% yield) was isolated.

Soluble THF, DCM, $CHCl_3$

Insoluble H_2O, MeOH

R_f 0.3 (SiO_2: DCM/MeOH (9:1))

MP > 200°C

^{1}H NMR (500 MHz, CHLOROFORM-*d*) δ = 1.23 (s, 9 H, CH_3 (Py)), 1.25 (s, 9 H, CH_3 (Py)), 1.59 (br. s., 3 H, CH_3 (Py)), 1.72 - 1.84 (m, 8 H, CH_2 (CyH)), 1.93 (m, 6 H, CH_2 (CyH)), 2.25 - 2.30 (m, 4 H, CH_2 (Linker)), 2.49 - 2.52 (t, ^3J=7.88, 2 H, CH_2 (Linker)), 2.53 - 2.63 (m, 6 H, CH_2 (CyH)), 3.38 (s, 3 H, CH_3 (PEG)), 3.53 - 3.57 (m, 2 H, CH_2 (PEG)), 3.64 (m, 54 H, CH_2 (PEG)), 3.77 - 3.80 (m, 4 H, CH_2 (PEG)), 3.84 - 3.88 (m, 4 H, CH_2 (PEG)), 4.10 - 4.12 (m, 2 H, CH_2 (PEG)), 4.36 (t, ^3J=7.25 Hz, 2 H, CH_2 (Linker)), 4.61 - 4.64

(m, 2 H, CH_2 (PEG)), 5.05 (tt, ^3J=12.22 Hz, ^4J=3.55 Hz, 2 H, CH (CyH)), 6.57 (d, ^4J=4.73 Hz, 2 H, CH (Per)), 8.02 (s, 2 H, CH (Per)), 8.45 (s, 1 H, CH (Per)), 8.55 (d, J=8.51 Hz, 1 H, CH (Per)), 9.72 (d, ^3J=8.51 Hz, 1 H, CH (Per))

^{13}C NMR (126 MHz, CHLOROFORM-*d*) δ = 9.78 (CH_3), 26.54, 27.77 (CH_2), 28.00, 28.39 (CH_3), 29.44, 34.84, 38.60 (CH_2), 53.92 (CH_3), 59.00 (CH), 68.47, 70.46, 70.50, 70.66, 70.80, 71.00, 71.90 (CH_2), 77.20, 78.74 (CH_2), 100.56, 117.50, 121.77, 121.89, 123.84, 29.09, 129.24, 129.34, 133.72 (C_q), 140.07, 143.17, 145.40, 148.70, 156.48, 157.90, 162.59, 163.90, 164.05 (CO, CN)

HR-MS (MALDI) m/z = calculated 1823.8323, measured 1823.9720 for M - C_2H_4O + K^+

FT-IR v [cm^{-1}] = 3355 (w), 3092 (w), 2930 (m), 2850 (m), 2365 (w), 1700 (m), 1620 (m), 1435 (m), 1285 (s), 1140 (s), 935 (s), 820 (s), 710 (s), 590 (m)

Substance 37

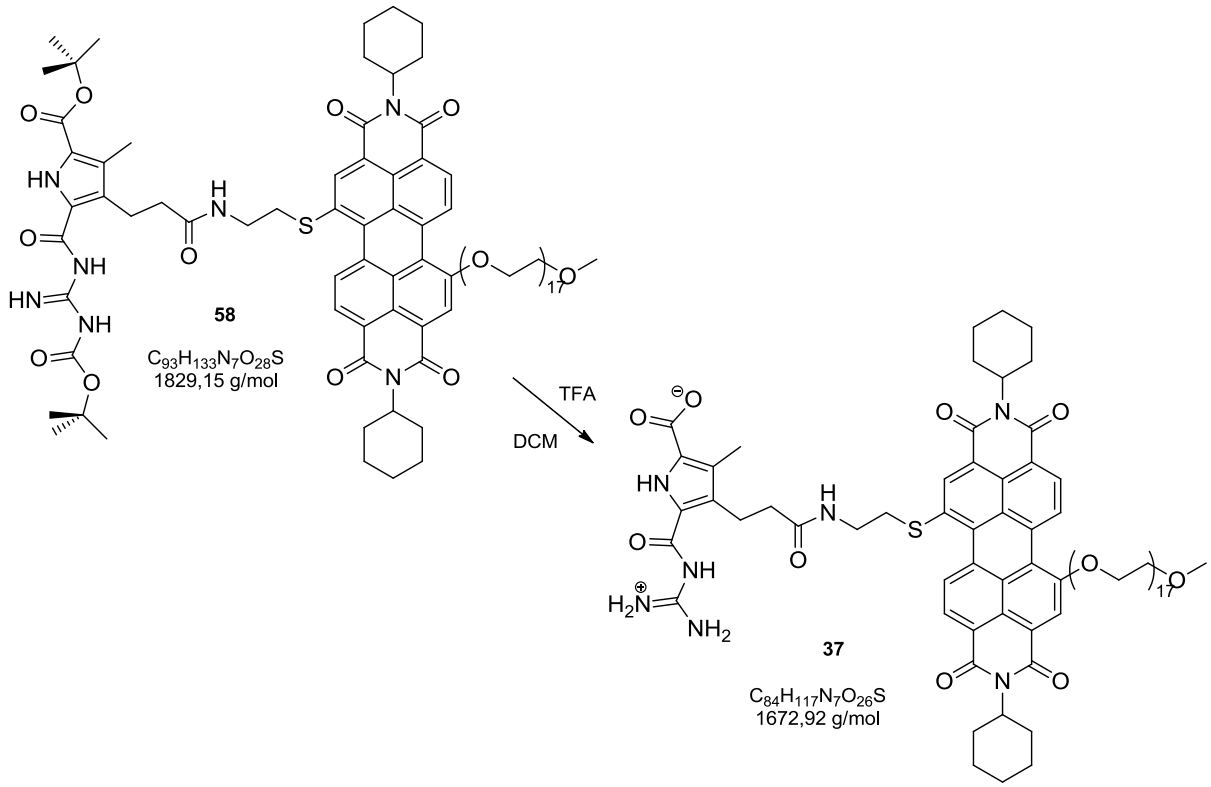

58 (25 mg, 14 µmol) was dissolved in a dichloromethane/TFA-mixture (5 mL:0.5 mL) and stirred for 24h. After evaporation of the solvent, 0.1M HCl (10 mL) was added and the suspension lyophilized. The remaining solid was dissolved in 0.5M NaOH (5 mL) and the pH was brought to 5.8 with 0.1M HCl. The suspension was stirred for 1h and the precipitate was filtered. The remaining solution was again lyophilized. To remove all salts, the solid was dissolved in tetrahydrofurane and filtered through a nylon membrane filter. The solvent was removed under reduced pressure to obtain a dark purple wax like substance (23 mg, 14 µmol, quant. yield).

Soluble THF, DCM

Insoluble H_2O, DMSO

R_f 0.7 (SiO_2: DCM/MeOH (9:1))

MP > 200°C

^{1}H NMR (500 MHz, THF-d^8) δ = 1.48 (s, 3 H, CH_3 (Py)), 1.72 - 1.78 (m, 6 H, CH_2 (CyH)), 1.82 - 1.87 (m, 6 H, CH_2 (CyH)), 1.89 - 1.95 (m, 8 H, CH_2 (CyH)), 2.53 - 2.54 (m, 2 H, CH_2 (Linker)), 2.58 (m, 2 H, CH_2 (Linker)), 2.64 (m, 2 H, CH_2 (Linker)), 3.22 (m, 2 H, CH_2 (Linker)), 3.41 (s, 3 H, CH_3 (PEG)), 3.48 (m, 24 H, CH_2 (PEG)), 3.52 - 3.54 (m, 8 H, CH_2 (PEG)), 3.59 - 3.62 (m, 8 H, CH_2 (PEG)), 3.69 - 3.73 (m, 8 H, CH_2 (PEG)), 3.79 - 3.81 (m, 8 H, CH_2 (PEG)), 4.01 - 4.03 (m, 4 H, CH_2 (PEG)), 4.47 (m, 4 H, CH_2 (PEG)),

4.82 - 4.89 (m, 4 H, CH_2 (PEG)), 5.29 - 5.34 (br. s., 2 H, NH), 5.48 (dd, J=6.46, 2.36 Hz, 2 H, CH (CyH)), 8.02 (br. s., 2 H, CH (Per)), 8.07 (br. s., 2 H, CH (Per)), 9.23 (br. s., 2 H, CH (Per)), 9.39 (br. s., 2 H, NH), 11.98 (br. s., 1 H, NH)

^{13}C NMR (151 MHz, THF-d^8) δ = 25.56, 25.70, 25.83 (CH_2), 27.65 (CH_3), 30.00, 30.34 (CH_2), 58.98 (CH_3) 70.45, 71.43, 71.58, 71.65, 71.84, 71.96, 72.98 (CH_2), 95.21 (CH), 121.98, 122.89, 129.77, 129.92, 134.14 (C_q), 157.62, 164.11, 164.27 (CO, CN)

HR-MS (MALDI) m/z = calculated 1894.7662, measured 1694.2801 for M + Na^+

FT-IR v [cm^{-1}] = 2960 (s), 2920 (s), 2865 (s), 2360 (w), 1695 (m), 1645 (s), 1460 (w), 1360 (m), 1245 (m), 1100 (s), 890 (w), 745 (s)

8. Abbreviations

$CHCl_3$	Chloroform
EtAc	Ethyl acetate
MeOH	Methanol
CyHex	Cyclohexane
DEE	Diethyl ether
H_2O	Water
NEt_3	Triethylene amine
DCM	Dichloromethane
K_2CO_3	Potassium carbonate
EtOH	Ethanol
DMAP	4-(Dimethylamino)-pyridin
HCTU	N,N,N′,N′-Tetramethyl-O-(6-chloro-1H-benzotriazol-1-yl)uronium hexafluorophosphate
DMF	Dimethylformamide
LiOH	Lithium hydroxide
NaOAc	Sodium acetate
SO_2Cl_2	Sulfuryl chloride
RT	Room temperature
HCl	Hydrochloric acid
AcOH	Acetic acid
n-Hex	n-Hexane

THF	Tetrahydrofurane
H_2SO_4	Sulfuric acid
TFA	Trifluoroacetic acid
NaOH	Sodium hydroxide
NMM	N-Methylmorpholin
PTCDA	Perylene tetracarboxylic acid bisanhydride
PEG-MME	Polyethylene glycol mono methyl ether (750 Dalton)

9. Bibliography

[1] http://witcombe.sbc.edu/water/artleonardo.html (09/06/2014)

[2] http://hammercodex.com/index.php (09/06/2014)

[3] W. M. Latimer , W. H. Rodebush, *J. Am. Chem. Soc.*, **1920**, 42, 1419-1433.

[4] F. Franks, *Water: A Matrix of Life*, Second Edition, Royal Society of Chemicals, Cambridge, **2000**.

[5] J. M. Lehn, *Supramolecular Chemistry, Concepts and Perspectives*, VCH, Weinheim, **1995**.

[6] H. R. Horton, L. A. Moran, K. G. Scrimgeour, M. D. Perry, J. D. Rawn, *Biochemie*, 4. Auflage, Pearson Studium, München, **2008**.

[7] J. D. Watson, F. H. Crick, *Nature* **1953**, *171*, No. 4356, 737-738.

[8] B. J. B. Folmer, R. P. Sijbesma, R. M. Versteegen, J. A. J. van der Rijt, E. W. Meijer, *Adv. Mater.* **2000**, *12*, 874-878.

[9] X. Zhan, A. Facchetti, S. Barlow, T. J. Marks, M. A. Ratner, M. R. Wasielewski, S. R. Marder, *Adv. Mater.* **2011**, *23*, 268-284.

[10] K. Tomizaki, R. S. Loewe, C. Kirmaier, J. K. Schwartz, J. L. Retsek, D. F. Bocian, D. Holten, J. S. Lindsey, *J. Org. Chem.* **2002**, *67*, 6519-6534.

[11] C. Li, H. Wonneberger, *Adv. Mater.* **2012**, *24*, 613-636.

[12] Y. Hisamatsu, S. Banerjee, M. B. Avinash, T. Govindaraju, C. Schmuck, *Angew. Chem. Int. Ed.* **2013**, *52*, 12550-12554.

[13] J. N. Israelachvili, *Intermolecular and Surface Forces*, Third Edition, Elsevier, Oxford, **2011**.

[14] C. A. Hunter, K. R. Lawson, J. Perkins, C. J. Urch, *J. Chem. Soc., Perkin Trans. 2* **2001**, 651-669.

[15] C. Fouquey, J.-M. Lehn, A.-M. Levelut, *Adv. Mater.* **1990**, *2*, 254-257.

[16] T. F. A. De Greef, M. M. J. Smulders, M. Wolffs, A. P. H. J. Schenning, R. P. Sijbesma, E. W. Meijer, *Chem. Rev.* **2009**, *109*, 5687-5754.

[17] M. M. J. Smulders, M. M. L. Nieuwenhuizen, T. F. A. de Greef, P. van der Schoot, A. P. H. J. Schenning, E. W. Meijer, *Chem. Eur. J.* **2010**, *16*, 362-367.

[18] C. Schmuck, *Eur. J. Org. Chem.* **1999**, 2397-2403.

[19] F. P. Schmidtchen, M. Berger, *Chem. Rev.* **1997**, *97*, 1609-1646.

[20] C. Schmuck, *Chem. Commun.* **1999**, 843-844.

[21] C. Schmuck, W. Wienand, *J. Am. Chem. Soc.* **2003**, *125*, 452-459.

[22] M. T. Fenske, W. Meyer-Zaika, H.-G. Korth, H. Vieker, A. Turchanin, C. Schmuck, *J. Am. Chem. Soc.* **2013**, *135*, 8342-8349.

[23] C. Schmuck, T. Rehm, F. Gröhn, K. Klein, F. Reinhold, *J. Am. Chem. Soc.* **2006**, *128*, 1430-1431.

[24] C. Schmuck, T. Rehm, K. Klein, F. Gröhn, *Angew. Chem. Int. Ed.* **2007**, *46*, 1693-1697.

[25] T. Fenske, *Schaltbare supramolekulare Nanostrukturen - Einflüsse externer Stimuli auf das Aggregationsverhalten von supramolekularen Strukturen*, Dissertation, Essen, **2011**.

[26] C. Huang, S. Barlow, S. R. Marder, *J. Org. Chem.* **2011**, *76*, 2386-2407.

[27] F. Würthner, *Chem, Commun.* **2004** , 1564-1579.

[28] G. Geissler, H. Remy (Hoechst AG), *Ger. Pat. Appl.*, DE 1130099, **1959** (*Chem. Abstr.* **1962**, *57*, P11346f).

[29] E. E. Jelley, *Nature* **1936**, *138*, 1009–1010.

[30] G. Scheibe, *Angew. Chem.* **1936**, *49*, 563.

[31] W. West, B.H. Carroll, *J. Chem. Phys*. **1951**, *19*,417.

[32] from a presentation of T. Pradeep, Professor at DST Unit of Nanoscience, Indian Institute of Technology Madras; http://www.dstuns.iitm.ac.in/teaching.php (08/04/2014)

[33] W. E. Ford, *J. Photochem.* **1987**,*37*, 189-204.

[34] F. Würthner, C. Thalacker, S. Diele, C. Tschierske, *Chem. Eur. J.* **2001**, *7*, 2245–2253.

[35] S. Ghosh, X.-Q. Li, V. Stepanenko, F. Würthner, *Chem. Eur. J.* **2008**, *14*, 11343-11357.

[36] T. E. Kaiser, H. Wang, V. Stepanenko, F. Würthner , *Angew. Chem. Int. Ed.* **2007**, *46*, 5541-5544.

[37] G. Gröger, V. Stepanenko, F. Würthner, C. Schmuck, *Chem. Commun*, **2009**, 698-700.

[38] R. Dobrawa, M. Lysetska, P. Ballester, M. Grüne, F. Würthner, *Macromolecules* **2005**, *38*, 1315-1325.

[39] F. Würthner, *Pure Appl. Chem.* **2006**, *78*, 2341-2349.

[40] E. Sariola-Leikas, M. Niemi, H. Lemmetyinen, A. Efimov, *Org. Biomol. Chem.* **2013**, *11*, 6397-6406.

[41] B. Gao, H. Li, H. Liu, L. Zhang,Q. Bai, X. Ba, *Chem. Commun.* **2011**, *47*, 3894-3896.

[42] Y. Liu, K.-R. Wang, D.-S. Guo, B.-P. Jiang, *Adv. Funct. Mater.* **2009**, *19*, 2230-2235.

[43] R. Samudrala, X. Zhang, R. M. Wadkins, D. L. Mattern, *Bioorg. Med. Chem.* **2007**, *15*, 186-193.

[44] S. Rehm, V. Stepanenko, X. Zhang, T. H. Rehm, F. Würthner, *Chem. Eur. J.* **2010**, *16*, 3372-3382.

[45] D. Görl, X. Zhang, F. Würthner, *Angew. Chem.* **2012**, *124*, 6434-6455.

[46] X. Zhang, D. Görl, V. Stepanenko, F. Würthner, *Angew. Chem. Int. Ed*. **2014**, *53*, 1270-1274.

[47] V. Percec, M. Peterca, T. Tadjiev, X. Zeng, G. Ungar, P. Leowanawat, E. Aqad, M. R. Imam, B. M. Rosen, U. Akbey, R. Graf, S. Sekharan, D. Sebastiani, H.W. Spiess, P. A. Heiney, S. D. Hudson, *J. Am. Chem. Soc.* **2011**, *133*, 12197-12219.

[48] N. Jouault, Y. Xiang, E. Moulin, G. Fuks, N. Giuseppone, E. Buhler, *Phys. Chem. Chem. Phys.* **2012**, *14*, 5718-5728.

[49] M. Duval, F. Boué, *Macromolecules* **2007**, *40*, 8384-8388.

[50] J. Baram, E. Shirman, N. Ben-Shitrit, A. Ustinov, H. Weissman, I. Pinkas, S. G. Wolf, B. Rybtchinski, *J. Am. Chem. Soc.* **2008**, *130*, 14966-14967.

[51] E. Krieg, E. Shirman, H. Weissman, E. Shimoni, S. G. Wold, I. Pinkas, B. Rybtchinski, *J. Am. Chem. Soc.* **2009**, *131*, 14365-14374.

[52] G. Golubkov, H. Weissman, E. Shirman, S. G. Wolf, I. Pinkas, B. Rybtchinski, *Angew. Chem. Int. Ed.* ***2009,*** 48, 926 -930.

[53] M. Merschky, *from small molecules towards supramolecular dendrimers*, Dissertation, Essen, **2010**.

[54] F. Würthner, V. Stepanenko, Z. Chen, C. R. Saha-Möller, N. Kocher, D. Stalke, *J. Org. Chem.* **2004**, *69*, 7933-7939.

[55] C. Schmuck, D. Rupprecht, U. Urban, N. Walden, *Synthesis* **2006**, 8996.

[56] J.-F. Ponsa, J.-L. Fauchèreb, F. Lamatya, A. Mollac, R. Lazaro, *Eur. J. Org. Chem*. **1998**, 853-859.

[57] G. Goretzki, E. Stephen Davies, S. P. Argent, W. Z. Alsindi, A. J. Blake, J. E. Warren, J. McMaster, N. R. Champness, *J. Org. Chem.* **2008**, *73*, 8808-8814.

[58] G. Santosh, E. Shirman, H. Weissman, E. Shimoni, I. Pinkas, Y. Rudich, B. Rybtchinski, *J. Phys. Chem. B* **2010**, *Vol. 114, No. 45*, 14389-14396.

[59] C. Shahar, J. Baram, Y. Tidhar, H. Weissman, S. R. Cohen, I. Pinkas, B. Rybtchinski, ACS Nano **2013**, *Vol. 7, No. 4*, 3547-3556.

[60] T. Heek, C. Fasting, C. Rest, X. Zhang, F. Würthner, R. Haag, *Chem. Commun.* **2010**, *46*, 1884-1886.

[61] J. van Herrikhuyzen, A. Syamakumari, A. P. H. J. Schenning, E. W. Meijer, *J. Am. Chem. Soc.* **2004**, *126*, 10021-10027.

[62] J. Lopez-Andarias, M. J. Rodriguez, C. Atienza, J. L. Lopez, T. Mikie, S. Casado, S. Seki, J. L. Carrascosa, N. Martin, *J. Am. Chem. Soc.* **2015**, *137*, 893-897.

[63] L. Bu, E. Pentzer, F. A. Bokel, T. Emrick, R. C. Hayward, *ACS Nano* **2012**, *6*, 10924-10929.

[64] P. Rajasingh, R. Cohen, E. Shirman, L. J. W. Shimon, Boris Rybtchinski, *J. Org. Chem.* **2007**, *72*, 5973-5979.

[65] H. Langhals, O. Krotz, K. Polborn, P. Mayer, *Angew. Chem. Int. Ed.* **2005**, *44*, 2427-2428.

[66] Z. Zhang, X. Zhang, C. Zhan, Z. Lu, X. Ding, S. He, J. Yao, Soft Matter, 2013, 9, 3089-3097.

[67] J. R. R. Tolkien: *The Hobbit or There and Back Again.* George Allen & Unwin, London **1937**, Quote of Thorin Oakenshield

[68] J. R. R. Tolkien: *The Hobbit or There and Back Again.* George Allen & Unwin, London **1937**, Quote of Thorin Oakenshield